Magnetotactic bacteria in sediment: Magnetotaxis, chemotaxis, and paleomagnetic implications

Xuegang Mao

München 2013

Magnetotactic bacteria in sediment: Magnetotaxis, chemotaxis, and paleomagnetic implications

Xuegang Mao

Dissertation
an der Fakultät für Geowissenschaften
der Ludwig–Maximilians–Universität
München

vorgelegt von
Xuegang Mao

München, den July 16, 2013

Erstgutachter: Prof.Dr. Stuart Gilder
Zweitgutachter: Dr. Ramon Egli
Tag der mündlichen Prüfung: November 13, 2013

Contents

List of Figures

List of Tables

Summary

The widespread magnetotactic bacteria (MTB) in freshwater and marine sediment have been studied over a few decades. In spite the fact that fruitful accomplishments have been achieved, magnetotactic bacteria behaviour in sediment is poorly known. Some hypothesis and models based on observations of cultured magnetotactic bacteria in water environment sometimes are not sufficient to reflect their real states in sediment. The main task of present thesis is to study magnetotactic bacteria behaviour in sediment, and the relation between magnetotaxis and chemotaxis.

The magnetic alignment of magnetotactic bacteria in water obeys a Langevin law derived from Brownian motion, while the alignment in sediment is controlled by mechanical interaction with the sediment matrix, resulting in an almost random distribution. A $\sim$1% alignment with the Earth magnetic field, however, is theoretically sufficient for providing swimming bacteria with a magnetotactic advantage for crossing typical oxygen gradients in sediment. Mechanical interactions between bacteria and sediment particles can also explain the observed positive correlation between magnetic moment and bacteria volume, which make some types of bacteria (e.g. *M. bavaricum*) appear largely overdesigned in terms of magnetosome number for performing magnetotaxis in water. Therefore, additional functionalities, such as energy derived from magnetite oxidation/reduction cycles, are not required to explain the observed magnetosome production. A series of experiments with controlled magnetic fields show that the original poor alignment of living magnetotactic bacteria is the starting point for the acquisition of a natural remanent magnetization (NRM) by magnetofossils derived from the dissolution of cells after their death. This NRM is proportional to the magnetic field and of the same order of magnitude as non-biogenic NRMs obtained with redeposition experiments. Therefore, magnetofossil-bearing sediments appear to be suitable NRM carriers for relative paleointensity studies.

The efficiency of polar magnetotaxis, and its combination with chemotaxis, has been studied in microcosms subjected to a variety of sedimentary conditions and magnetic field

configurations. Both types of polar magnetotactic bacteria investigated (cocci and *M. bavaricum*) can migrate vertically over macroscopic distances to reach their optimum living depth if the field polarity corresponds to the environment where they originated from (i.e. downward-pointing magnetic field in the Northern hemisphere). If the magnetotactic advantage is removed by performing the same experiments in zero field, the *M. bavaricum* population decreases, but cells are capable of reaching their optimum living depth relying only on chemotaxis. Cocci, on the other hand, disappear in such conditions. Similar results are obtained if the field polarity is reversed. In this case, *M. bavaricum* cells that migrated in the correct direction must have been capable of adapting their polar magnetotactic response to an environment where the chemical gradient is reversed with respect to the magnetic field. Finally, cells that are already living in their optimum depth range might require magnetotaxis only to counteract bioturbation-related solid diffusion in sediment, which tend to disperse them vertically, or to move up and down in a given depth range for metabolic requirements that cannot be satisfied at a single depth in sediment. Experiments in zero field for as long as ∼160 days show that cocci already living in their optimum depth range are unaffected by the lack of magnetotaxis, while the *M. bavaricum* population initially decrease, but does not disappear.

Overall, these results prove the magnetotactic advantage of cells that need to reach their optimum living environment after major sediment disturbance. This advantage is strongest for cocci, while *M. bavaricum* appears to be capable of migrating on the basis of chemotaxis alone. Once cells are located in their optimum living range, the situation appears reversed: cocci are not favoured by the magnetic field in maintaining their depth in sediment, while the *M. bavaricum* population decreases in zero fields. This difference might reflect the fact that cocci are relatively immotile under optimal conditions, while *M. bavaricum* needs to migrate continuously within a certain depth range

Microcosm experiments on polar magnetotaxis show that bacteria are able to switch their swimming direction depending on the chemical environment, as also predicted by current magneto-aerotaxis model. However, the predicted swimming direction under strictly anoxic conditions could never be observed under the microscope. Observation of living *M. bavaricum* cells swimming into a pH gradient, on the other hand, revealed that swimming direction switching is triggered by a single concentration threshold of different substances (e.g. O_2 and H^+) rather than a lower and an upper oxygen threshold.

Chapter 1

Introduction

In 1958, Salvatore Bellini, a medical doctor working at the Institute for Microbiology at the University of Pavia (Italy), discovered motile bacteria that reacted to the Earth magnetic field while examining water samples from sources around Pavia for pathogens (Frankel, 2009), which he called "magnetosensitive bacteria" in two unpublished manuscripts (Bellini, 2009a,b). This sensational discover was ignored by the scientific community and was effectively lost until Richard P. Blakemore, unaware of Bellini's findings, rediscovered these bacteria in a pond in Woods Hole (Massachusetts) and called them with the name by which they are known today: "magnetotactic bacteria" (Blakemore, 1975). Blakemore was able to show that the swimming direction of these bacteria is determined by the Earth magnetic field surrounding them, thanks to chains of "iron-rich particles" (later identified as magnetite) which acted like microscopic compass needles. The ability of magnetotactic bacteria to align with magnetic fields and swim along field lines is known as magnetotaxis. This discover generated immediate interest in the scientific community, and later studies demonstrated how the biomineralized magnetic crystals, known as magnetosomes, and the arrangement of such crystals in chains, is precisely controlled by the cell, so that the resulting magnetic moment is maximized with respect to the amount of iron used for this purpose (Frankel, 2009; Frankel et al., 1979). Such maximization requires magnetosomes to be grown within a very narrow grain size range for which they contain a single magnetic domain. It represents a tantalizing fingerprint of natural selection, especially when considering that inorganic synthesis of magnetic nanocrystals with similarly well-constrained properties is an impossible task for nowadays best technologies.

Magnetotaxis (i.e. the ability to swim along magnetic field lines) is combined with chemotaxis to help magnetotactic bacteria place themselves in the oxic-anoxic transition

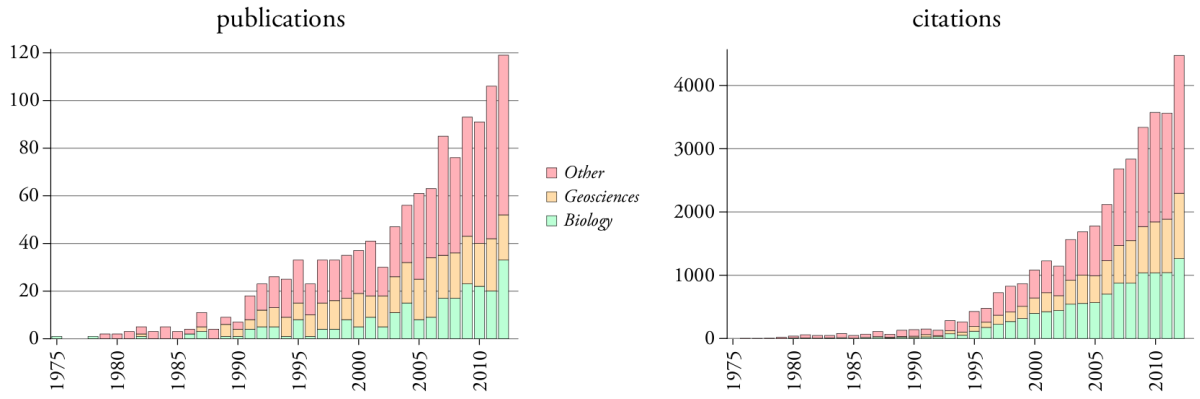

Figure 1.1: Number of publications (left) and citations (right) related to magnetotactic bacteria, obtained from the ISI Web of Science databank with the search key "magnetotactic bacteria OR magnetofossils OR magnetosomes OR biogenic magnetite". The "biology" and "geosciences" categories correspond to "microbiology, biotechnology, applied microbiology" and "geochemistry, geophysics, multidisciplinary geosciences", respectively

zone of chemically stratified environments, which is their preferred living environment (Frankel et al., 1997). The advantage of magnetotactic bacteria over other chemotactic organisms is believed to be given by their alignment in the magnetic field, which reduces a three-dimensional search for an optimal environment to a much faster one-dimensional search (Frankel, 1984). The unique characteristics of magnetosome biomineralization and magnetotactic behaviour (see Bazylinski and Frankel, 2004; Blakemore, 1982; Faivre and Schüler, 2008, for reviews) have attracted a broad interdisciplinary interest, as testified by exponentially growing number of publications related to magnetotactic bacteria (Figure 1.1).

Discovery of fossil magnetosomes in deep-sea sediments (Kirschvink, 1982; Kirschvink and Chang, 1984; Petersen et al., 1986; Vali et al., 1987) and later in sedimentary rocks (see Kopp and Kirschvink, 2008, for a review of magnetofossil findings), triggered the interest of the paleomagnetic community for magnetotactic bacteria as potential carriers of natural remanent magnetization (Mcneill and Kirschvink, 1993). Because magnetite particles of magnetosome size are dissolved under sulfidic conditions encountered in anoxic marine sediments (Canfield and Berner, 1987; Karlin, 1990; Tarduno, 1994), magnetofossils have been reported as the dominant carrier of paleomagnetic signals only in few pre-Quaternary locations (Kopp and Kirschvink, 2008) despite the ubiquitous occurrence of magnetotactic bacteria in aquatic environments. The recent development of new rock magnetic techniques for the identification of magnetofossils in complex magnetic mineral

mixtures typically occurring in sediments (Egli, 2004a; Egli et al., 2010) led to discovering that magnetofossils are widespread in the geological record (Roberts et al., 2012). Putative magnetofossil findings have been reported for up to 3.4 billion years old stromatolitic cherts (Chang and Kirschvink, 1989), and, more controversially, in 3.6 billion years old carbonate globules of the Martian meteorite ALH84001 (Thomas-Keprta et al., 2000). These findings, if further confirmed, are interesting because, besides proving the existence of life on Mars, they would provide a mean for inferring the existence of a planetary field during epochs for which classical paleomagnetic records are likely erased by high-temperature metamorphism.

Besides their relevance as paleomagnetic carriers, magnetofossil concentration and morphology variations in sediment are expected to reflect the influence of paleoenvironmental conditions on magnetotactic bacteria communities living in sediment. For example, correlations between magnetofossil morphology and glacial/interglacial cycles (Hesse, 1994), as well as the sedimentary organic carbon flux (Yamazaki and Kawahata, 1998), have been reported. Elevated magnetofossil concentrations (Lippert and Zachos, 2007) and unusual magnetite crystals of supposedly biological origin (Schumann et al., 2008) characterize some sedimentary records during the Paleocene-Eocene Thermal Maximum (55 million years), when one of the most abrupt and dramatic climate events of the Cenozoic occurred. Roberts et al. (2011) used magnetofossil, calcareous nannofossil, and dust records in Eocene pelagic carbonates to conclude that magnetotactic bacteria abundance in pelagic marine environments is limited by organic carbon flux and dissolved iron availability. This hypothesis has been used to infer natural iron fertilization in the Southern Ocean during glacial periods characterized by increased concentrations of elongated magnetofossils (Yamazaki and Ikehara, 2012). Finally, (Bishop and Egli, 2011) proposed that ^{60}Fe iron produced by a supernova explosion $\sim$2.8 million years before present is recorded by magnetofossils in pelagic carbonates. These examples among many other published results (Figure 1.1) demonstrate the increasing interest gained by magnetotactic bacteria in geosciences.

Despite the growing interest on magnetotactic bacteria in geosciences, many fundamental questions relevant for paleomagnetic and paleoenvironmental applications remain unanswered. For example, the excellent alignment of freely swimming magnetotactic bacteria with the Earth magnetic field, as observed under the microscope, is not necessarily replicated in sediment, which is their natural living environment in most cases. Yet the acquisition of a natural remanent magnetization (NRM) by magnetofossils likely depends on the initial alignment of living bacteria. The naive model of magnetofossils left *in-situ*

by the post-mortem dissolution of well-aligned bacteria living in sediment would generate a saturated remanent magnetization that is orders of magnitudes larger than observed NRM amplitudes. Chain collapse occurring after the dissolution of stabilizing biological structures in the cell (Kobayashi et al., 2006), would reduce or even completely erase the magnetofossil NRM, possibly explaining the NRM intensities observed in magnetofossil-rich sediments (Mcneill and Kirschvink, 1993). On the other hand, we now know that these sediments contain mostly intact magnetofossil chains (Egli et al., 2010; Roberts et al., 2012), so that the initial magnetofossil NRM acquisition mechanism must rely on a more complicated process. Because of the different NRM acquisition mechanisms of magnetofossils – which originate directly in sediment – on one hand, and of magnetic particles depositing from the water column on the other, the corresponding NRM acquisition efficiencies might be drastically different, leading to apparent variations in paleointensity records that might be interpreted as Earth field variations while just reflecting compositional variations of the magnetic remanence carriers (Yamazaki and Solheid, 2011).

Paleoenvironmental reconstructions based on magnetofossil abundance and/or morphology, on the other hand, require a detailed knowledge of the ecological requirements of magnetotactic bacteria and on the modulation of their "magnetotactic advantage" over other organisms competing for the same resources. Although the basic mechanisms of magnetotaxis have been explained (Frankel et al., 1997), many questions are not yet answered. For example, laboratory experiments where nutrients or iron sources have been added to sediment hosting living populations of magnetotactic bacteria have never produced a cell number increase, as one would expect from the claimed (e.g. Roberts et al., 2012) correlation between sedimentary organic carbon flux and magnetofossil concentration. The abundance of magnetotactic bacteria might be influenced by competition with other organisms for the same resources, and therefore by the magnetotactic advantage over other chemotactic organisms. This advantage is directly related to the natural selection of magnetotactic bacteria with best capability to migrate across chemical gradients. One of the factors that influence this capability is the alignment of magnetotactic bacteria in sediment, which in turn depends on the magnetic moment and the volume of cells. Unfortunately, current magnetotaxis models are not capable of explaining the observed correlation between magnetic moment and cell volume, and the apparent excess of magnetosome production in some types of bacteria (e.g. Spring et al., 1993). This problem led to the formulation of alternative hypotheses on the role of magnetosome production, such as the "magnetosome battery hypothesis", according to which magnetosomes acts as

intracellular energy storage based upon partial oxidation of magnetite to maghemite and subsequent reduction (Vali and Kirschvink, 1991).

The goal of this PhD thesis is to answer the following questions:

- How well are magnetotactic bacteria aligned in sediment?
- What is the magnetotactic advantage in sediment?
- How is magnetotaxis combined with chemotaxis?
- Do magnetofossils acquire a NRM, and, if yes, how does this occur?

with the observation of natural populations of magnetotactic bacteria in sediment or under conditions that are as close as possible to a sedimentary environment. Such observations are much more difficult and time consuming than analogous experiments with magnetotactic bacteria cultures, because of the much smaller concentration of cells and the impossibility to observe them directly in sediment. On the other hand, wild-type magnetotactic bacteria are continuously subjected to natural selection and degeneration effects typical of cultures can be excluded. Degeneration effects are not negligible: for example, cultured cells tend to grow magnetosome chains containing gaps, and the coercivity of such chains, which is a measure for their degree of "perfection", is systematically much smaller than that magnetofossils and enriched wild-type magnetotactic bacteria (Egli, 2004a; Pan et al., 2005b).

Different aspects of magnetotaxis and NRM acquisition by magnetofossils are handled in six Chapters, each focusing on results obtained with a given type of experimental procedures, as summarized in the following:

chapter 2. This chapter reports measurements of the alignment of magnetotactic bacteria in sediment. It is shown that the observed alignment in sediment – despite being much lower than in water – is sufficient to provide a magnetotactic advantage for cell swimming across typical oxygen gradients in sediment. Furthermore, only the observed alignment in sediment explains the correlation between magnetic moment and cell volume, without the need for additional hypotheses magnetosome functionality. NRM acquisition experiments in controlled fields are used to show that magnetofossils acquire a magnetization in the mixed layer of sediments, and that this magnetization is of the same order of magnitude as that obtained from redeposition experiments. This result is reassuring, because it shows that magnetofossil-bearing sediments are suited to relative paleointensity investigations.

This chapter is at the same time a manuscript submitted to *Geochemistry, Geophysics, Geosystems*.

chapter 3. In this chapter, the reaction of natural magnetotactic bacteria populations to changes of the oxygen gradient in sediment microcosms is investigated with a specially designed glove box in which the atmospheric oxygen concentration can be controlled. Temporal changes in the oxygen profile affect the magnetotactic bacteria population, although it is evident than other factors are also involved in controlling their position in sediment. Experiments with a CO_2-atmosphere have been performed to test the reaction of bacteria population to a change of pH in sediment. Finally, microscope observation of magnetotactic bacteria under strictly anoxic conditions inside the glove box failed at detecting bacteria swimming along the opposite direction with respect to observations in oxygen-saturated water, which would be expected from the polar magnetotaxis model of Frankel et al. (1997). Therefore, oxygen cannot be the only factor regulating magnetotaxis.

chapter 4. In this chapter the magnetotactic advantage is tested with microcosms subjected to different magnetic field configurations. Absence of a magnetic field eliminates the magnetotactic advantage, while periodically switched fields are be used to test situations where polar magnetotaxis becomes a disadvantage. The effect of these magnetic field configurations on the total population of two types of magnetotactic bacteria (cocci and *Magnetobacterium bavaricum*) and on their vertical distribution in sediment is monitored over time. Unexpected results that did not point to a clear magnetotactic advantage have been obtained. These results, which cannot be explained with current magnetotaxis models, have been used to design detailed experiments for testing magnetotaxis in sediment, as discussed in chapter 5.

chapter 5. This chapter describes microcosm experiment designed to track the vertical migration of the same two types of magnetotactic bacteria investigated in chapter 4, under different magnetic field configurations. The main parameters controlling these experiments are the starting position of specially marked cells in sediment (above, at, or below their optimal living depth), and field configurations in which magnetotaxis is either eliminated, does not provide an advantage or a disadvantage, or provides one of both. Consistent results for all combinations of starting positions and field configurations provide a first systematic investigation of polar magneto-chemotaxis inside the natural living environment of magnetotactic bacteria. Comparison of these results with observation under the microscope clearly demonstrates that magneto-chemotaxis is regulated by a number of factors that are difficult to reproduce outside the sedimentary environment.

chapter 6. This chapter provides the missing bridge between magnetotaxis experiments in sediment, and direct observation of magneto-chemotaxis under the optical microscope. The fortuitous discover of the response of *Magnetobacterium bavaricum* cells to pH-gradients has been used to perform systematic observations on swimming direction changes produced by an environment containing a combination of two repellents, namely oxygen and excessively acidic conditions. These observations demonstrate that the two-threshold response to oxygen concentrations originally postulated for polar magneto-aerotaxis (Frankel et al., 1997) is best replaced by single thresholds of substances promoting one or the other direction of flagella rotation. It also appears that the swimming direction of *Magnetobacterium bavaricum* is controlled by chemical concentrations, rather than gradients.

In summary, new models have been obtained for magnetofossil NRM acquisition, and for magnetotactic mechanisms in sediment. These models provide a first basis for further research aimed at better understanding both the paleomagnetic and the environmental significance of magnetofossils.

Chapter 2

Magnetotaxis and acquisition of a detrital remanent magnetization by magnetotactic bacteria populations in sediment:first experimental results and theory

This chapter was based on paper: Mao, X., Egli, R., Petersen, N., Hanzlik, M. Zhao, X. Magnetotaxis and acquisition of a detrital remanent magnetization by magnetotactic bacteria populations in sediment : first experimental results and theory. Geochem. Geophys. Geosyst. under review (2013).

Abstract

The widespread occurrence of magnetotactic bacteria (MTB) in several types of marine and freshwater sediment, and the role of fossil magnetosomes (magnetofossils) as main remanent magnetization carriers therein, has important implications for paleoenvironmental reconstructions and for sediment paleomagnetism. Despite numerous studies on MTB biology and on magnetofossil preservation in geological records, no information is yet available on magnetotaxis in sedimentary environments (i.e. the ability to align with magnetic fields and efficiently move across chemical gradients) and on the mechanism by which magnetofossils possibly record the Earth magnetic field. This paper provides for the first time experimental evidence for these processes. Unlike the case of MTB bacteria freely swimming in the water column, active MTB in sediment are poorly aligned with geomagnetic

fields. Nevertheless, this alignment appears just sufficient for supporting magnetotaxis across the typical thickness of oxygen gradients. Sediment magnetotaxis appears to be the only mechanism capable of explaining the observed magnetic moments of individual MTB in terms of selective pressure. A proportional detrital remanent magnetization (DRM) is acquired by magnetofossils within the mixing layer of sediment exposed to 0-160 μT fields. Current models of DRM acquisition based on flocculation are not applicable to magnetofossils, because MTB are primarily present in sediment as 'non-flocculable' magnetic carriers. Instead, the observed DRM acquisition can be explained by a dynamic equilibrium between magnetic forces and randomizing forces due to bioturbation-induced rearrangement of contact points between sediment particles.

2.1 Introduction

Magnetotactic bacteria (MTB) represent one of the most intriguing examples of biological synthesis of iron minerals. These minerals (magnetosomes) have unique magnetic properties, and the development of rock magnetic techniques for their identification led to discovery of the widespread occurrence of MTB in several types of marine and freshwater sediment, and the dominant role of fossil magnetosomes (magnetofossils) as main remanent magnetization carriers therein (Egli et al., 2010; Roberts et al., 2012). Besides the obvious paleomagnetic relevance of magnetofossil-bearing sediments, concentration and morphology of magnetofossils has been linked with paleoenvironmental conditions (e.g. Hesse, 1994; Roberts et al., 2011; Yamazaki and Ikehara, 2012).

Despite abundant literature is now available on MTB biology (Bazylinski and Frankel, 2004; Faivre and Schüler, 2008) and on magnetofossil preservation in geological records (Kopp and Kirschvink, 2008), no information is yet available on magnetotaxis in sedimentary environments (i.e. the ability to navigate with the geomagnetic field and efficiently move across chemical gradients) and on how magnetofossils can possibly acquire a natural remanent magnetization (NRM). This information, however, is essential to understand the environmental control of MTB populations, and for relative paleointensity determinations based on magnetofossil-bearing sediment. Therefore, we provide for the first time experimental evidence and theoretical models for magnetotaxis and acquisition of a detrital remanent magnetization (DRM) by magnetofossils.

2.2 Materials and methods

2.2.1 Sediment preparation and MTB populations

Carbonaceous, sandy to loamy sediment containing living MTB has been collected from lake Chiemsee, Germany (47°52'23" N, 12°24'25" E) using the procedures described in Pan et al. (2005b), and from a small pond with ∼1 m maximum water depth in proximity of our laboratory (48°35'14.98" N, 12°04'43.71" E). Collected sediment was transferred to glass aquaria (microcosms) at ambient temperature, where a stationary chemical stratification with stable MTB populations formed in ∼9 days within ∼3 cm from the sediment-water interface. These aquaria served as material source for all experiments. Sediment from Chiemsee contains predominantly cocci, a large, rod-shaped bacterium known as *Magnetobacterium bavaricum* (Jogler et al., 2010), and, occasionally, unidentified magnetotactic vibrios (Figure 2.1). In addition to these MTB types, a large, ovoid coccus (Kolinko et al., 2012) occurs dominantly in pond sediment (Figure 2.1c). These bacteria exhibit polar magnetotaxis (Frankel et al., 1997): when collected in the northern hemisphere (as in our case), they consistently swim towards the magnetic N when observed under normal (oxic) conditions in the hanging drop assay. We refer to this behavior as N-seeking (NS), and to the opposite behavior as S-seeking (SS), regardless of their effective polarity inside the sediment.

2.2.2 MTB swimming path tracking

All observations of living MTB have been performed with a specially equipped optical microscope (section A.1). For accurate swimming path tracking in controlled magnetic fields, the whole equipment was placed in a magnetically shielded room with <0.5 μT residual fields, and AF demagnetized in order to eliminate field inhomogeneities caused by objectives and other slightly magnetic parts. Fields comprised between 0 and 85 μT have been applied with 3 pairs of Helmholtz coils along directions parallel to the objective plane. Swimming trajectories of *M. bavaricum* and ovoid cocci in selected field intensities (Figure 2.2a,b) have been tracked with real-time image processing. About 1000 trajectories for each type of bacterium and each field step have been collected and analysed for determining mean cell alignment with the applied field (section A.1).

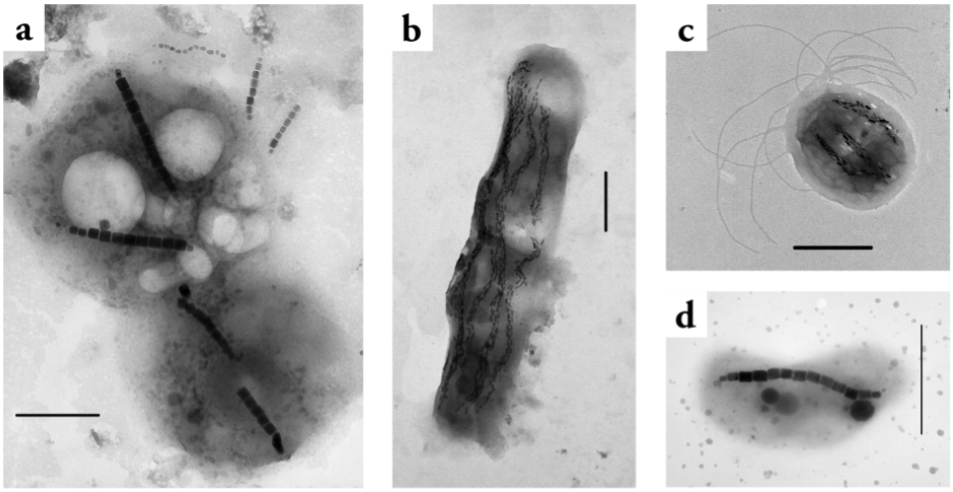

Figure 2.1: Transmission electron micrograph (TEM)images of wild-type MTB found in sediment from lake Chiemsee and a small pond. Scale bars are 1 μm. (a) Two cocci containing two chains of prismatic magnetosomes each. (b) *M. bavaricum*, containing 5 chain bundles of tooth-shaped magnetosomes. Chain bundles are heavily distorted by drying artifacts. (c) 'Watermelon' coccus containing three chain bundles of tooth-shaped magnetosomes. (d) Vibrio containing a single chain of prismatic magnetosomes.

2.2.3 Pulsed field experiments

MTB-containing sediment taken from the uppermost ∼3 cm of Chiemsee microcosms was transferred into 2 cm plastic cubes and allowed to stabilize in a 0.86 mT horizontal field for 20 minutes. Short, ∼0.1 T magnetic pulses were applied by capacitor discharge through a split coil placed around the plastic cube at various angles to the constant field (section A.2). The pulses are of sufficient intensity for switching the magnetic moment of cells forming large angles with the pulse direction (Hanzlik et al., 2002). After each pulse, 20 μl sediment samples were taken at three different points in the plastic cube with a micropipette. Each sample was diluted with 100 μl distilled water and homogenized in microtubes. 10 μl aliquots of the homogenized solution were transferred to a microscope slide and prepared for a hanging drop assay. A horizontal field was used to separate cells with unswitched moments, which swim towards the magnetic N (NS), from switched cells, which swim towards the opposite direction (SS). Switched and unswitched cells were allowed to accumulate on opposite sides of the water drop and counted. Experiments were repeated with six sediment-filled cubes in order to gain sufficient statistical significance.

2.2.4 DRM experiments

MTB-containing sediment from the topmost 2 cm of Chiemsee or pond microcosms was transferred to a separate container and thoroughly mixed in order to randomize particle orientations. The mixed sediment slurry was successively poured into 22×22 mm cylindrical plastic cups previously placed at the centre of three Helmholtz coil pairs producing a homogeneous magnetic field with known intensity (0.4-158 μT) and direction (∼50°inclination). The samples were allowed to rest in controlled fields for times comprised between 12 hours and 14 days (see section A.3). Sediment porosity ϕ, estimated as 1-(sample dry mass)/(sample volume)/(density of $CaCO_3$), was ∼88% at the beginning of the experiment. Initial water loss by evaporation produced a ∼15% and ∼33% reduction of sample diameter and thickness, respectively. Porosity was not allowed to decrease below 68%, and shrinkage cracks did not occur.

In a first series of experiments (samples A-C), cups were sealed with a glued lid at the end of the intended DRM acquisition time, in order to avoid water loss during subsequent measurements. A second series of experiments (samples D) was conducted in a similar manner, except for dividing the acquisition time into two intervals characterized by distinct field directions. For this purpose, samples have been sealed as described above after 52 hours and turned upside down, remaining in this position until the end of the experiment after 14 days. A third series of experiments (samples F) has been conducted in the same manner as for samples A-C with 14 days acquisition time, using four sets of Helmholtz coils with field intensities comprised between 0.4 and 158 μT.

Sediment samples obtained from the three experiment series have been immediately transferred to a shielded room with <0.5 μT residual field. Remanent magnetization measurements were performed with a vertical 2G cryogenic magnetometer integrated with an automatic sample handling and AF demagnetization system (Wack and Gilder, 2012). Three-axis AF demagnetization was performed in 1 mT steps up to 30 mT, 2 mT steps between 30 and 60 mT, and 5 mT steps between 60 and 90 mT. After complete NRM demagnetization, anhysteretic remanent magnetization (ARM) was imparted with 0.1 mT DC field and 90 mT peak AF field, and subsequently demagnetized with same AF steps used for NRM. Finally, a 0.2 T isothermal remanent magnetization (IRM) was imparted with an electromagnet, and subjected to the same AF demagnetization procedure. IRMs acquired in 0.2 T and 1 T are practically identical, and IRM(0.2T) is therefore identified with M_{rs} throughout the paper.

Control samples deprived of MTB and, more in general, of SD magnetite, have been

prepared by selective chemical dissolution with the citrate-bicarbonate-dithionite (CBD) method (Mehra and Jackson, 1958) modified for optimal extraction efficiency of magnetosomes (section A.3). CBD-treated sediment (samples C) has been used to perform identical DRM experiments as described above. Finally, AF demagnetization curves of ARM and IRM have been measured on fully dried, untreated sediment powder firmly compressed in plastic cups. These AF demagnetization curves serve as reference for the magnetic properties of sediment, because mechanical unblocking of magnetic particles in strong fields can be excluded.

2.3 Orientation of active MTB in water

The orientation of a bacterium with magnetic moment $\mathbf{m}$ in presence of a homogeneous magnetic field $\mathbf{B}$ is controlled by combined action of the magnetic torque $\mathbf{T}=\mathbf{m}\times\mathbf{B}$, and of randomizing forces associated to Brownian motion in water. If self-propulsion is neglected, the probability density function for the angle θ between $\mathbf{m}$ and $\mathbf{B}$ under thermal equilibrium is proportional to the Boltzmann factor e^{U/k_BT}, where k_BT is the energy of thermal perturbations at the absolute temperature T, and $U = mB\cos\theta$ is the magnetic potential energy (Kalmijn, 1981). The probability density function of θ is therefore coincident with the Von Mises-Fisher distribution.

$$\mathcal{F}(\theta,\varkappa) = \frac{\varkappa}{4\pi\sinh\varkappa}\exp(\varkappa\cos\theta) \tag{2.1}$$

with concentration parameter $\varkappa = mB/(k_BT) \geq 0$ and expectation $\langle\cos\theta\rangle = \mathcal{L}(\varkappa)$ where $\mathcal{L}(\varkappa) = \coth\varkappa - \varkappa^{-1}$ is the Langevin function. Assuming that flagella rotation has no effect on cell orientation, the mean alignment of swimming MTB in water is given by

$$\zeta \quad = \langle\cos\theta\rangle \quad = \mathcal{L}\left(\frac{mB}{k_BT}\right) \tag{2.2}$$

(Frankel and Blakemore, 1980).

Magnetic moment estimates from observation of swimming cells in rotating fields (Frankel and Blakemore, 1980; Petermann et al., 1989; Petersen et al., 1989), U-turns caused by a sudden field reversal (Esquivel and De Barros, 1986), and direct magnetic measurements of single cells (Dunin-Borkowski, 1998; Proksch et al., 1995), are affected by large uncertainties. Furthermore, the orientation model described above is derived from the Brownian motion of non-motile particles and does not consider possible effects related to

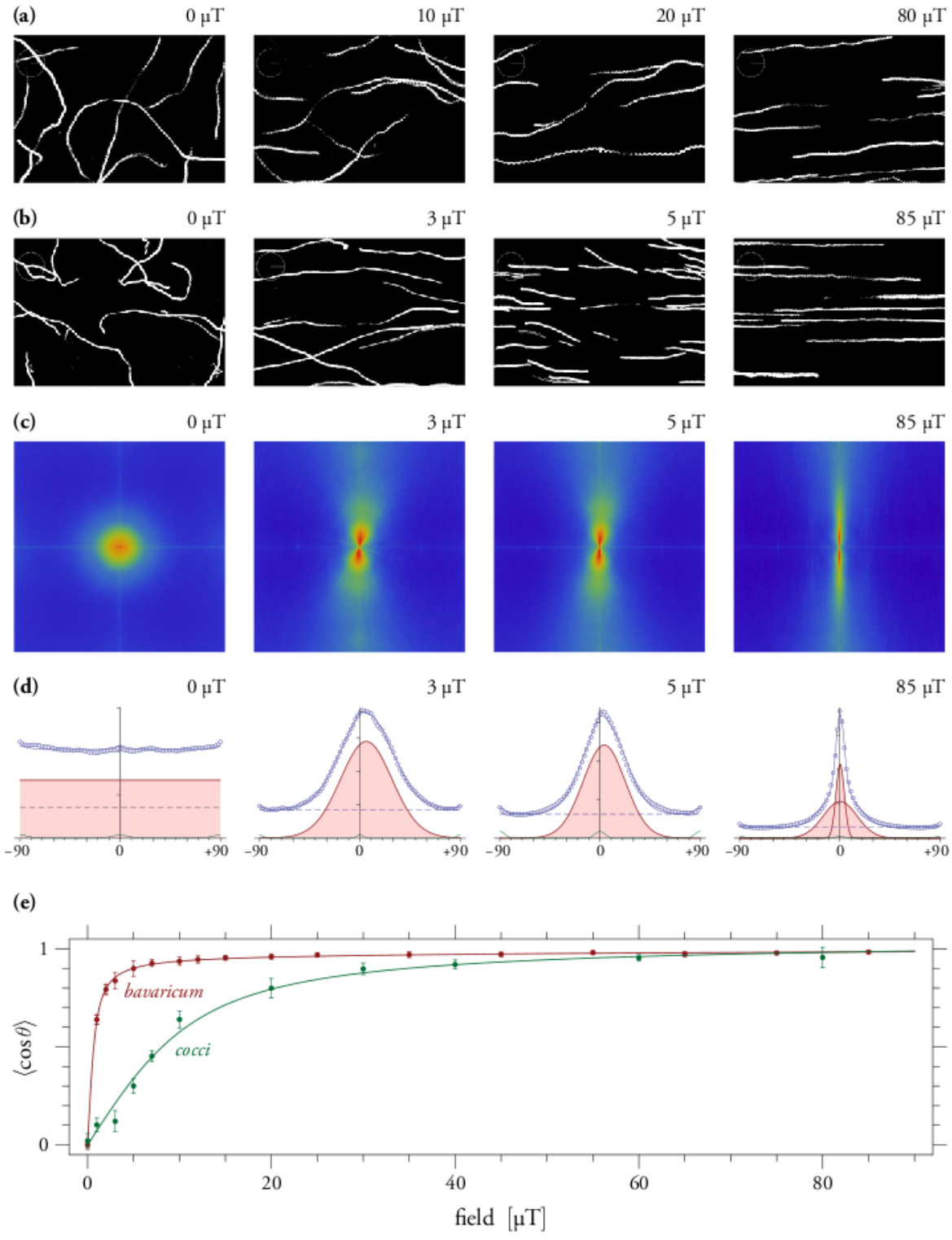
(a)
0 µT
10 µT
20 µT
80 µT
(b)
0 µT
3 µT
5 µT
85 µT
(c)
0 µT
3 µT
5 µT
85 µT
(d)
0 µT
3 µT
5 µT
85 µT
−90
0
+90
(e)
1
0
⟨cos θ⟩
bavaricum
cocci
0
20
40
60
80
field [µT]

cell propulsion. Rigorous verification of eq. (2.1-2.2) relies on direct tracking of swimming trajectories. A single study (Kalmijn, 1981), appears to confirm the validity of eq. (2.2) in >10 μT fields and no data are available in smaller fields. Therefore, we have systematically investigated the orientation of two wild-type bacteria (ovoid cocci and *M. bavaricum*) in precisely controlled fields of intensities comprised between 0 and 85 μT (Figure 2.2). The distribution of cell orientations empirically derived from large numbers of traces (section A.1) is in good agreement with eq. (2.1) (Figure 2.2d). Furthermore, the resulting mean alignments of both types of bacteria can be fitted by eq. (2.2) within experimental errors (Figure 2.2e). And the mean magnetic moments deduced from Langevin fits are slightly inconsistent with independent estimates obtained with the rotating field method and U-turn method (Table 2.1), which is likely because the latter two methods are associated to uncertain parameters (e.g. viscous drag and shape factor). Our result confirms that MTB alignment in water is controlled by Brownian motion and that self-propulsion effects are negligible. Furthermore, the two types of bacteria have very different alignment capabilities, due to the factor ∼13 difference in magnetic moment; in particular, *M. bavaricum* reaches 80% alignment in 2 μT (i.e. only ∼6% of the minimum geomagnetic field intensity).

Figure 2.2 ***(preceding page)*****:** Statistical analysis of MTB orientation in water in 0-85 μT fields. (a) Example of trajectories by ovoid cocci (white), as seen under the optical microscope in a horizontal field with indicated intensities. The wiggling trace in 20 μT is a typical feature of cocci, and results from the two-dimensional projection of helicoidal trajectories (Nogueiral and Barros, 1995). (b) Same as (a) for *M. bavaricum*. (c) Averaged Fourier amplitude spectra obtained from ∼100 trajectory images of *M. bavaricum* for each field intensity (color scale from zero in blue to maximum in red), reflecting the dominant texture (e.g. Redon et al., 1998) produced by cell orientation. (d) Angular distribution of the Fourier spectra in (c), obtained by integration over sectors (dots), which coincide with the distribution of trajectory angles, rotated by 90°(section A.1). The distributions are modelled with the sum of a constant background (dashed), and the theoretical function expected from straight trajectories produced by MTB with a Von Mises-fisher distribution of orientations (red line with shading). A single function was sufficient to fit all distributions, except for the one in 85 μT, where two functions have been used. A third contribution (green) is a spurious effect due to the rectangular image boundaries. (e) Mean alignment of ovoid cocci (green) and *M. bavaricum* (red) in 0-85 μT fields, derived from trajectory analysis as in (a-d). Lines are least-squares fit of data with eq. (2.2).

Table 2.1: Magnetic moments (in fAm^2) of *M. bavaricum* and ovoid cocci, determined with (1) a Langevin fit of mean swimming trace alignments (Figure 2.2), (2) rotating fields (Frankel and Blakemore, 1980), (3) U-turn, induced by instantaneous field reversing (Esquivel and De Barros, 1986), and (4) total magnetosome volume deduced from electron microscopy, multiplied by the spontaneous magnetization of magnetite.

Method	***M.bavaricum***	**Ovoid cocci**
(1) **Langevin**	11.7±0.28	0.86±0.28
(2) **Rotating field**	7.4±2.3	0.77±0.24
(3) **U-turn**	9.4±2.3	1.9±0.65
(4) **Electron microscopy**	14.4–36	4.8–9.6

2.4 Orientation of active MTB in sediment

The orientation of active MTB in unconsolidated sediment cannot be observed directly; however, it can be deduced from pulse field experiments where an appropriated sequence of magnetic pulses is applied to sediment containing an initial population of exclusively NS bacteria, as it is the case for our microcosms. The cell magnetic moment can be switched by a sufficiently strong and rapid pulse given at large angles (>90°) to the initial moment direction, causing the bacterium to swim in the opposite direction and become SS. If the same experiment is performed on a large number of bacteria with different orientations, the fraction of SS cells obtained after pulse application is a function of the original distribution of magnetic moment directions in sediment, and of the pulse field direction with respect to the field to which they are continuously exposed.

We begin our analysis with the simplest case of a single bacterium in water, whose magnetic moment $\mathbf{m}$ is fully aligned with an external field $\mathbf{H}_0$. A magnetic pulse $\mathbf{H}_p(t)$ is now applied at an angle ψ to $\mathbf{H}_0$, causing immediate rotation of $\mathbf{m}$ by an angle $\varepsilon(t)$ away from the chain axis, and delayed rotation of the whole cell by an angle $\beta(t)$ towards $\mathbf{H}_p$. Solutions of the equations governing $\beta(t)$ and $\varepsilon(t)$ (see section A.2) show that moment switching by a given $\mathbf{H}_p(t)$ occurs only for pulse field angles exceeding a critical value ψ_c>90°, which depends on the viscous drag that opposes cell rotation, on pulse intensity

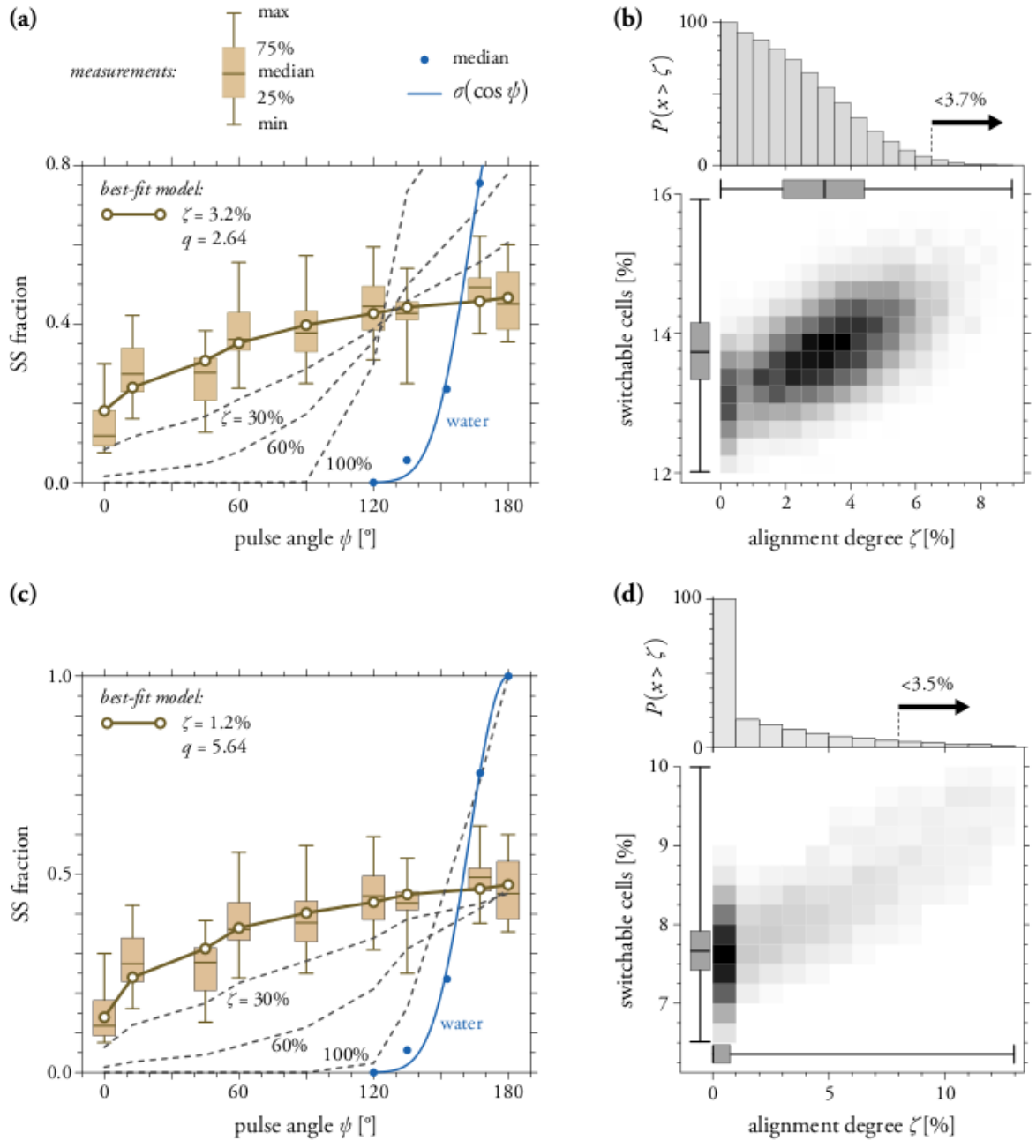
(a)
measurements:
max
75%
median
25%
min
median
σ(cos ψ)
best-fit model:
ζ = 3.2%
q = 2.64
ζ = 30%
60%
100%
water
SS fraction
pulse angle ψ [°]
(b)
P(x > ζ)
<3.7%
switchable cells [%]
alignment degree ζ [%]
(c)
best-fit model:
ζ = 1.2%
q = 5.64
ζ = 30%
60%
100%
water
SS fraction
pulse angle ψ [°]
(d)
P(x > ζ)
<3.5%
switchable cells [%]
alignment degree ζ [%]

and timing, and on the magnetic moment and anisotropy of the magnetosome chain. Because of natural statistical variations in cell size, shape, and magnetic moment, even a single MTB population (e.g. *M. bavaricum*) is characterized by a range of ψ_c-values comprised between 90°and 180°. Therefore, only a fraction $\sigma(\cos\psi)$ of bacteria is switched on average by a single pulse. This fraction has been determined experimentally for *M. bavaricum* in water (Figure 2.3), and is conveniently parametrized by $\sigma(x) = \mathcal{H}(-x)|x|^q$, where $\mathcal{H}$ is the Heaviside unit step function, and $q \approx 11$. The 20-180°range of pulse angles for which magnetic moments are switched is in good agreement with theoretical calculations (section A.2). The exponent q reflects the freedom of cells to rotate under the action of a pulsed field: 100% switching (i.e. $q \to 0$) applies to totally immobilized cells in sufficiently strong fields, while intermediate values are expected for MTB cells in sediment, where pore geometry limits free rotation. The total fraction of randomly oriented magnetic moments that can be switched by a single magnetic pulse is $1/(2q + 2)$ and is comprised between 50% for immobilized cells ($q \to 0$) and 4% for freely swimming cells ($q \approx 11$).

We now generalize the pulse field model described above to the case of sediment containing NS bacteria whose chain axes are represented by unit vectors $\mathbf{u} = (\sin\theta\cos\lambda, \sin\theta\sin\lambda, \cos\theta)$ where θ is the angle to the applied field $\mathbf{H}_0$, and $\mathcal{F}(\theta, \varkappa)$ the corresponding probability density function (eq. 2.1). If a single pulse is given along the unit vector $\mathbf{p}=(\sin\psi, 0, \cos\psi)$

Figure 2.3 *(preceding page)*: Estimates of *M. bavaricum* alignment in a 0.86 mT field with magnetic pulse experiments. (a,c) Fraction of SS bacteria created in sediment by a sequence of pulse fields imparted at angles of 0, 12.6, 45, 60, 90, 120, 135, 167.4, and 180°to the aligning field. SS fractions (brown box charts) have been measured after each pulse, and a 45°reset pulse was given before proceeding with the next pulse. Data obtained with 120, 135, 152.7, 167.4 and 180°pulses in water are shown for comparison (blue dots), along with best-fit (blue line, $q \approx 11$). Measurements in sediment (box charts) are compared with best-fit models (solid line with dots) calculated for MTB whose orientations has been assumed to be fixed during the whole experiment, regardless of magnetic moment switching (a), or has been assumed to equilibrate with the 0.86 mT field after each pulse (b). The models are based on a Von Mises-Fisher distribution $\mathcal{F}(\theta, \varkappa)$ generating a mean alignment $\zeta = \mathcal{L}(\varkappa)$, with a proportion σ of switchable cells for given angle between chain axis and magnetic pulse. Models obtained with much higher alignments (30%, 60%, and 100%, dashed lines) are shown for comparison. (b,d) Monte Carlo simulations of best-fit models obtained with a Poisson model of cell counts. Each chart shows the joint probability density of the model parameters (white = 0, black = maximum) expressed by the mean alignment ζ and the total fraction $1/(2q+2)$ of cells switched by a single pulse. The marginal distribution of ζ is plotted above each chart: ζ<7% with >95% probability in both cases.

, a fraction $\sigma(\mathbf{u}\cdot\mathbf{p})$ of bacteria with chain axes parallel to $\mathbf{u}$ will be switched and becomes SS. The statistical distributions of SS and NS moment directions after this pulse are given by

$$\begin{aligned} s(\theta,\lambda;\psi) &= \mathcal{F}(\theta,\varkappa)\sigma(\sin\theta\sin\psi\cos\lambda+\cos\theta\cos\psi) \\ n(\theta,\lambda;\psi) &= \mathcal{F}(\theta,\varkappa)[1-\sigma(\sin\theta\sin\psi\cos\lambda+\cos\theta\cos\psi)] \end{aligned} \tag{2.3}$$

respectively (section A.4). These distributions cannot be measured experimentally; however, the fractions $N(\psi)$ and $S(\psi)$ of NS and SS bacteria – given by integration of eq. (2.3) over the unit sphere – can be determined by counting NS and SS bacteria with the hanging drop assay. NS and SS counts after a single pulse are not sufficient for determining the parameters of $\mathcal{F}$ and σ . In order to obtain these parameters, which ultimately define the mean alignment of cells in sediment, a sequence of pulses has been applied at angles $\{\psi_0,\psi_1,\psi_2,\cdots\}$, where ψ_{2i}=45°represents a 'reset' pulse, and $\psi_{2i+1}=\psi_1,\psi_3,\cdots$ are distributed between 0 and 180°. The interpretation of cell counting results depends on whether individual cell orientations do not change between consecutive pulses (full correlation) or equilibrate with the applied field before the next pulse is given (lack of correlation). The case of full correlation is expected for MTB that are inactive inside the sediment, while complete lack of correlation represents the case of motile bacteria that could displace themselves between pulses. Not knowing the real conditions inside the sediment, expected NS and SS proportions for both cases have been calculated on the basis of eq. (2.3) (section A.4).

Results of experiments performed in a 0.86 mT constant field with pulses applied at 9 different directions, for a total of >13,000 cell counts, are shown in Figure 2.3. SS fractions obtained for each pulse direction are characterized by an increasing trend from S_1 ≈0.13 at ψ_1=0°to S_{18} ≈0.45 at ψ_{18}=180°. These values have been compared with models based on eq. (2.3) and a various combinations of alignment degrees (expressed by $\mathcal{L}(\varkappa)=\zeta$) and pulse field responses (expressed by the integral of $\sigma(x)=|x|^q$ over $-1\le x\le 0$ for given q). Best fit to the experimental data is obtained with ζ ≈3.2% for fixed orientations, and ζ ≈1.2% if full equilibrium after each pulse is assumed. In order to evaluate the significance of these results, a Monte Carlo approach has been used to create 10,000 simulations of the experimental data, on the basis of a Poisson model of cell count statistics (section A.4). Best-fit parameters ζ and q have been calculated for each simulation, obtaining 10,000 values of (ζ,q) that define an empirical probability distribution of the mean alignment ζ and the total fraction $1/(2q+2)$ of randomly oriented cells that can be switched by a single pulse (Figure 2.3b,d). This probability distribution gives an upper limit for ζ , with

Table 2.2: Magnetic properties of sediment used for NRM acquisition experiments (pressed dry powder and wet samples with 12 hours, 3 days, 4 days, and 14 days NRM acquisition time). C1 and C2 are CBD-treated wet sediment samples from which MTB and magnetosomes have been dissolved. NRM was acquired in a 47 μT field with 49°inclination. δ is the inclination shallowing, defined as the difference between field inclination and NRM inclination after 50 mT AF demagnetization. ARM was acquired in a 100 μT DC field, and IRM in a 0.2 T field. S is the ratio between IRM and saturation IRM (acquired in a 1 T field). χ_a is the ARM susceptibility, and χ_n is the NRM susceptibility, calculated as NRM divided by the field in which it was acquired. LC, BS, and BH are the low-coercivity component and two components attributed to magnetofossils, respectively, as obtained from coercivity analysis of ARM and IRM AF demagnetization curves (Figure 2.4).

Sample	Time	δ	NRM μAm^2/kg	ARM μAm^2/kg	IRM mAm^2/kg	S	χ_a/M_{rs} mm/A	χ_n/M_{rs} mm/A	χ_n/χ_a
Powder	–	–	–	226	1.45	–	1.962	–	–
LC				*11.20%*	*37.70%*		*0.584*		
BS				*59.20%*	*47.70%*		*2.437*		
BH				*29.60%*	*14.60%*		*3.966*		
A3	12 h	∼0°	26	112	1.17	0.965	1.204	0.593	0.493
B2	3 d	∼10°	26	120	1.25	0.937	1.211	0.557	0.46
B3	4 d	∼10°	11.9	149	1.3	0.954	1.438	0.244	0.17
B4	14 d	∼5°	11.1	155	1.64	0.949	1.189	0.181	0.152
B5	14 d	∼5°	14.7	200	1.71	0.954	1.473	0.23	0.156
F	14 d	–	–	–	–	–	–	0.208	–
C1	*12 h*	*∼0°*	*2.17*	*9.37*	*0.26*	*0.845*	*0.452*	*0.222*	*0.492*
C2	*12 h*	–	–	*15.6*	*0.376*	*0.851*	*0.522*	–	–

$\zeta \leq 7\%$ at 95% confidence level. On the other hand, inferences about the degree of MTB motility inside the sediment are not possible, since limit assumptions about the correlation of individual cell orientations between consecutive pulses produced equally good fits to experimental data. Overall, our experiments show that living MTB cells in sediment are very poorly aligned by geomagnetic fields, unlike the case of freely swimming cells in water.

2.5 DRM acquisition experiments

In order to verify that magnetofossils represent the mean remanence carriers in our DRM experiments, we performed coercivity analysis of detailed AF demagnetization curves of ARM and IRM (Egli, 2003). Results (Figure 2.4) confirm the presence of two magnetic components with coercivity distributions and ratios χ_a/M_{rs} between ARM susceptibility

and (section A.3 and Table 2.2) typical of magnetofossils (Egli, 2004a; Ludwig et al., 2013). These components contribute to ∼89% of the bulk ARM and ∼62% of the bulk IRM, respectively. The presence of SD magnetite as dominant remanence carrier is confirmed by selective chemical dissolution experiments, where ∼92% of ARM and ∼78% of IRM is lost in CBD-treated sediment. The ratio between IRMs acquired in 0.2 and 1 T, respectively, is >0.93, and thermomagnetic measurements (not shown) indicate a Curie temperature of ∼580°C. Therefore, we conclude that remanence carriers are SD magnetites, mostly in form of intact magnetosome chains. Average cell counts in samples taken at the time of DRM acquisition experiments amounted to 40-100 cells/μl for *M. bavaricum* and for cocci. Using the magnetic moments reported in Table 2.1 and assuming random orientations, the estimated contribution of living MTB to M_{rs} amounts to 0.4-1μAm^2/kg, compared to ∼1.4 mAm^2/kg for bulk M_{rs} measurements (Table 2.2). With these results we conclude that living cells provide a negligible contribution to the total magnetization; therefore, almost all magnetosome chains are expected to occur inside non-motile (dead) MTB or to be freely dispersed in sediment after cell dissolution (i.e. magnetofossils).

DRM acquisition experiments have been conducted in ∼47 μT fields with ∼50°inclination and acquisition times of 0.5, 3, 4, and 14 days (Table 2.2). In all cases, except for CBD-treated sediment samples, NRM directions are consistent with the applied field (Figure 2.4e-f). Zijderveld plots of MTB-bearing sediments with 12 h acquisition time display a single direction that is fully demagnetized in ∼80 mT. Sediments with intermediate acquisition times (3-4 days) are characterized by slightly curved inclination trends, with expected inclination values in the 0-20 mT range, and up to 10°shallowing between 50 and 80 mT. This shallowing is consistent with observed sample contraction over the first few days. After 14 days, inclination shallowing decreases to 5°. CBD-treated samples acquire a ∼10 times smaller NRM. The resulting small magnetic moments (∼1-10 nAm^2) are close to measurement noise level; nevertheless, directions compatible with the applied field are recognizable in sample C1. Overall, NRM intensities are correlated with porosity: the acquisition efficiency, expressed by the ratio χ_n/M_{rs} between NRM susceptibility and M_{rs} , decreases from ∼0.58 mm/A for ϕ ≈0.88 to ∼0.2 mm/A for ϕ ≈0.68 . A similar trend is observed if NRM susceptibility (= NRM/H) is normalized by ARM susceptibility (Table 2.2). Analogous results have been obtained with gelled DRM experiments (Carter-Stiglitz et al., 2006).

The evolution of DRM upon sediment compaction is exemplified by the three acquisition stages (0.5, 3-4 and 14 days) shown in Figure 2.5. NRM demagnetization curves

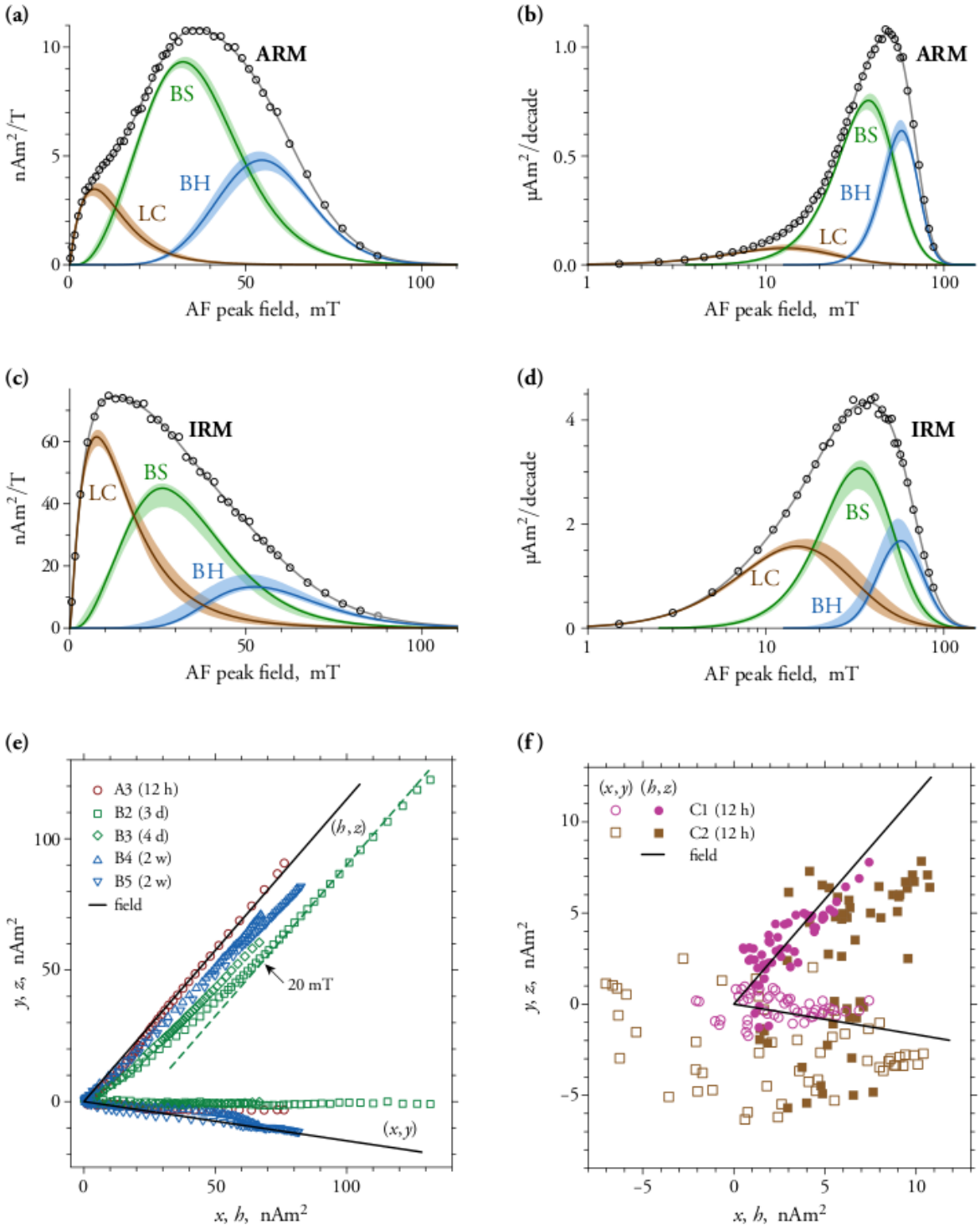
(a)
ARM
BS
BH
LC
nAm²/T
AF peak field, mT
(b)
ARM
BS
BH
LC
μAm²/decade
AF peak field, mT
(c)
IRM
LC
BS
BH
nAm²/T
AF peak field, mT
(d)
IRM
BS
LC
BH
μAm²/decade
AF peak field, mT
(e)
A3 (12 h)
B2 (3 d)
B3 (4 d)
B4 (2 w)
B5 (2 w)
field
(h,z)
20 mT
(x,y)
y, z, nAm²
x, h, nAm²
(f)
(x,y) (h,z)
C1 (12 h)
C2 (12 h)
field
y, z, nAm²
x, h, nAm²

can be expressed as the sum of two end-members, which are proportional to (1) the AF demagnetization of ARM, as measured in dry sediment, and (2) an exponential curve with ∼12 mT median destructive field, respectively. The two end-members are particularly well distinguishable after 3-4 days, and the relative contribution of the exponential one decreases monotonically with increasing acquisition times, almost disappearing after 14 days. On the other hand, wet sediment AF demagnetization curves of ARM and IRM, obtained immediately after NRM demagnetization, are similar to the corresponding counterparts measured on dry sediment. While χ_n/M_{rs} decreases by ∼50% during the first 4 days, the relative contribution of the ARM-like end-member to total NRM increases steadily, reaching 95% after 14 days (Figure 2.5c). The transitional nature of the exponential end-member excludes the possibility that it originates from magnetic particles with large NRM/ARM ratios, leaving us with the hypothesis that it is related to mechanical unblocking.

In order to verify this hypothesis, acquisition experiments were modified by introducing a sudden change in magnetic field direction after a given time t_1 . For example, 14 days total acquisition time with t_1=52 hours produced the same two NRM components of Figure 2.5, each pointing to a different direction (Figure 2.6a,b). Preservation of the 'exponential' component in these experiments is due to sample sealing at t_1, which prevents further water losses. Coercivity analysis of the full NRM vector (section A.3) was used to isolate the directions of the two NRM components (Figure 2.6c), whereby the curvature of Zijderveld plots is entirely caused by the overlapping range of unblocking fields. The directions of the exponential component coincides with the field applied after t_1 , while the ARM-like component remains closer to the initial field direction. These results can be

Figure 2.4 ***(preceding page)*:** Coercivity analysis of detailed AF demagnetization curves of ARM (a-b) and IRM (c-d) for powdered sediment. Coercivity distributions (dots) are shown on a linear field scale ($\Delta M/\Delta H$, left) and on a logarithmic field scale ($H \ln 10 \times \Delta M/\Delta H$, right). They have been fitted with a linear combination of skewed Gaussian functions representing three magnetic components (solid lines) labeled as LC (low-coercivity), BS (biogenic soft), and BH (biogenic hard). The shaded band around curves represents a confidence interval derived from 25% and 75% quantiles of solutions obtained from 5000 Monte Carlo simulations of measurement errors. The solid gray line is the modelled coercivity distribution obtained from the sum of the three components. (e-f) Zijderveld diagrams obtained from AF demagnetization of NRM (symbols) for MTB-bearing sediments (e) and CBD-treated sediments in which MTB and magnetosomes have been dissolved (f). Solid black lines are projections of the applied field on the (x, y)-plane and the (h, z) -plane, with $h = (x^2 + y^2)^{1/2}$ being the horizontal component.

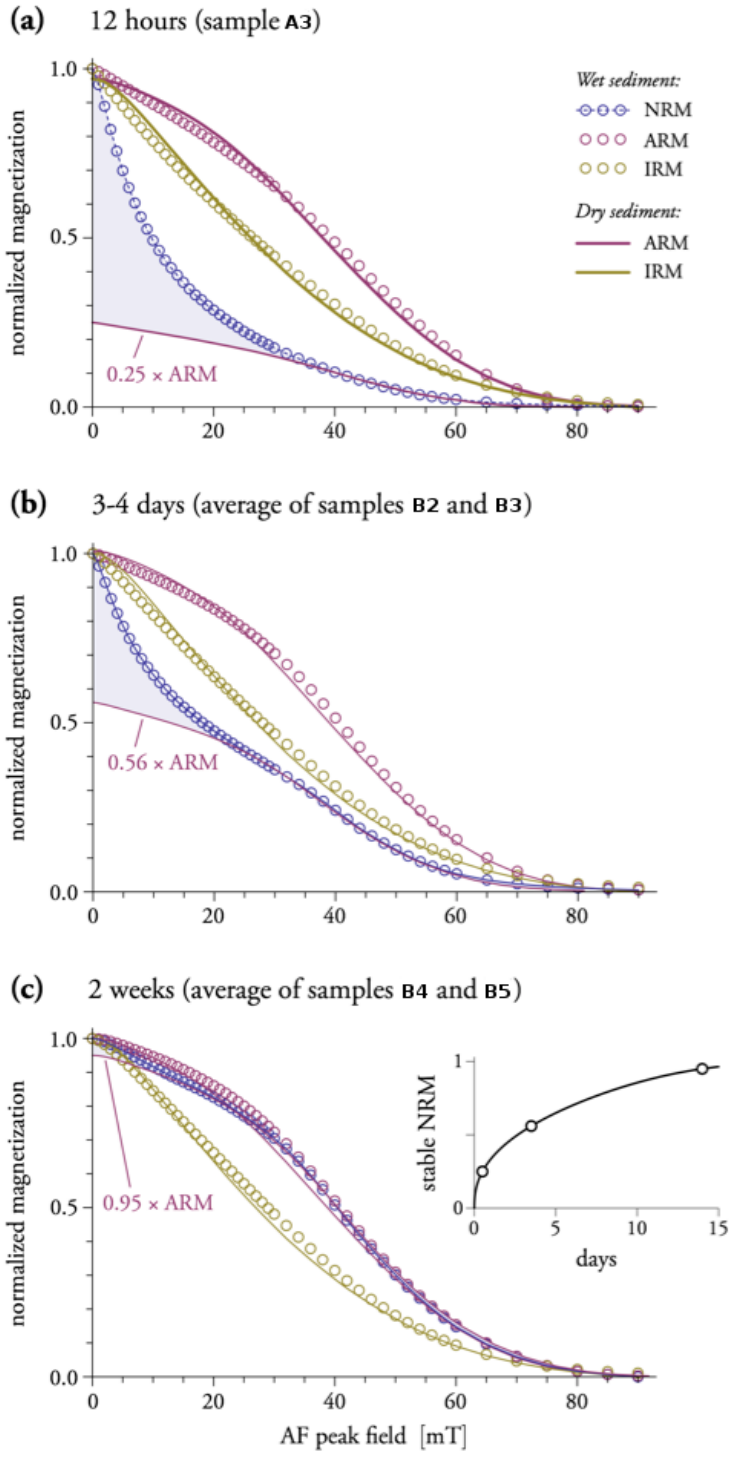
(a) 12 hours (sample A3)
normalized magnetization
1.0
0.5
0.0
0
20
40
60
80
Wet sediment:
NRM
ARM
IRM
Dry sediment:
ARM
IRM
0.25 × ARM
(b) 3-4 days (average of samples B2 and B3)
normalized magnetization
0.56 × ARM
(c) 2 weeks (average of samples B4 and B5)
normalized magnetization
0.95 × ARM
stable NRM
1
0
0
5
10
15
days
AF peak field [mT]

explained by faster equilibration of loosely bounded magnetization carriers contributing to the exponential component.

Finally, DRM acquisition experiments performed in 0.4-158 μT fields during 14 days (Figure 2.6d) confirm the linearity of DRM over this range of field intensities, with proportionality constant χ_n/M_{rs}=0.208 mm/A . Using $\chi_n/M_{rs} \approx 2\zeta/H$ for weakly aligned SD particles (section A.5), we obtain a mean alignment $\zeta \approx 8 \times 10^{-5}\mu_0 H[\mu\text{T}]$ of magnetofossil chains in sediment with ∼68% porosity.

2.6 Discussion

2.6.1 Magnetotaxis

The displacement of MTB is described in mathematical terms by a biased random walk, whose efficiency is quantified by the mean alignment $\zeta = \langle \cos\theta \rangle$. Generally, cell alignment can be considered 'good' if ζ>0.8 (Frankel, 1984): in water, this condition is verified if $mB > 5k_BT$(eq.2.2). Given B>35μT for the geomagnetic field, a magnetic moment of ∼0.6 fAm^2 is required for efficient magnetotaxis in water, independently of cell size. For comparison, observed magnetic moments are up to 100 times larger and positively correlated with cell volume (Figure 2.7c). This correlation holds regardless of MTB morphology (e.g. spherical, elongated, multicellular) and geomagnetic field intensity or inclination (i.e. Equator vs. mid latitudes). Therefore, simple considerations about MTB alignment in water cannot explain the observed magnetic moments. A more elaborated magnetotaxis model (Esquivel and De Barros, 1986) considers the possibility of collisions between MTB and suspended particles in water, introducing a new perturbation source (Figure 2.7a). Detailed statistical analysis of this model (section A.6) shows that the mean cell alignment is still formally described by eq. (2.2), as for Brownian motion, if the thermal perturbation

Figure 2.5 ***(preceding page)*:** Detailed stepwise AF demagnetization of NRM, ARM, and 0.2 T-IRM (dots) for NRM acquisition times of (a) 12 hours, (b) 3-4 days, and (c) 14 days in a 47 μT field with ∼50°inclination. All curves are normalized with the initial values of NRM, ARM, and IRM, respectively. AF demagnetization curves of ARM and IRM are similar to their counterparts measured on pressed powders of dried sediment (solid lines). AF demagnetization curves of NRM can be modelled as linear combination of ARM data (solid line) and an exponential function (dashed area). The relative contribution of the NRM component with ARM-like properties increases monotonically with increasing acquisition time (insert in c).

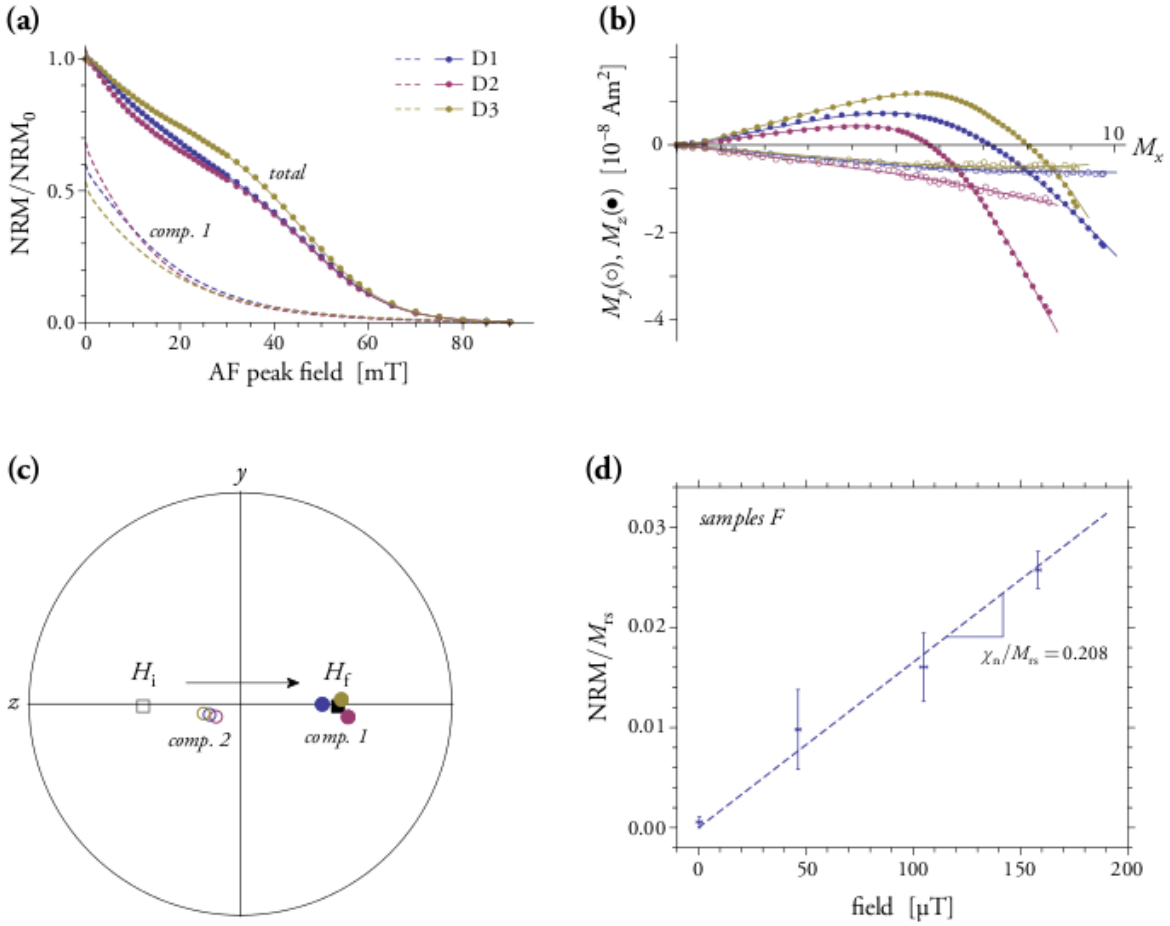

Figure 2.6: AF demagnetization curves (a) and Zijderveld diagram (b) of NRM acquired during 14 days by samples D1-D3 in a 46 μT field with 52°inclination. The samples have been sealed and turned upside down after 52 hours. The full NRM vector after each AF step has been fitted with a linear combination of two coercivity components similar to those identified in Figure 2.5. The AF demagnetization curves of component 1 are shown in (a) as dashed lines. A fixed direction has been assumed for each component. The curved trends of the Zijderveld diagram (dots) are perfectly reproduced by the model (solid lines) and can be explained by the overlapping coercivity ranges of the two components. (c) Stereographic plot of field directions before (H_i) and after (H_f) turning the samples upside down, expressed in sample coordinates, and directions of the two NRM components. (d) NRM acquired during 14 days in 0.4, 46, 105, and 158 μT fields with ∼50°inclination.

energy k_BT is replaced by the energy $E_c = (36\pi)^{1/3}\eta v_0 \phi_s V^{2/3}$ of collisions in environments with constant volume density ϕ_s of suspended particles, and by $E_c = 4\eta V v_c$ for environments with constant collision rates v_c, with η being the dynamic viscosity of water, V the cell volume, and v_0 the MTB swimming velocity. This model reproduces the observed correlation between m and V (Figure 2.7c). However, the condition $mB = 5E_c$ for 'good' alignment in B=50 μT is fulfilled by v_c ≈15 Hz and ϕ_s ≈0.8%, respectively, which appear to be vastly excessive for aquatic environments where MTB populations have been observed (Kim et al., 2005; Simmons et al., 2004). Such conditions, on the other hand, could be encountered at the sediment/water interface.

Assessment of magnetotactic effectiveness changes radically for MTB populations living in sediment. In this case, alignment in geomagnetic fields is small, probably of the order of ∼1%. A useful term of comparison for passive MTB displacement in sediment is the diffusion of Brownian particles in porous media (Kluijtmans and Philipse, 1999), where the role of Brownian motion is taken by bioturbation. Bioturbation can be modelled as a solid diffusion process characterized by a diffusion coefficient D_{bt} (Meysman et al., 2005). Estimates of D_{bt} are comprised between 0.003-0.03 cm^2/yr for pelagic sediments (Berner, 1980) and 0.1-100 cm^2/yr on the continental shelf (Mulsow et al., 1998; Solan et al., 2004). MTB alignment is affected by changes in the microscopic structure of sediment, due to a rearrangement of particle contacts. Once the shear strength is overcome, a certain work E_{bt} is performed in order to rearrange individual particles surrounding MTB cells (Figure 2.7b): this work can be understood as a randomizing energy equivalent to that of Brownian motion, so that eq. (2.2) remains valid if k_BT is replaced by E_{bt}. Estimates of E_{bt} can be obtained by modeling sediment as a colloidal hard-sphere dispersion with low-shear viscosity η_{ls} (Cheng et al., 2002). Using $6D_{bt}/d_s$ as the diffusion velocity of particles with size d_s, the work required to displace one of them by the size of a MTB cell with volume V in a medium with viscosity η_{ls}, is

$$E_{bt} = 18\pi \frac{D_{bt}\eta_{ls}}{d_s} \left[\frac{6V}{\pi}\right]^{2/3} \tag{2.4}$$

(section A.6). If E_{bt} replaces k_BT in eq. (2.2), the observed correlation between cell volumes and magnetic moments is obtained with 1% mean alignment in 35 μT and realistic values of D_{bt}, η_{ls} and d_s (Figure 2.7c).

Magnetotactic effectiveness must be evaluated by asking whether a certain mean alignment (i.e. ζ ≈0.01) is sufficient for supporting sufficiently fast displacements across the

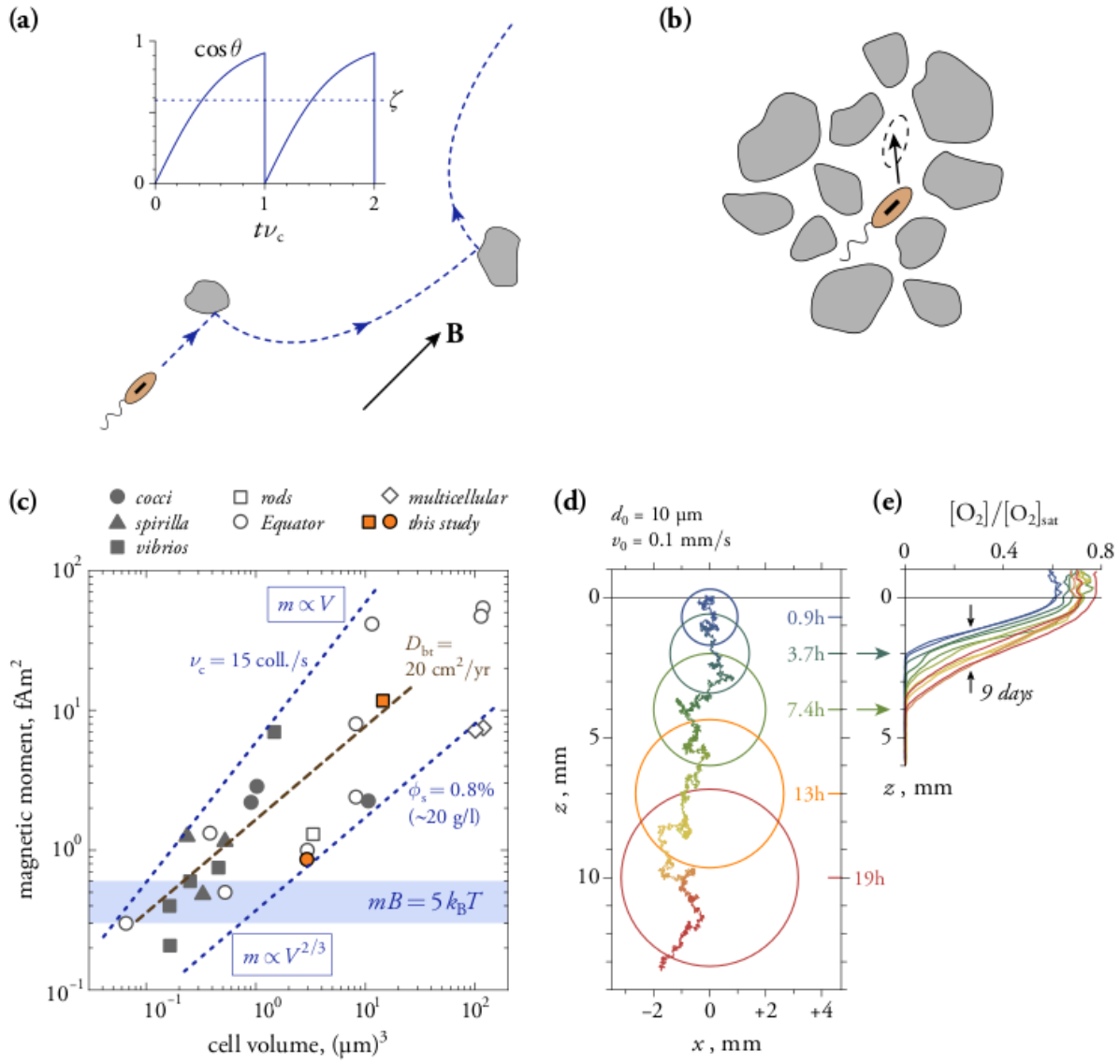
(a)
cos θ
ζ
1
0
0
1
2
tν_c
B
(b)
(c)
cocci
spirilla
vibrios
rods
Equator
multicellular
this study
m ∝ V
ν_c = 15 coll./s
D_bt = 20 cm²/yr
φ_s = 0.8% (~20 g/l)
mB = 5 k_B T
m ∝ V^2/3
magnetic moment, fAm²
cell volume, (μm)³
(d)
d_0 = 10 μm
v_0 = 0.1 mm/s
0.9h
3.7h
7.4h
13h
19h
z , mm
x , mm
(e)
[O_2]/[O_2]_sat
9 days
z , mm

typical thickness of chemical gradients. For this purpose, we model MTB displacement in terms of a biased random walk consisting of a sequence of microscopic segments $\mathbf{r}_i = d_s\mathbf{u}_i$, where d_s is the mean free path length (Wheatcroft et al., 1990), which might be identified with typical sediment particle sizes, and $\mathbf{u}_i$ are unit vectors described by $\mathcal{F}(\theta, \varkappa)$ (eq.2.1) with $\varkappa = 3\zeta \approx 0.03$. If v_p is the effective forward swimming velocity inside pores, and γ the fraction of total time spent in successful microscopic displacements, the total displacement $\mathbf{r}(t) = (X, Y, Z)$ after time t in a vertical field is statistically given by the expectations:

$$\begin{aligned} \langle X(t)\rangle = \langle Y(t)\rangle &= 0 \\ \langle Z(t)\rangle &= \gamma v_p \zeta t \end{aligned} \tag{2.5}$$

and variances

$$\langle X^2(t)\rangle = \langle Y^2(t)\rangle = \langle Z^2(t) - \langle Z(t)\rangle\rangle = 2D_{mt}t, \tag{2.6}$$

where $D_{mt} = (1-\zeta)^2\gamma v_p d_0/2$ is an equivalent diffusion constant (Berg, 1993) that describes

Figure 2.7 *(preceding page)*: Evaluation of magnetotaxis models. (a) Collision model in water. Collisions produce sudden deviations of the swimming path, followed by progressive realignment in the magnetic field . The graphics shows the instantaneous alignment (solid line) after two collisions, and its average over time (dashed line). (b) Biodiffusion model in sediment. Solid diffusion forces the rearrangement of sediment particles, including MTB (arrow), requiring a certain energy that acts as randomizing force against alignment in the geomagnetic field. (c) MTB magnetic moment vs. cell volume (data from this study and Dunin-Borkowski (1998),Erglis et al. (2007),Esquivel and De Barros (1986), Hanzlik (1999), Lins et al. (2005),Meldrum et al. (1993),Nogueiral and Barros (1995), Proksch et al. (1995), Winklhofer et al. (2007)). Conditions for 80% mean alignment in typical geomagnetic fields are shown for Brownian motion (horizontal, shaded band), and for aquatic environments (dotted lines) where collisions with suspended particles occur at a fixed rate ($m \propto V$ with v_c=15 collisions/s) or with a fixed volume concentration of suspended material ($m \propto V^{2/3}$ with ϕ_s=0.8% , corresponding to ∼20g/l of sediment material with a density of 2.7 g/cm^3). The dashed line shows conditions for 1% mean alignment in 35 μT in sediment with D_{bt}=20 cm^2/yr, d_s=10 μm, and η_{ls}=3.5 mPa$\cdot$s for a hard sphere colloidal dispersion with 70% porosity after Cheng et al. (2002). (d) Mathematical simulation of a biased random walk (line) for a bacterium with velocity v_0=0.1 mm/s in sediment with grain size d_s=10 μm, exposed to a vertical field that gives a 1% mean alignment (see text for additional model parameters). Circles indicate the expectation (centres) and standard deviations (radii) of cell position at given times. (e) Oxygen concentrations profiles measured in our microcosms (lines), as function of sediment depth and time after microcosm preparation (color code from blue = day 1 to red = day 9).

the random component of the displacement of a large number of cells. The systematic component of displacement, on the other hand, is equivalent to an advective flow with velocity $\gamma v_p \zeta$ along the magnetic field. The velocity of MTB inside pores is reduced with respect to the velocity v_0 in pure water by hydrodynamic friction between cell and pore walls. Experiments on confined Brownian motion between plates yield v_p/v_0 ≈0.3 for latex spheres very close to a glass wall (Faucheux and Libchaber, 1994): this value can be considered as a lower limit for the motion of cells in sediment pores. On the other hand, γ is controlled by the unavailable fraction of pore volumes. Diffusion models of Kim and Torquato (1992) give $\gamma \approx [1-(1-\phi)(1+\beta)^3]^{1.36}$, where ϕ is the sediment porosity and β the ratio between the sizes of cells and sediment particles, respectively. Using ϕ ≈0.8 for superficial sediment (Berner, 1980), and assuming β=1/4 for 2.5 μm cells in sediment with d_s=10 μm, we obtain γ ≈0.5. Typical swimming velocities v_0=0.1 mm/s of wild-type cocci in water (Hanzlik, 1999), along with v_p/v_0 ≈0.3 , yield D_{mt} ≈23 cm^2/yr. An example of random walk generated with these parameters is shown in Figure 2.7d. The additional contribution of solid biodiffusion to the random component of displacement is accounted by replacing D_{mt} in eq. (2.6) with D_{mt}+D_{bt}.

Magnetotaxis is the dominant component of displacement over lengths and times larger than critical values that satisfy $\langle Z^2(t)\rangle = \langle Z(t)\rangle^2$, i.e.:

$$\begin{aligned} L_c &= d_s \frac{(1-\zeta)^2}{\zeta}[1+\frac{D_{bt}}{D_{mt}}] \\ t_c &= \frac{d_s}{v_p}[\frac{1-\zeta}{\zeta}]^2[1+\frac{D_{bt}}{\gamma D_{mt}}] \end{aligned} \tag{2.7}$$

In the example of Figure 2.7d (D_{bt}= 0,γ=1), L_c ≈1 mm and t_c ≈1 hour. For comparison, the thickness of the dissolved oxygen gradient was 2 mm in newly prepared microcosms, and slowly increased to 4 mm within ∼9 days, probably because of a reduction of the respiration rate as organic matter is consumed (Figure 2.7e). Similar oxygen gradients have been observed in sediment from different freshwater microcosms (Flies et al., 2005a), while thicker gradients (5-30 mm) are characteristic of deep-sea sediments hosting living MTB communities (Petermann and Bleil, 1993). In all cases, magnetotaxis appear to dominate over typical oxic-anoxic interface (OAI) thickness. The time required to cross the OAI by actively swimming bacteria with characteristics taken from the above example is comprised between 3 and 8 hours. ATP storage in MTB cells (Blakemore, 1982) can be used to estimate how long it takes for a cell to consume its energy reserves by continuous swimming. Considering the efficiency of flagella propulsion (Purcell, 1997), and using

v_0=0.1 mm/s we obtain ∼22 hours (section A.6), which appear to be sufficient for crossing the OAI, even by assuming that only 50% of energy reserves are available for this purpose.

2.6.2 DRM acquisition by MTB

For the purpose of understanding DRM acquisition, the sediment column can be divided into a top, so-called mixed layer where sediment is thoroughly mixed by living organisms (bioturbation), overlaid to the historical layer where no mixing occurs (Katari and Tauxe, 2000) (Figure 2.8). The thickness L of the mixed layer is independent of sedimentation rate and is proportional to the organic carbon flux to the sediment, with values comprised between 2 and 10 cm (Trauth et al., 1997). Two important parameters describe the fate of a sediment particle in the mixed layer: these are the diffusive transport time $t_D = L^2/D_{bt}$ (i.e. the time required to cross the mixed layer by diffusion), and the residence time $t_s = L/s$ (i.e. the time required to reach the historical layer with given sedimentation rate s). The ratio $t_D/t_s = sL/D_{bt}$ is usually <1, implying that particles in the mixing layer – as suggested by its name – are thoroughly mixed before entering the historical layer. Solid diffusion produces a microstructural rearrangement of sediment particles upon braking of inter-grain forces with two important consequences, i.e. (1) the abatement of shear strength as consequence of thixotropy (Barnes, 1997), and (2) continuous reorientation of sediment grains. The latter means that magnetic moments associated with individual DRM carriers are expected to be in dynamic equilibrium with the geomagnetic field H over a timescale t_D – as long as they reside in the mixing layer. This equilibrium is quantified by the 'alignment susceptibility' $Q = 2\zeta(H)/H$, where ζ is the mean alignment of magnetic moments in the geomagnetic field H , so that NRM=QM_rsH is obtained for SD carriers of DRM. DRM experiments with gelatin-stabilized sediment have been used to show that Q is positively correlated with sediment porosity for ϕ<0.86 , and constant above this critical value (Carter-Stiglitz et al., 2006) (Figure 2.8e). The critical porosity $\phi \approx$0.86 is close to the percolation threshold of jammed spheres, i.e. the volume concentration of randomly packed spheres for which a macroscopic network of contact points develops (Powell, 1979), testifying the importance of mechanical interactions between sediment particles in regulating DRM intensity.

Physical DRM models are based on dynamic equations that describe the rotation of magnetic particles under the combined action of (1) a magnetic torque, (2) randomizing forces, and (3) elastic or viscous forces. DRM acquisition by settling in water or diluted slurries has been modeled as equilibrium between (1) and (2), with randomizing forces

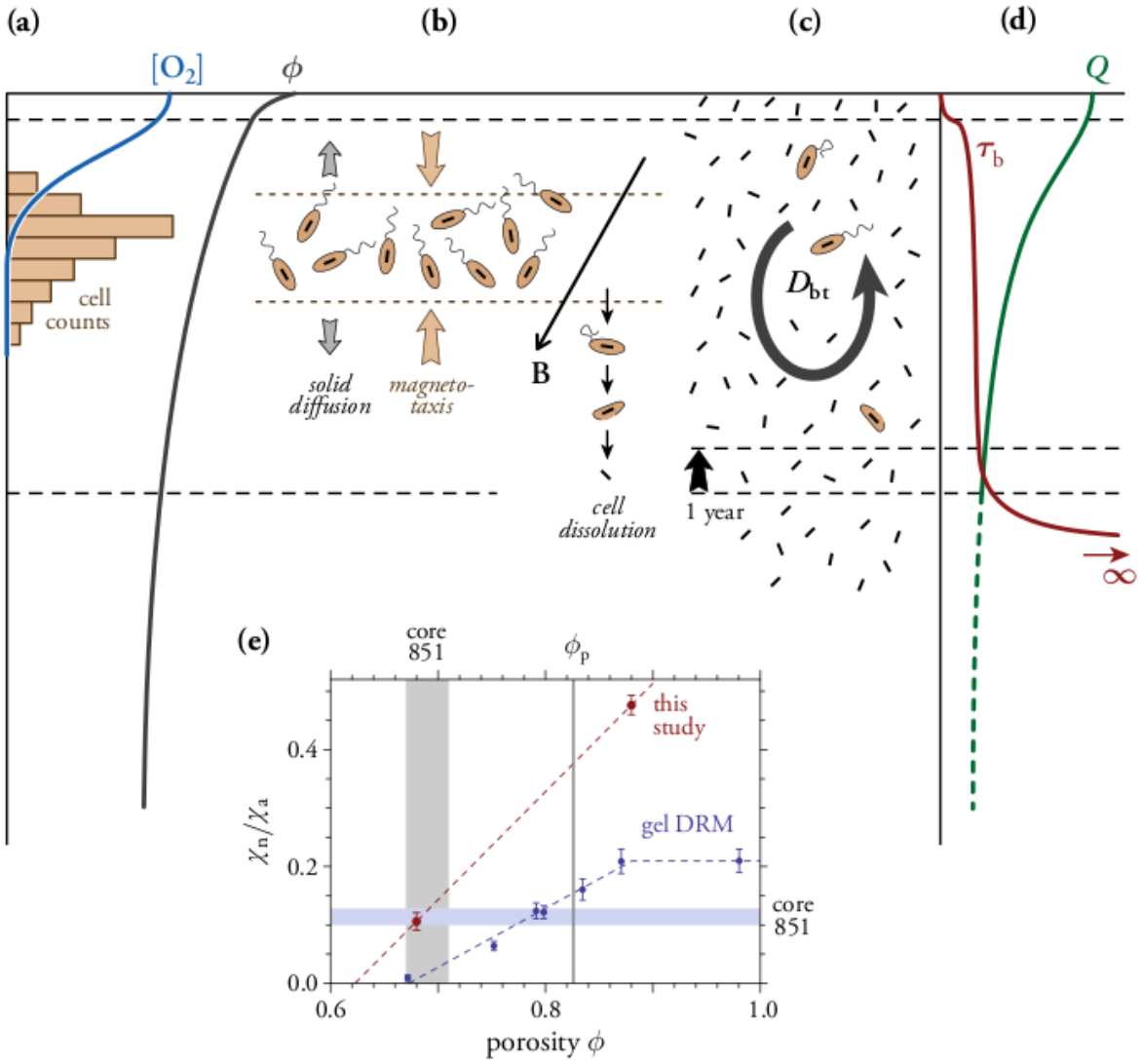
(a)
(b)
(c)
(d)
[O2]
ϕ
Q
cell
counts
solid
diffusion
magneto-
taxis
B
cell
dissolution
Dbt
1 year
τb
∞
(e)
core
851
ϕp
this
study
gel DRM
core
851
χn/χa
0.0
0.2
0.4
0.6
0.8
1.0
porosity ϕ

being represented by Brownian perturbations of energy k_BT(Tauxe et al., 2006). On the other, hand, DRM acquisition in sediment has been linked to (1) and (3) through the yield strength, which determines the possibility of acquiring a DRM, and Bingham viscosity, which regulates the time constant τ_b of particle rotation (Shcherbakov and Shcherbakova, 1987). In this model, DRM acquisition relies on irreversible displacement of contact points between sediment particles. The required breakage of sediment microstructure is thereby attributed to magnetic forces alone; however, bioturbation is an additional source of continuous microstructural rearrangements, during which magnetic torques can produce a directional bias. Therefore, an inverse correlation is expected between the time constant τ_b of DRM on one hand, and bioturbation intensity, expressed by the solid diffusion constant D_{bt} , on the other hand. Actual values of $\tau_b < t_D$ in the mixed layer are difficult to estimate: Katari and Tauxe (2000) did not observe a significant change of NRM direction in the top 0.5-4 cm of marine sediment exposed to a different field direction for 3 weeks, concluding that mixed layer DRM is stable (i.e. not at equilibrium with the field), except for the top-

Figure 2.8 ***(preceding page)*:** Magnetofossil DRM acquisition model. (a) Typified sediment profile with dissolved oxygen concentration [O_2], MTB cell counts, and sediment porosity ϕ. The upper and lower dashed lines delimit the sediment-water interface affected by resuspension, and the lower limit of the mixed layer, below which the historical layer begins. (b) Living MTB maintain themselves within the oxic-anoxic interface (dashed lines) counteracting solid diffusion caused by bioturbation by magnetotaxis in the geomagnetic field $\mathbf{B}$. Dead bacteria diffuse in the mixed layer and cell material is eventually dissolved before incorporation of the fossil chain in the historical layer after a relatively long residence time of 10-100 years. (c) Concentration of living MTB is negligible with respect to magnetofossils. Magnetofossils are accumulated during their residence time in the mixed layer and redistributed by bioturbation, which is quantified by the solid diffusion constant D_{bt}. The lower boundary of the mixed layer, as well as the sediment-water interface, raise with time, so that a thin layer of magnetofossils is incorporated in the historical layer every year. (d) Expected profiles of the 'alignment susceptibility' Q , i.e. the magnetofossil mean alignment normalized by field intensity, and of the typical time τ_b required to reach a dynamic equilibrium with the geomagnetic field. Divergence of τ_b is expected in the historical layer because of thixotropic increase of the shear strength of undisturbed sediment. (e) DRM intensity, normalized by ARM acquired in the same DC field (χ_n/χ_a), vs. sediment porosity ϕ. Data for gelatin experiments with material from ODP core 851 (blue dots) is redrawn from Carter-Stiglitz et al. (2006), after conversion of sediment weight fraction into porosity assuming a density of 2.71 g/cm^3 for calcium carbonate particles. Typical porosity (vertical gray band) and χ_n/χ_a (horizontal light blue band) of the topmost meter of core 851 are from Lyle et al. (1995) and Meynadier et al. (1995), respectively. ϕ_p is the percolation threshold of hard spheres after Powell (1979).

most 0.5 cm affected by resuspension. In our experiments, on the other hand, we observed an evident change of NRM direction over 14 days. The apparent incompatibility between these results might be reconciled by assuming different equilibration times reflecting D_{bt} . Furthermore, thixotropic effects induced by our sample preparation method, by which sediment was thoroughly stirred, cannot be excluded. Nevertheless, the assumption of complete sediment mixing, which is also part of the Katari and Tauxe (2000) DRM model, is hardly compatible with the maintenance of an out-of-equilibrium NRM over the long residence time (10-1000 years) of sediment particles in the mixed layer.

Magnetofossil DRM starts with active MTB occurring at the oxic-anoxic interface (OAI) (Figure 2.8a). Although active MTB populations have been observed in the water column of eutrophic environments (e.g. Kim et al., 2005; Simmons et al., 2004), sediment is the natural living environment of MTB for organic carbon fluxes comprised between 0.5 and 20 g/(m^2yr) (Petermann, 1994). Observed OAI depths are inversely correlated to organic carbon fluxes and do not exceed ∼3 cm in sediment hosting living MTB populations (Petermann and Bleil, 1993). Oxygen diffusivity in sediment (D_{ox} ≈190 cm^2/yr) is much larger than solid diffusion in the mixed layer (Rabouille and Gaillard, 1991); therefore, chemical stratification is not significantly perturbed. Given the observed OAI depths, active MTB populations occur in the mixed layer under normal circumstances, and magnetotaxis is sufficiently effective to maintain them near the OAI (Figure 2.8b). Dead cells, on the other hand, are expected to passively diffuse in the mixed layer, until incorporation in the historical layer (Figure 2.8c). Long residence times are probably sufficient for complete dissolution of dead MTB, exposing magnetosome chains to direct interactions with sediment particles.

The dramatic volume decrease that accompanies cell dissolution could favor a much higher alignment of 'naked' chains in pore water; on the other hand, magnetite is known to adhere on clay particles under near-neutral pH conditions (Galindo-Gonzalez et al., 2009), so that magnetosome chains standing free in sediment pores might not occur. Another potential effect of cell dissolution is the collapse of magnetosome chains deprived of their biological support structures (Kobayashi et al., 2006), with consequent destruction of the original magnetic moments. Our experiments do not support the occurrence of such processes in the mixed layer. The coercivity components BS and BH with χ_a/M_{rs}>2 mm/A (Table 2.2) are incompatible with the magnetic properties of collapsed chains (χ_a/M_{rs}<1 mm/A), and only the low-coercivity component LC, contributing to ∼10% of the bulk ARM, could represent collapsed magnetofossils. On the other hand, measured DRM in-

tensities point to ∼1% alignment of SD magnetization carriers in the geomagnetic field, similarly to what observed with living MTB, thereby excluding strong alignments after cell dissolution.

Our experiments were designed to reproduce DRM acquisition by (mostly) intact magnetosome chains at different stages before and after reaching the historical layer. The first stage is that of a sediment slurry with 88% porosity (sample A3), which is typical for material within ∼2 cm from the sediment-water interface, and is characterized by $Q \approx 0.59$ mm/A . Its porosity is close to the percolation threshold mentioned above. This means that sediment particles – including magnetization carriers – are only weakly linked to each other, but already with sufficient strength to hold a stable NRM. Strong AF fields, however, unblock ∼75% of the magnetization carriers before their switching field is reached, so that AF demagnetization curves of NRM are characterized by an exponential decrease in the 0-40 mT range (Figure 2.5a). Full equilibrium with the ambient field is reached in <14 days (component 1 in Figure 2.6). The remaining magnetization carriers are mechanically blocked in AF fields up to 100 mT and require a longer time to equilibrate with the ambient field (component 2 in Figure 2.6).

Porosity is an exponentially decreasing function of sediment depth within the mixed layer, reaching values comprised between 67 and 80% at the boundary with the historical layer (Mulsow et al., 1998). Samples B4-5 with 68% porosity might therefore represent sediment that has just entered the historical layer. They are characterized by $Q \approx 0.2$ mm/A , and acquisition times up to 2 months (not shown) do not change this value significantly. This means that Q and τ_b are decreasing and increasing functions of depth in the mixed layer, respectively (Figure 2.8d). AF demagnetization curves of NRM at 68% porosity are no longer affected by mechanical unblocking and are almost identical in shape to AF demagnetization of ARM (Figure 2.5c). The proportionality between NRM and ARM demagnetization curves reflects common remanent magnetization carriers. Differences with IRM demagnetization curves, on the other hand, are entirely attributable to the low-coercivity component LC (Table 2.2), which is characterized by ∼6 times smaller χ_a/M_{rs} than the magnetofossil components BS and BH. Component LC is also ∼6 times less efficient in acquiring a DRM: its reduced DRM acquisition efficiency might be attributed to smaller magnetic moments or larger particle volumes.

We conclude this discussion with an estimate of NRM intensity that non-SD DRM carriers would produce with the same alignment 'susceptibility' Q observed with magnetofossils. In this case, NRM intensity is given by NRM$=QM_{rs}r_dH$, where r_d is the ratio

between the remanent magnetic moments of DRM carriers before and after the application of a saturating field (section A.5). According to the DRM model of Tauxe et al. (2006), 3 μm composite flocs are characterized by r_d ≈0.11, and using Q ≈0.2 mm/A we would obtain NRM/M_{rs} ≈0.18 in a 10 μT field, which compares well with experimental values of 0.15-0.25 obtained by the authors from redeposition experiments with <3 ppt salinity (section A.5).

2.7 Conclusions

Unlike the case of aquatic environments, living MTB in sediment are poorly aligned with the geomagnetic field. Nevertheless, 1% alignment in a vertical field appear to be sufficient for supporting magnetotaxis, expressed by the capability of crossing the typical thickness of oxygen gradients. Furthermore, mechanical interactions between cells and sediment particles can explain the observed correlation between magnetic moment and volume of MTB. Therefore, magnetosome production appears to be controlled by selective pressure in sedimentary environments. Because nutrient availability (Petermann, 1994) and ability to reach the ideal sediment depths are two important factors controlling MTB growth, our results can serve as starting point for the future development of ecological models for magnetofossil abundances.

Current flocculation models for DRM acquisition (Tauxe et al., 2006) are not applicable to magnetofossil NRM, because MTB are primarily present in the mixed layer of sedimentary columns as 'non-flocculable' magnetic carriers. Typical residence times in the mixed layer (10-1000 years) are sufficiently long to enable homogenous dispersion of dead MTB by solid diffusion and subsequent dissolution of cell material. Our experiments do not support evidence for magnetosome chain collapses during this time, nor did we find indications that the sudden volume decrease accompanying cell dissolution leads to full alignment of free-standing chains in sediment pores. These observations suggest that magnetofossil chains adhere to sediment particles, and that adhesion prevents a further collapse. Our experiments show that magnetofossils acquire a proportional DRM when sediment with typical porosities encountered in the mixed layer is exposed to 0-100 μT magnetic fields. The corresponding mean alignment of magnetic moments in a field B expressed in μT is thereby given by $\zeta \approx 8 \times 10^{-5} B$. Because of bioturbation-driven solid diffusion, a dynamic equilibrium with the applied field is expected over the residence time of particles in the mixed layer. Experiments with previously stirred sediment suggest that

equilibrium is reached in ∼1 month; however, longer equilibration times can be expected in undisturbed sediments in sediments characterized by smaller biodiffusion coefficients. The DRM acquisition efficiency of magnetofossils appears to be similar to that of other magnetization carriers, so variations in their relative concentration might not excessively alter relative paleointensity records. On the other hand, SD properties of magnetofossils make them an ideal 'tracer' for sediment mixing and early diagenetic processes (e.g. recrystallization), which affect the NRM of all remanence carriers. For this purpose, systematic investigation of DRM acquisition by magnetofossil-bearing sediment will be necessary.

Acknowledgements

This work has been made possible by the generous support of the German Research Foundation (DFG grants EG 294/1-1 and EG294/2-1), the Ludwig-Maximilians University (pond infrastructure), and the China Scholarship Council (CSC), who provided three-year funding for X. Mao.

Chapter 3

An experimental test of magneto-aerotaxis in sediment with wild-type magnetotactic bacteria

Abstract

Magnetotactic bacteria (MTB), prevalent in freshwater and marine sediment, accumulate in the top sediment, approximately at the oxic and anoxic interface (OAI). Magneto-aerotaxis is widely used to explain MTB behaviour and distribution in sediment but is rarely tested by experiment. We tested this model in sediment with wild-type MTB by controlling oxygen concentration in a glove box. The results revealed that the variation of oxygen concentration did not alter MTB behaviour. No south seeking MTB were detected in anoxic condition. The depth distribution of MTB responded to transient changes in oxygen gradient change, but not to the disappearance of it, in which case MTB profiles remained similar to the profiles observed under normal conditions. These observations suggests that magneto-aerotaxis of wild-type bacteria in sediment works in a different manner, and is probably controlled by several chemical parameters besides oxygen.The concept of magneto-aerotaxis in sediment should be updated based on these observations.

3.1 Introduction

Magnetotactic bacteria (MTB), a large variety of aquatic micro-organisms of various morphologies (rod-shaped, vibrio, spirillum, coccus and ovoid et al.) are ubiquitous in chemically stratified salt and freshwater sediment or water column. They mineralize intracellular

iron minerals of single domain magnetite and/or greigite (magnetosomes), by which they orient and navigate along geomagnetic field lines, which is known as magnetotaxis (Blakemore, 1975, 1982; Frankel, 1984). The phenomenon that MTB swim consistently in one direction, also in absence of a chemical gradient, either parallel (north-seeking, shortly NS) or antiparallel (south-seeking, shortly SS) is called polar magnetotaxis. Other types of MTB (e.g. spirilla) swim in either direction along magnetic field lines in absence of a chemical gradient, and this phenomenon is called axial magnetotaxis. Most MTB in nature display polar magnetotaxis. The advantage of magnetotaxis is believed to benefit MTB to search optimal living condition in sediment (Frankel and Bazylinski, 2009).

When observed under the light microscope in the so-called hanging drop assay, polar MTB are fully aligned and swim toward the magnetic North of a horizontal field, accumulating on the corresponding side of the water drop. These observations performed on freely swimming bacteria in water are unlikely to apply in a sedimentary environment, where strong mechanical constrains and chemical interaction greatly alter MTB behaviour. Unlike in water drop assay, MTB alignment in sediment with respect to external field is in order of 1%, so that the displacement of bacteria over time is described by a biased random walk, rather than directed swimming (see chapter 2). Similar to non-magnetic bacteria, MTB are also influenced by chemical stimuli: this phenomenon is called chemotaxis. The influence of chemotaxis on MTB swimming direction in natural sediment is expected to be significant, because MTB are only detected in the top few cm (Flies et al., 2005a; Pan et al., 2005a; Petermann and Bleil, 1993; Petersen et al., 1989), while a much wider distribution extending to the bottom of sediment aquaria would be expected if the same swimming direction is maintained all the time. In this case, chemotaxis plays a role in either preventing MTB going too deep or guiding them to turn upward in order to satisfy metabolic requirements. That means MTB swimming direction, or swimming polarity (i.e. NS and SS) must switch according to chemical environment. This phenomenon was first discovered by Frankel et al. (1997) and explained with a combination of magnetotaxis and chemotaxis called magneto-aerotaxis.

The model magneto-aerotaxis is based on observation of cultured magnetococci (MC-1) aerotactic response in oxygen gradient. In a water drop assay with oxygen saturation, strain MC-1 displays polar magnetotaxis, accumulating at the magnetic N (Figure 3.1a). MC-1 cells in a flat capillary with oxygen gradient and a horizontal field display evident aerotactic behaviour by swimming away from high oxygen concentration towards low oxygen concentration and finally form a population band where the oxygen concentration is

supposed to be optimal (O_2opt) for the bacteria growth (Figure 3.1b, top). If the field direction is reversed, the band tends to disperse into two separate bands (Figure 3.1b, bottom) advancing in opposite direction. The formation of two bands after field reversal is explained by postulating a two-state aerotactic sensory mechanism with two oxygen thresholds. As long as the oxygen concentration is larger than the upper threshold (oxic conditions), cells swim parallel to the magnetic field towards the magnetic N (NS, blue cells in Figure 3.1b). By doing so in a natural chemical gradient, they move to regions with smaller oxygen concentrations until they reach the lower oxygen threshold: here they switch the swimming direction and become SS (red cells in Figure 3.1b). In water drop assays, water is rapidly saturated with oxygen and cells are systematically NS, even in absence of an oxygen gradient (Figure 3.1a). If this model is applied to natural sedimentary environments where oxygen concentration decreases with depth (Spring et al., 1993), MC-1 cells in the top sediment are exposed to an oxygen-rich environment where the swimming direction (NS in the Northern hemisphere) points downwards. This brings the cell to greater depths; however, endless downward swimming is prevented by a change in swimming direction occurring when the cells have come to a depth where the lower oxygen threshold has been crossed. This oxygen-controlled vertical migration results in MTB concentration at the oxic and anoxic interface (OAI), which can be regarded as the optimal oxygen requirement. The model is illustrated in Figure 3.1c.

Although magneto-aerotaxis is generally used to interpret MTB behaviour in sediment, a direct validation of this model with wild-type MTB living in sediment has not been possible. Yet such validation is very important, because of the complex interplay of the following typical sedimentary conditions that are not well replicated in water: (1) poor alignment with the magnetic field and strong mechanical constraints, (2) complex chemical environment, and (3) possible differences between wild-type and cultured bacteria. In addition, although most MTB are microaerophilic (Bazylinski, 2003; Paasche Øand Larsen, 2010), the role of oxygen in MTB ecology in sediment environment is poorly known. The potential application of MTB as bio-marker in study of paleoenvironment (Chang and Kirschvink, 1989; Snowball et al., 2002) also depends on a full understanding of the role of oxygen in regulating the occurrence of MTB populations. In artificial environments, oxygen influences the growth of MTB cultures and the synthesis of magnetosomes and their morphology (Blakemore et al., 1979, 1985; Li and Pan, 2012). In this chapter, we aim to (1) test the validation of magneto-aerotaxis in sediment environment and (2) investigate oxygen ecological role in MTB growth.

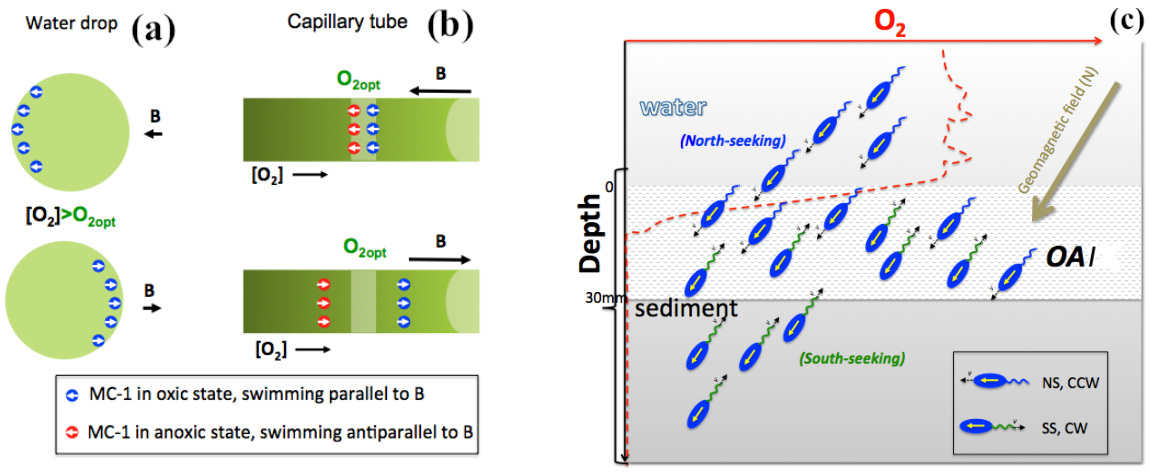

Figure 3.1: Magento-aerotaxis model in water and sediment. (a) Polar magnetotactic MC-1 in a water drop swim persistently in one direction relative to magnetic field B. Due to oxygen saturation in the water drop, all cells present north seeking behaviour. (b) In a flat capillary, oxygen concentration increases to the right and field B points to the left. MC-1 cells form a population band at a site where oxygen concentration is believed optimal O_{2opt} for MC-1 growth (top figure). NS (blue) and SS (red) swim frequently back-and-forth within the band. When the field direction is reversed (bottom), the band tends to disperse and form two separate bands containing NS and SS respectively. (c) Magneto-aerotaxis model in sediment (geomagnetic N). Oxygen penetration from air and oxygen consumed by organisms in the water and sediment lead to formation of oxygen gradient (dashed red line) which decreases with depth. MTB mostly occur in the uppermost few cm (here 30 mm) and generally concentrate at the oxic and anoxic interface (OAI) where oxygen concentration is supposed to be optimal for cell growth. MTB above OAI swim downward along the geomagnetic field lines by rotating flagella couterclockwise (north seeking motility, blue flagella); when MTB swim below OAI, they reverse flagella rotation direction (clockwise) and swim upward (south seeking motility, green flagella). The opposite occurs in the southern hemisphere. Figures are after Bazylinski and Frankel (2004); Frankel et al. (1997).

Because MTB behaviour observations are carried out in open air or oxygen-rich environment (e.g. water drop assay), polar magnetotactic bacteria grown in the Northern hemisphere are consistently observed in their NS state (Figure 3.1a). Full testing of the magneto-aerotaxis model requires observations performed under anoxic conditions. For this purpose, MTB-containing sediment was placed in an oxygen-controlled glove box where the oxygen concentration could be reduced to zero and all observations were carried out in a well-defined atmosphere. This treatment allows various MTB in the sediment, with different species-specific oxygen requirement, to experience their oxygen threshold (if exists) below which south seeking motility might be present (if magneto-aerotaxis model is valid). We can therefore test if (1) SS bacteria start to become observable in decreasing oxygen concentrations, (2) the depth distribution of MTB changes as response to a change in the oxygen gradient, and (3) the total MTB population changes in response to gradient changes.

3.2 Materials and methods

Top sediment from Lake Chiemsee (southern Germany) has been collected with a bottom grab sampler and transferred into a few glass aquarium in the laboratory. Sediment was thoroughly stirred and allowed to stabilize for few months in order to reach stationary stratification with finer silt particles on the top and sandy particles on the bottom. About 3-5 cm water was kept above the sediment: evaporation was compensated by adding distilled water. Two wild-type MTB: *M. bavaricum* and cocci (Figure 3.2) were dominant in the sediment (Pan et al., 2005a; Petersen et al., 1989) and were examined in this study. *M. bavaricum* is described in Hanzlik et al. (1996); Jogler et al. (2010); Li et al. (2010); Spring et al. (1993) in term of its morphological, magnetic and phylogenetic characters. Cocci (Figure 3.2) (ca. $\sim 1\mu$m in diameter) have two bundles of flagella, 2-4 chains of prismatic magnetosomes, phosphorus inclusions and swim in a helical way (Hanzlik et al., 1996; Pan et al., 2009).

A glove box (Figure 3.3) was used to control oxygen concentration in the sediment and water, from oxygen saturation to a completely anoxic environment (no oxygen gradient). An anoxic atmosphere was created in the glove box by a continuous flow of N_2 gas with $<1\%$ impurities. Residual oxygen was removed by washing the inflowing gas in a FeCl solution. When the original greenish color of the solution started to fade after some days, fresh FeCl was added. A slight overpressure inside the glove box prevented atmospheric

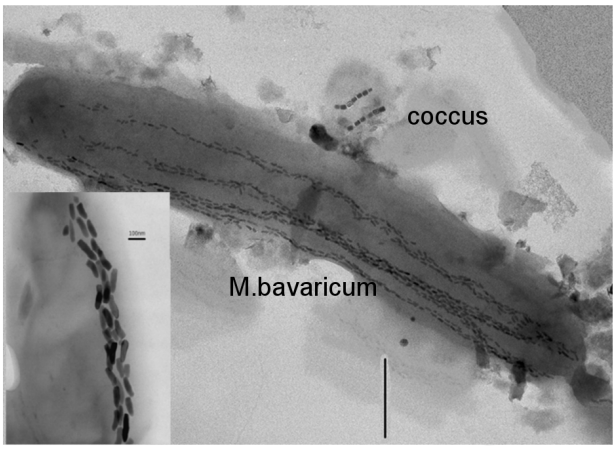

Figure 3.2: Transition electron micrograph of uncultured *M. bavaricum* (insert is amplified chain) and a coccus from lake Chiemsee, south of Germany. Coccus contains 2-4 chains of prismatic magnetosomes and are propelled by two bundles of flagella attached to one side of the cell. The vertical bar is 1μm. The bar of the insert is 100 nm.

contaminations. Sediment, microscope, oxygen sensor and other equipment required for this experiment were placed in this glove box. All microscope observations and population measurements were carried out in the same atmosphere used to control the oxygen gradient in the aquarium. Procedures of sediment sampling, observation under light microscope and oxygen profiles are similar to those described in chapter 4. Oxygen profiles were measured every 1-13 hours over periods of time where fast changes could be expected, and before and after sediment profiles have been taken for bacteria counts. Regular sampling of the top sediment (every 12-24 hours) has been performed in order to detect SS bacteria at different sediment depths by hanging drop assay. SS bacteria, if present, can be detected because sampling and observation took place in the same anoxic atmosphere. Sediment mini-cores (24 mm long) were sliced every 2 mm and diluted with distilled water to make sediment hanging drops. MTB counts obtained in this way for each slice are used to reconstruct the depth distribution of NS and SS bacteria. *M. bavaricum* and cocci numbers were counted directly under microscope. Due to relative homogeneity of this sediment microcosm, only a single sediment profile each time was enough to estimate bacteria vertical distribution and population change in this microcosm.

3.3 Results

3.3.1 MTB behaviour in changing oxygen concentration

Before moving the aquarium in the glove box, oxygen and MTB profiles have been measured to provide a reference initial state (Figure 3.4a, day 0). Nitrogen gas began to flew in the glove box from 2012/2/17 (day 6). Then the oxygen concentration in the sediment started

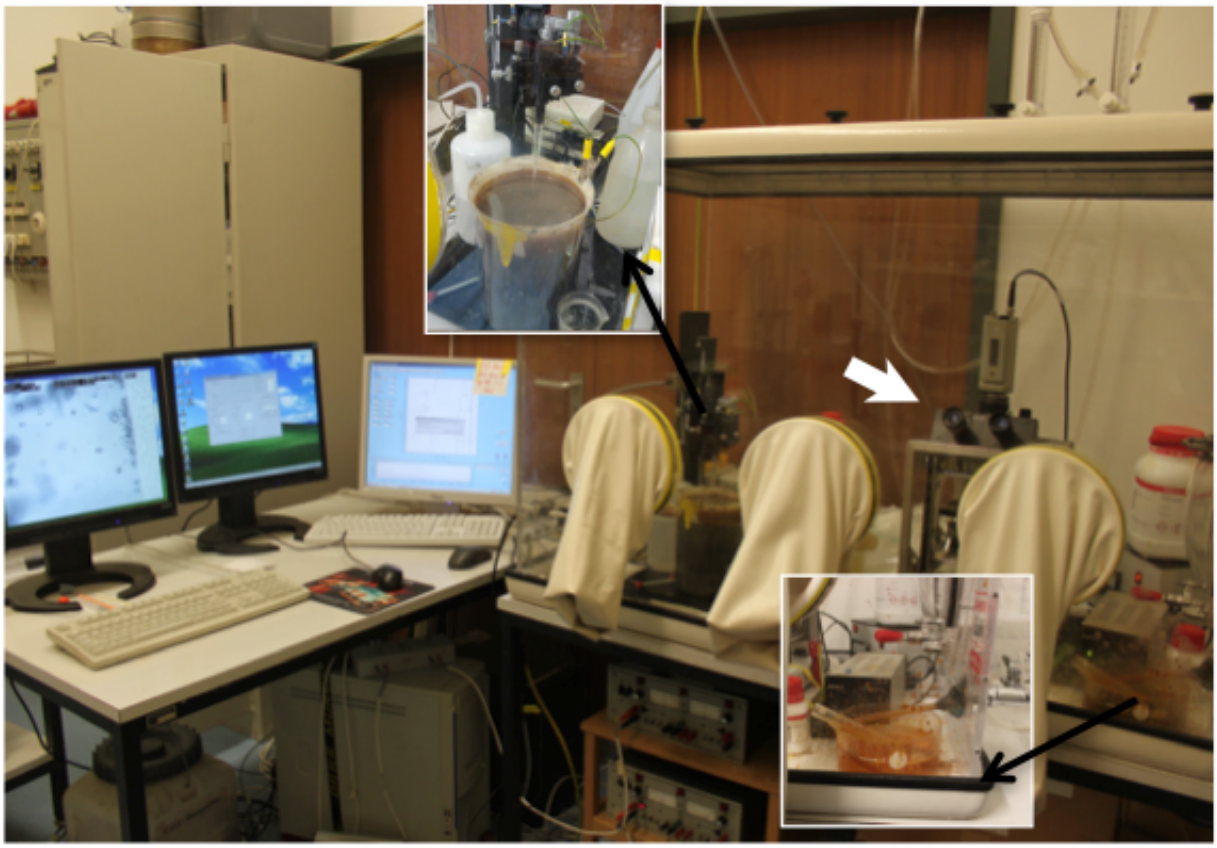

Figure 3.3: Experimental setup with a glove box containing sediment microcosm placed under a movable oxygen microprobe for measuring oxygen profiles (top insert), and an optical microscope equipped with Helmholtz coils for observation of MTB in a controlled magnetic field (magnetodrome, white arrow, see section A.1). The glove box with 3 gloves for experiment operations is air-sealed, and the atmosphere inside it is controlled by a regulated flow of N_2 or CO_2 through an input and output valve. Oxygen impurity is removed by washing the gas in a green Fe^{2+}-solution that slowly oxidises, producing an orange precipitate of iron oxyhydroxides (bottom insert). The oxygen microprobe from the company Unisense (top insert) has a diameter of 50 μm, spatial resolution 50 μm and a sensitivity of 0.3μmol/L. It can be inserted in the sediment without disturbing the vertical stratification for measuring O_2 profiles. The oxygen profile and MTB behaviours can be spontaneously monitored by the computer programme (left-hand side).

to decrease and the oxygen gradient moved upward (see oxygen profiles in Figure 3.4a, b, c). About one month later (2012/3/20), the oxygen gradient started to vanish as oxygen concentration decreased to zero in both water column and sediment (see oxygen profile in Figure 3.4d). The gas flew continuously for another week (2012/3/27) to remove residual oxygen in the sediment. During this process, only a few SS MTB were detected in some samples (Table 3.1); however, this result is not dissimilar from what is observed under normal conditions. Abundant north seeking MTB behaved identically as their counterparts in air. We also observed the same cells in oxygen-saturated water, without detecting any difference. In order to test whether SS cells could be produced by exposure to substances typically encountered in anoxic sediment, we prepared a sulphide solution by dissolving 0.025 mol/l Na_2S in oxygen-free water inside the glove box, and added this solution to the hanging drop assay. *M. bavaricum* immediately reduced its swimming speed while cocci stopped immediately.

The glove box was then open to air until oxygen concentration in the sediment recovered to the initial conditions (see oxygen profile Figure 3.4k) and subsequently refilled with CO_2. The sediment was kept in dark to avoid oxygen generation due to photosynthesis. CO_2 dissolution reduced the sediment pH to ∼4-6. In CO_2 gas, *M. bavaricum* became gradually immotile and slowed down. Two weeks later as the oxygen gradient disappeared (see oxygen profile Figure 3.4l), the motility of 20-30% of *M. bavaricum* cells was so greatly reduced that they could not reach the edge of the water drop, while cocci could not be detected. Immotile *M. bavaricum* cells recovered their usual swimming velocity upon exposure to fresh air for few minutes and many cocci appeared again after a few days in air.

A large number of new, slightly magnetic organisms appeared under anoxic conditions (created in a N_2-atmosphere), sometimes even exceeding the MTB counts. These organisms appeared to be slightly magnetic when exposed to a rotating magnetic field, and resembled the magnetic protists reported by Bazylinski et al. (2000) in a salt pond, although TEM pictures were not taken for confirmation. A short video of these organisms can be seen in Appendix C-6. Non-magnetic organisms, apparently swallowing MTB, also appeared under anoxic conditions (Appendix C-7). All these unidentified organisms disappeared after the sediment was exposed to fresh air.

3.3.2 Vertical distribution and population change

The vertical distribution of *M. bavaricum* and cocci corresponding to oxygen profiles are respectively shown in Figure 3.4 and Figure 3.5. In presence of an oxygen gradient, *M.*

Table 3.1: South and north seeking MTB counts measured during three days while sediment oxygen profiles decreased from normal (2012-03-01) to zero (2012-03-20). Each sample contained 0.89 μl sediment

			M. bavaricum			cocci		
Date (profile)[1]	Oxygen [2]	Depth	NS	SS[3]	SS%	NS	SS	SS%
2012/3/1(c)	Zero	0-2mm	765	2	0.3%	420	140	25%
		2-4mm	1473	0	0%	480	14	2.8%
		6-8mm	282	0	0%	180	3	1.6%
2012/3/9 (d)	Zero	0-2mm	51	0	0%	480	24	4.8%
		2-4mm	220	0	0%	380	4	1.0%
2012/3/20 (e)	Zero	2-4mm	332	3	0.90%	25	0	0%

1. Sediment profiles corresponding to those in Figure 3.4 and Figure 3.5
2. Oxygen concentration at the water-sediment interface.
3. All SS observed in the whole experiment are listed and not reproducible.

bavaricum showed a bimodal distribution peaking at 0-5 mm and 10-20 mm (Figure 3.4a, b, c), with a few cells below 20 mm. *M. bavaricum* below 20 mm soon disappeared as oxygen concentration decreased to 60 μmol/L in the water column (Figure 3.4b). As oxygen concentration decreased to zero and oxygen gradient vanished, *M. bavaricum* peaked only at 0-5 mm (Figure 3.4d, e, f) without cells below 10 mm. At the same time, no MTB were ever detected in the overlying water column. After 40 days continuously in anoxic environment, the bimodal distribution tended to partially recover (Figure 3.4h, i) and completely recovered in air (Figure 3.4k). In order to test if fluctuation of vertical distribution was due to immotile bacteria in anoxic condition, a sediment profile was taken in anoxic condition and then counted in air. The vertical distribution (Figure 3.4g) was identical with previous profile (Figure 3.4f) that was sampled and counted in zero oxygen. *M. bavaricum* peaked at around 4-6 mm in CO_2 atmosphere without cells below 10 mm.

Cocci, on the other hand, showed clear uni-modal distribution. In oxic condition, cocci peaked at 6 mm (Figure 3.5a,k). As oxygen concentration decreased, the population peak moved to the water-sediment interface (Figure 3.5b,c,d,e,f). In stable anoxic condition, the peak gradually moved to 6 mm (Figure 3.5h,i,j) and the distribution completely recovered in air (Figure 3.5k), same as in oxic condition (Figure 3.5a,k). Cocci motility test (comparison

between Figure 3.5f,g) showed same results as *M. bavaricum*. Very few cocci were detected in CO_2 atmosphere (Figure 3.5l).

The cell counts of *M. bavaricum* and cocci per μl sediment are shown in Figure 3.6. Total populations dropped as oxygen concentration decreased (from profiles a, b, c to profile d). Relatively constant and high population occurred in both stable oxic and anoxic environments. *M. bavaricum* and cocci significantly dropped in the CO_2 atmosphere, in particular with a hint of cocci extinction.

3.4 Discussion

3.4.1 Validating magneto-aerotaxis with wild-type MTB in sediment

Unlike non-magnetic bacteria, the aerotactic behavior of MC-1 is combined with magnetotaxis, so that NS and SS cells swimming parallel and antiparallel to the magnetic field, respectively, are expected depending on the oxygen concentration. Accordingly, SS cells are not expected in the classic hanging drop assay. They are, however, expected in hanging drop assays performed under strictly anoxic conditions.

Successful test of the magneto-aerotaxis model with NS and SS counts in hanging drop assays under controlled atmospheres relies on the verified situation that only a very small fraction of SS cells ($<5\%$) is occasionally detected in sediment from the Northern hemisphere (Frankel and Bazylinski, 2009; Zhang et al., 2010). In our sediment, the SS fraction is $<5\%$, and consists mainly of cocci, spirilla, and some other unidentified species. The SS fraction is even smaller for SS *M. bavaricum*. The reason for the occurrence of SS cells in oxygen-saturated water in the Northern hemisphere is unclear. According to the magneto-aerotaxis model of Frankel et al. (1997), all NS should become SS under anoxic conditions, in contradiction with our experiments, where the SS fraction was $<5\%$ in all but one case, where 25% SS cells have been counted. This case, however, could never be reproduced. Because oxygen concentration reduces gradually from saturation to zero, the oxygen concentration threshold that makes NS cells become SS does not appear to exist for the observed MTB types. This suggests that *M. bavaricum* and wild-type cocci do not perform the same type of magneto-aerotaxis observed with MC-1 (Frankel et al., 1997), or that other factors are responsible for the swimming direction of cells in a magnetic field. MTB sensitivity to oxygen thresholds below the detection level of the oxygen microprobe

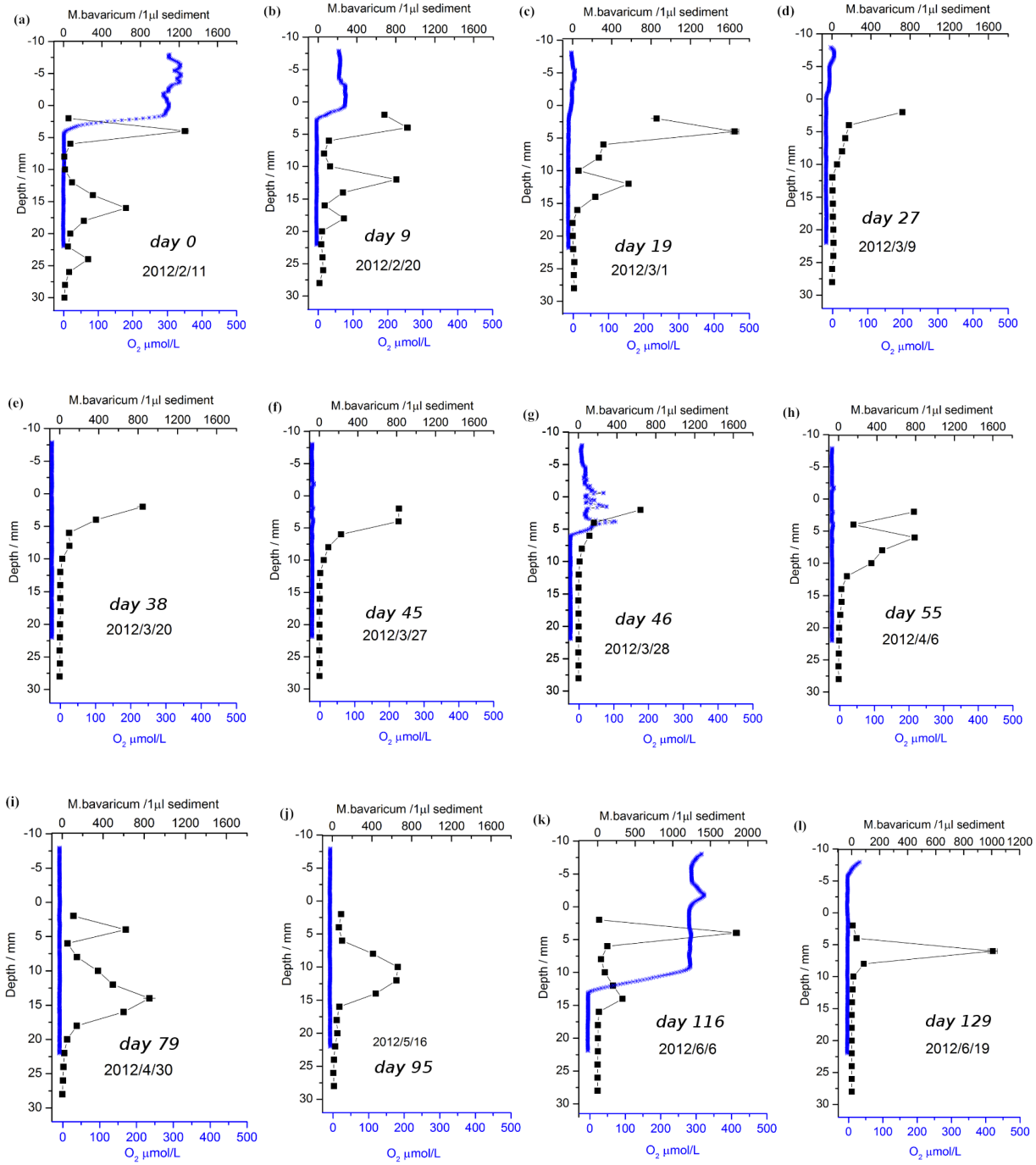

Figure 3.4: Oxygen profiles (blue) and *M. bavaricum* vertical distribution (black). Some examples: (a) profile taken before putting the sediment inside the glove box, (g) after opening the glove box for some hours; (k) after opening the open glove box for a few days; (l) in CO_2-atmosphere. All profiles except (a) and (l) were taken in a N_2-atmosphere

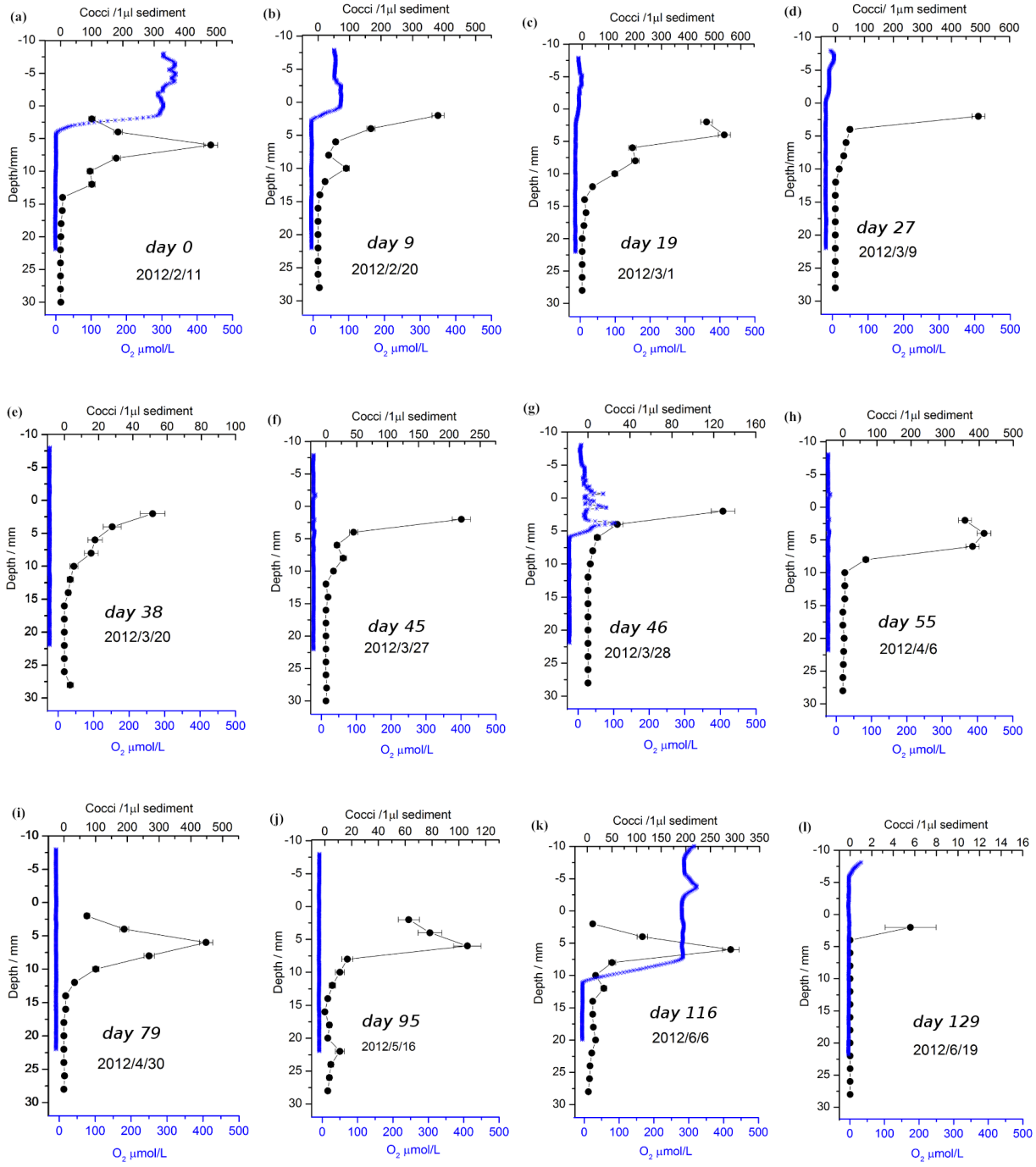

Figure 3.5: Oxygen profiles (blue) and cocci vertical distribution (black). Some examples: (a) profile taken before putting the sediment inside the glove box, (g) after opening the glove box for some hours; (k) after opening the open glove box for a few days; (l) in CO_2-atmosphere. All profiles except (a) and (l) were taken in a N_2-atmosphere

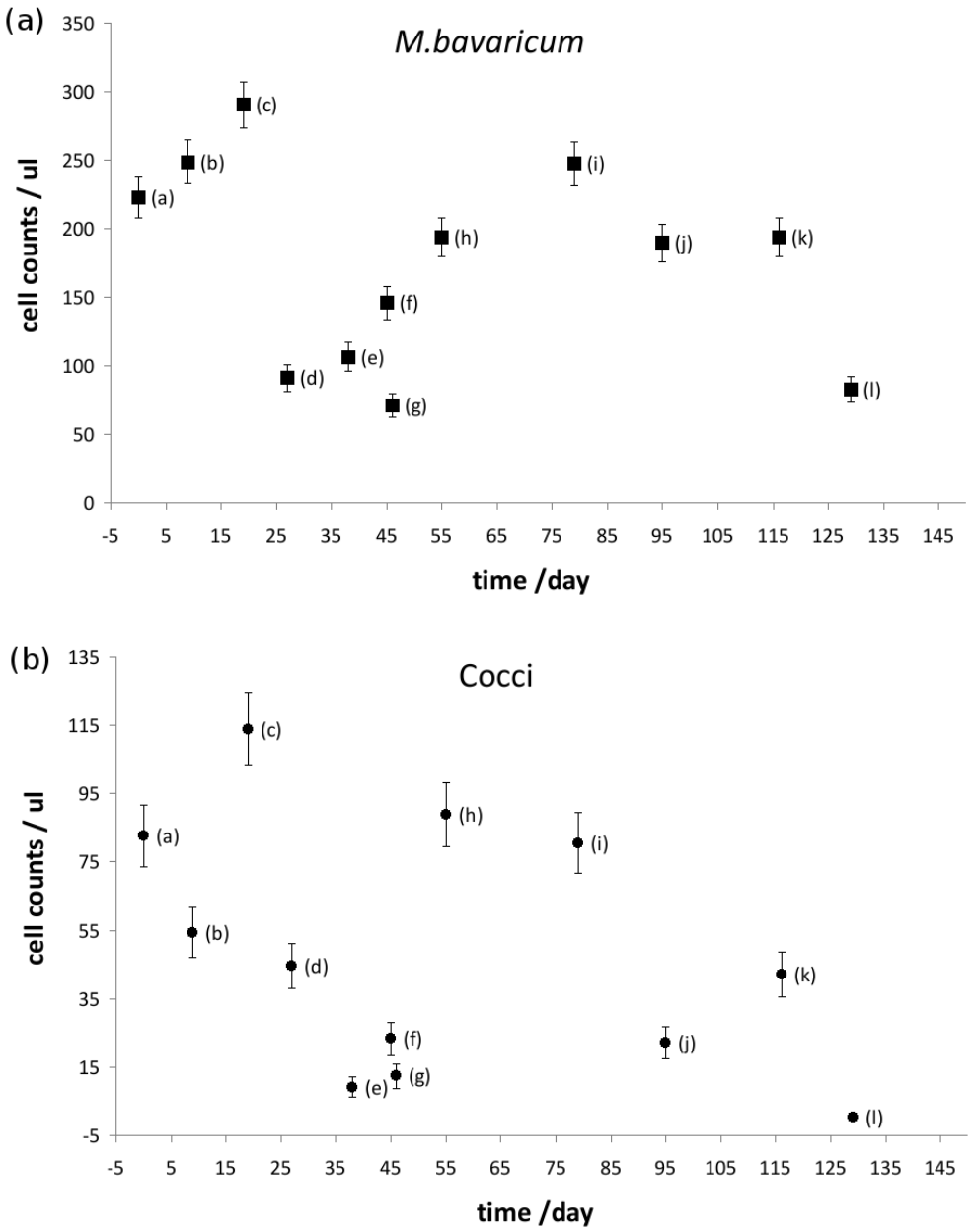

Figure 3.6: Total bacteria concentration (per μl sediment) of *M. bavaricum* (a) and cocci (b) as a function of time. The data points were obtained by integration of the profiles (labels beside data points) in Figure 3.4 and Figure 3.5 with respect to depth. Some examples: (a) profile taken before putting the sediment inside the glove box, (g) after opening the glove box for some hours; (k) after opening the open glove box for a few days; (l) in CO_2-atmosphere. All profiles except (a) and (l) were taken in a N_2-atmosphere. The error bar was square root of cell count.

(0.3 μmol/L) can be excluded for two reasons: first, constant overpressure and N_2 washing in a FeCl solution ensured oxygen removal and lack of atmospheric contamination. Second, any residual oxygen would be consumed by the sediment.

Aerotactic behaviour can also be inferred from MTB vertical distribution change with oxygen variation. If MTB vertical distribution correlates with oxygen gradient and MTB accumulation coincides with optimal oxygen concentration, evident change of MTB vertical distribution would be expected when oxygen changes. With other words, when oxygen is completely removed, MTB would be expected to uniformly distribute in the sediment, again, this contradicts our results: the MTB depth distribution did not change significantly long after removing the oxygen gradient, except during the transient phase where the oxygen gradient moved upwards. Therefore, aerotaxis appears to be active only under transient conditions, while other factors must control the depth distribution of MTB under stationary conditions. This might explain the lack of a strong correlation between MTB depth distribution and oxygen gradient (Flies et al., 2005b; Jogler et al., 2010).

Overall, the classic model of magneto-aerotaxis is not directly verified by our observations. But we do not exclude the possibility of magneto-aerotaxis in sediment. The results suggest that oxygen is likely not, at least for *M. bavaricum* and cocci in our sediment, the only stimulus that changes the polarity of magnetotaxis. MTB might respond only to a combination of different substances. This problem is further investigated in chapter 6, where a modified magneto-chemotaxis model is proposed.

3.4.2 Why could magneto-aerotaxis not be detected in sediment?

In the following, we discuss two possible reasons for the apparent lack of observations supporting magneto-aerotaxis in sediment:

1. *Oxygen requirements.* Most MTB are microaerobic or anaerobic. In our experiments, *M. bavaricum* and wild-type cocci concentrate in the uppermost 0-10 mm sediment where the oxygen concentration under normal conditions is as high as 200 μmol/L (Figure 3.4, Figure 3.5). If aquaria are exposed to pure oxygen, both *M. bavaricum* and wild-type cocci move down by few mm (Kerstin Reimer, personal communication), so that the minimum sediment depth at which living cells are detected appears to be correlated with the oxygen gradient. On the other hand, the maximum sediment depth, which is the expected place where NS bacteria become SS, is unrelated to the oxygen gradient. Because this depth did not increase under anoxic conditions, the process by which NS cells become SS appears to be controlled by other factors.

2. *Dependence on other electron acceptors.* For aerotactic bacteria such as *E. coli*, nitrate or fumarate works as alternative electron acceptor (Taylor et al., 1999). The same might be true for *M. bavaricum* and/or cocci, in which case magnetotaxis under anoxic conditions is controlled by a different electron acceptor. However, the depth distribution of *M. bavaricum* appears to be unrelated to nitrate concentrations and the specific growth requirements of this bacterium are unknown.

3.5 Conclusions

In this study, we have conducted experiments to test the magneto-aerotaxis model in sediment containing wild-type magnetotactic bacteria. The most characteristic nature of this model, namely the occurrence of SS bacteria under anoxic condition, could not be observed. The depth distribution of MTB responded to transient changes in oxygen gradient, but not to the disappearance of it, in which case MTB profiles remained similar to the profiles observed under normal conditions. These observations suggests that magneto-aerotaxis of wild-type bacteria in sediment works in a different manner, and is probably controlled by several chemical parameters besides oxygen.

Chapter 4

Study of magnetotaxis advantage in stable sediment: magnetotactic bacteria in Earth's field, zero field and alternating field

Abstract

In this study, we assess magnetotactic advantage in sediment by long-period observations of natural MTB populations of cocci and *M. bavaricum* in an aquarium exposed to the following magnetic field configurations: (1) geomagnetic field in the laboratory (∼44 μT with 71°downward inclination), (2) zero field, and (3), a ∼100 μT vertical field whose polarity is switched every 24 hours. Comparison of MTB populations in the geomagnetic field with those observed after long (∼6 months) exposure to a zero field provides a first, simple quantification of magnetotaxis advantage in sediment. This comparison is complicated by extremely large spatial and temporal variations of MTB populations, whereby the cell concentration at any given depth can vary by a factor 5 between consecutive samplings within few days, and between profiles taken at few cm distance. Nevertheless, repeated sampling during normal and zero field exposure allowed detecting a decrease of MTB concentrations in absence of a magnetic field: this effect was clearer for *M. bavaricum*, whose mean concentration was 13.1± 6.1 cells/μl before cancelling the geomagnetic field, and 5.8± 1.2 cells/μl during ∼6 months in zero field, with no clear temporal trend suggesting an extinction. Cell numbers recovered to initial values within ∼1.5 months after the geomagnetic field was reset, and dropped again during a second period of ∼1.5 month in zero

field. Cocci displayed a larger temporal variability with 11.7 ± 4.5 cells/μl during stable periods in the geomagnetic field, and 11.5 ± 4.3 cells/μl during zero field experiments. The absence of a magnetic field does not appear to produce cocci extinction in ∼6 months, nor was a significant change in depth distribution observed. A second experiment in which the polarity of a vertical magnetic field was switched on a daily basis produced a moderate decrease of *M. bavaricum* concentrations and nearby extinction of cocci.

Overall, both types of MTB benefit from the presence of a magnetic field with correct polarity (i.e. pointing downward in the northern hemisphere), and this benefit appears stronger for *M. bavaricum* than for cocci. While *M. bavaricum* drops very rapidly after the onset of zero field conditions, recover to normal concentrations after restoring the geomagnetic field appears gradual and might be explained by its natural duplication rate. On the other hand, cocci are intolerant to reversed magnetic fields, as expected from the polar magneto-aerotaxis model of Frankel et al. (1997), confirming the active role of magnetotaxis in sediment, while *M. bavaricum* is only partially affected. The reason for this difference is unclear and might point to a different magnetotactic mechanism for *M. bavaricum*.

4.1 Introduction

In presence of external magnetic field, magnetotactic bacteria (MTB) in water environment are aligned and swim along the magnetic field lines. This behaviour–known as magnetotaxis is expected to be advantageous for searching optimal living habitat in chemically stratified sediment, which can be realized in two ways: by reducing searching path from three dimension to one dimension (Kirschvink, 1980) and/or by improving MTB sensing ability (Smith et al., 2006). Reducing searching path depends on good alignment with external field. The study of magnetotactic bacteria orientation in sediment revealed that the alignment degree along the magnetic field is as low as 1% which is however sufficient for successful magnetotaxis in sediment (see chapter 2).

The unsuccessful search polar magneto-aerotaxis in uncultured cocci (chapter 3), which appear to persist in a NS state even under anoxic conditions can in principle be explained by a complex reaction to a range of other stimuli, such as tactile ones, that cannot be reproduced under the optical microscope. On the other hand, it is also possible that magnetotaxis of our MTB populations works on fundamentally different principles. For instance, MTB swimming consistently downwards in the geomagnetic field could efficiently

escape bioturbation-induced sediment resuspension by re-entering the sediment as fast as possible. In this case, cells would never need to reverse swimming direction, provided that it stops moving when a suitable depth in sediment is reached. Therefore, the use of magnetotaxis for maintaining MTB near the oxic-anoxic interface needs to be tested directly in sediment, because the complex combination of chemical and tactile conditions cannot be reproduced under the microscope. The simplest test that serves this purpose is the comparison of MTB abundance in the same microcosm under different magnetic field configurations. Cancelling the geomagnetic fields, in particular, eliminates magnetotaxis, because MTB no longer have a preferred swimming direction and they can solely rely on chemotaxis for displacement. A decrease in MTB abundance would therefore indicate that magnetotaxis effectively provided a biological advantage.

A different experiment is used to test two known types of magnetotaxis: axial magnetotaxis, in which the geomagnetic field just provides a reference axis for directed swimming in both directions, as observed with the spirillum *M. magnetotacticum*, and polar magnetotaxis, in which cells subjected to given conditions (i.e. oxygen concentration above a threshold) swim only in one direction, parallel or antiparallel to the magnetic field, as observed with MC-1 cultured cocci (Frankel et al., 1997). For this purpose, the polarity of a vertical or inclined magnetic field is switched at a certain rate (e.g. once a day) so that a reference axis is provided, while the field direction (in particular its vertical component) is zero on average. Such field would still support axial magnetotaxis, but not polar magnetotaxis, since during half of the cycles, when the field points upwards, the polarity of all cells make them swim away from the oxic-anoxic interface (Frankel et al., 1997).

4.2 Materials and methods

4.2.1 Sediment

Top sediment from Lake Chiemsee (southern Germany) has been collected with a bottom grab sampler and transferred into a $30 \times 20 \times 20$ cm glass aquarium in the laboratory. Sediment was thoroughly stirred and allowed to stabilize for few months in order to reach stationary stratification with finer silt particles on the top and sandy particles on the bottom (Figure 4.1a insert). About 3-5 cm water was kept above the sediment: evaporation was compensated by adding distilled water. A stable oxygen gradient formed after $\sim$5 days (see section 4.2.4) and was maintained unaltered for the entire experiment duration. Observation under the microscope confirmed the presence of abundant populations

of MTB, including the rod-shaped *M. bavaricum* and cocci (Pan et al., 2005a). These two types of bacteria provided the most stable and easy-to-observe populations: therefore, our experiments focus on the characterization of these two types of MTB.

4.2.2 Magnetic field settings

The stabilized aquarium was put at the center of three ∼1×1 m Helmholtz coil pairs used to control the magnetic field over the volume occupied by the sediment. The coils were connected with precision power supplies for passive field regulation. The geomagnetic field in the laboratory had an intensity of ∼44 μT with 71°downward inclination.

Near-to-zero field conditions have been obtained by regulating the power supplies over several days in order to obtain averages close to zero. Figure 4.1 shows a nearly instantaneous field map over the area occupied by the sediment measured on a single day after zero field setting. Maximum field deviations from zero are of the order of 1.5 μT, and tend to average out over time, so that a systematic vertical field component is not expected over the long experiment duration. Assuming a maximum systematic error of 0.3 μT on the vertical component, the resulting alignment of bacteria in sediment would be <1% of the typical alignment under normal conditions, making the 'residual' magnetotaxis at least 100 times less effective than usual.

Vertical alternating fields have been obtained with the same Helmholtz coil system and an electronically controlled commutator (Figure 4.2 insert) that switches contacts every 24 hours, so that the field points upwards or downwards every second day.

4.2.3 MTB characterization

Estimates of MTB populations and vertical distributions of cell concentration as a function of space and time in the top 2.5 cm sediment have been obtained as follows. Before and during the experiments, 7 or 8 homogeneously distributed sediment profiles were sampled on a regular basis (every 15 or 30 days) (Figure 4.3a). Sediment profiles were taken in form of mini-cores (⊘ 5 mm) with a drinking straw, which easily penetrate in the topmost ∼3 cm unconsolidated sediment. After sealing the top end with plasticine, the straw was retrieved from sediment (Figure 4.3b). The mini-core contained in the straw was pushed forward by applying some pressure on the sealed end of the straw, and sliced in 1 mm increments. Each slice was diluted with distilled water (200 μl) and homogenized in microtubes. 10 μl sediment solution (containing ∼0.614 μl sediment) was placed on a cover slid and turned

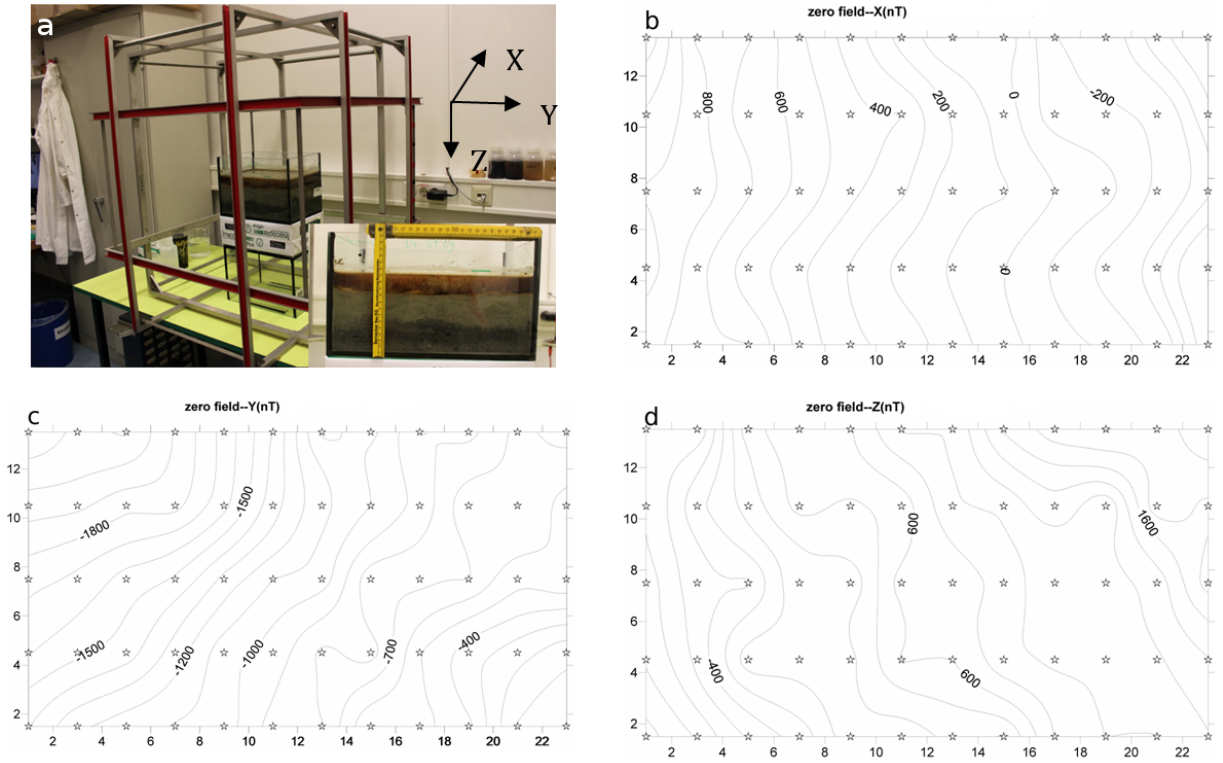

Figure 4.1: Experimental setup for magnetotactic bacteria in zero field. (a) The close-to-zero field condition was generated by 3 pairs of Helmholtz coils, in which sediment (insert) was placed at the center. Three components of magnetic field inside the coils were indicated at the right top. The geomagnetic field inside the coil (no electric current) in three components were: X=-12.9μT, Y=4.7 μT, Z=41.8 μT. (b, c, d) Maps of three components of zero field. The unit is nT. Numbers in horizontal and vertical axis were the dimension reference of the sediment area. Stars in the maps were the control sites for field measurement.

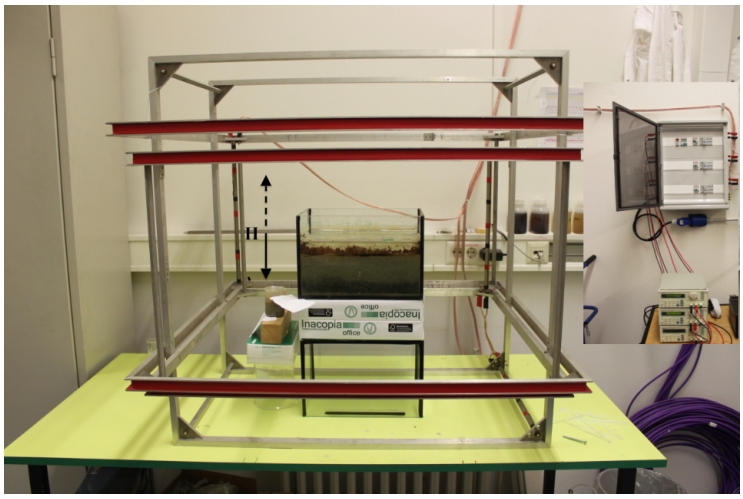

Figure 4.2: Experimental setup for magnetotactic bacteria in alternating field. Sediment was placed in the center of 3 Helmholtz coils which two pairs were used to compensate horizontal and vertical field components and the third pair was responsible for reversing vertical field component. The switch upward and downward field every 24 hours was executed by an electronically controlled commutator (insert). The downward field intensity was 118–121.5 μT and upward field intensity was -123– -120μT.

it upside down to make a hanging drop on a rubber O-ring. The sample was put in magnetodrome (Davila, 2005; Hanzlik et al., 2002; Petermann et al., 1989), an instrument consisting of optical microscope and 2 pairs of Helmholtz coils for generating homogeneous field, to let MTB move to the water/air edge in the droplet. Cells swimming out of the sediment can no longer be observed after ∼20 min in a horizontal magnetic field, so that *M. bavaricum* and cocci were always counted after 20 min exposure to a horizontal magnetic field in the magnetodrome.

Vertical MTB distributions were determined by averaging cell counts from 7 or 8 individual mini-cores as described above. Standard errors were identified with the standard deviation of the mini-cores counts at each depth. These errors are always larger than statistical counting fluctuations derived from a Poisson distribution (i.e. is the error associated to n counts), reflecting true heterogeneities in the aquarium (Table 4.1). The origin of this heterogeneities and their correlation with bioturbation is unclear. Jogler et al. (2010) reported the case of one aquarium with no detectable *M. bavaricum* cells, which was abundantly bioturbated by tubificious worms. However, several initially identical aquaria in our laboratory, which evolved in time to lesser or larger sediment reworking by those worms, did not show a systematic correlation between biotrubation and MTB populations. For each field setup (i.e. geomagnetic field, zero field, alternating field), average profiles have been calculated from all sampling dates (Figure 4.9) in order to determine the equilibrium population established under these conditions. Because of the large temporal fluctuations sometimes observed in twin aquaria kept under identical conditions, we verified mean MTB

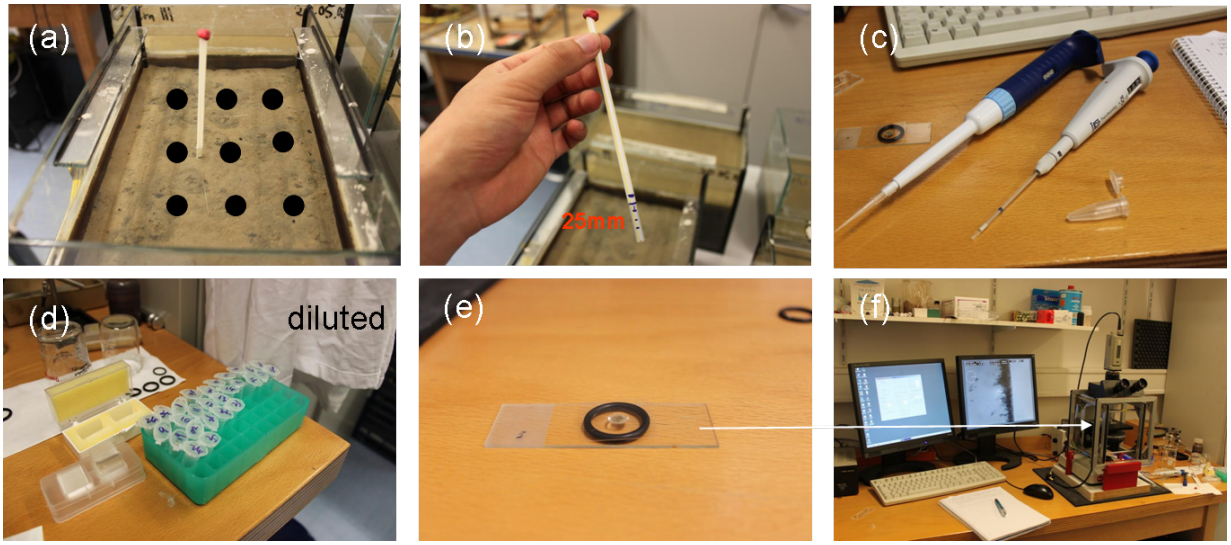

Figure 4.3: Procedure of sampling and measurements. (a) 7 or 8 sediment mini-cores were sampled around the 9 areas indicated by black dots; (b) A mini-core, 25 mm long, was taken by a drinking plastic straw; (c, d) The mini-core was sliced every 1 mm increment and diluted with distilled water; (e) A drop of 10 μl solution was made to be a hanging drop over a plastic O-ring; (f) MTB number was directly obtained under the magnetodrome.

populations in a twin aquarium constantly exposed to the geomagnetic field at the time when the ∼6 month zero-field experiment was ending (red triangles in Figure 4.7).

The method described above for quantifying MTB populations in sediments might underestimate the real number of cell in sediment, because there is no mean to verify that all cells are active and swim out of the sediment in the hanging drop assay. In fact, it is possible that most cells in sediment are inactive. However, the cell counting procedure was identical for all experiments, so that any variation is attributable to a true change in the population of active MTB in sediment.

4.2.4 MTB evolution as the reformation of chemical stratification

In order to monitor the formation of stable MTB populations after the preparation of a sediment-filled aquarium, we used the same sediment material to prepare a microcosm. Preparation started with filling a 500 ml glass baker with homogenized sediment slurry (Figure 4.4). A clearly recognizable sediment-water interface formed after 1 hour. Oxygen profiles have been measured in water and sediment with a microprofiling system from company Unisense (www.unisense.com), consisting of a computer-controlled vertical stage equipped with an oxygen microsensor (OX50) with 50 μm external tip diameter and 0.3

Table 4.1: An example to indicate large spatial variation of MTB population in the sediment by comparing standard deviation and Poisson error of MTB counting in each depth (average of 7 profiles).

Depth (mm)	Mean	Standard deviation	Min.	Max.	Poisson error
1	2.6	2.4	0	7	1.6
2	4.4	6.6	0	19	2.1
3	37.3	92.0	0	246	6.1
4	42.4	87.4	0	240	6.5
5	91.1	125.9	5	330	9.5
6	150.1	157.8	7	375	12.3
7	61.3	84.4	7	235	7.8
8	36.3	44.5	2	133	6.0
9	25.7	20.5	4	60	5.1
10	23.1	13.7	3	37	4.8
11	36.9	52.0	5	153	6.1
12	27.6	22.8	4	76	5.3
13	33.9	22.4	4	68	5.8
14	40.1	33.4	6	99	6.3
15	41.9	38.9	9	99	6.5
16	37.9	31.4	4	84	6.2
17	46.4	64.5	2	185	6.8
18	45.3	62.7	1	170	6.7
19	24.9	33.1	3	82	5.0
20	26.6	44.2	0	122	5.2
21	22.6	35.8	0	101	4.8
22	12.9	12.2	2	34	3.6
23	11.3	11.3	0	30	3.4
24	9.7	12.1	0	34	3.1
25	18.6	19.9	1	56	4.3

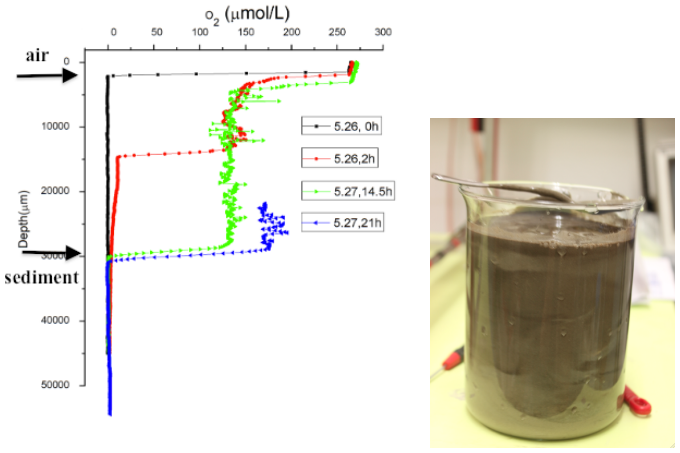

Figure 4.4: Reformation of oxygen gradient in sediment. The sediment in one 500 ml baker was first stirred completely to form sediment slurry (see the sediment in baker on the right-hand side). Oxygen profiles have been measured with an oxygen microsensor from company Unisense (see text). It was amounted on an engine to automatically measure oxygen profiles without disturbing the vertical stratification. The two arrows beside vertical axis refers to air-water interface and water-sediment interface.

μM detection limit. Initial O_2 measurements revealed anoxic conditions in the entire suspension, due to rapid oxygen consumption by sediment previously coming from an oxygen-free environment. A steep oxygen gradient forms and moves down in the water column within the first few hours (Figure 4.4), until it reaches the sediment-water interface after ∼14.5 hours. The initial fast progress of the OAI in the water column (∼1.2 mm/h) comes to a halt as soon as the sediment-water interface is reached. MTB profiles have been measured at regular intervals, first on a daily basis (day 2 until day 6), then every two days until day 10, every four days until day 18, and then occasionally until day 123.

4.3 Results

4.3.1 Initial evolution of MTB populations in the geomagnetic field

During the first 2 days of the newly formed sediment column of the microcosm (day 0 to day 2), MTB were scattered at all depths, with an incipient formation of a peak in the topmost 2 mm. This peak, located exactly at the OAI, developed steadily during the next day, producing a population increase of both *M. bavaricum* and cocci (Figure 4.5 and Figure 4.6). As far as cocci are concerned, the peak increased in amplitude until day 4, and

was followed by a sudden population drop with no significant change in depth distribution. A second increase, always in form of a sharp peak at the OAI, was observed at day 18. Interestingly, the population of cocci tended to spread out into larger depths from day 44 on, although no changes of the oxygen gradient have been observed since day 16. A similar evolution occurred for *M. bavaricum*, which reached its first population maximum at day 18, with an unusually shallow depth distribution within 1-2 mm from the OAI that has never been observed again at a later point. After this first population maximum, a second peak developed at ∼13 mm depth on day 68, and the depth distribution remained wider at later points.

Overall, even taking into account unavoidable heterogeneities between profiles taken at different points in the microcosm, the initial evolution of MTB populations can be outlined. Initially, cells are scattered at all depths, reflecting the homogeneity of the initial slurry. 2-3 days after the OAI has penetrated the sediment, a first sharp MTB peak develops within 2 mm from the OAI. An initial increase of MTB population occurs entirely in this peak for both *M. bavaricum* and cocci, while the homogeneous cell concentration at larger depths remains constant. The OAI-related peak eventually reaches a first maximum at day 4 for cocci and day 18 for *M. bavaricum*. A second maximum is reached by cocci at day 18, always within 2 mm from the OAI. Until this point, the depth distribution of both MTB types conforms to the classic picture of population maxima at or just below the OAI. From day 18 on, however, MTB populations start to spread over greater depths with no change of the OAI depth, and sometimes a second peak clearly appears ∼10 mm below the OAI. The reason for this change is not clear; however, MTB profiles taken after ∼1 month from microcosm formation do not show any systematic changes in time. Random fluctuations in depth distribution are expressed by the transient development of peaks located either 1-3 mm from the OAI, or ∼6-10 mm deeper.

4.3.2 Total MTB population in the geomagnetic field, zero field and alternating field

MTB population changes in geomagnetic field, zero field and alternating field are shown in Figure 4.7 (data in Table B.1). *M.bavaricum* decreased from 13.1 ± 6.1 cells/μl in geomagnetic field to 5.8±1.2 cells/μl during the following ∼6 months in zero field. The population recovered to the initial value 12.2 ±5.3 cells/μl in geomagnetic field for 1.5 months and decreased 8.0±1.4cells/μl in zero field. The similar decrease of population density also occurred to alternating field in which *M.bavaricum* decreased to 6.9±2.3 cells/μl. Inter-

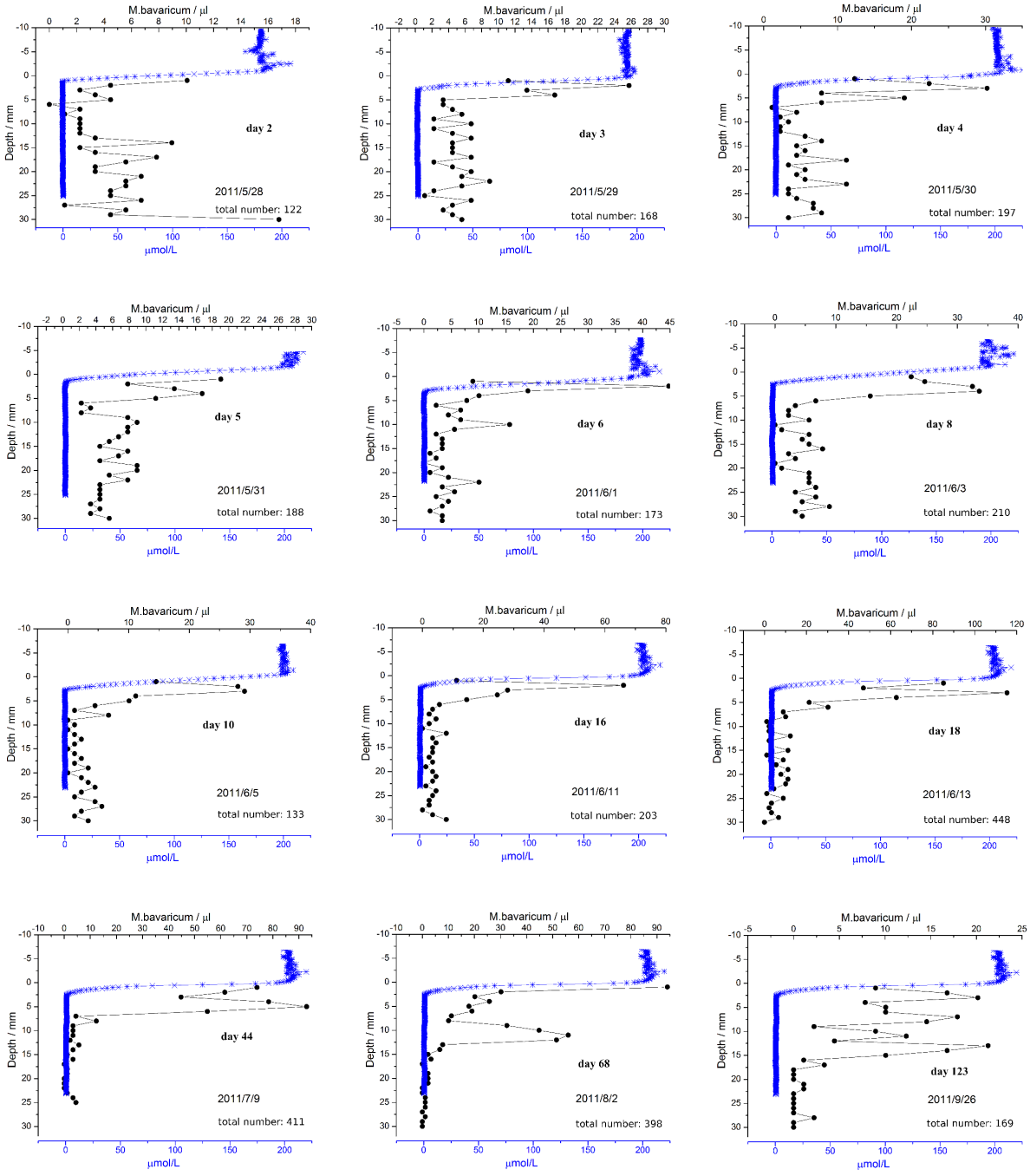

Figure 4.5: Initial evolution of *M. bavaricum* including vertical distributions (black) and total number (inserts) with oxygen gradient (blue).

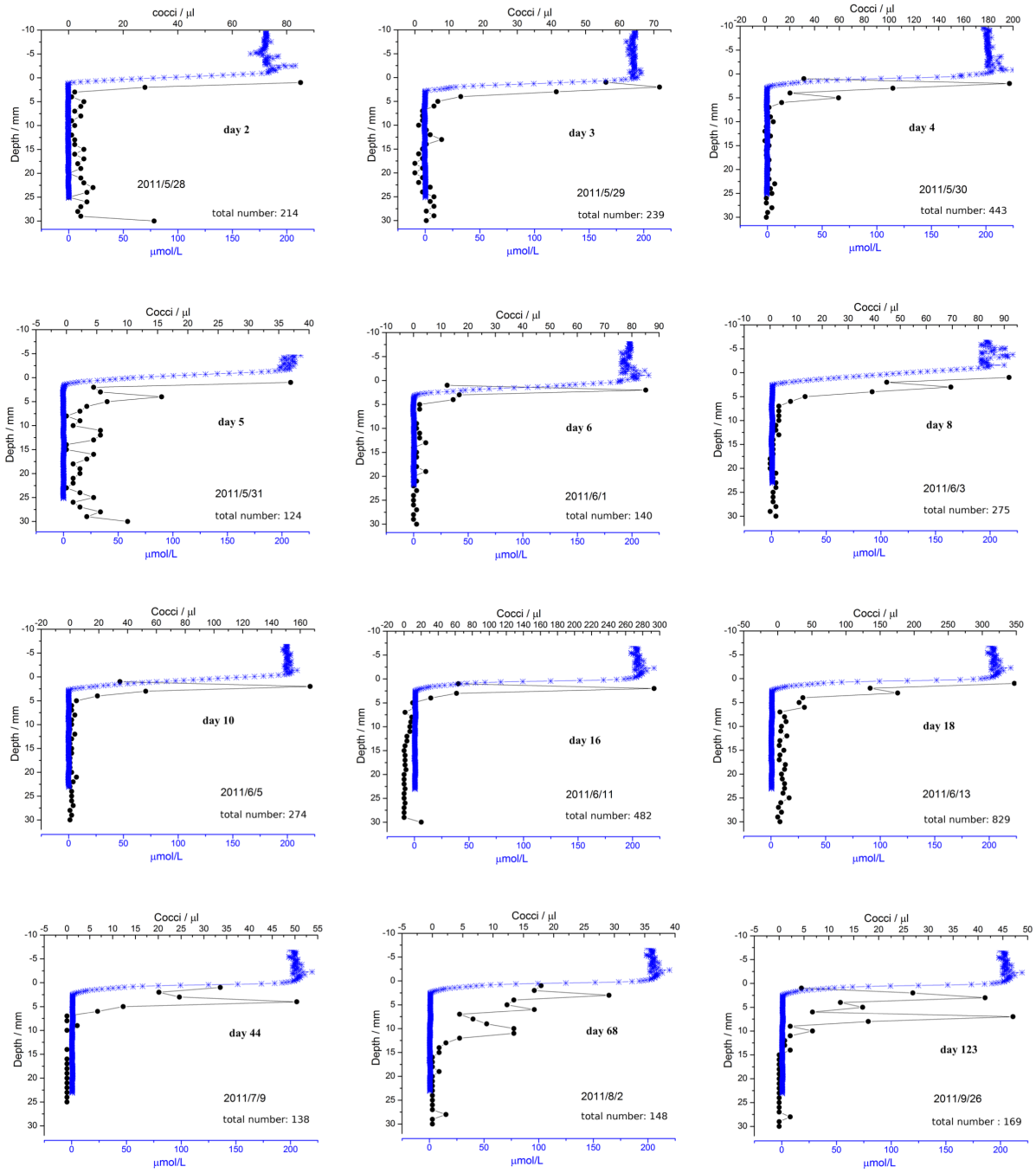

Figure 4.6: Initial evolution of cocci including vertical distributions (black) and total number (inserts) with oxygen gradient (blue).

Table 4.2: A summary of MTB population density in Earth's field, zero field and alternating field. Kolmogorov-Smirnov test accompanied with null hypothesis is used to test the difference of population density in zero field and alternating field from that in Earth's field. If null hypothesis is rejected, the two datasets are seen different, otherwise are same. In principle population density in Earth's field is larger than that in zero field and alternating field, which can be supported by rejection of null hypothesis (i.e. two datasets are different). Because after first and second zero-field settings, MTB took time to recover in Earth's field, during which population density was still low, population density in Earth's field was calculated based on selected data(see Table B.2 and Table B.3). Population density in zero field and alternating field was the average of all single profiles in corresponding field settings (see Table B.2 and Table B.3).

Field setting	Cells/μl	Kolmogorov-Smirnov test	
		95% confidence level	Confidence level for rejecting null hypothesis
M.bavaricum			
Earth's field	14.6± 9.6	—	—
zero field	6.7 ± 4.3	Rejected	99%
alternating field	7.5 ± 4.8	Rejected	99%
coci			
Earth's field	9.9 ± 6.8	—	—
zero field	10.5± 11.4	Not Rejected	85%
alternating field	0.5± 0.8	Rejected	99%

estingly, *M.bavaricum* in zero field and alternating field did not indicate extinction even over 6 months. In addition, at the end of alternating field, many small MTB, presumably spirilla or vibiros, were observed. These bacteria belonged to polar MTB but displayed frequent back-forward motion at the water edge. Two measurements were obtained and plotted in Figure 4.7a ('green cross symbols').

Cocci displayed large variation with population density 11.2± 4.4 cells/μl in Earth's field and 10.7± 4.4 cells/μl in zero field. The population difference between Earth's field and zero field can be tested by statistical analysis. According to two-sample Kolmogorov-Smirnov test with null hypothesis, based on two datasets: individual profiles in Earth's field and zero field (data in Table B.2), the null hypothesis (i.e. two datasets are same) is rejected at 85% confidence level. If using averaged population density in Earth's field and zero field (cocci in Figure 4.7b), the null hypothesis (i.e. two datasets are same) is rejected at 66% confidence level. Therefore, the two datasets (i.e. in Earth's field and zero field) can

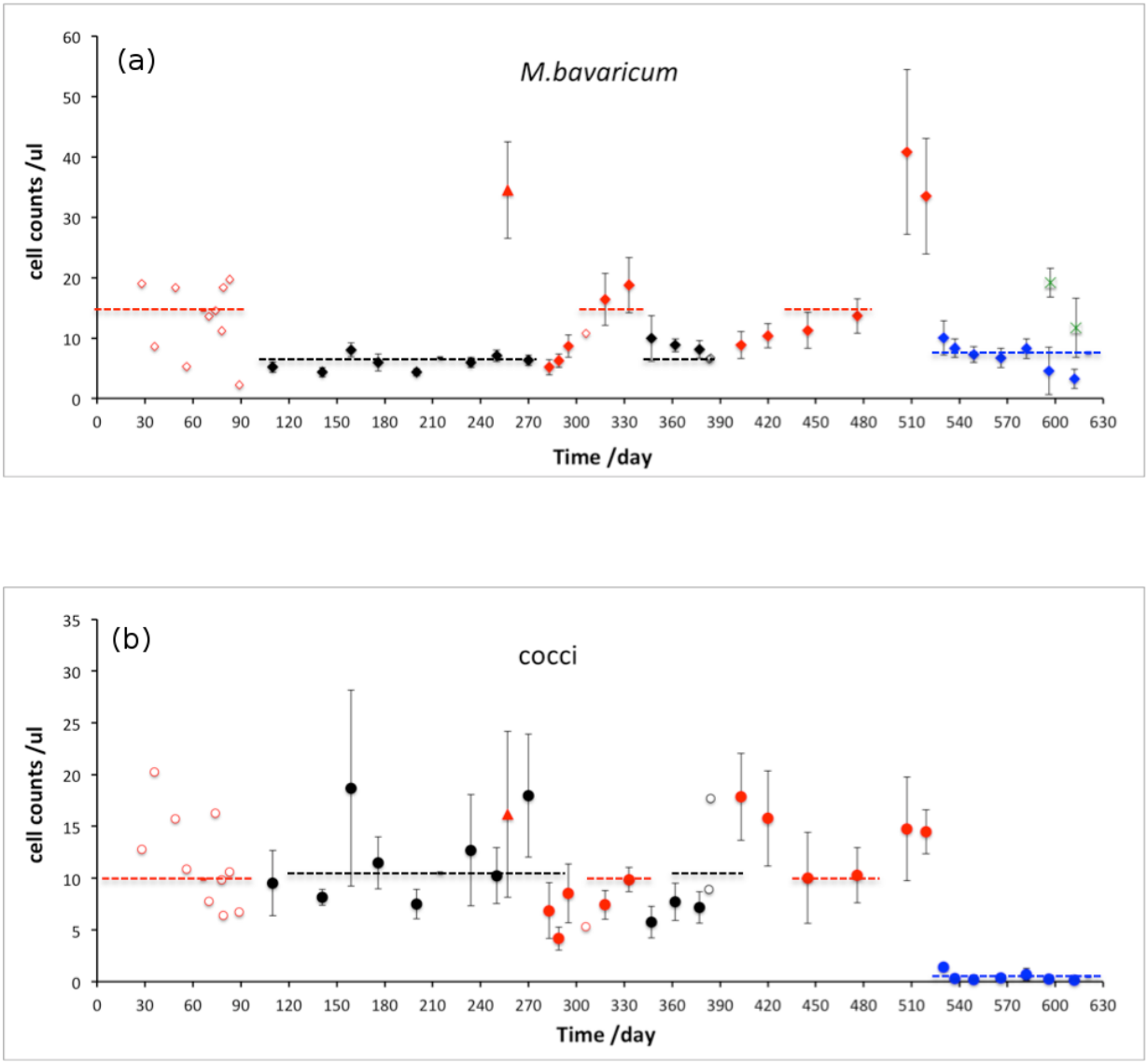

Figure 4.7: Population changes of *M.bavaricum* (a) and cocci (b) in Earth's field (red symbols), zero field (black symbols) and alternating field (blue symbols) as a function of time. Filled symbols represent averaged population density of 7 or 8 profiles (25 mm long) and smaller open symbols represent population density of single profile. Horizontal dashed lines refer to mean concentration in zero field (black), Earth's field (red) and alternating field (blue) (see data in Table 4.2). The data for these two plots are shown in Table B.1. Red filled triangle represents one sediment constantly in Earth's field. At the end of alternating field experiment, we detected many spirilla or vibrios MTB (hereafter termed spirilla) which were polar magnetotaxis MTB but displayed frequent back-forward motion at the water-air edge in a hanging drop assay. The population density is plotted in (a) with green cross symbols.

be seen same with high confidence level. Cocci in alternating field experienced dramatic decrease from 13.9±3.1 cells/μl in Earth's field to 0.5±0.5 cells/μl, almost extinction.

4.3.3 Vertical distribution

Vertical distributions of *M. bavaricum* and cocci from individual profiles taken in the geomagnetic field, in zero field, and in alternating field are shown in Figure 4.8. This figure gives an idea of the large scatter of bacteria concentrations in time and in space, with most values comprised between 5 and 50 cells/μl. Depth distributions are better recognizable on averages of all profiles corresponding to a given field condition (Figure 4.9).

The vertical distribution of cocci in the geomagnetic field is a unimodal function staring within ∼1 mm from the sediment-water interface, where oxygen concentration is ∼50% of saturation, and peaking at 5-15 mm depth, 3 mm below the level where O_2 drops below measurable levels. The maximum depth for the occurrence of cocci is ∼10 mm. *M. bavaricum* occurs over a slightly larger range of depths (i.e. 1- 25 mm), as also reported by Jogler et al. (2010); however, its depth distribution has a bimodal character, with a first, usually more pronounced peak at ∼6 mm depth, and a second, broader one, which is not always present in individual profiles (Figure 4.10), at 13-18 mm depth. Despite the presence of MTB at the sediment-water interface, MTB cells could never be detected in the water column. Overall, MTB occur within, and especially below the oxic-anoxic interface (OAI) as observed in other freshwater microcosms (Flies et al., 2005a), marine sediment (Petermann and Bleil, 1993), as well as eutrophic water columns (Kim et al., 2005; Moskowitz et al., 2008). In case of measurements in the water column, MTB were rigorously confined to depths below the deepest limit of the OAI, defined as where O_2 drops below measurable levels. The occurrence of MTB above this limit in sediment might be due to microscopic O_2 fluctuations, or to the disturbing effect of bioturbation.

Average profiles of cocci taken in zero-field are similar to profiles in the geomagnetic field and only slightly wider in the deeper range. The distribution appears slightly bimodal, due to some individual profiles with strongly bimodal character (Figure 4.10); however, this feature is not a systematic characteristic of cocci in zero field. The depth distribution of *M. bavaricum* does also not appear to change significantly in zero field, except for a clear, proportional concentration decrease at all depths (Table 4.2, Figure 4.9). Cocci profiles obtained in the alternating field are characterized by drastic decrease of cell concentration, with few cells occurring only in a limited depth range closer to the OAI (i.e. 1-13 mm). The depth distribution of *M. bavaricum*, on the other hand, becomes more evidently bimodal,

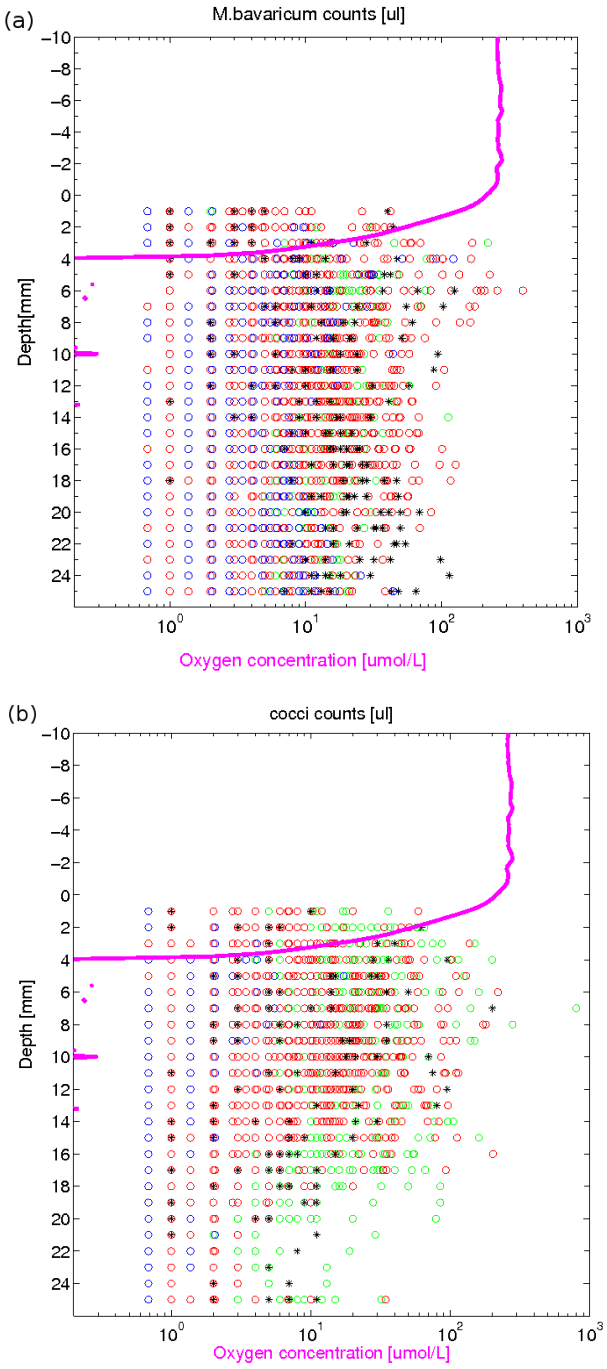

Figure 4.8: Vertical distribution of *M. bavaricum* (a) and cocci (b) by plotting all individual counts against depth. The water/sediment interface is at 0 depth. One oxygen profile is also plotted in the same coordinate.(○ in Earth's field; ○ in zero field; ○ in alternating field; ∗ reference sediment constantly in Earth's field)

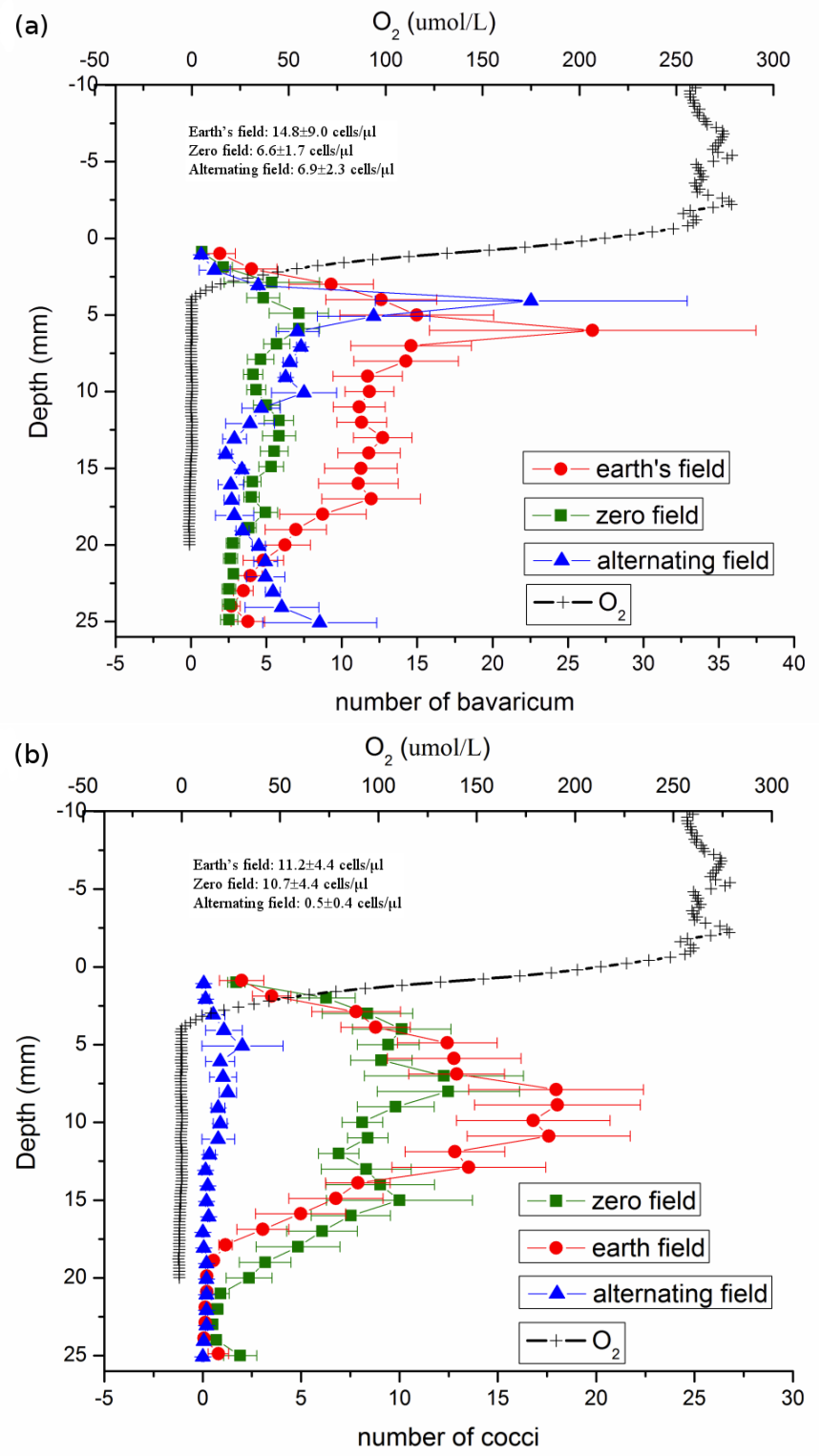

Figure 4.9: Vertical distribution (average profile) of *M. bavaricum* (a) and cocci (b) in Earth's field, zero field and alternating field. The population intensities in three field settings are inserted.

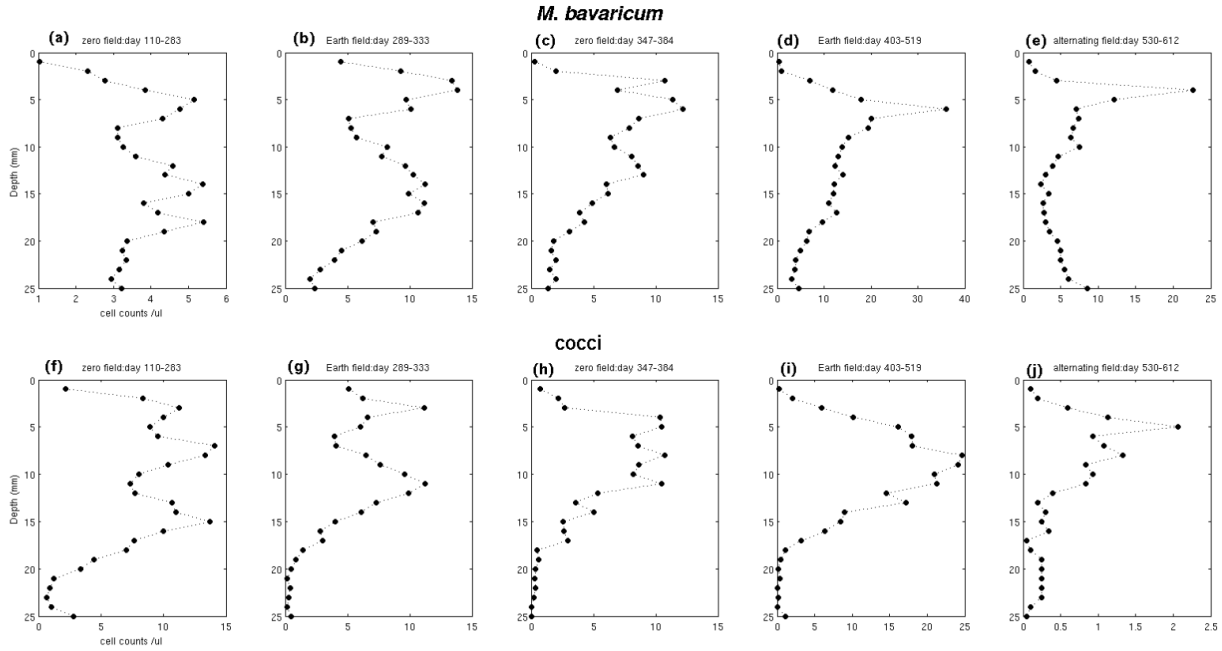

Figure 4.10: Overview of MTB vertical distribution (average profiles) in each field setting

with the upper peak moving up by 2 mm, and a lower peak forming at >24 mm depth. The cell concentration drops to almost zero at intermediate depths around ∼15 mm.

4.4 Discussion

4.4.1 Magnetotactic advantage

A clear effect of zero field conditions can only be observed with *M. bavaricum*, whose concentration, as inferred with the hanging drop assay, decreased by a factor ∼2 immediately after the beginning of the experiment. The mean concentrations appeared to remain constant over the ∼6 months experiment duration, without evidence for any further decrease. After re-establishing normal geomagnetic conditions, mean concentrations increased slowly during ∼1.5 months. A second experiment with zero-field conditions produced a similar concentration drop. Several explanations for these observations are possible, as summarized in the following models.

A) *True population decrease.* In this case, we assume that cell counts with the hanging drop assay reflect, or are at least proportional to, the real concentration of cells in sediment. The sudden concentration decrease at the onset of zero-field conditions,

and the slow recovery as the geomagnetic field was re-established, can be interpreted as the consequence of magnetotactic advantage removal. *M. bavaricum* might continue surviving indefinitely relying on chemotaxis as other bacteria do. However, the lack of preferred cell orientation produces a three-dimensional random walk pattern with substantially longer times and higher energies required to obtain macroscopic displacements in sediment.

B) *Cells become non-motile.* In this case, we assume that the true cell concentration of *M. bavaricum* in sediment did never change systematically, and that the apparent 50% drop observed with the hanging drops assay during zero-field conditions is due to the fact that 50% of the cells become non-motile. Slow apparent population recovery at the end of the experiment is due to an increasing number of cells becoming motile again. The reason for motility loss could be related to the lack of correlation between cell magnetotactic polarity (i.e. swimming direction), and change of environmental conditions. This concept can be clarified with the following example. Consider a cell with polar magnetotaxis under normal field conditions, which is located above the OAI, therefore exposed to high oxygen (HO) concentrations. In this case, according to the model of Frankel et al. (1997), the cell will be north-seeking (NS), swimming downward to greater depths until low oxygen (LO) concentrations are reached. If magnetic field is removed, the cell will still be NS, but will swim at random, continuing to remain exposed to HO conditions for much longer time. If unfavourable (in this case HO) conditions will persist beyond a certain amount of time – within which better conditions are usually found with magnetotaxis – the cell might enter into an 'emergency state' and become inactive, until casual events such as bioturbation will eventually bring it again into a more suited environment. Lack of a magnetic field will therefore increase the number of cells that enter into this state at any time. This hypothesis has an important drawback, because it assumes that the MTB population remains constant while 50% of individual cells are in such unfavourable conditions that they loose motility – but do not die. This endurance capability might be attributed to *M. bavaricum* on account of its unusual size and thick external membrane, the situation by which 50% of the cells loose motility appears as clear disadvantage.

C) *Degeneracy.* This scenario is based again on the assumption that the true MTB concentration in sediment remained constant, but some cells degenerate and no longer

synthesize magnetosomes. This kind of degeneracy is observed in old MTB cultures, where fewer and fewer cells have a measurable magnetic moment. In this case, unlike cultures, degeneracy is induced by the lack of a magnetic field: if a random mutation produces non-magnetic cells with intact chemotactic capabilities, these cells have exactly the same survival probability as their magnetic counterparts. An increased number of non-magnetic cells will result in an apparent decrease of MTB concentration in sediment, because these cells are no longer counted in the hanging drop assay.

Models B) and C), although rejecting a population decrease in zero-field conditions, actually imply a magnetotactic advantage. In B), loss of motility is induced by unfavourable conditions, which are a direct consequence of magnetotaxis lack. In C), it is assumed that non-magnetic cells suffer from some sort of disadvantages under normal field conditions, so that magnetotaxis is actually an advantage. Therefore, all three models for explaining the zero-field experiment imply that there is a magnetotactic advantage for *M. bavaricum* in sediment.

While the existence of a magnetotactic advantage for *M. bavaricum* in sediment is proved by the zero-field experiment, the apparent insensitivity of cocci to the cancellation of magnetotaxis is puzzling. A possible explanation for the difference between the two types of bacteria comes from the activity of individual cells within the preferred depth range in sediment. While MTB populations as a whole were already living at preferred depths at the beginning of the zero-field experiments, therefore not needing to move from there, individual cells within the same depth distribution might require changing depth according to their internal state. In this case, the observed depth distributions could be a dynamic equilibrium of cells moving up and down between upper and lower limits. This hypothesis is particularly well suited for explaining the bimodal distribution of *M. bavaricum* (Figure 4.9a), and the independent development of two peaks in newly formed microcosms (Figure 4.5 and Figure 4.6).

In fresh microcosms prepared from homogenized slurry, sediment taken at any depth contains particles with compositions corresponding to a wide range of depths in the original sedimentary column. Therefore, the same combination of nutrients can be found everywhere during initial formation of a new microcosm, and the only factor influencing the depth distribution of MTB is the oxygen gradient. Indeed, the initial depth distributions of cocci and *M. bavaricum* are identical and tightly concentrated at the OAI. This stage produces a first MTB 'bloom', and, in case of cocci, a second one, with an increase in total

population by a factor 2-4. Once the 'bloom' is over (day 44 in Figure 4.5) a second population peak develops at greater depths, ∼10 mm below the first one, without any change of the oxygen concentration profile. From this point on, the depth distributions of *M. bavaricum* and cocci extend ∼20 mm and 15 mm below the OAI, respectively. Especially in case of *M. bavaricum*, individual profiles taken in mature microcosm often display the shallower or the deeper population peak in a clear manner. These observations can be interpreted as population oscillations at given depths, with each peak signalling a localized 'blooming', or as a migration of cells within the usual range of living depths.

Vertical 'shuttling' could satisfy specific metabolic requirements related to substances that are usually not found at same depth in stratified environments (except for freshly prepared, homogenized microcosms). This hypothesis is particularly appealing for *M. bavaricum*, given the observation that some cells contain filled sulphur inclusions and appear darker than other 'empty' cells. Dissolved sulphides could not be detected in similar microcosms hosting *M. bavaricum* (Jogler et al., 2010); however, *M. bavaricum* could obtain sulphur from solid phases in deep sediment. In this case, the typical cycle of individual cells could consist in a 'deep' phase, where sulphur is accumulated inside the cell, followed by a 'shallow' phase where the incorporated sulphur is oxidized. One could in this case expect a correlation between the proportion of dark cells and depth in sediment, which could never be observed. However, in case of a stationary, dynamic 'shuttling' between two depth ranges, both ranges would contain equal amounts of empty cells (i.e. just arriving or just leaving) and full cells (i.e. just leaving or just arriving).

If the vertical 'shuttling' hypothesis applies to *M. bavaricum*, and to a lesser extent, or not at all, to cocci, it can explain the experimental results in zero field. Lack of magnetotaxis makes vertical 'shuttling' rely exclusively on chemotaxis, with increased energy costs, and it becomes obvious that MTB performing such 'shuttling' are more affected by zero-field conditions than MTB cells that tend to maintain a constant depth, such as cocci. This hypothesis, if verified, provides interesting insights into MTB metabolism.

4.4.2 Magnetotaxis polarity

Frankel et al. (1997) observed two different mechanisms by which magnetotaxis is combined with chemotaxis in which they called magneto-aerotaxis. The first mechanism, observed on the spirillum *M. magnetotacticum*, is called axial magneto-aerotaxis. Cells sense oxygen concentrations continuously while moving, thereby perceiving a temporal $[O_2]$ increase or decrease (temporal sensory mechanism). The swimming direction is almost instantaneously

controlled by the temporal trend in oxygen concentration: if $[O_2]$ increases, cells are leaving the OAI by swimming upwards, and the swimming direction is soon reversed. In this case, the cell will swim downwards and sense a $[O_2]$ decrease, in which case it will change swimming direction again. Axial magneto-aerotaxis is thus characterized by a continuous change of swimming direction around the OAI. Field polarity is indifferent, because cells determine their swimming direction on the basis of a sensed chemical gradient. Indeed, field reversal applied to a *M. magnetotacticum* culture did not change cell stratification. A second magneto-aerotaxis mechanism, called polar magneto-aerotaxis, was observed in a cultured coccus MC-1. In this case, cells sense $[O_2]$ and determine their swimming direction with respect to the magnetic field according to a threshold mechanism. As long as $[O_2]$ is above an upper critical threshold (HO), cells are presumably located above the OAI and will consistently swim along a direction that brings them further down. In the Northern hemisphere, this direction corresponds to the magnetic N, and bacteria will be North-seeking (NS). The opposite occurs in the Southern hemisphere. As cells continue to swim downwards, they eventually cross the OAI and, at a later point, a lower critical $[O_2]$-threshold (LO). As soon as sensed $[O_2]$ drops below this threshold, cells will reverse their swimming direction. In the Northern hemisphere, they become South-seeking (SS), because the magnetic South pole points upwards. This mechanism gives a consistent swimming direction with respect to the magnetic field for the HO and LO states. If magnetic field is reversed, HO-cells, which are already above the OAI, will swim upward, and LO-cells, which are already below the OAI, swim downwards. In both cases, cells swim away from the OAI and disperse, as observed with MC-1 in water.

Polar and axial magneto-aerotaxis can be distinguished in the hanging drop assay. Recalling that this assay is performed in normal atmosphere, and that the water drop is soon saturated with oxygen, polar magnetotaxis with MTB from the Northern hemisphere is manifested by consistent NS swimming, because cells are in HO state (i.e. 'above' the OAI). On the other hand, axial magnetotaxis, which is based on temporal sensing of oxygen gradients, does not produce a consistent swimming direction, because uniform saturation with O_2 produces a random signal that makes cells change their swimming direction continuously and oscillate back and forth. According to the hanging drop assay, both cocci and *M. bavaricum* perform polar magneto-aerotaxis. When these MTB reach the northern edge of the drop, they display different swimming pattern, i.e. 'ping-pong' motion for cocci and short excursions performed with backward swimming (chapter 6). These, however, appear to be tactile responses, since freely swimming cells are consistently

NS before reaching the edge of the water drop. Attempts to observe SS cells in their LO state, however, failed systematically (chapter 3), raising some questions about the validity of the polar magneto-aerotaxis model for uncultured bacteria.

Experiments in alternating field can probe the existence of polar and axial magneto-aerotaxis directly in sediment. Field direction switching will not affect axial magneto-aerotaxis as discussed above, while it transform magnetotaxis advantage into a disadvantage in case of polar magneto-aerotaxis. Our results with cocci exposed to an alternating field support the hypothesis that they perform polar magneto-aerotaxis, because cell number experienced a rapid drop close to a complete extinction. Interestingly, the residual cell population appears more concentrated around the OAI, while the opposite would be expected by cells swimming in the wrong directions, as seen with MC-1 in water (Frankel et al., 1997). This result can be interpreted in terms of better survival chances near the OAI. Again, as discussed for the zero-field experiment, the cell concentration drop could be apparent, if cells become non-motile as consequence of prolonged exposure to LO or HO states.

M. bavaricum, on the other hand, is affected by alternating fields in a similar manner as with zero fields in terms of population decrease. Interestingly, the bimodal nature of its depth distribution becomes more pronounced, with a $\sim$2 mm upward shift of the upper peak, and a $>$5 mm downward shift of the lower peak. The divergence of the two peaks can be explained with polar magneto-aerotaxis; however, the persistence of an apparently stable population indicates some fundamental differences with cocci. Two possibilities are discussed in the following:

A) After a field reversal, *M. bavaricum* cells move in the wrong directions, spreading the upper and lower population peaks. The situation is reversed during normal polarity periods, so that the divergence of the two peaks does not continue indefinitely. This situation, however, impedes successful cell migration over long distances. The persistence of a stable – although reduced – population might be due to the capability of *M. bavaricum* to endure adverse conditions for long periods of time. In this case, longer experiments in alternating field should be performed to see if the population finally declines.

B) *M. bavaricum* can 'switch' its polar magneto-aerotaxis under critical conditions, as explained with the following example. Consider a cell in its LO state in sediment from the Northern hemisphere. At some point, the cell becomes SS in order to move up in sediment. Its LO state will end soon under normal conditions. On the other

hand, the same action in a reversed field brings the cell further down in sediment and its LO state persists. At a certain point, the cell might switch its polarity mechanism, becoming NS in a LO state. Switched cells would therefore be able to use magnetotaxis in the reversed field. Because the geomagnetic field does not reverse during the lifetime of individual cells, the evolutionary advantage of such capability is unclear. A possible explanation is based on the presence of strong, localized chemical gradients, for example around decomposing organic matter. In this case, cells located right below such localized gradients would need to reverse their polar magneto-aerotaxis in order to successfully exploit such gradients.

4.5 Conclusions

The existence of a magnetotactic advantage in sediment has been confirmed for *M. bavaricum*, while ambiguous results have been obtained for cocci. On the other hand, cocci conform to our current knowledge about polar magneto-aerotaxis, while *M. bavaricum* appears capable of enduring periods of reversed field polarity, where magnetotactic advantage becomes a disadvantage. The main limitation of the experiments described in this chapter appears to be the incapability to track the actual displacement of individual cells in sediment. Temporal fluctuations in cell concentrations can always be interpreted as (a) true population fluctuations or (b) fluctuations in the proportion of motile or magnetic cells. Furthermore, changes in depth distribution might result from cell migration or from cell multiplication/death at given depths. Nevertheless, the evolution of MTB populations and depth distributions in freshly prepared microcosms strongly support the hypothesis that individual cells, especially in the case of *M. bavaricum*, might 'shuttle' within a certain depth range in order to satisfy different metabolic requirements.

The interpretation problems raised here are addressed in the next chapter, where MTB migration in sediment is specifically investigated.

Chapter 5

Magnetotactic bacteria migration in sediment and interaction between magnetotaxis and chemotaxis

Abstract

Current knowledge on MTB motility is based on observations performed in water, mainly with cell cultures. Several assumptions in existing models of magnetotaxis are not applicable to sedimentary environments. For example, magnetotactic advantage is not based on a high degree of cell alignment in the geomagnetic field, since mean alignments of only ∼1% have been observed in sediment (chapter 2). Hanging drop assays suggest polar magnetotaxis for two types of MTB occurring in our microcosms, namely unidentified cocci and *M. bavaricum*; however, the behavior predicted by polar magnetotaxis under anoxic conditions could never be observed (chapter 3), questioning the correctness of polar magnetotaxis models for those MTB populations. Finally observation of MTB populations in sediment during zero-field experiments pointed to contradictory results: while cocci appeared unaffected by the lack of magnetotaxis, *M. bavaricum* cell concentration decreased but did not disappear after ∼6 months. On the other hand, periodic reversals of the magnetic fields drove cocci almost into extinction, but had a similar effect on *M. bavaricum* as zero-field condition. Analysis of the depth distribution of MTB during these experiments and during stabilization of freshly prepared microcosms gave indirect hints to a migration of cells within a certain depth range below the OAI. A series of experiments specifically designed to assess cell migration in sediment under a variety of chemical and magnetic conditions are presented here. Results indicate that active cell migration occurs

under normal conditions in sediment, according to current models of magneto-aerotaxis. If magnetotactic assistance to vertical migration is suppressed in zero-field or horizontal field experiments, displaced cells of *M. bavaricum* are capable of reaching suitable depths with chemotaxis, while the same capability was not observed on cocci. Furthermore, *M. bavaricum* seems capable of adapting to a reversed magneto-aerotaxis polarity, contrary to the case of cocci. These results confirm current magneto-aerotaxis models for MTB populations in sediment, although the response to anoxic conditions might not be controlled by oxygen concentration alone. Fundamental differences exist between the magnetotactic behaviors of *M. bavaricum* and cocci, which might reflect different adaptation strategies.

5.1 Introduction

Magnetotactic bacteria can be imagined as living compass needles that passively align with the geomagnetic field. As a result, they swim straight along magnetic field lines in water, instead of performing a random walk like other chemotactic bacteria (Berg and Brown, 1972): this phenomenon is called magnetotaxis (Blakemore, 1982). Cell alignment in water, as induced by typical geomagnetic field intensities, is almost perfect. In sediment, cell alignment is heavily disturbed by mechanical interactions with other particles, so that MTB are characterized by a mere $\sim$1% alignment with the geomagnetic field (chapter 2). Nevertheless, this alignment is sufficient to provide MTB cells with a clear preferred direction when moving over $>$1 mm distances in typical sediment. Except for places on Earth located at or near the magnetic Equator, geomagnetic field lines are inclined, so that moving along those lines produces a change in depth, which, in case of horizontally stratified environments, is accompanied by exposure to different environmental conditions. Because the preferred environment of MTB is the oxic-anoxic interface (OAI), where dissolved oxygen concentrations drop below 1% of saturation, magnetotaxis can be used as an efficient tool for reaching the OAI, and staying within a certain depth range (Flies et al., 2005a; Simmons et al., 2004). In order for magnetotaxis to accomplish this task, the swimming direction of cells needs to be changed according to the chemical environment. The combination of magnetotaxis and chemotaxis, i.e. the ability to change swimming direction according to the presence of chemical attractants or repellants (Adler, 1975), is called magneto-aerotaxis (Frankel et al., 1997).

The chemotactic response of MTB is not limited to oxygen (aerotaxis): sensitivity to light (phototaxis, Chen et al. 2011; Shapiro et al. 2011), redox potential (Simmons et al.,

2006; Zhang et al., 2010), temperature (thermaltaxis, Chen et al. 2011) has been observed in some MTB. On the other hand, the correlation of MTB depth distributions in sediment and chemical conditions (e.g. O_2, pH and S^{2-}) is not always obvious (Bazylinski et al., 1995; Jogler et al., 2010; Kim et al., 2005; Moskowitz et al., 2008; Paasche Øand Larsen, 2010; Petermann and Bleil, 1993; Simmons et al., 2004). The OAI appears to provide consistently an upper limit for MTB populations (Flies et al., 2005a; Petermann and Bleil, 1993), however, correlations with other substances relevant for bacterial metabolism (NO_3^-, Fe^{2+}) are elusive (Jogler et al., 2010). Furthermore, fluctuations in depth distributions can be observed in apparently stationary environments with no changes of the oxygen gradient (chapter 4). The complexity of chemotactic responses makes experiments performed in aqueous conditions (e.g. Smith et al., 2006) hardly comparable with sediment. This might explain why the polar magnetotaxis under anoxic conditions could never be observed under the optical microscope (chapter 3). Another limitation of current magnetotaxis models is the difficulty in explaining the magnetotactic advantage of MTB at the geomagnetic Equator, where directed swimming along the field lines does not produce any benefit in horizontally stratified environments.

In order to obtain a better insight of magnetotaxis and chemotaxis, as they occur in undisturbed sediment with the original richness of chemical and tactile stimuli, we designed a series of experiments where different combinations of favorable and unfavorable conditions are reproduced, and monitored the evolution of natural populations of cocci and *M. bavaricum*.

5.2 Definitions

In order to keep an overview of all experiments described in this chapter, we introduce some definitions that are consistently used for experimental description and discussion.

5.2.1 Definitions related to polar magnetotaxis

The combination of magnetotaxis (MT, i.e. the ability to swim with a consistent bias parallel to the geomagnetic field) and chemotaxis (specifically aerotaxis) has been called magneto-aerotaxis (M-A, Frankel et al. 1997). Here, we use the concept of M-A to describe combinations with all forms of chemotaxis. While the polarity of the geomagnetic field is indifferent for axial M-A, it plays a fundamental role in case of polar M-A, which is apparently the form of magnetotaxis that characterize cocci and *M. bavaricum*. In polar

M-A, the swimming direction of cells with respect to the magnetic field vector is determined by chemical conditions through a threshold mechanism (Frankel et al., 1997). Here, we group all chemical conditions into three categories according to the corresponding depth in sediment with respect to the optimal living depth. These categories are: (1) high-oxygen conditions (HO), referring to positions in sediment above the optimal depth, (2) normal conditions (NO), referred to positions within the optimal depth range, and (3) low-oxygen conditions (LO), referring to positions in sediment below the optimal depth. According to the polar M-A model, the swimming direction of cells is determined by their position (HO, NO, LO) in sediment. HO cells are expected to move downward, which, for the Northern hemisphere, means that the swimming direction is parallel to the field vector. HO cells are easily observed in the hanging drop assay because of oxygen saturation, and the swimming direction points to the magnetic North (North-seeking cells, NS). In the Southern hemisphere, the situation is reversed, and HO cells are South-seeking (SS). On the other hand, LO cells are expected to move upward, which, for the Northern hemisphere, means that the swimming direction is antiparallel to the field vector, (i.e. SS).

Because of the different dependence of the swimming direction on the magnetic field in the two hemispheres, we denote with 'correct magnetotaxis' all situations where the field has the correct polarity with respect to the hemisphere that MTB represent: our bacteria, which evolved in the Northern hemisphere, perform 'correct magnetotaxis' in all experiments where the magnetic field points downwards. If the field direction is reversed, making MTB swimming incorrectly for their biological requirements (e.g. LO cells swimming downwards), we speak of 'incorrect magnetotaxis'. Incorrect magnetotaxis is realized in our experiments by exposing microcosm to upward-pointing magnetic fields.

In analogy with correct and incorrect magnetotaxis we introduce the concept of 'indifferent magnetotaxis' to denote magnetotaxis in horizontal fields, and 'no magnetotaxis' to denote experiments performed in zero field. The term indifferent is referred to the lack of magnetotaxis effectiveness when the chemical stratification is parallel to the field.

5.2.2 Definitions related to the magnetic moments of cells

As already reported by Blakemore (1975, 1982), MTB with polar magnetotaxis are characterized by a well defined swimming direction in the hanging drop assay: for example, cocci and *M. bavaricum* in our microcosms are consistently NS, and only very few SS cells are occasionally seen. The proportion of NS and SS cells is larger than 1000:1. SS cells are believed to form by chance and play an important role in allowing polar MTB survive

the many geomagnetic field reversals occurred over geologic epochs. The use of NS and SS terms in defining the polarity of MTB cells is clear within the context of microscope observations, where cells are systematically in a HO state, but becomes confusing when applied to the sediment, since LO cells are expected to display opposite swimming directions. Therefore, we call 'normal MTB' (N) those cells from the northern hemisphere that are NS in the hanging drop assay: with other words, the vast majority of cells found in natural sediment. The few cells showing opposite behaviour in the hanging drop assay are called 'reversed MTB' (R). This definition avoids misunderstandings in interpreting microcosm experiments performed in reversed fields. In the case of a microcosm from the northern hemisphere exposed to a downward-pointing magnetic field, all N cells perform correct magnetotaxis, and all R cells perform incorrect magnetotaxis (which is a reason for the few numbers of R cells). If the same microcosm is exposed to an upward-pointing magnetic field, all N cells perform incorrect magnetotaxis, and all R cells perform correct magnetotaxis. Finally, if the microcosm is exposed to a horizontal field, magnetotaxis is indifferent.

The nearly complete lack of naturally occurring R cells in our microcosms can be exploited for tracing cell displacements. This is done by artificially creating a large population of R cells. R cells are easily created by reversing their magnetic moment with a strong magnetic pulse, as explained in chapter 2. Reversing the magnetic moment makes a NS cells in the hanging drop assay becoming SS while being in HO state: this is the definition of an R cell in the northern hemisphere. If R cells are created only at specific depths in sediment, their migration is easily tracked by observing R cells in surrounding sediment. R cells therefore serve as 'tracers' of magnetotaxis or chemotaxis.

5.3 Experiments and methods

We concentrate our investigations on two wild-type MTB occurring in Lake Chiemsee (southern Germany): *M. bavaricum*, a large ($\sim$10 μm long), rod-shaped bacterium with $\sim$40 μm/s swimming velocity in water (Spring et al., 1993), and round cocci ($\sim$1 μm diameter) with swimming velocities of up to 1 mm/s in water (Cox et al., 2002). See chapter 2 for a detailed description. All experiments have been performed with aquaria or microcosm prepared with surface sediment from Lake Chiemsee, which has been collected with a bottom grab sampler. Freshly collected sediment was transferred into several 30×20×20 cm glass aquaria in the laboratory, which served as sediment source for all experiments

described here. Aquaria were allowed to stabilize for few months under constant laboratory conditions. About 3-5 cm water was kept above the sediment and evaporation was compensated by adding distilled water.

Microcosms have been prepared by transferring sediment slurry from aquaria into 1 L glass bakers. The slurry was thoroughly stirred and allowed to rest for at least 1 week in order to rebuild a stationary stratification hosting stable MTB populations. The evolution of chemical gradients and MTB populations during the stabilization phase is described in chapter 4.

5.3.1 Experiments on horizontal migration

Horizontal migration experiments have been performed in a 30×20×20 cm aquarium denoted with H1 (Figure 5.1). A 10 cm wide sediment band on one side of the aquarium was subjected to several ∼0.1 T magnetic pulses, imparted with a coil (see chapter 2) placed within few mm from the sediment-water interface. The coil was moved all over the sediment band, in order to expose the uppermost ∼25 mm of sediment to a sufficiently strong field capable of reversing the magnetic moments of favourably oriented MTB cells. As explained in chapter 2, magnetic moments of MTB in sediment are almost randomly oriented, so that only ∼12% of all cells are reversed by a single pulse. Repeated application of pulses can increase the proportion of R cells to ∼50%. At the end of the pulse treatment described above, ∼50% of R cells could be found in the uppermost 25 mm of treated sediment, while only N cells occurred in remaining parts of the aquarium. The boundary between sediment containing R cells and 'normal' sediment is not sharp, due to the dimensions of the pulse coil, and a ∼2 cm wide transition zone must be taken into account.

The aquarium was subsequently placed at the centre of a Helmholtz coil system producing a homogeneous, sub-horizontal magnetic field pointing to the side of the aquarium containing R cells. The field had an intensity of 133 μT and was pointing slightly downwards with an inclination of 17°(Figure 5.1). The expected result of this experiment is a lateral migration of polar MTB. Specifically, R cells in HO state, which could initially be found only in the pulsed area, are expected to migrate towards the remaining part of the aquarium, in which case they would be detected by regular sediment sampling near the pulsed area.

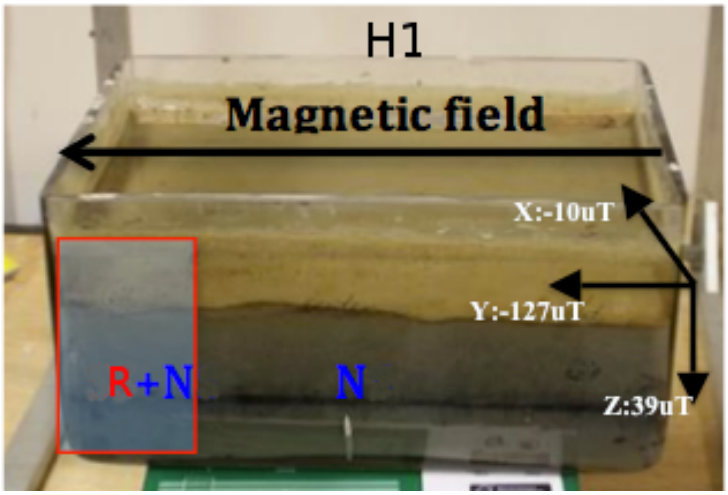

Figure 5.1: Sediment in horizontal field. The left part (red rectangular area.) about 10 cm wide of the aquarium containing MTB-bearing sediment was subject to pulse treatment many times to convert N-cells into R-cells while the other part was untreated (see text). This sediment was placed in a horizontal field (field direction and intensity was inserted) pointing to the R-cell side. A downward inclination 17°was induced.

5.3.2 Experiments on vertical migration

Vertical migration experiments have been performed on 8 microcosms (labelled as M1-M8) prepared so, that they consist of two sediment layers separated by a sharp boundary. At the beginning of each experiment, one of the two layers (alternatively the bottom one or the top one) contains R cells, and migration of those cells in the other layer under different field conditions, i.e.: upward and downward pointing fields for correct and incorrect magnetotaxis of R cells, and horizontal fields or zero fields for indifferent magnetotaxis, is closely monitored. R cells are tracked as migration tracers, and the evolution of N and R cells in time is used as an indicator for beneficial or adverse effects of magnetotaxis.

Microcosms have been prepared with the following procedure:

Microcosms with R cells on top. The starting point is a stabilized microcosm, and an aquarium where sediment has been treated with pulsed fields in order to obtain ∼50% R cells, similarly to the aquarium preparation described in section 5.3.1. Superficial sediment containing R cells has been taken from the aquarium and transferred to a sieve. Sediment slurry in the sieve has been allowed to 'rain down' in the water column of the microcosm, and gently deposits over the existing sediment. If this preparation step is performed carefully, the interface with existing sediment remains sharp. Between 15 and 25 mm sediment containing R cells has been deposited in this way.

Microcosms with R cells on the bottom. In this case, a stabilized microcosm has been repeatedly exposed to pulsed fields, as with the aquarium described in section 5.3.1, in order to obtain ∼50% R cells in the uppermost 25 mm of microcosm sediment. Untreated sediment containing exclusively N cells has been subsequently deposited on the top of the

existing sediment with the same system used to prepare microcosms with R cells on the top. The final result was a microcosm where sediment contains R cells below a sharp boundary located 25-28 mm below the sediment-water interface.

The top layer of all microcosms was initially saturated with oxygen, due to the preparation method, however, the usual oxygen gradient developed within few days (data not shown), because oxygen is rapidly consumed in sediment. Therefore, MTB in the bottom layer enter soon into a LO state, being >25 mm further down with respect to the OAI. On the other hand, at least some *M. bavaricum* cells in the thinnest top layer (15 mm) are in a HO state. R cells in HO and LO states are expected to migrate down or up, respectively, crossing the sharp boundary between the two sediment layers and appearing in the layer that originally did not contain any R cells. This vertical migration can be influenced or even prevented by different magnetotaxis configurations. Exposing microcosms to an upward-pointing magnetic field provides the correct setup for R cells magnetotaxis: therefore, migration corresponding to HO and LO states of R cells (i.e. SS and NS, respectively) should be observed. On the other hand, incorrect magnetotaxis is obtained for R cells if the microcosm is exposed to a downward-pointing magnetic field, and indifferent magnetotaxis is obtained with horizontal field or no magnetotaxis with zero field. Field setups are always referred to R cells, because these are the only cells that initially occur in one layer but not the other, and allow migration tracking.

5.3.3 Summary of experimental setups

The experimental setups for the horizontal migration (H1) and the vertical migration (M1-M8) experiments, as well as the experiments in zero field (Aquarium 1) and alternating field (Aquarium 2) described in chapter 4 are summarized in Table 5.1. The first 5 columns of this table summarize the experimental setup, followed by a column where experimental results are predicted in accordance with the M-A model of Frankel et al. (1997). These predictions (referring to R cells whenever it applies) are compared with experimental observations of migration behaviour, and changes in total population. The temporal evolution of *M. bavaricum* and cocci populations, as well as the detection of magnetotaxis-assisted migration, or chemotactic migration without magnetotaxis (vertical migration in horizontal fields or in zero fields), are summarized in the last three columns.

MTB populations in vertical sediment profiles, obtained with the method described in chapter 4, have been measured at the beginning of the experiment, i.e. within 1-2 days from microcosm preparation, and after 10-14 days (M1-M8) or longer periods of time for

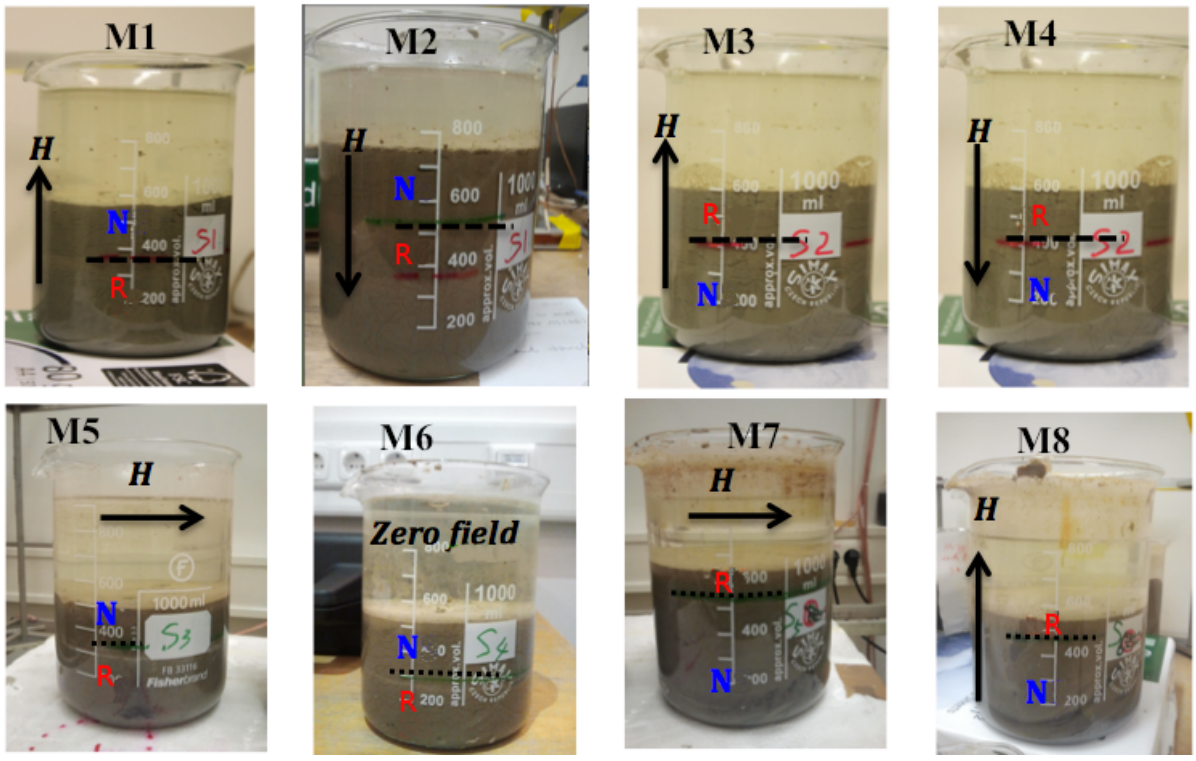

Figure 5.2: Overview of experiments on vertical migration. 8 microcosms (1L glass bakers) were prepared according to the description in section 5.3.2. Magnetic field direction is marked by black arrow with sign "H". The boundary between top and bottom sediments is marked by black dashed line. The location of R-cells and N-cells is marked in red "R" and blue "N" respectively.
From left to right and from top row to bottom row, M1: R cells in bottom layer, correct magnetotaxis; M2: R cells in bottom layer, incorrect magnetotaxis; M3: R cells on top, correct magnetotaxis; M4: R cells on top, incorrect magnetotaxis; M5: R cells in bottom layer, horizontal field (indifferent magnetotaxis); M6: R cells in bottom layer, zero field (no magnetotaxis) ; M7: R cells in thin top layer, horizontal field (indifferent magnetotaxis); M8: R cells on thin top, correct magnetotaxis. Magnetic field intensity (except the zero field), including vertical field and horizontal field, is identical with present geomagnetic field in mid latitude ($\sim$ 50 μT). M6 was put in a magnetically shielded room where residual magnetic intensities of three components were: 0.33 μT, -0.05 μT and $\pm$0.11 μT, close to "zero field".

the other experiments (i.e. H1) and the experiments described in chapter 4.

5.4 Results

5.4.1 Horizontal migration (H1)

R cells of *M. bavaricum* or cocci could not be detected outside of the pulsed sediment area after four months. Knowing the migration speed of MTB cells from vertical migration experiments (see section 5.4.3-5) to be >0.3 mm/day, we expect R cells in HO state to have moved horizontally by >36 mm if they were continuously swimming, so that at least some R cells would have definitively abandoned the pulsed area. The fact that this was not the case implies that polar MTB must be able to stop swimming and/or reverse their magnetotactic behaviour after some time. Short stops have been observed by following *M. bavaricum* cells under the optical microscope while swimming into an area with increased sediment particle density. Some cells came at rest after hitting a sediment particle, and resumed swimming if the field was reversed for a short time, probably in response to a tactile stimulus created by cell rotation during field reversal.

Figure 5.3 shows sediment profiles taken in the pulsed area at the beginning of the experiment and after four months. The total population of N and R cells of *M. bavaricum* decreased significantly during this time (Figure 5.3a), similarly to what observed in zero field (chapter 4). On the other hand, no decreasing population trend can be recognized for cocci (Figure 5.3b). Again, similar results have been obtained in zero field.The fraction of R cells is not expected to change significantly with time, because horizontal fields do not favour N or R cells ('indifferent' magnetotaxis). Indeed, the fraction of R cells of *M. bavaricum* did not decrease over four months, although an interesting downward migration can be observed (Figure 5.3c). On the other hand, R cells of cocci have not been found after four months (Figure 5.3d) while N cells of cocci increased by about two times.

5.4.2 R cells on top, correct magnetotaxis (M3)

This experiment reproduces the normal conditions existing in the Southern hemisphere. In this case, R cells would be the 'normal' MTB expected in sediment, except for the fact that they have been created by switching their magnetic moment, instead of naturally evolving in environments where the magnetic field points upwards. Because R cells are located in the uppermost 25 mm, which is the normal depth range of MTB in our microcosms,

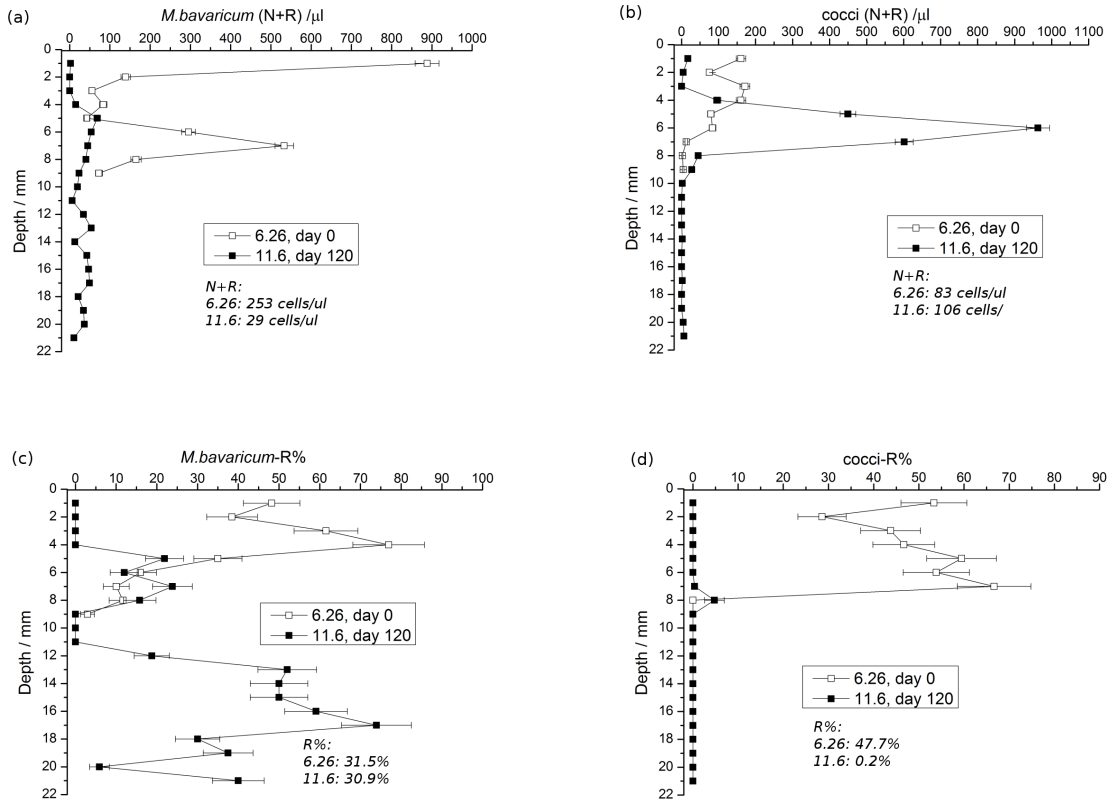

Figure 5.3: MTB profiles of aquarium H1 taken over the pulsed area immediately after pulse treatment (open squares) and after four months (filled squares). (a) N and R cells of *M. bavaricum*, (b) N and R cells of cocci, (c) fraction of R cells of *M. bavaricum*, and (d) fraction of R cocci. The initial depth range of R cells is limited by the size of the pulsed field coil, whose field intensity declines with increasing distance from coil.

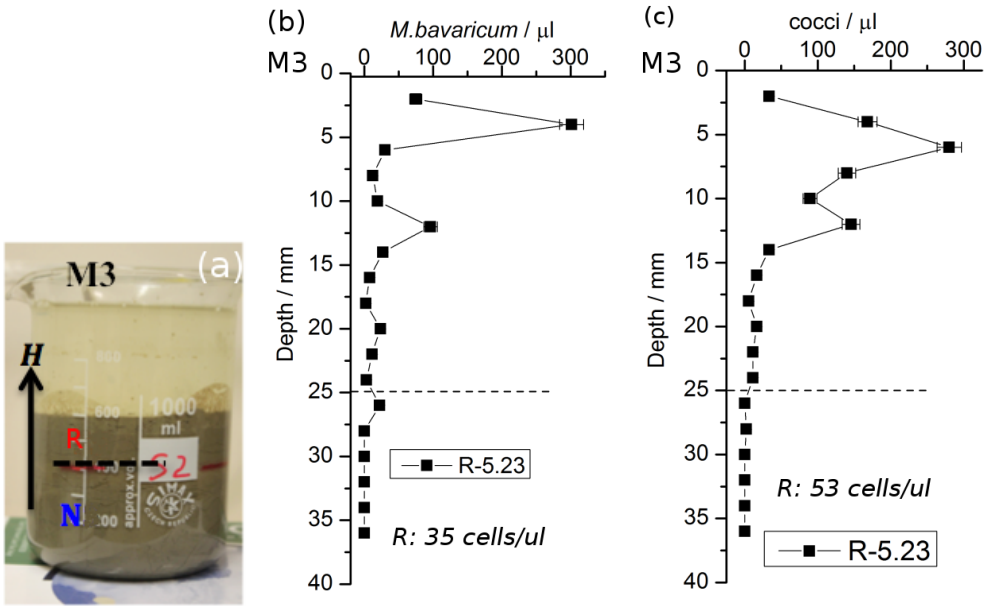

Figure 5.4: (a) Microcosm M3, with boundary between sediment layers 25 mm below the sediment-water interface marked with a dashed line. (b) Depth distribution of R cells of *M. bavaricum* after 14 days from microcosm preparation. (c) Same as (b), for R cells of cocci.

vertical migration is not expected. At the same time, magnetotaxis is incorrect for N cells, whose number is expected to decline with time.

The vertical distribution of R cells after 14 days is shown in Figure 5.4. Practically no cells have been detected below 25 mm and few cells detected near the interface between the two layers might have been passively moved by bioturbation. On the other hand, N cells of both *M. bavaricum* and cocci were hardly detectable after 14 days (not shown). This experiment confirms the prediction of M-A. Furthermore, R cells created by reversing their magnetic moment are undistinguishable from R cells evolved in an environment corresponding to the Southern hemisphere.

5.4.3 R cells on top, incorrect magnetotaxis (M4)

This is the same case as section 5.4.2, with the only difference that the magnetic field points downwards. In fact, microcosm M3 has been used in this experiment, after reversing the direction of the magnetic field. The initial condition of M4 is therefore depicted by Figure 5.4, with no N cells and a population of R cells with normal depth distribution. In this case, R cells occur in the right range of depths, but perform incorrect magnetotaxis.

The M-A model predicts that the vertical distribution of R cells tends to spread out, accompanied by a population decline.

Indeed, *M. bavaricum* decreased markedly, while cocci became practically extinct in 7 days (Figure 5.5). The decrease in *M. bavaricum* concentration was particularly evident in the topmost 10 mm, and can be explained by R cells in HO state, which move upwards because of incorrect magnetotaxis and become exposed to an even more oxic environment. R cells of *M. bavaricum* have been detected in the bottom layer, indicating a downward migration that can be explained in a similar manner by incorrect magnetotaxis of LO cells. M-A predictions are overall confirmed, and suggest that cocci succumb more rapidly to incorrect magnetotaxis than *M. bavaricum*

5.4.4 R cells in bottom layer, correct magnetotaxis (M1)

This experiments aims at testing the upward migration of cells in LO state by correct magnetotaxis. R cells in microcosm M1 are initially confined in the bottom layer below 25 mm depth and exposed to an upward-pointing field (Figure 5.6). All R cells are expected to be in LO state and would therefore move upward according to the M-A model. This would be the first observation of magnetotaxis by LO cells, which has never been possible under the microscope (chapter 3). Vertical profiles of R cells measured after 7 days show that cells have fully migrated inside the upper layer, reaching the usual vertical distributions expected for *M. bavaricum* and cocci. Migration has occurred without any population decrease, demonstrating that LO cells can move several cm in sediment under unfavourable conditions. The minimum migration velocity implied by this experiment is $\sim$3.6 mm/day, but might actually be much higher, since profiles have not been measured before 7 days from experiment beginning. Much higher velocities, of the order of 10 mm/day, are predicted by calculations based on the mean alignment of MTB in sediment (see chapter 2).

5.4.5 R cells in bottom layer, incorrect magnetotaxis (M2)

Microcosm M2 was prepared from M1 after adding a new, 25 mm thick sediment layer containing only N cells. This experiment reproduces the same situation as in section 5.4.4, with R cells confined to $>$25 mm depth. However, the field points now downwards, so that R cells, which are in a LO state, would migrate further down according to the M-A model. A strong population decrease is therefore expected. In any case, no R cells are expected to migrate in the upper layer.

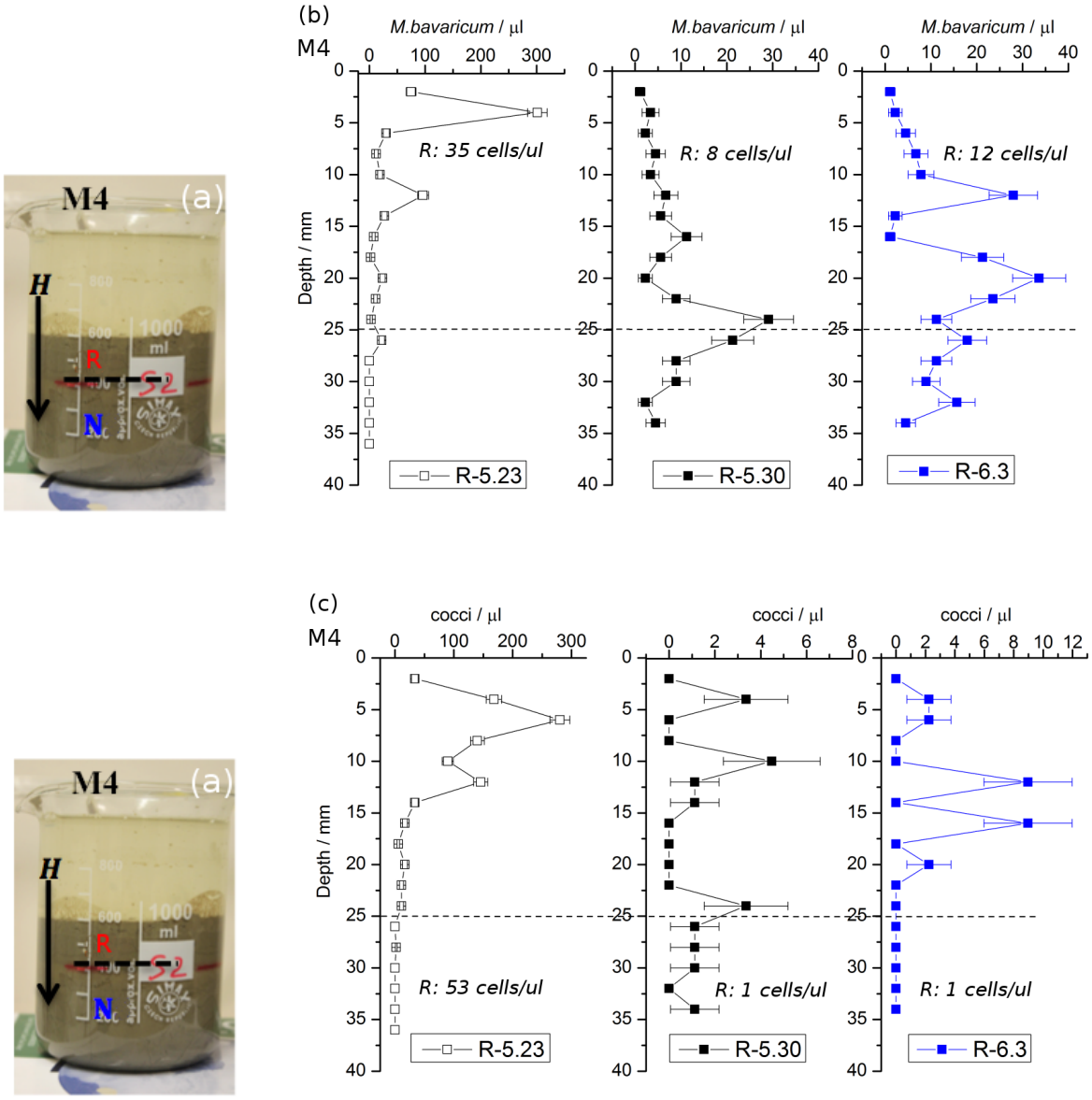

Figure 5.5: (a) Microcosm M4, identical to M3 but exposed to a downward-pointing magnetic field from the day 5.27. (b) Vertical profile of *M. bavaricum* (R cells) at the beginning of the experiment (left, coinciding with Figure 5.4b), and after 3 and 7 days (middle and right). (c) Same as (b) for R cells of cocci.

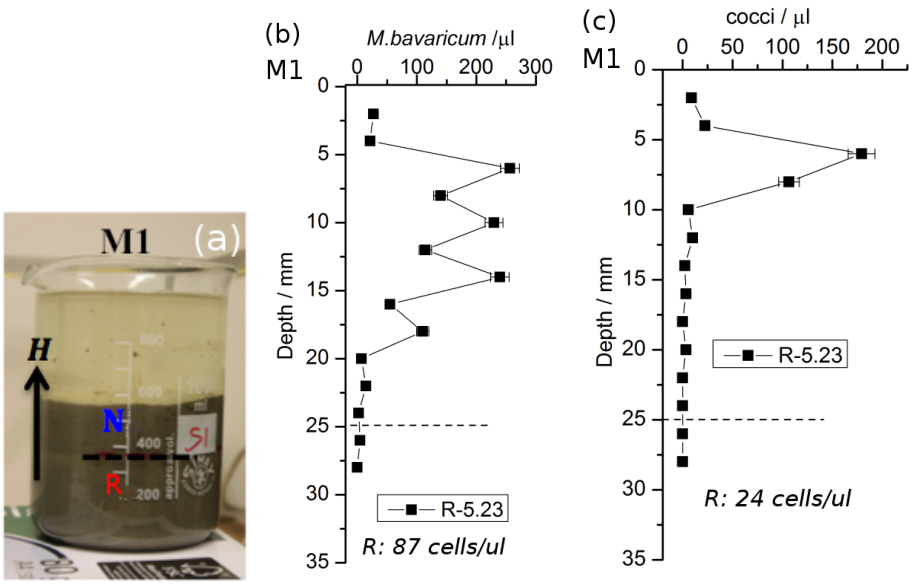

Figure 5.6: (a) Microcosm M1, with boundary between sediment layers 25 mm below the sediment-water interface marked with a dashed line. (b) Vertical profile of R cells of *M. bavaricum*, initially confined within the bottom layer, after 7 days exposure to an upward pointing magnetic field. (c) Same as (b) for R cells of cocci.

MTB profiles taken after 4 days (Figure 5.7), revealed the first surprise of this experiment series: R cells of *M. bavaricum* partially migrated inside the upper layer and the total population decreased slightly. This result implies that LO *M. bavaricum* moved in the opposite direction with respect to M-A predictions. Because the predicted behaviour of LO cells has been observed under correct magnetotactic conditions (section 5.4.4), this experiments demonstrates the capability of *M. bavaricum* to switch its polar magnetotaxis response when subjected to incorrect magnetotaxis. With other words, R cells in LO state have spontaneously converted into N cells, conforming the existing field conditions. The slight population decrease might be attributed to the time required for this adaptation to occur. R cocci, on the other hand, disappeared after 4 days, demonstrating their incapability to cope with incorrect magnetotaxis.

5.4.6 R cells on thin top, correct magnetotaxis (M8)

This experiment is in principle identical to the one described in section 5.4.2, with the only difference that the R-cell-containing top layer has been made as thin as possible (15 mm, Figure 5.8a), in order to capture the migration of *M. bavaricum* cells in HO state, assisted by correct magnetotaxis. After 14 days, high concentrations of R cells could be

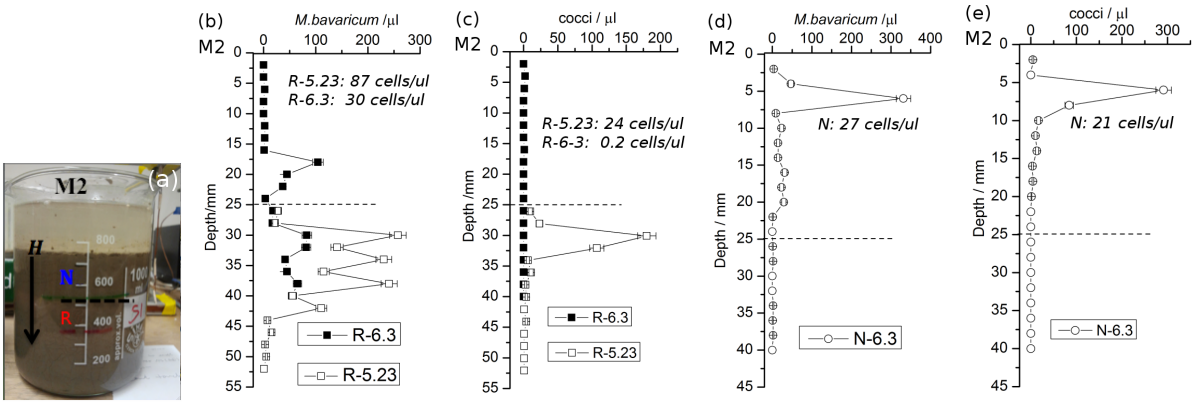

Figure 5.7: (a) Microcosm M2, obtained from M1 by adding 25 mm of sediment containing exclusively N cells. The boundary between sediment layers 25 mm below the sediment-water interface is marked with a dashed line. From 5.30, M2 was moved in downward field. (b) Vertical profile of R cells of *M. bavaricum* at the beginning of the experiment (empty squares) and after 4 days (solid squares). (c) Same as (b) for R cells of cocci. (d) Vertical profile of N cells of *M. bavaricum* after 4 days. (e) Same as (d) for N cells of cocci.

detected in vertical profiles down to 20 mm, and few cells have been found down to 27 mm. This experiment demonstrates the vertical migration of HO cells, as predicted by the M-A model. The concentration of N-cells, on the other hand, decreased significantly, due to incorrect magnetotaxis.

5.4.7 R cells in bottom layer, horizontal field (M5)

Microcosm preparation was identical to M1 (section 5.4.4). R cells in LO state inside the bottom layer are exposed to a horizontal field (Figure 5.9a). In this case, magnetotaxis does not provide any preferred direction for vertical migration (indifferent magnetotaxis). The M-A model predicts that LO cells would swim horizontally, with no systematic vertical migration, and cell concentration would decrease with time, due to unfavorable conditions. Therefore, we expect the initial vertical distribution of R cells to spread out slightly and decrease.

Cocci, though being abundant at the beginning of the experiments, disappeared completely after 14 days, regardless of N or R. R cells of *M. bavaricum*, on the other hand, migrated into the top layer, as if a vertical field was present. Because the horizontal field provides no bias for vertical displacement, the migration of R cells must be attributed to chemotaxis alone, in which case cells must have been able to reverse their swimming direction, and therefore polarity, several times while being still in LO state. This is because the

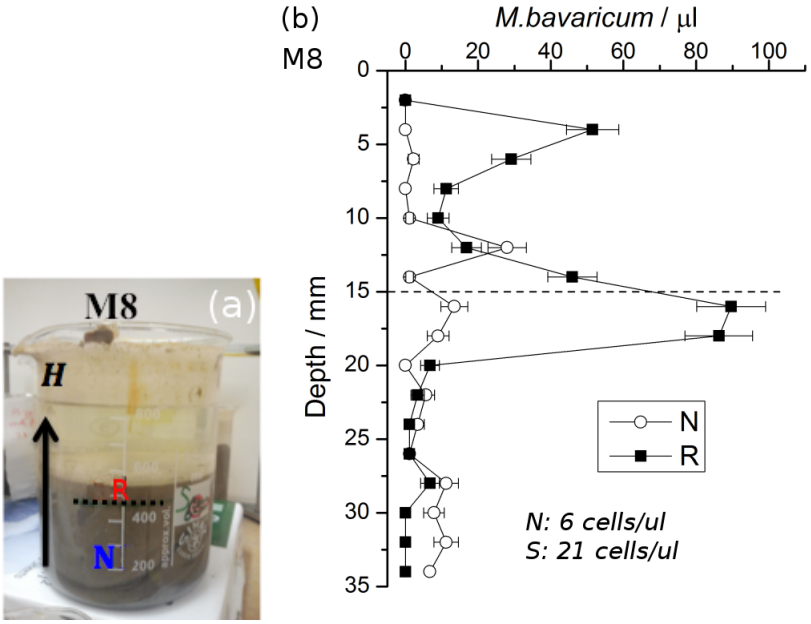

Figure 5.8: (a) Microcosm M8, with boundary between sediment layers 15 mm below the sediment-water interface marked with a dashed line. (b) Vertical profile of R and N cells of *M. bavaricum*, 14 days after beginning of the experiment.

vertical position of cells maintaining the same polarity can only be subjected to random fluctuations in absence of a magnetotactic bias. This result confirms the capability of *M. bavaricum* to reverse its polarity if required by environmental conditions, so that R cells become N cells and vice-versa. This phenomenon was also observed in case of LO cells with incorrect magnetotaxis (section 5.4.5), and occurred in this case with minimal decrease of the total population.

5.4.8 R cells in thin top layer, horizontal field (M7)

This experiment is similar to the previous one performed in a horizontal field (section 5.4.7); however, R cells are confined in a thin top layer in order to study the vertical migration of *M. bavaricum* cells in HO state. This experiment was inconclusive, because N as well as R cells remained in the top layer during 14 days (Figure 5.10). R cells concentrations decreased markedly, although this effect is not imputable to magnetotaxis and might just represent a random fluctuation. N and R cells of cocci, on the other hand, were undetectable after 14 days.

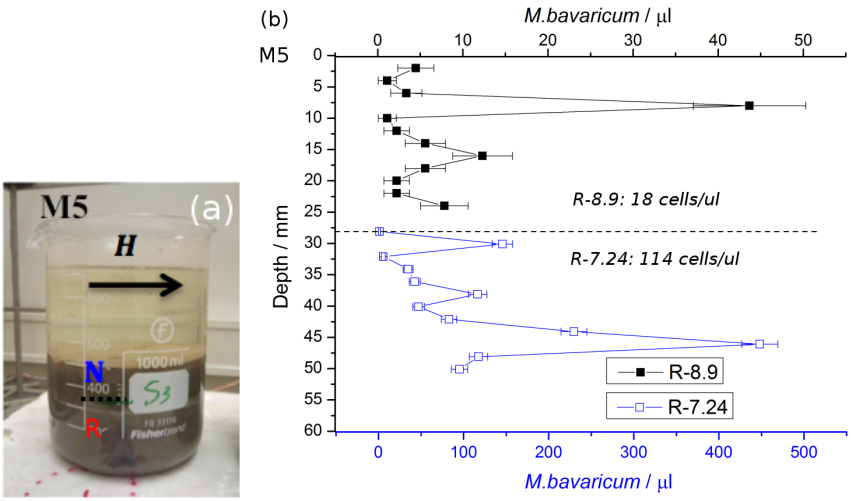

Figure 5.9: (a) Microcosm M5, with boundary between sediment layers 28 mm below the sediment-water interface marked with a dashed line. (b) Vertical profile of R cells of *M. bavaricum*, before the top layer was added (open squares) and 14 days after the top layer was added (filled squares). Note that because there were still many R cells of *M. bavaricum* below 28 mm but not shown in the profiles after 14 days, the count of *M. bavaricum* above 28 mm was actually larger than presented.

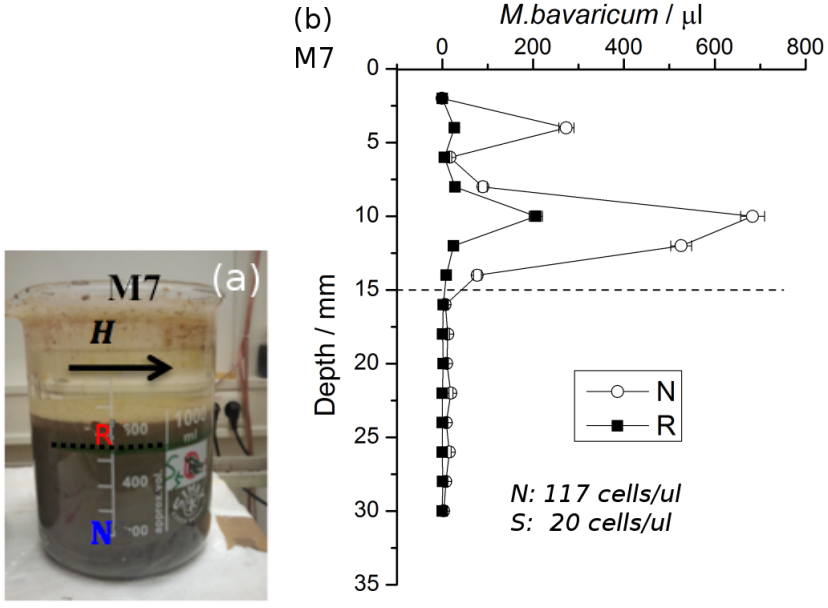

Figure 5.10: (a) Microcosm M7, with boundary between sediment layers 15 mm below the sediment-water interface marked with a dashed line. (b) Vertical profile of N and R cells of *M. bavaricum* after 14 days from experiment beginning.

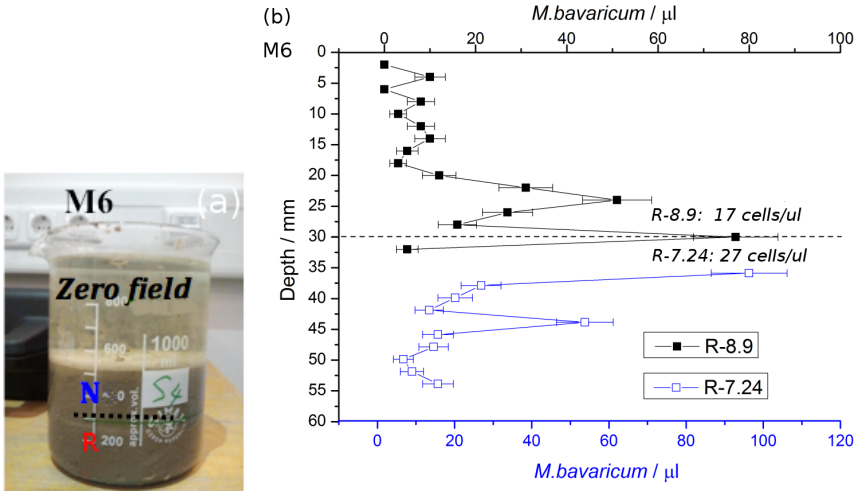

Figure 5.11: (a)Microcosm M6, with boundary between sediment layers 30 mm below the sediment-water interface marked with a dashed line. (b) Vertical profile of R cells of *M. bavaricum*, before the top layer was added (open squares) and 14 days after the top layer was added (filled squares). Note that because there were still many R cells of *M. bavaricum* below 30 mm but not shown in the profiles after 14 days, the counts of *M. bavaricum* above 30 mm was actually larger than presented.

5.4.9 R cells in bottom layer, zero field (M6)

This experiment aims at testing the vertical migration of LO cells in zero field. The M-A model predicts that cells diffuse randomly in zero field, and population declines. R, as well as N cells of cocci disappeared after 14 days, though they were abundant at the beginning of the experiment. This result contrasts with a zero field experiment described in chapter 4, where cocci were practically unaffected by ∼6 months in zero field. The reason for this difference might be due to the fact that zero field conditions in the experiment of chapter 4 have been set on a stabilized aquarium. Here, the only stabilized layer is the bottom one, which, however, as seen by other experiments with incorrect magnetotaxis (section 5.4.5), is too deep for cocci to survive without help of magnetotaxis. The top layer, on the other hand, was created at the beginning of the experiment, and is therefore far from being stabilized.

R cells of *M. bavaricum* migrated into the top layer after 14 days, without significant decrease of the total population (Figure 5.11). This result confirms the possibility for *M. bavaricum* to migrate by chemotaxis alone, as already seen in section 5.4.7.

Table 5.1: Summary of experiments on magnetotaxis in sediment with *M. bavaricum* (b) and wild-type cocci (c). N = normal, R = reversed (pulsed), LO = low oxygen (too deep), HO = high oxygen (too shallow), MA = magneto-aerotaxis, Pop. = trend in total population, MT = evidence of displacement by magnetotaxis, CT=evidence for displacement for chemotaxis alone, b=bav, c=cocci, n.a.= not available. Symbols: ⇑= field direction (up); $\frac{R}{N}$= R cells on top and N cells in bottom layer; →= no significant change; ∼= strong oscillations; ↘= population decrease with no hint to extinction; ↓= population decrease with hint to extinction; √=magnetotactic displacement in the right direction can be deduced; ×=magnetotactic displacement in the unfavourable direction cannot be deduced; —=magnetotactic displacement is not observed. ?= unclear

Experiment	Field	Scheme	Location	Magnetotaxis	Prediction from MA	Observation	Pop.	MT	CT
M3 14 days (control)	⇑	25 mm $\frac{R}{N}$	OK for R	OK for R	R: No changes	R: No changes	R-b→ R-c→	— —	— —
M4 7 days	⇓	25 mm $\frac{R}{N}$	OK for R	wrong for R	Depth profiles of R spread out and population declines slowly.	R-b drops in upper 10 mm, and spreads out below 25 mm. R-c practically disappear.	R-b↘ R-c ↓	× ×	× ×
M1 7 days	⇑	25 mm $\frac{N}{R}$	R in LO state	OK for R	R moves up by backward swimming	R moves up (∼3.5 mm/day)	R-b→ R-c →	√ √	— —
M2 4 days	⇓	25 mm $\frac{N}{R}$	R in LO state	wrong for R	R moves down by backward swimming and die out.	R-b moves up ∼2.5 mm/day and decrease. R-c die out.	R-b↘ R-c ↓	√ ×	√ ×
M8 14 days	⇑	15 mm $\frac{R}{N}$	R-b partially in HO state	OK for R	R-b appear below 15 mm by forward swimming	R-b peak appears at 20-15 mm (∼0.36 mm/day)	R-b→	√	—
Aquarium 2 60 days	⇑⇓	Only N	OK	50% wrong	Spread out and decline.	R-b spread out and declines but does not disappear. N-c practically disappear, especially in >15 mm.	R-b↘ R-c ↓	× ×	× ×
M5 14 days	⇒	28 mm $\frac{N}{R}$	R in LO state	indifferent	Spread out and decline.	R-b appears in <24 mm R-c disappear	R-b→ c ↓	— —	√ ×
M7 14 days	⇒	15 mm $\frac{R}{N}$	R-b partially in HO state	indifferent	Spread out and decline.	R-b: no change in depth distribution. Both R-b and N-b in <15 mm. Decline not observed.	b→ c ↓	—	?
H1 120 days	⇐ I=17°	R |N	OK for N and R	In different. Slightly biased to N	Spread out and slight decline	Part of R-b movess down (0.1 mm/day). R-c disappear. N-b declines. N-c oscillate and increase	b↘ c∼	— —	— —
M6 14 days	0	28 mm $\frac{N}{R}$	R-b in LO state	n.a	No change in depth for R and population decline	R-b appear in <28 mm and slightly decrease. R-c disappear.	b↘ c ↓	— —	√ ×
Aquarium 1 180 days	0	Only N	OK	n.a	No change in depth and decline	R-b declines but does not disappear. N-c oscillate with no clear decrease	b↘ c∼	— —	? ?

Table 5.2: Summary of magnetotaxis observations on *M. bavaricum*. MT = Magnetotaxis, M-A = Magneto-aerotaxis, HO = high-oxygen state, LO = low-oxygen state.

Depth of *M. bavaricum*	Correct MT	Incorrect MT	Indifferent or no MT
Correct position	***Simulation of S-hemisphere.*** **M3**: →, *R-cells behave normally in reversed field*	***Test for incorrect polarity in favourable environment.*** *M-A predicts spread out and consequent population decline* **M4**:↘ spread out. *As expected from M–A if cells maintained their original polarity for 14 days* **Aquarium 2**: ↘ spread out. *As expected from M-A, at least part of the cells continued to use MT.*	***Test for no preferred polarity in favourable environment.*** *Horizontal field could support MT in non-vertical gradients.* **Aquarium 1**: ↘ no moves. *Zero field: same depth distribution, with reduced but stable population over 6 months.* **H 1**: ↘ apparent moves according M–A. *Horizontal field: slight field inclination favoured bimodal depth distribution of R cells and unimodal distribution of N cells.*
HO (partially) Too shallow	***Test for active magnetotaxis.*** **M8**: → moves down (forward). *As expected from polar M–A in HO state*		***Test for active chemotaxis.*** **M7**:→. *Test performed in horizontal field. No change in depth distribution observed.*
LO Too deep	***Test for active magnetotaxis*** **M1**: → moves up (backward). *As expected from polar M-A in LO state*	***Test for incorrect polarity in unsuited environment.*** *M-A predicts downward migration and extinction.* **M2**: ↘ moves up. *Possible only if polarity has changed spontaneously, at least in some cells*	***Test for active chemotaxis.*** **M5**: ↘ moves up, Test performed in horizontal field. Veritical component of MT is random. Appearance in upper layer could arise from diffusion alone. **M6**: ↘ moves up. *Test performed in zero field. Appearance in upper layer supports effective chemotaxis.*

Table 5.3: Summary of magnetotaxis observations on cocci. MT = Magnetotaxis, M-A = Magneto-aerotaxis, HO = high-oxygen state, LO = low-oxygen state.

Depth of cocci	Correct MT	Incorrect MT	Indifferent or no MT
Correct position	***Simulation of S-hemisphere.*** **M3**: →, *R-cells behave normally in reversed field*	***Test for incorrect polarity in favourable environment***. *M–A predicts spread out and consequent population decline.* **M4**:↓. *As expected from M-A if cells maintained their original polarity for 14 days* **Aquarium 2**: ↓ no spread out. *Cells become non-motile*	***Test for no preferred polarity in favourable environment***. *Horizontal field could support MT in non-vertical gradients.* **Aquarium 1**: → (large variations). *Zero field: same depth distribution, with strong population oscillations but no decrease on average over 6 months.* **H 1**: → (large variations). *Horizontal field: R cell extinguished after a strong population decrease, N cells recovered. No systematic change in depth distribution.* **M5, M6, M7:**↓. *R and N cells extinguished in the freshly prepared top layer, in contrast to the survival capability in stabilized sediment such as Aquarium 1.*
HO Too shallow	***Test for active magnetotaxis***. n.a		***Test for active chemotaxis***. n.a
LO Too deep	***Test for active magnetotaxis*** **M1**: → moves up (backward). *As expected from polar M–A in LO state*	***Test for incorrect polarity in unsuited environment***. *M-A predicts downward migration and extinction.* **M2**: ↓ does not move. *Cells become non-motile?*	***Test for active chemotaxis.*** **M5**: ↓, **M6**: ↓. *Rapid disappearance supports the hypothesis that chemotaxis is not used.*

Table 5.4: Properties of *M. bavaricum* and cocci, as deduced from experiments.

	Active M-A	**Magnetotactic advantage**	**Active chemotaxis when no MT**	**Can reverse MT polarity**	**Type of magnetotaxis**
	Capability to reach favourable depth according to M-A model. Experiment: M1, M3, M8.	*Expressed in comparison with population in zero field.* Experiment: Aquarium 1.	*Capability to reach favourable depth in zero or horizontal field.* Experiments: M5, M6.	*Capability to reverse MT polarity when field polarity is wrong.* Experiments: M2, M4.	
Cocci	Yes	Unclear	No	No	Fixed polar
M. bavaricum	Yes	Yes	Yes	Yes (from LO in$<$ 10 days)	Switchable polar

5.5 Discussion

Results of experiments with microcosms M1-M8, as well as experiments in large aquaria described in chapter 4, are summarized in Table 5.1. These experiments can be classified according to (1) the position of MTB in sediment relatively to their optimum depth, and (2) the direction and polarity of the magnetic field with respect to the polarity of MTB (i.e. normal or reversed) and the chemical gradient. In the latter case, which is important in case of polar magnetotaxis, we distinguish between:

(2a) *correct magnetotaxis*, which corresponds to the typical situation encountered in nature (i.e. normal MTB in a downward pointing field or reversed MTB in an upward pointing field),

(2b) *incorrect magnetotaxis*, in which the field is reversed with respect to the typical situation encountered in nature (i.e. normal MTB in a upward pointing field or reversed MTB in an downward pointing field),

(2c) *no magnetotaxis*, when experiments are conducted in zero field and MTB have no preferred swimming direction, being therefore in the same situation as non-magnetic bacteria performing magnetotaxis,

(2d) *indifferent magnetotaxis*, when a magnetic field is present, but is perpendicular to the dominant chemical gradient (i.e. horizontal), so that there is no preferred vertical swimming direction,

(2e) *alternation of correct and incorrect magnetotaxis*, when the vertical magnetic field component is reversed periodically, so that there is no preferred vertical swimming direction on average, but magnetotaxis is incorrect 50% of the total time.

The magnetotactic situations described above have been used to test whether MTB can maintain a stable population at their natural living depth, or if they can successfully migrate to this depth when placed under HO (i.e. near the sediment-water interface) or LO (i.e. below the OAI) conditions. These experiments thus test the influence of a magnetic field on the chemotactic response of MTB in their natural environment. Experiment results for *M. bavaricum* and cocci, classified according to the abovementioned criteria, are summarized in Table 5.2 and Table 5.3 and discussed in the following.

5.5.1 Correct position and correct magnetotaxis

These experimental conditions correspond to the natural case, when sediment is not heavily disturbed. It therefore represents the reference situation that serves as comparison for all other experiments. Microcosm M3 represents this situation for reversed MTB cells and can therefore be considered as a simulation of bacteria grown in the Southern hemisphere. As expected in such case, the population of reversed cells remains stable for both *M. bavaricum* and cocci. Because these "Southern hemisphere" cells have been created by reversing their magnetic moment and did not develop naturally, the microcosm M3 experiment proves that cells do not possess an intrinsic chemical polarity, i.e. a distribution of different chemoreceptors placed at the two ends of the cells along the magnetic axis. This hypothesis is particularly suggestive for *M. bavaricum*, given its large size and very elongated, rigid body. In this case, however, reversed cells created with a magnetic pulse would have their receptors exchanged with respect to their NS or SS swimming direction, possibly producing an incorrect response to chemical gradients and consequent population decline, which was not observed in this case. Therefore, cells must either sense chemical concentrations or chemical gradients by a temporal mechanism, in which case the position of chemical receptors is indifferent. The second mechanism, temporal gradient sensing, has been observed in non-magnetic bacteria performing chemotaxis (Macnab and Koshland, 1972).

5.5.2 Correct position and incorrect magnetotaxis

A logical function of magnetotaxis, and more in general, motility, consisting in allowing cells to escape from unfavourable chemical conditions and move into a suitable environment. For example, the magnetotactic advantage of cells brought to the sediment-water interface after a major bioturbation event has been discussed in chapter 2 by calculating the time required by MTB to reach their usual living depth below the OAI. These calculations showed that, because of the poor alignment of cells living in sediment with the external field, magnetotaxis becomes effective only over macroscopic displacements of $\sim$1 mm. On smaller scales, MTB are expected to move almost randomly in a similar manner as non-magnetic chemotactic cells. According to these results, magnetotaxis, and even motility, might not be necessary for cells that are already correctly positioned in a stable chemical gradient. On the other hand, as especially evident with *M. bavaricum*, the depth distribution of cells is much wider than the typical width of the oxygen gradient, and, in many cases, it is

evidently bimodal, with maximum cell concentrations at ∼6 and ∼16 mm depth. Bimodal depth distributions are suggestive of two groups of cells moving up and down within a 2-25 mm living depth range. Such 'vertical shuttling' might be caused by different metabolic requirements requiring substances that do not coexist in a single depth in sediment, as for instance nitrate and sulphide. In this case, magnetotaxis is still required to optimize vertical migration within the living zone.

A second reason for using magnetotaxis under stationary conditions is related to constant sediment mixing caused by bioturbation. As discussed in chapter 2, mixing is described by a solid diffusion constant D_{bt} of the order of 0.1-100 cm^2/yr for the type of sediment used in our experiments. In this case, cells would be randomly displaced by a distance $(2D_{bt}t)^{1/2}$ over time t, being eventually transported to unfavorable depth if this diffusion mechanism is not counteracted by magnetotaxis

Experiments in which the depth distribution of MTB in sediment is undisturbed, but the magnetic field is reversed with respect to the normal situation encountered in nature, are therefore useful for evaluating the magnetotactic activity of cells under stationary environmental conditions. Such conditions have been created with reversed MTB in microcosm M4. In this case, cells have been reversed *in-situ* by a magnetic pulse, without disturbing their natural distribution, and exposed to a downward-pointing magnetic field. Under such conditions, immotile cells would not be affected by the incorrect field polarity, and the total MTB population would remain stable. However, a population decline was observed for reversed *M. bavaricum* within 7 days, accompanied by an increased spread of the depth distribution, while reversed cocci almost disappeared during this time. Normal cells, on the other hand, were not affected by the experiment, demonstrating that the population decline observed on reversed cells is indeed caused by the incorrect field polarity. This experiment shows that magnetotaxis is continuously used by MTB, also under stationary conditions, and not only after major disturbances. The expected passive displacement $(2D_{bt}t)^{1/2}$ of cells produced by sediment mixing over the duration $t = 7$ days of the experiment is comprised between 0.6 and 19 mm, so that correct magnetotaxis might be required for overcoming adverse consequences of sediment mixing, as well as for 'vertical shuttling' within the typical living range of MTB. The hypothesis that motility, and therefore magnetotaxis, is required only to overcome sudden sediment disturbances is therefore discarded by the experiment with microcosm M4.

A similar experiment has been described in chapter 4. In this case, normal MTB in a stable aquarium have been exposed to a vertical magnetic field whose polarity was

switched every 24 hours, so that normal and reversed field conditions are obtained every second day. This experiment, in which magnetotaxis is incorrect during 24 h every second day, produced the same results observed in microcosm M4. The 1.5 years stabilization time of the aquarium reduced the organic matter content in the upper ∼3 cm of sediment so that a reduction of the maximum solid diffusion constant by bioturbation is expected. Using $D_{bt} < 20$ cm^2/yr, we obtain a ∼3 mm maximum passive displacement of cells by sediment mixing during the 24 h duration of reversed field conditions. Because the depth range of living MTB in this aquarium was > 2 cm (Figure 4.9), passive displacement of cells by sediment mixing in a reversed magnetic field is not a probable cause for the observed population decline. Therefore, results from both experiments suggest that MTB continuously migrate within a given range of depths to meet metabolic requirements, and that magnetotaxis assists individual cells during migration.

5.5.3 Incorrect position and correct magnetotaxis

Microcosm experiments with correct field polarity, in which reversed bacteria are initially confined within unusual (i.e. excessively deep or shallow) depth ranges were aimed at testing the long-range efficiency of magnetotaxis and the capability of individual MTB cell to reach the correct position in sediment within a reasonable time. Because the natural depth distribution of *M. bavaricum* and cocci begins at only ∼2 mm depth (Figure 4.9), it is easier to create a microcosm in which reversed MTB are located below the usual depth range than above, as in microcosm M1. The experiment with microcosm M1 is also particularly interesting, because, in order to move upward in the sediment column, normal MTB need to be SS and reversed MTB need to be NS. In both cases, cells need to swim in the opposite direction with respect to what is systematically observed in the hanging drop assay, including assays performed under strictly anoxic conditions (chapter 3). This experiment would therefore prove the capability of wild-type MTB to perform polar magnetotaxis with both swimming directions in their natural environment, despite unsuccessful observations with the optical microscope. Indeed, reversed cells located at >25 mm depth in microcosm M1, that is below the usual depth range for both *M. bavaricum* and cocci (Figure 5.8), migrated upwards in an upward field, reaching their usual position within 7 days.

Similar results have been obtained with the opposite situation in which reversed cells were confined within the uppermost 15 mm of sediment in Microcosm M8. Although most *M. bavaricum* cells are normally found in this depth range, the natural depth distribution of this bacterium can exceeds 20 mm (Figure 4.9), so that some reversed cells should migrate

to those depths by SS swimming (corresponding to NS swimming for normal cells). This migration has also been experimentally confirmed (see chapter 6).

The experiments described in this section confirm that polar magnetotaxis in sediment from the Northern hemisphere is performed by cells that are NS if located above their usual depth range and SS if located below their usual depth range, as observed by Frankel et al. (1997) with cultured cocci in their culture medium. The impossibility to observe SS wild-type MTB in the hanging drop assay, regardless of oxygen concentration, must therefore be related to experimental deviations that deviate in some manner from what is required for performing polar magnetotaxis. A possible explanation is given in chapter 6.

5.5.4 Incorrect position and incorrect magnetotaxis

Experiments performed with reversed cells located outside their usual living depth and exposed to a magnetic field with incorrect polarity (i.e. pointing downward), represent the most threatening situation for MTB performing polar magnetotaxis, because the swimming polarity (i.e. NS or SS) determined by the environment is expected to drive the cells into the wrong direction, running into a worse environment. Unlike axial magnetotaxis, polar magnetotaxis appear to be disadvantageous in such conditions, leading to MTB extinction. Indeed, experiments with microcosm M2, where reversed cells located at $>$25 mm depth where exposed to a magnetic field pointing downward, leaded to the complete disappearance of cocci within 4 days, and to an evident population reduction for *M. bavaricum*. This result implies that cocci were killed by the unfavourable environment into which they were forced by magnetotaxis, or at least they became non-motile, so that they could not be counted with the hanging drop assay. In both cases, this experiment demonstrates the disadvantage of polar magnetotaxis in case of wrong combinations of field polarity and chemical gradient. This is not a problem during natural field reversals on Earth, because such reversals occur over geological time scales, and therefore over millions of MTB generations, giving polar MTB the chance to evolve with correct polarity without damage. On the other hand, reversed gradients could be encountered in sediment on a small scale, for example around a 'reduction spot' caused by unusual concentrations of decomposing organic matter. MTB located just below such spot would be exposed to a kind of reversed chemical gradient, in which conditions corresponding to a deep, anoxic sedimentary environment are encountered when moving up, instead of moving down. Because such 'inverted gradients' are always of local nature, MTB extinction is not expected. However, the 'inverted gradient' scenario described above appears to be a disadvantage

for polar magnetotaxis, whose existence must be justified by other advantages over axial magnetotaxis.

A completely unexpected observation could be made in microcosm M2. The microcosm preparation method ensures a very sharp (< 1 mm) upper boundary for reversed MTB cells. Because the expected polar magnetotaxis mechanism drive reversed MTB further down in sediment, any observation of reversed cells above the initial upper boundary (i.e. at depths < 25 mm) would imply that the magnetotactic mechanism has been adapted to the new situation. This was indeed the case for *M. bavaricum*, whose depth distribution at the end of the experiment expanded upwards by ∼7 mm. There are two possible explanations for this observation: (1) some cells were able to switch the control of flagella rotation, so that HO and LO conditions lead to rotation senses that are opposed to the 'normal' ones, or (2) cells correctly polarized for the new environment evolved upon cell division. The second hypothesis requires sufficiently rapid cell division under adverse conditions. Although the cell division rate of *M. bavaricum* in sediment has never been measured, a crude upper limit can be obtained from the zero-field-experiment described in chapter 4. Here, a stabilized, sediment-filled aquarium was kept in zero field for ∼160 days. These conditions produced a decrease of the *M. bavaricum* population. After re-establishing the original magnetic field, total cell counts doubled in ∼25 days. Assuming that this apparent population increase was entirely produced by cell division (and not by cell mobility artefacts), <2.5% of the initial population of reversed *M. bavaricum* cells in microcosm M2 can evolve favourably and migrate upwards every day. Taking into account the total population decrease of reversed cells in microcosm M2, only ∼5% of the initial population is expected to be found above 25 mm depth, while 9% has been observed experimentally (Figure 5.7). Therefore, considering also the unfavourable environmental conditions for reversed cells in microcosm M2, the cell division hypothesis appears highly unlikely, leaving us with the possibility that *M. bavaricum* cells can 'switch' their polar magnetotaxis if required.

Another argument against the cell division hypothesis comes from the observation that reversed cocci in microcosm M2 disappeared in 4 days. If natural selection of suitably polarized cells had occurred with *M. bavaricum* cells, there is no apparent reason for preventing natural selection to work in the same manner with cocci, unless a much smaller cell division rate is assumed. This unique capability of *M. bavaricum* is confirmed by the switching field experiment described in chapter 4 and mentioned in section 5.5.2, where the magnetic field polarity was switched every 24 h. Also in this case, the *M. bavaricum* population declined but reached a stationary equilibrium, while cocci were practically

extinguished, as expected from their incapability to adapt to field reversals. Finally, the spontaneous reversal of the magnetotaxis polarity of individual *M. bavaricum* cells has been directly observed under the microscope, as reported in chapter 6.

5.5.5 Correct position and no magnetotaxis

Magnetotaxis is simply eliminated by exposing MTB to a zero field environment. In this case, motile cells have no preferred swimming direction and the only possibility for them to displace in a chemical gradient is to move for longer time along directions where a favourable chemical gradient is sensed, similarly to chemotaxis performed by non-magnetic bacteria. Experiments with stabilized microcosms in zero field are thus aimed at testing the capability of MTB to rely only on simple chemotaxis, as non-magnetic bacteria do. The most systematic experiment with this purpose was described in chapter 4, where an aquarium was placed in a zero field environment for ∼160 days while periodically monitoring the MTB population in it. The clear outcome of this experiment was that cocci were not affected by zero field conditions, while *M. bavaricum* rapidly reached a new equilibrium in which the total population decreased by ∼54% and remained constant during the entire experiment duration.

The insensitivity of cocci to zero field conditions can be explained with the following hypotheses:

(1) *Cocci are not motile while being in a favourable sedimentary environment.* In this case, cells would not move from their original position, which also means that they are not using magnetotaxis under normal conditions. This hypothesis is rejected by the observation that cocci disappear if the magnetic field is reversed (i.e. microcosm M4 and Aquarium 2 in Table 5.3), which means that they are motile and perform magnetotaxis when a field is present. Furthermore, sediment bioturbation would make immotile cells diffuse away from their optimal depth. Using the diffusion constants discussed in section 5.5.2, this is expected to occur in 160 days.

(2) *Chemotaxis is sufficiently efficient to keep cocci within a favorable range of depths.* In absence of major disturbances, chemotaxis is sufficient for cocci to maintain themselves within an optimal depth range, counteracting the steady, slow sediment mixing caused by bioturbation.

Because hypothesis (1) is contradicted by other experiments, it appears that a magnetotactic advantage does not exist for cocci living in sediment with a stationary chemical

gradient and no external disturbances. Magnetotaxis proves to be important only when cocci are significantly displaced from their natural living depth, as discussed in the next section.

M. bavaricum, on the other hand, definitively benefits from a magnetotactic advantage even in undisturbed sediment, as seen by the population decrease in zero field. The observed difference between *M. bavaricum* and cocci can be explained by assuming that (1) *M. bavaricum* has worse chemotactic capabilities than cocci, or (2) individual *M. bavaricum* cells must move continuously within a certain range across a chemical gradient to satisfy their metabolic requirements, while individual cocci can live at same depths for long time. The first assumption is not supported by any additional evidence. Furthermore, the chemotactic capabilities of *M. bavaricum* are demonstrated in zero field experiments where cells are not placed within their optimum depth range: in this case, *M. bavaricum* cells are able to displace towards favourable depths relying solely on chemotaxis, while cocci do not display such ability (see section 5.5.6 coming as next). Therefore, the observation that *M. bavaricum* has a clear magnetotactic advantage while living in its optimal depth range, despite its chemotactic capabilities, is a further hint that its metabolism requires 'vertical shuttling' as discussed in section 5.5.2.

5.5.6 Incorrect position and no magnetotaxis

If reversed MTB cells are confined to unfavourable depth ranges in sediment exposed to zero field, their only survival chance consist in reaching their usual depth range by chemotaxis alone. This situation, realized with microcosm M6, probes the magnetotactic advantage of MTB in situations where the sediment is disturbed macroscopically. Reversed *M. bavaricum* cells in zero field were indeed capable of moving upwards by ∼30 mm in 14 days, at the cost of a slight population decrease. Reversed cocci, on the other hand, disappeared. This experiment demonstrates that a magnetotactic advantage exists for both types of bacteria, but is strongest for cocci, which are not capable of relying only on chemotaxis when displaced from their usual living depth. The reason for the observed difference between *M. bavaricum* and cocci could be related to the better endurance of *M. bavaricum* under adverse conditions, maybe because of its large cell size and thick membrane, which enables cells to survive long enough for the less efficient chemotaxis to become effective.

5.5.7 Horizontal and vertical motility in horizontal fields

One of the most puzzling aspects of magnetotaxis is the possible existence of a magnetotactic advantage for MTB living at the geomagnetic Equator, where the magnetic field is perpendicular to the vertical chemical gradient of sediments. In this case, the magnetic field cannot assist cells in vertical migration, and in case of polar MTB, equal amounts of NS and SS cells have been found in freshwater and marine sediments in sites with $<4°$magnetic inclination (Frankel et al., 1981). Because a horizontal field does not support vertical magnetotaxis, Frankel et al. (1981) proposed that the horizontal alignment of MTB would be advantageous to bacteria of either polarity in reducing detrimental vertical motion, compared to a pure random walk. This hypothesis relies on a large alignment of MTB with the magnetic field in sediment, as believed at the time on the basis of microscope observations of swimming cells in water. Our findings of a $\sim$1% alignment of MTB living in sediment (chapter 2) excludes this explanation, because the real MTB displacement in a horizontal field is almost random. The second explanation proposed by Frankel et al. (1981) for the magnetotactic advantage of bacteria living at the geomagnetic equator appears more reasonable and relies on a more efficient escape response from localized unsuited spots in sediment.

Even in case of small alignment with the external field, a systematic horizontal migration of polar MTB would be expected for cells located at the extremes of the usual range of living depths in an intuitive polar magnetotaxis model. Such migration, however, was not observed in the experiment described in section 5.4.1. A simple explanation of this result is based on the purely random nature of the vertical component of the swimming path. This means that, while swimming with a slight horizontal bias provided by the magnetic field during a given time, 50% of all cells will end at a different depth that makes them change polarity (i.e. NS become SS and vice-versa). Overall, a preferred horizontal swimming direction does therefore not exist over long distances. As for the case of zero field experiments with MTB located at natural depths, the total *M. bavaricum* population decreased, while cocci were subjected to large fluctuations with no significant changes in total cell number. Similarities between zero and horizontal field experiments include the depth distribution of *M. bavaricum*, whose vertical spread increases significantly.

5.5.8 Incorrect position in horizontal fields

Finally, we discuss the situation of MTB located outside their usual living range when subjected to a horizontal field. As for the same situation in zero field (Section 5.5.6), MTB must rely solely on chemotaxis for vertical displacement, because the horizontal field does not provide any vertical bias. Indeed, similar results are obtained as for zero field, with *M. bavaricum* being able to reach its usual living depth, and cocci disappearing within few days.

5.6 Conclusions

The large number of experiments described in section 5.5 for different combinations of field and environmental conditions provide useful constraints for the magnetotactic properties of *M. bavaricum* and cocci. Although both types of bacteria perform polar magnetotaxis, important differences exist between them, as summarized in Table 5.4. In the following, individual magnetotactic properties are discussed for *M. bavaricum* and cocci.

5.6.1 Magnetotactic advantage under stationary conditions

Stationary conditions, defined by a stable chemical gradient and the absence of strong external disturbances, require only a minimum motility of MTB in order to contrast the slow process of sediment mixing. As demonstrated by zero field experiments, cocci can maintain themselves within a suitable depth range with chemotaxis alone, without undergoing a detectable population decrease over $\sim$160 days. Therefore, magnetotaxis does not provide any advantage to cocci in such situation, in comparison with non-magnetic chemotactic bacteria. A magnetotactic advantage, on the other hand, exists for *M. bavaricum* under the same experimental conditions. Because *M. bavaricum* is otherwise capable of relying on chemotaxis alone for escaping unfavourable environments, the magnetotactic advantage under stationary conditions can be explained by the necessity of *M. bavaricum* cells to move up and down within a certain depth range, probably because of metabolic requirements that cannot be satisfied by staying at a fixed depth. In this case, a better efficiency of vertical displacement is advantageous. This hypothesis needs further experimental validation.

5.6.2 Magnetotactic advantage after major disturbances

Major sediment disturbance produced by bioturbation can displace MTB into sediment depths that do not provide a suitable living environment. In this case, rapid vertical migration is essential for surviving such events. *M. bavaricum* and cocci are capable of reaching their optimum living depth by magnetotaxis without any decrease in cell counts. On the other hand, if the magnetic field is removed, so that simple chemotaxis is the only mean for vertical migration, *M. bavaricum* is still capable of reaching its optimum living depth, although at cost of a significant population decrease, while cocci undergo extinction under the same conditions. This proves that a significant magnetotactic advantage exists for both types of bacteria when long-range displacement is required. This advantage is more pronounced for cocci, where magnetotaxis is mandatory for survival, while *M. bavaricum* can rely solely on chemotaxis, probably because of longer endurance under unfavourable conditions.

5.6.3 Adaptation capability of polar magnetotaxis

Polar magnetotaxis is sensitive to the field polarity, and becomes disadvantageous in all cases where the field polarity is incorrect with respect to the chemical gradient. Such situations can be encountered in natural sediment in proximity of localized gradients around decomposing organic matter. As expected, cocci are negatively affected by all situations where the field polarity is incorrect, as seen by rapid disappearance. *M. bavaricum*, on the other hand, possess the surprising ability to adapt to such situations by reversing its magnetotactic polarity, at least for part of the whole population. This adaptation behaviour appears to be excessively rapid for being attributed to natural selection over several cell generations, as also supported by direct observation under the optical microscope (chapter 6).

Chapter 6

Direct observation of magneto-chemotaxis on individual magnetotactic bacteria

Abstract

The motion of magnetotactic bacteria (MTB) is the result of the joint action of passive alignment in a magnetic field (magnetotaxis), and the response to chemical stimuli (chemotaxis). As far as the response to oxygen concentration is concerned, the combination of magnetotaxis and chemotaxis is called magneto-aerotaxis. In this chapter we investigate the response of individual wild-type cells of *Magnetobacterium bavaricum* to a pH gradient in oxygen-saturated water. The combination of two distinct chemical stimuli (oxygen and pH) creates a complex response of swimming cells observed under the optical microscope with the hanging drop assay. The normal swimming direction of *M. bavaricum* in oxygen-rich water is towards the magnetic N (N-seeking cells, shortly NS). As NS cells swimming in near-neutral water enter a region with different pH, two different behaviours are observed: (1) cells stop abruptly or after some slowdown, or (2) some cells become S-seeking (SS) or engage a rapid back-and-forth (oscillatory) motion along a certain pH front. If the field direction is reversed, formerly oscillatory cells become in most cases consistently NS and in few cases consistently SS. The oscillatory motion can be explained by the combined action of two repellents (oxygen and acidity) on bacteria that perform polar magnetotaxis with a temporal sensing mechanism, in analogy to the magneto-aerotaxis model of Frankel et al. (1997). On the other hand, however, *M. bavaricum* appears to be able to "switch" the link between chemical sensing and flagella motion, so that some cells become SS in oxygen-rich

water, even when far from any pH-gradient. This ability appears to be an adaptive mechanism that enables cells to survive in environments where the chemical gradient is reversed with respect to the usual magnetic field direction, as also observed in sediment (chapter 5).

6.1 Introduction

The ability of magnetotactic bacteria (MTB) to migrate along magnetic field lines is known as magnetotaxis (Blakemore, 1975, 1982; Frankel, 1984). While magnetotaxis determines a preferred axis for the swimming path, the swimming direction (parallel or antiparallel to the field) is given by the sense of flagella rotation (clockwise or counter-clockwise), which is in turn controlled by the chemical environment (chemotaxis). The combination of these two phenomena has been called magneto-aerotaxis by Frankel et al. (1997), in the case of a response to oxygen concentration. Depending on the way of flagella rotation which is affected by the chemical environment, Frankel et al. (1997) distinguished the cases of axial and polar magneto-aerotaxis. Axial magneto-aerotaxis, as observed in magnetic spirilla, is based on the detection of a chemical gradient (i.e. a spatial change of concentration), probably through a temporal sensing mechanism by which cells compare concentrations measured in successive time intervals while moving through the gradient (Berg and Purcell, 1977). Axial magnetotaxis has no preferred swimming direction: if the cell is moving towards more favourable conditions, it keeps swimming along the same direction, while the swimming direction is reversed in case of movement towards less favourable conditions. If cells performing axial magnetotaxis are observed in a homogeneous environment with negligible concentration gradients, such as the oxygen-saturated water drop of a hanging drop assay, the temporal sensing mechanism cannot detect real concentration changes and is affected by random fluctuations. In this case, cells will change their swimming direction at random times, performing a characteristic 1-D oscillatory motion around a mean position.

Polar magneto-aerotaxis, on the other hand, appears to be controlled by an upper and a lower oxygen concentration threshold. In the model of Frankel et al. (1997), based on observations on cultured cocci, cells exposed to oxygen concentrations larger than the upper threshold do consistently swim towards one magnetic pole (for example N), while the same cells exposed to concentrations smaller than the lower threshold consistently swim towards the other magnetic pole. The swimming polarity depends on the direction of the magnetic field with respect to the oxygen gradient in which the cells were grown: if the magnetic N points against the oxygen gradient (i.e. the oxygen concentration decreases

when moving towards it), cells will swim towards the magnetic N (north seeking, NS) in oxic environments, and towards the magnetic S (south seeking, SS) in anoxic environments. In chemically stratified environments, this type of magnetotaxis will keep MTB within a range of depths comprised between the lower and the upper oxygen concentration thresholds. This range of depths coincides with the oxic-anoxic interface (OAI) of sediment or water column. In the hanging drop assay, MTB are exposed to oxygen saturation, and are therefore consistently NS if grown in the Northern hemisphere, and SS if grown in the Southern hemisphere.

The two types of magnetotaxis are easily distinguishable in the hanging drop assay, with an oscillatory behaviour being characteristic of axial magneto-aerotaxis and consistent swimming directions for polar magneto-aerotaxis. According to this criterion, *M. bavaricum* performs polar magneto-aerotaxis. However, all attempts to observe SS cells under strictly anoxic conditions, as expected from polar magneto-aerotaxis, gave negative results for both *M. bavaricum* and wild-type cocci (see chapter 3). On the other hand, the existence of SS migration in sediment has been shown with dedicated experiments (chapter 5), proving that magneto-chemotaxis involves both swimming directions despite the impossibility to observe them in the hanging drop assay. SS migration might be induced by other substances instead of oxygen, in which case a lower oxygen concentration threshold does not exist. In the experiments reported by Frankel et al. (1997), such repellents might occur only in the anoxic zone of the MTB culture, forming a concentration gradient that is opposed to that of oxygen. Such opposed gradients (e.g. ammonia and sulphide) are common in stratified environments (Froelich et al., 1979) and might be essential for reversing the swimming direction observed under oxygen saturation. Another unexpected magneto-chemotactic pattern of *M. bavaricum* observed in sediment is the ability to switch polarity in case of unfavourable combinations between oxygen gradient and vertical magnetic field, so that cells are SS under oxic conditions.

In general, it appears that magnetotaxis is controlled by chemotaxis, as well as responses to physical stimuli such as light (magneto-phototaxis, Chen et al. 2011; Shapiro et al. 2011), and contact with solid obstacles (tactile response, Spormann and Wolfe 1984). Information from specialized receptors must therefore be combined into a single signal that determines the sense of flagella rotation. In order to investigate this mechanism, systematic experiments have been performed with the hanging drop assay in presence of a pH gradient. In this case, MTB cells are exposed to two independent chemical stimuli, which can provide consistent or contradictory signals to the flagella motor, depending on

the position inside the hanging drop.

The pH of typical freshwater and marine MTB habitats is comprised between 5.5 and 9.8 (Jogler et al., 2010; Lefèvre et al., 2011; Mann et al., 1990; Pan et al., 2005a). In general, pH decreases across the OAI, with more acidic conditions in the anoxic zone. For example, Jogler et al. (2010) reported a pH decrease from 8.5 above the OAI of carbonate-rich sediment, to 7-7.5 at greater depths. The minimum depth for the occurrence of *M. bavaricum* usually coincide with a level where dissolved oxygen drops to half of the saturation value, while maximum depths are not correlated with other dissolved ions such as nitrate, ammonia, or pH. Nevertheless, since MTB grow only in defined pH ranges (Blakemore et al., 1979; Martatea and Blakemore, 1981), they might possess a chemotactic response to H^+ or OH^- ions. Furthermore, pH might affect flagella rotation, since the flagella motor is driven by a proton flux (Eisenbach, 2004).

6.2 Preliminary observations

The initial motivation for studying the reaction of MTB to pH gradients came from hanging drop observations of *M. bavaricum* in a suspension of sediment particles taken from 2-3 cm depth in the aquaria described in chapter 4. Dark greyish sediment from this depth acquired a reddish color when dried in air, testifying the formation of iron oxide from Fe^{2+}. *M. bavaricum* cells approaching non-oxidized sediment particles sometimes engaged a rapid sequence of swimming direction reversals, which was not observed with sediment taken from above the OAI. This observation leads to the hypothesis that the unusual behaviour of *M. bavaricum* was due to Fe^{2+} diffusing from sediment particles. Therefore, further hanging drop observations have been performed by adding a freshly prepared $\sim$1 mM Fe^{2+}-solution on the magnetic N side of the hanging drop. When NS *M. bavaricum* cells reached the boundary with the added solution, they engaged a similar sequence of swimming direction reversals. Because the Fe^{2+}-solution had a pH of $\sim$4.5, subsequent experiments have been designed for the purpose of investigating the response of *M. bavaricum* to pH gradients. Wild-type cocci, which are also abundant in sediment used for these experiments, did never switch their swimming direction in proximity of sediment particles, nor in Fe^{2+}- or pH-gradients. Therefore, all subsequent experiments were focused on *M. bavaricum*.

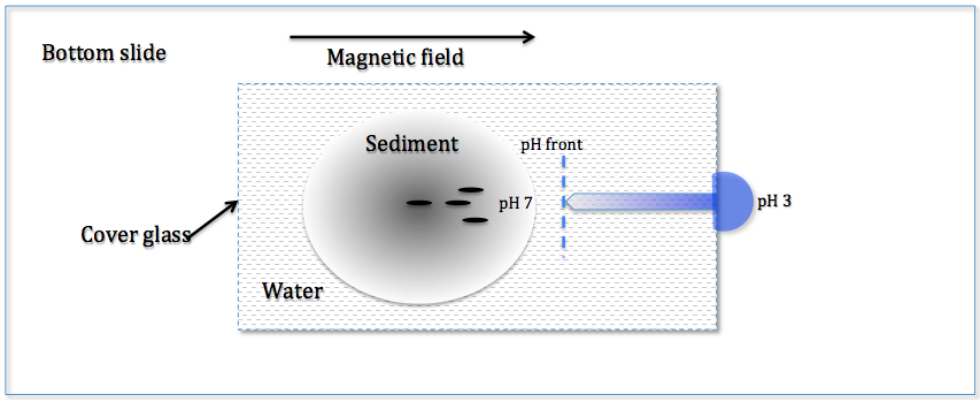

Figure 6.1: Sketch for observing *M. bavaricum* in pH gradient. A drop of diluted *M. bavaricum*-containing sediment was placed on a bottom slide and surrounded with distilled water, which was then covered by a thin glass. A drop of pH solution (e.g. pH 3) was added to one side of the cover glass. The diffusion of pH solution towards the sediment side created a pH gradient whose front was indicated by a vertical dashed line. Magnetic field was against to pH gradient.

6.3 Experiments

A series of aqueous solutions with pH values ranging from 1 to 12 has been prepared by successive dilution of a 1 M solution of HCl in distilled water. The pH of each solution has been tested with a pH sensor from Unisense. The behaviour of *M. bavaricum* cells in a pH gradient was observed with a modified hanging drop assay prepared as follows. ∼0.5 ml of MTB-containing sediment was taken with a micropipette from an aquarium at 5-10 mm depth (see chapter 4), and transferred to a glass slide. ∼1ml distilled water (pH 7.35) were added on the top of the sediment drop in order to create a clear water rim around the sediment. A cover glass was placed on the sediment-water preparation in order to create a thin film of homogeneous thickness. Finally ∼0.1 ml of pH solution has been added on one side of the cover glass, providing an acid or basic reservoir that slowly diffuses into the sediment-water solution under the cover glass. The thin layer of solution below the cover glass prevents turbulent mixing and ensures the establishment of a pH gradient, which slowly diffuses inside the cover glass (Figure 6.1).

This preparation procedure is inadequate for the production of stationary, controlled gradients: all observations have been performed within 30 min from cover slide preparation, before the gradient front reaches sediment, which acts like a buffer. On the other hand, it avoids long exposure of MTB to artificial environments, which might eventually

modify their response to chemical stimuli. The glass slide was immediately placed under a specially equipped optical microscope (magnetodrome, see section A.1), for the observation of bacteria in controlled horizontal fields. A magnetic field pointing to the side of the pH solution front was applied in order to make NS cells swimming out of the sediment towards the pH gradient (right in Figure 6.1).

Solution of the diffusion equation for the experimental setup shown in Figure 6.1 gives a rough idea of the evolution of the pH gradient over time. For this purpose, diffusion in the water film under the cover slide is modeled with the 1-D diffusion equation:

$$\frac{\partial C}{\partial t} = D\frac{\partial^2 C}{\partial x^2} \tag{6.1}$$

where $C = C(t, x)$ is the concentration of a given ion (i.e. H^+ or OH^-) as a function of time t since contact with the pH solution, and distance x from the cover slide edge (i.e. $x = 0$ at the right end of the cover slide in Figure 6.1). Furthermore, $D = 2.3 \times 10^{-9} m^2/s$ is the self-diffusion constant of water at room temperature. The initial condition is given by:

$$C(0, x) = C_0 \mathcal{H}(x) \tag{6.2}$$

where C_0 is the concentration of the solution in contact with the cover slide, and $\mathcal{H}$ is the Heaviside step function ($\mathcal{H}$=0 for $x < 0$ and $\mathcal{H}$=1 for $x > 0$). Suitable boundary conditions must be set at x=0 , and on the other end of the cover slide, i.e. $x = -L$, where $L \approx$2 cm is the width of the cover slide. Because the drop of solution added near x=0 is much thicker than the water film under the cover slide, we assume it to be an infinite reservoir, in which case

$$C(t, x = 0) = C_0 \tag{6.3}$$

is the boundary condition in x=0 . The other end of the cover slide is a physical barrier with no flux, so that

$$\frac{\partial C(t, x)}{\partial x}|_{x=-L} = 0 \tag{6.4}$$

is the boundary condition at $x = -L$. Numerical solutions of eqs.(6.1-6.4) obtained with Mathematica are shown in Figure 6.2 for a 2 cm cover slide and a pH 3 solution with concentration $C_0 = 10^{-3}$ M of H^+-ions. The numerical solutions of Figure 6.2 show that relatively sharp pH front propagates under the cover slide for the first ∼30 min. During this time, the left-hand side of the cover slide is unaffected by the pH solution. The pH front disappears completely after 2 hours, when the pH of the entire water film starts

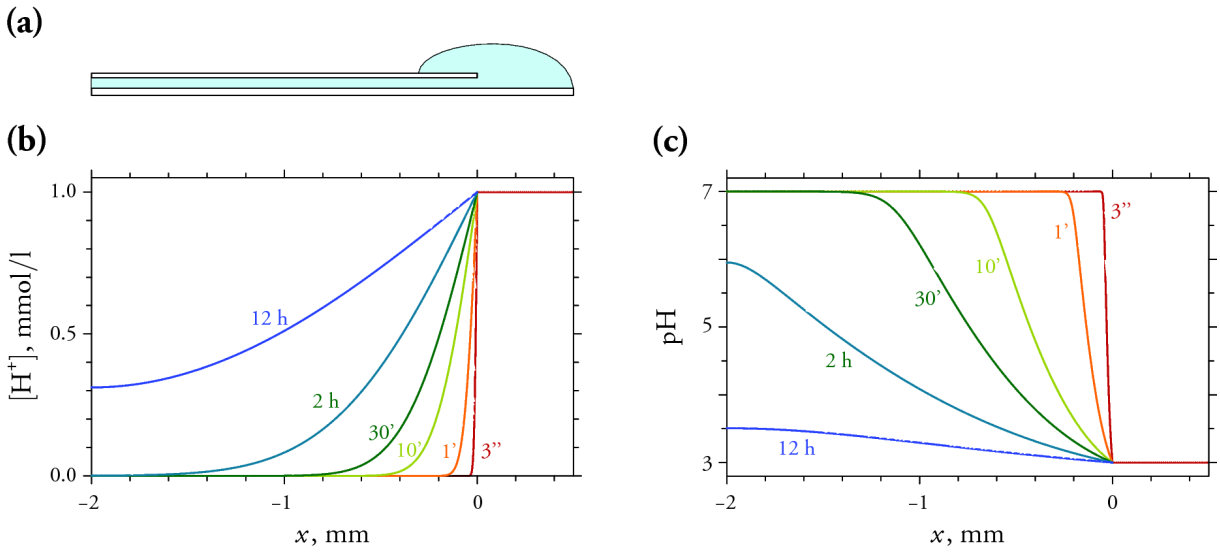

Figure 6.2: (a) Sketch showing a vertical section of the glass slide with pH solution added to the right (not to scale). (b) Profiles of H^+-concentration through the water film on the glass slide shown in (a), after given times since the addition of a pH 3 solution. (c) pH-values corresponding to the profiles shown in (b).

to decrease until it reaches the same pH of the original solution. This simulation of the diffusion process show that observations made within the first ∼30 min show MTB cells swimming from a nearly neutral environment into a pH gradient.

Experiments with pH 1 and pH 12 solutions killed MTB cells before sufficiently long observations cold be made; therefore, experiments were limited to solutions with pH values comprised between 2 and 11. In this case, MTB swim out of the sediment, as in the regular hanging drop assay, until they reach the gradient front, where they come to a sudden stop (pH 4-11, see a video Appendix C-4). Motility could not be resumed by reversing the magnetic field, or by removing the pH solution in order to slowly recover near-neutral conditions: therefore, we assume that these cells died as a consequence of inadequate environmental conditions. If solutions with pH 2-3 are used to create a gradient, some *M. bavaricum* cells behave as described above, while other cells start to engage a rapid sequence of swimming direction reversals when coming close to the region where other cells are killed. This oscillatory behaviour continues as long as the field is oriented so, that the magnetic N points to the side where the pH solution has been added. A field reversal makes NS cells swim continuously away from the pH front. If the field is reset to the original direction, the same NS cells swim continuously until they reach the pH front,

where they engage the same oscillatory behaviour observed before (see a video Appendix C-3). Finally, few NS cells spontaneously reverse their swimming direction when approaching the pH gradient, becoming SS and swimming away from the pH front. The SS swimming behaviour is interrupted by brief NS excursions, but the net cell displacement corresponds to SS polarity (see a video Appendix C-3).

The observations presented in this chapter focus on two main aspects of the above-mentioned behaviour of *M. bavaricum*, namely the swimming velocity of NS cells as they approach the pH front, and the type of magneto-chemotaxis observed once the cells are immersed in a pH gradient.

6.3.1 *M. bavaricum* velocity in pH gradient

M. bavaricum velocity was measured by calculating the ratio between fixed distances of ~0.2 mm (hereafter referred as steps) traced by individual cells, and the time interval covered by the corresponding video frames. In order to follow the swimming path beyond the limited view field of the objective, the stage was moved from time to time in order to keep track of the same cell until it reached the pH front. The swimming velocity of individual *M. bavaricum* in pH 4-11 is shown in Figure 6.3. Because *M. bavaricum* swims out of sediment, goes through neutral water (pH 7) and finally encounters the pH front (Figure 6.1), the first steps represent velocity variations related to the sediment-water transition, while the last steps represent velocity responding to pH front. Almost all *M. bavaricum* cells abruptly stop to swim when entering the pH gradients created with pH 4-11 solutions, while the cell body continues to vibrate with the same frequency observed during normal swimming, but larger amplitude. Normal swimming is not resumed if the magnetic field is reversed as it often occurs when cells stop near a sediment particle. If a rotating field is applied, these cells rotate round one end of the body, unlike the case of dead and normally swimming cells, which rotate around the body centre (see video in Appendix C-4). This behaviour suggests that although flagella rotation is not interrupted, the configuration of individual flagella (rotation sense and orientation) is such that the net propulsion force is zero.

In general, the swimming velocity of individual cells starts with irregular variations due to the sediment-water transition, followed by a regular trend reflecting constant, slightly increasing, or slight decreasing velocities. This trend continues until the pH gradient is reached. Here, the following trends are observed: (1) velocity decrease (e.g. in pH 5.5 and pH 8.6-11), (2) velocity increase (e.g. in pH 4, pH 6 and pH 7), and (3) constant velocity

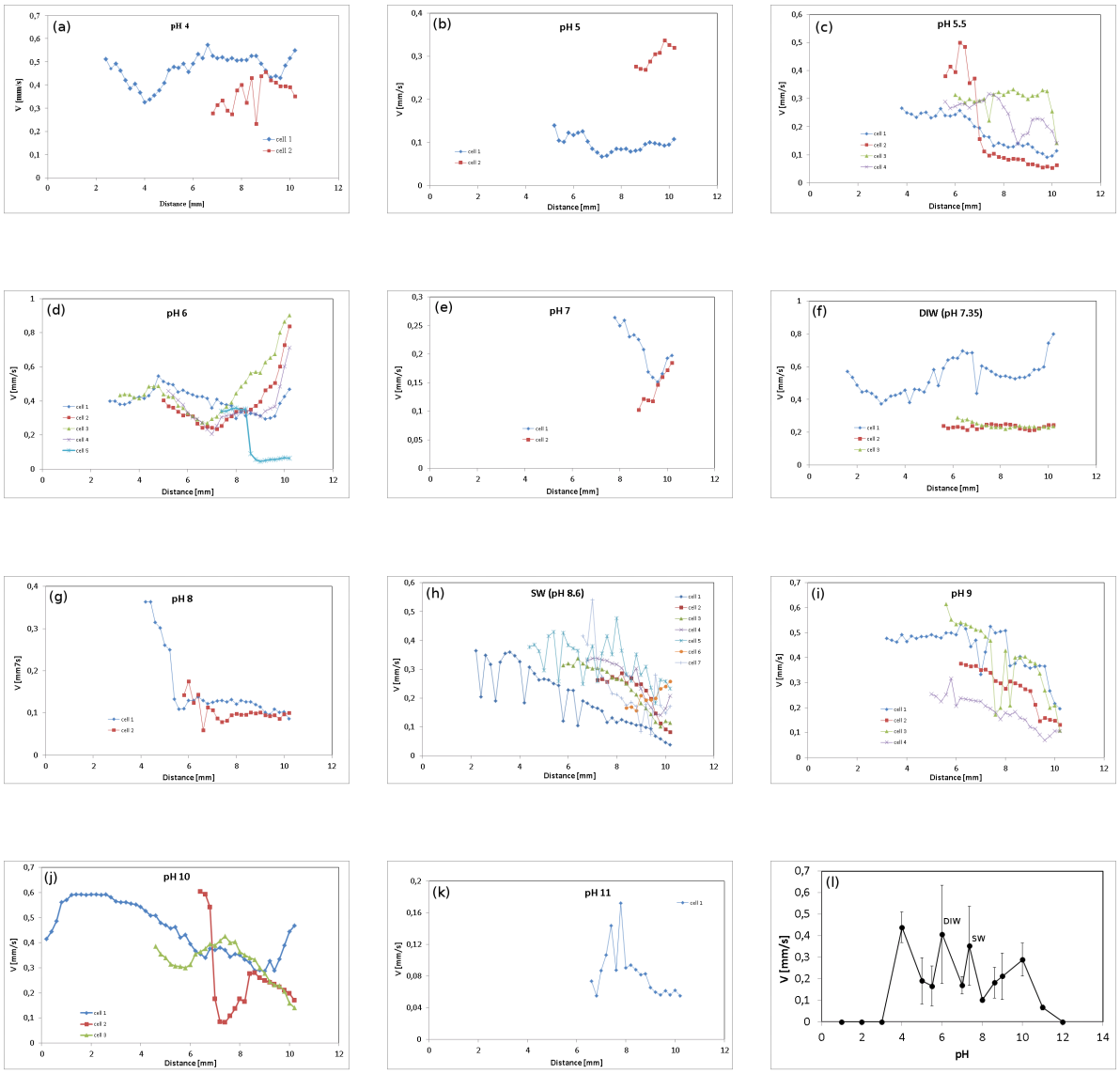

Figure 6.3: *M. bavaricum* velocity in pH (4-11) gradients. Using the setup in Figure 6.1, (a-k) the swimming velocity of single *M.bavaricum* under light microscope was recorded up to 10.2 mm where cells stopped in pH solution. DIW represented distilled water and SW was sediment water above sediment-water interface. (l) Average velocity (average of the last ten steps) in each pH gradient. *M. bavaricum* quickly lost its motility in pH 1 and pH 12, in which average velocity was taken zero. Because *M. bavaricum* in pH 2,3 displayed frequent back-and-forth swimming, the average velocity was taken zero as well.

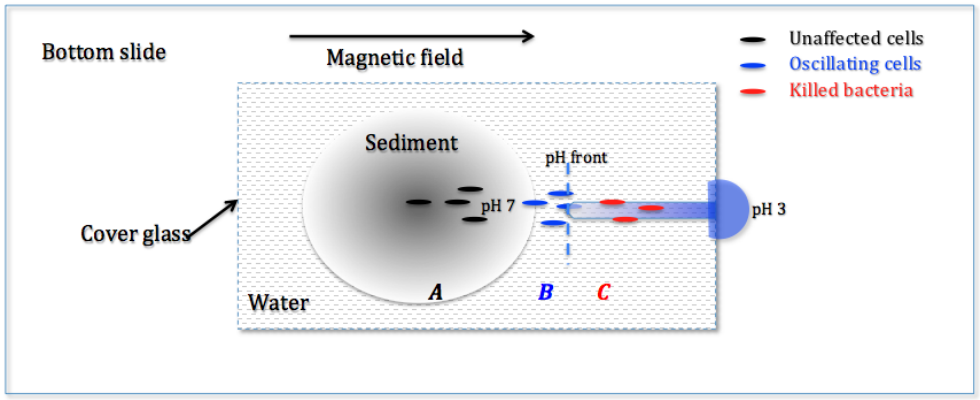

Figure 6.4: *M. bavaricum* behaviour in pH 2 or pH 3 gradient is described in the 3 zones. In magnetic field pointing to the right side, cells in zone A kept swimming out of the sediment towards pH front. Some cells swimming into pH solution stopped immediately in zone C. *M. bavaricum* in zone B (close to pH front) displayed frequent back-and-forth motion. As the field direction was reversed, cells in zone B swam towards zone A without oscillating behaviour. If initial field direction was restored, those *M. bavaricum* that entering zone B recovered their back-and- forth motion again.

(e.g. pH 5, cell 2,3 in DIW and pH 8). Such trends are not always systematic, even under identical experimental conditions, probably because the response of individual cells depends also on their internal state, in addition to the external environment. Nevertheless, a more or less gradual velocity decrease is prevalent for pH $>$ 8 and occurs even in experiments prepared with sediment water (SW, pH 8.6), in which case the adverse effect of excessively basic conditions can be excluded. These observations suggest that additional factors, such as nutrient availability and oxygen, might influence the swimming velocity besides pH. The average swimming velocity in the pH gradient, calculated from the 10 last steps before motion stop, shows a slight decrease with increasing pH. However, the significance of this trend is questionable, given the low number of observations (Figure 6.3l). Overall the swimming speed of *M. bavaricum* appears to be comprised between 0.1 and 0.4 mm/s over a wide range of pH values between 4 and 11.

6.3.2 Magneto-chemotaxis behaviour

When swimming into pH gradients created with pH 2-3 solutions, *M. bavaricum* cells display a complex swimming behaviour that is not seen if solutions with other pH values are used. This behaviour is best described by dividing the cover slide into three zones,

labeled with "A", "B" and "C" according to the increasing proximity to the pH solution (Figure 6.4). If the magnetic field points to the side of the cover slide where the pH solution is added, NS cells swim out of the sediment and continue to do so as long as they are in zone A. Some cells swim until a sudden and irreversible stop in zone C, where they are presumably killed by excessively acidic conditions. Other cells show a distinct swimming behaviour as soon as they reach zone B. In most cases, they engage an oscillatory movement produced by switching of swimming direction every 0.5-1 s. There is no bias in favour of one direction, so that individual cells oscillate around a mean positions for up to ∼30 min (Figure 6.5a). More careful control on pH amount (i.e. the pH diffusion rate with time) allows to observe the evolution of this oscillatory phenomenon. If pH gradient is not such sharp and cells have enough time to response to pH gradient, large part of cells (>50%) become SS when encountering the pH front, thereby reversing the swimming direction to swim away the pH front (Figure 6.5b). The newly formed SS bacteria occasionally switch their swimming direction for short periods of time (0.5-1 s), however, the net swimming direction is strongly biased the magnetic S. As the pH front moves towards the left side with time (Figure 6.1), this SS behaviour dominates until to an area (zone B) where backward swimming is replaced by frequent back-and-forth motion (Figure 6.5a).

According to these observations, zone A can be identified with the portion of water film under the cover slide that is not yet reached by the pH gradient, and zone B with part of the pH gradient that is sensed by *M. bavaricum* without being killed. In zone C, the pH drops below a specific survival threshold and cells are killed (Figure 6.2). If the magnetic field was reversed during the experiments, oscillating bacteria in zone B ceased to switch swimming direction and began to swim regularly as NS cells (90-95%) or SS cells (5-10%). In a reversed field, formerly oscillating NS cells swim back into zone A, while SS cells advance towards zone C, where they eventually stop (Figure 6.5c). If the original field direction is restored, motile NS and SS cells (if not stop in zone C) will return to their original position in zone B and engage the same oscillatory behaviour observed before field reversal (Figure 6.5a). A situation similar to that produced by field reversal is obtained if the field is turned by 90°(Figure 6.5d). Also in this case the oscillatory behaviour ceases and cells begin to swim consistently parallel or antiparallel to the field according to their polarity.

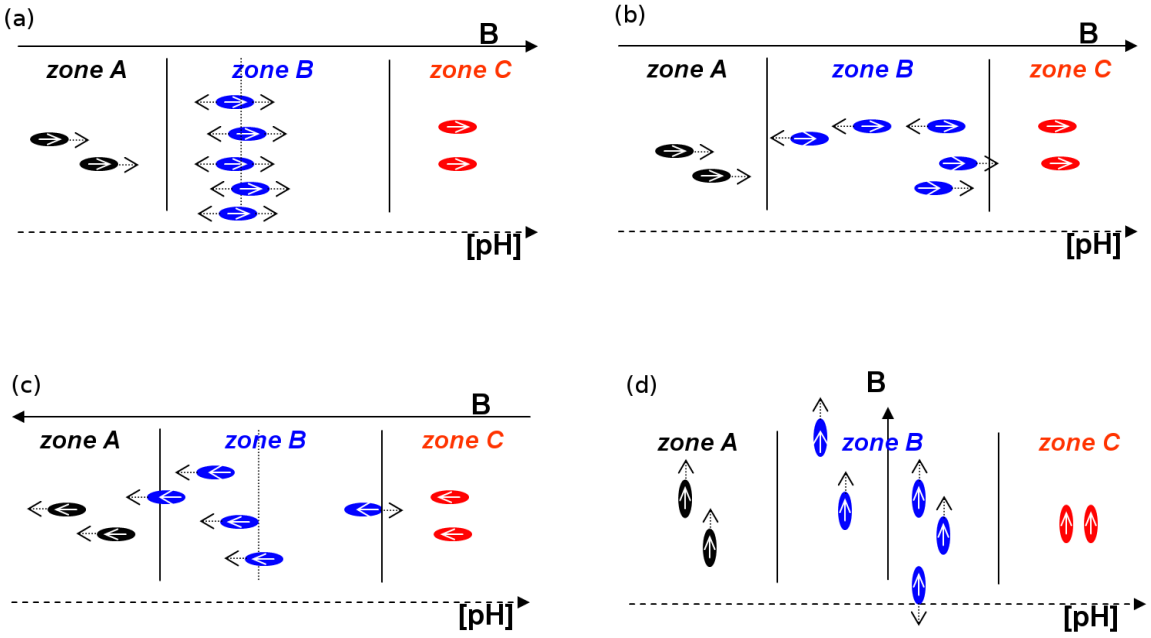

Figure 6.5: Back-and-forth motion and magnetic polarity switch in pH 2 or pH 3 gradient. (a) In some area of zone B (e.g. around the dotted line), frequent backward and forward motion are identical in velocity and distance. Bacteria magnetic polarity in this case is difficult to determine except by reversing field direction as in (c). (b) In zone B, some bacteria (in some case >50%) swim backward (become SS) until they come to the area in zone B as in (a) where back-and-forth motion occurs. The non-switched NS cells will enter zone C and be killed. (c) After field reversal, NS and SS swim in opposite direction without oscillatory motion. SS fraction (∼5-10%) is practically smaller than NS. Finally, SS will be killed in zone C and NS get to zone A. (d) Similar to (c) except that the field direction rotates by 90°, and also NS and SS swimming direction.

6.4 Discussion

A detailed insight in the behaviour of oscillating cells in zone B has been obtained by digitizing video (Appendix C-3) (Figure 6.6). The first example (Figure 6.6a-b) represents a large cell that oscillated with unusually large amplitude, which allowed a detailed track of the swimming path. The swimming path is composed of discrete sections characterized by constant swimming velocities with alternating sign, as deduced from the saw-tooth pattern of the x-coordinate $x(t)$. The y-coordinate, on the other hand, remain constant with little random fluctuations, as expected from the good alignment of cells with a magnetic field parallel to x. The asymmetry of the saw-tooth pattern is due to the fact that the swimming velocity of SS tracks is consistently $\sim$37% smaller than that of NS tracks. During SS tracks, *M. bavaricum* cells display an evident, rapid wiggling around the mean velocity vector, which is probably due to flagella rotating against their natural curl, therefore protruding far from the cell body instead of being wound around it, as during NS tracks (Steinberger et al., 1994). This observation show that polar magnetotaxis is intrinsically asymmetric. This asymmetry is evident in water, but might be irrelevant inside the sediment, where the displacement of cells is controlled by the "permeability" of the material, rather than the swimming velocity itself. The example of Figure 6.6a-b clearly shows that oscillations around a mean position are not random, being caused by swimming direction changes occurring at two fixed relative distances from the pH front.

Most *M. bavaricum* cells in zone B oscillate much more rapidly than the example discussed above, as seen in Figure 6.6d. Most cells change their swimming direction with a frequency $\sim$6 Hz, so that NS and SS tracks last for only 2-3 video frames. In this case, data are too noisy to discriminate between NS and SS swimming velocities; nevertheless, the mean velocity is similar in all examples shown in Figure 6.6. Differences in the amplitude of the oscillatory behaviour are thus caused by different rates of swimming direction switching. The example of Figure 6.6d is interesting because it is the only one depicting a cell that is freely swimming in water, without the influence of nearby sediment particles. The progressive decreasing trend of the mean x-position is probably due to the advancing pH front. In both examples of Figure 6.6a-d, the magnetic field was switched while the cells were NS. After field switching, cells continue to be NS and swim away from the pH front.

The last example (Figure 6.6e-f) was chosen because it depicts two oscillating cells that are only 50 μm apart from each other. These cells can be assumed to be subjected to the same environmental conditions. Before the field is switched, both cells oscillate around mean positions that display the same trend. The field is switched when both cells

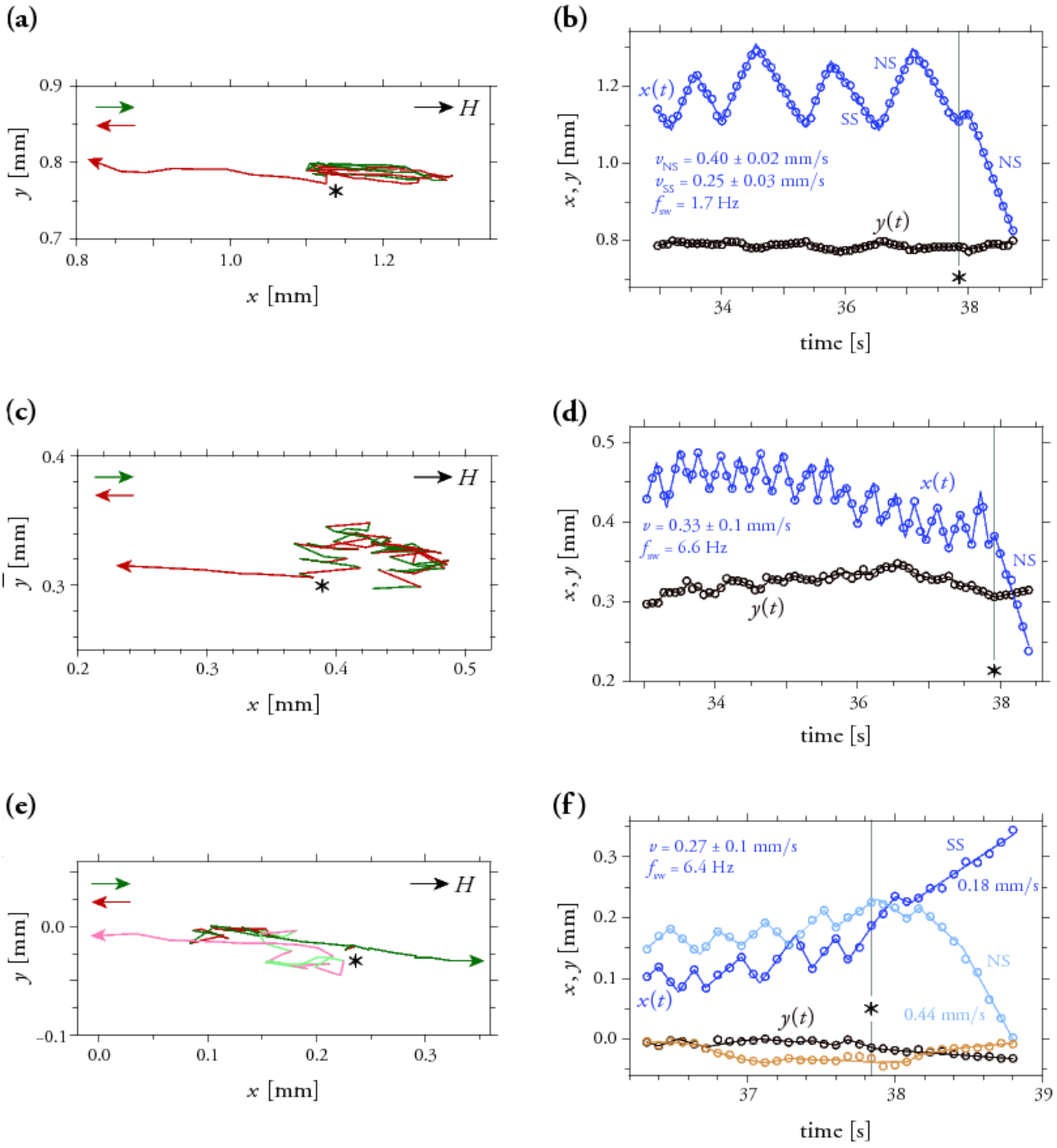
(a)
(b)
(c)
(d)
(e)
(f)
H
y [mm]
x [mm]
x(t)
y(t)
NS
SS
x, y [mm]
time [s]
v_NS = 0.40 ± 0.02 mm/s
v_SS = 0.25 ± 0.03 mm/s
f_sw = 1.7 Hz
v = 0.33 ± 0.1 mm/s
f_sw = 6.6 Hz
v = 0.27 ± 0.1 mm/s
f_sw = 6.4 Hz
0.18 mm/s
0.44 mm/s

as NS, yet one cell remains NS, as in the previous example, while the other cell becomes SS and swims toward the pH front. Because of identical external conditions, the different behaviour of the two cells must be attributed to internal, cell-specific factors.

6.4.1 pH tolerance and sensing by *M. bavaricum*

Experiments with MTB cells swimming into a controlled pH solution show that *M. bavaricum* continues to swim past the gradient front in pH values ranging from 4 to 11. For comparison, the pH of our carbonaceous sediment is comprised between ∼8.6 at the sediment-water interface and 7-7.5 at greater depths (Jogler et al., 2010). Lower pH values might be encountered on a microscopic level, due to fast decomposition of organic matter in microscopic spots. Long-term exposition to a CO_2 atmosphere (chapter 3) lowers the sediment pH to 4-6. In this case, the motility of *M. bavaricum* cells observed under the microscope in the same atmosphere is greatly reduced. The oscillating behaviour observed for cells entering a pH gradient obtained with pH 2-3 solutions can be interpreted as the successful reaction to a repellent. Such behaviour is not seen with steeper gradients created with more acidic solutions because of the finite time required for pH sensing, which lets the cells swim into a deadly environment.

Prolonged permanence of *M. bavaricum* cells in excessively acidic or alkaline conditions

Figure 6.6 *(preceding page)*: Oscillatory swimming paths of selected *M. bavaricum* cells in zone B (left plots) digitized from video Appendix C-3, and corresponding x- and y-coordinates as a function of time (right plots). In left plots, green and red sections of the swimming paths correspond to swimming velocities pointing to the right and the left, respectively. The magnetic field is pointing to the right (black arrow), until it is reversed at $t = 37.8$ s. The point at which this occurs is marked by an asterisk in all plots. In right plots, the coordinates $x(t)$ and $y(t)$ of the swimming path (circles) have been fitted with straight segments denoting a constant swimming velocity. Before the field is reversed, positive and negative slopes of $x(t)$ denote NS and SS cells, respectively, while the opposite is true after field reversal (asterisk). (a-b) Large *M. bavaricum* cells performing unusually large oscillations, which allowed precise determination of the swimming path. The asymmetric saw-tooth pattern in (b) reflects distinct, but consistent NS and SS swimming velocities. The cell was NS when the field has been reversed. (c-d) Same as (a-b) for a smaller cell performing smaller and faster oscillations. (e-f) Same as (c-d) for two very close cells (darker and lighter colours). In this case one cell (darker color) becomes SS when the field is switched, and therefore continues to swim towards the pH front. The isolated switching of the swimming direction after field reversal is a tactile response due to the collision with a sediment particle.

produces a sudden stop in forward motion. Some cells continue to vibrate as if flagella rotation would continue. Observations in rotating field (see section 6.3.1) support the hypothesis that flagella are no longer wrapped around the cell, as it is the case during normal forward swimming of NS cells (Spring et al., 1993). Instead, flagella might have become untangled, maybe because of opposed rotation directions. This can explain the lack of forward motion of the whole cell.

6.4.2 Magneto-chemotaxis in pH gradients under oxygen saturation

The oscillating behaviour of *M. bavaricum* in zone B resembles the swimming behaviour of spirilla in the hanging drop assay. However, the causes must be completely different. In absence of a gradient, the temporal sensing mechanism of spirilla is subjected to random fluctuations and measures essentially noise, triggering reversals of the swimming direction at random times. The oscillation of *M. bavaricum* in zone B, on the other hand, is very regular (Figure 6.6), and it occurs in proximity of zone C, where excessively acidic conditions suppress cell motility. This means that the concentration of H^+ ions in zone B is abundantly above the noise level of the cell sensory mechanism, so that changes in swimming direction are triggered deterministically either by concentration gradients or by concentration thresholds. In order to obtain more information about the triggering mechanism, two models are constructed in the following, based on different assumptions about how a repellent is sensed by *M. bavaricum*. In both models, the concepts of NS and SS are referred to bacteria grown in the Northern hemisphere, where NS brings cells to greater depths in sediment or water columns.

Model 1: Gradient sensing

In this model, it is assumed that the swimming direction of *M. bavaricum* is switched by a positive repellent gradient, i.e. if the repellent concentration increases with time along the swimming path. Gradient sensing can be realized by a temporal mechanism with which the cell compares the concentrations $C_1 = C(x(t))$ and $C_2 = C(x(t + \Delta t))$ of a repellent along the swimming path $x(t)$, as measured in successive time intervals Δt, where C is the concentration of H^+-ions. In this case, the gradient along the swimming path is given by $G(x) = C_2 - C_1$.

Because *M. bavaricum* cells are consistently NS in gradient-free hanging drop assays, both with oxygen saturation and under anoxic conditions, this swimming direction must be considered as a sort of "default" state. Furthermore, switching of the swimming direction

must occur only if a gradient exceeds a positive threshold G_0 : without such threshold, random switching would occur in absence of gradients because of the noise in $G(x)$, as it is observed with spirilla.

According to this model, *M. bavaricum* cells are consistently NS as long as they are in zone A. In zone B, the concentration of H^+-ions increases rapidly (Figure 6.2), along with the gradient, until the threshold G_0 is reached. At this point, cells become SS and swim away from the pH front. This phenomenon can explain the observation of SS cells forming in zone B, however, an additional switching mechanism is needed to explain the oscillating cells in the same zone. Such mechanism can be constructed by assuming that cells switch their swimming direction again, when the amplitude of the negative gradient sensed while being SS falls below a second threshold G_1 , which signals that the cell is at a "safe" distance from the repellent. The second swimming direction switching makes the cells becoming NS again, and moving back to the pH front, where another switching cycle begins.

This model, however, fails at explaining the behaviour of oscillating *M. bavaricum* cells when the magnetic field is reversed. This is because gradient sensing produces axial magnetotaxis, which is insensitive to magnetic field reversals. For example, if the magnetic field is reversed while a cell is SS, this cell will swim back towards higher concentrations of H^+-ions, sensing again a positive gradient in excess of G_0 . This triggers another change in the swimming direction, and the cell becomes NS, swimming away from the pH front in the reversed field. If, on the other hand, the field is reversed while oscillating cells are NS, all of them will continue to be NS and swim away from the pH front. In both cases, oscillating cells must become NS when the field direction is reversed. This result, however, is contradicted by observations formerly oscillating cells becoming SS after field reversal (e.g. Figure 6.6e-f).

Model 2: Threshold sensing

In this model, it is assumed that the swimming direction of *M. bavaricum* is switched by a specific repellent threshold signal sensed by the cell. Along with Berg and Purcell (1977) it is assumed that the capture of repellent molecules by receptors is a diffusion-controlled process. This produces a certain delay between the repellent concentration $C(x(t))$ along the swimming path $x(t)$ of the cell, and the "internal" concentration $C_{int}(t)$ felt by chemoreceptors. The relationship between C and $C_{int}(t)$ is established by the diffusion equation. In order to keep the conceptual model as simple as possible, diffusion is modelled in one dimension across a fixed distance L_0 . The boundary conditions are

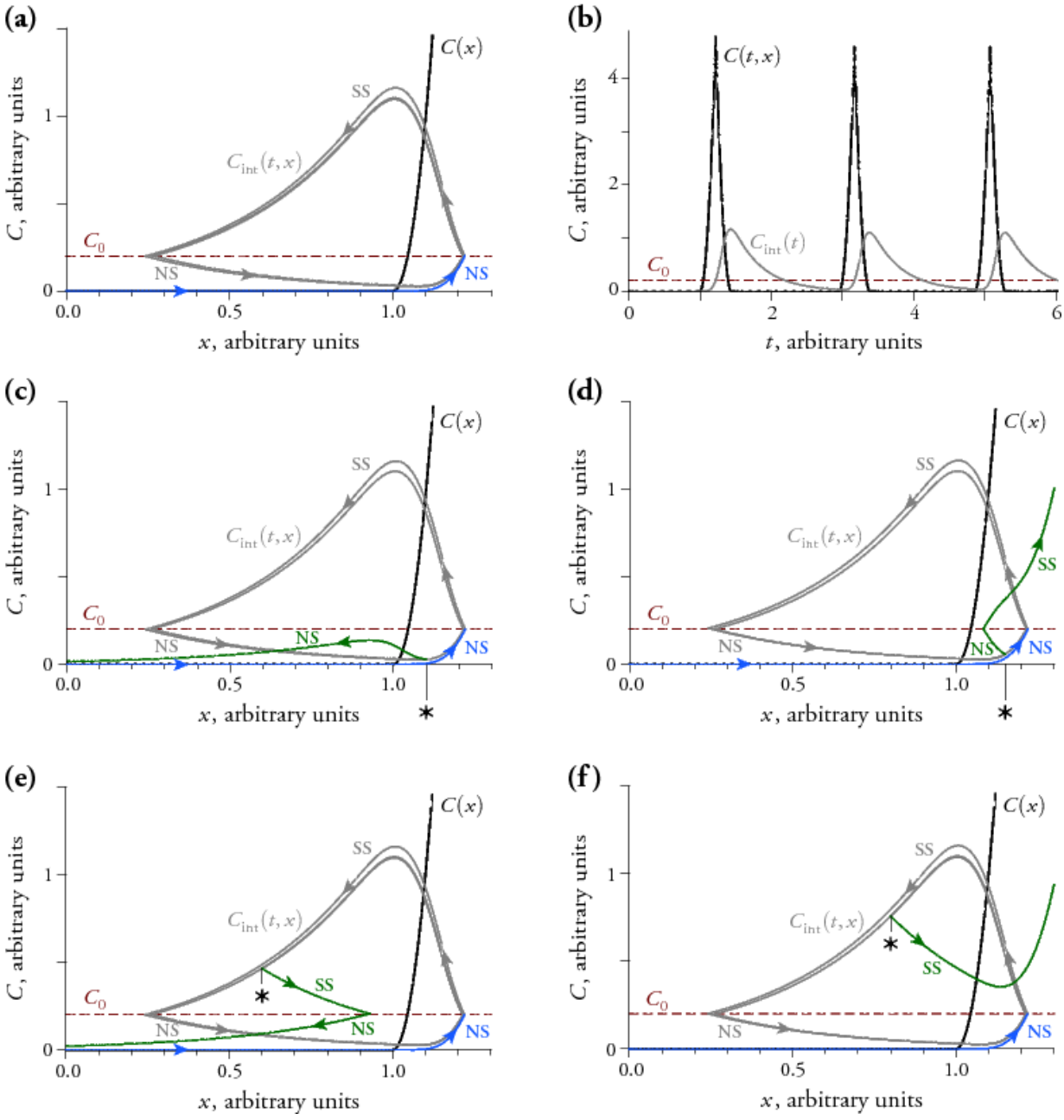
(a)
C, arbitrary units
C(x)
SS
C_int(t,x)
C_0
NS
NS
x, arbitrary units
(b)
C, arbitrary units
C(t,x)
C_int(t)
C_0
t, arbitrary units
(c)
C, arbitrary units
C(x)
SS
C_int(t,x)
C_0
NS
NS
NS
x, arbitrary units
(d)
C, arbitrary units
C(x)
SS
C_int(t,x)
SS
C_0
NS
NS
NS
x, arbitrary units
(e)
C, arbitrary units
C(x)
SS
C_int(t,x)
SS
C_0
NS
NS
NS
x, arbitrary units
(f)
C, arbitrary units
C(x)
SS
C_int(t,x)
SS
C_0
NS
NS
x, arbitrary units

then given by $C(x(t))$ on one side, and $C_{int}(t)$ is the concentration measured on the other side at a distance L_0 . In modelling a cell approaching a pH front, the initial condition is $C(x(t))$=0 and $C_{int}(t)$=0 in zone A, where C is the concentration of H^+-ions. Cells are initially NS, so that $x(t) = vt$, where v is the swimming velocity. In zone B, $C(x(t))$ starts to increase, and the same happens to $C_{int}(t)$ with some delay caused by diffusion across L_0 . Simulations of this process are shown in Figure 6.7. When $C_{int}(t)$ reaches a critical threshold C_0 , the swimming direction is switched and the cell becomes SS, moving back towards the starting point. C_{int} continues to increase as long as $C > C_{int}$, and starts to decay slowly as the repellent zone is left. If the cell remains SS, C_{int} will eventually decrease below a threshold that makes the cell becoming NS again. For convenience, we

Figure 6.7 ***(preceding page)*:** Simulations of the oscillatory swimming pattern of *M. bavaricum* in zone B, according to model 2 explained in the text. All diagrams except (b) represent a fixed concentration profile of a repellent along x. The concentration profile is taken from the solution of the diffusion equation on a glass slide (Figure 6.2). (a) A NS cell starting at x=0 swims with constant velocity along $+x$ and enters in the zone x>1 where $C(x)$>0 . The signal $C_{int}(t)$ of the sensed repellent starts to increase with a certain delay due to diffusion (blue line with arrow indicating the swimming direction), until it reaches a threshold C_0 that makes the cell becoming SS and swimming back along $-x$. C_{int} continues to increase for a while and then slowly decreases as the repelling zone is left (grey curve with arrow indicating the swimming direction). When C_{int} decays back to C_0 , the cell is at a "safe" distance from the repellent and becomes again NS. The swimming direction is reversed, but C_{int} continues to decay until the repelling zone is reached again, and the cycle is repeated (grey lines with arrows). The cell continues to reverse its swimming direction any time C_{int} increases above C_0 or decrease below C_0 , oscillating between two values of x. (b) Shows the same process as (a) in a graphics where $C(x(t))$ and $C_{int}(t)$ are plotted as functions of time. The delayed response of C_{int} to changes in C is clearly visible. Peaks of C correspond to the position x where the cell changes from NS to SS. (c-f) Same as in (a), except for the fact that the magnetic field is switched from $+x$ to $-x$ at a point marked with an asterisk. C_{int} after field reversal is shown with a green curve. In (c-d) the field is reversed while the cell is NS: in (c) this occurs at a point where C_{int} is sufficiently small and no longer increases above C_0 . In this case, the cell remains NS and swim away from the repellant front in the reversed field. In (d), C_0 is eventually exceeded and the cell becomes SS. Because the field is reversed, it will swim further towards $+x$ and higher repellant concentrations. In (e-f) the field is reversed while the cell is SS: in (e) this occurs at a point where C_{int} is sufficiently small to decay below C_0 before the repellent zone is entered, so that the cell becomes NS and swim away from the repellent front in the reversed field. In (f), C_{int} does not decay below C_0 before the repellent zone is entered, so that the cell remains SS and swims further towards $+x$ and higher repellent concentrations.

assume this threshold to be identical with C_0 . The cell is now far from the repellent zone and C_{int} continues to decrease until this zone is reached again. At this point, diffusion makes C_{int} increase and exceed C_0 a second time, and the cell becomes SS. This cycle is repeated indefinitely in the same manner, as long as $C(x)$ is constant, producing periodic functions of $x(t)$, $C(x(t))$ and $C_{int}(t)$. The periodicity of $x(t)$ represents the oscillatory behaviour of the cell around a mean position that coincides with the repellent front.

The key factor producing an oscillatory behaviour is the delay that accompanies changes of the sensed signal C_{int} with respect to the repellent concentration $C(x(t))$ around the cell. Without such delay, the cell would switch its swimming direction within an infinitesimal interval around the position x for which $C(x) = C_0$, so that the cell would appear at rest, in contradiction with observations. Another way to generate an oscillatory behaviour is to introduce two thresholds: one, C_0 , for increasing C_{int} , and another one, $C_1 < C_0$, for decreasing C_{int}. This mechanism would be similar to the principles of thermostatic regulation, where different "turn-on" and "turn-off" temperatures are chosen to avoid continuous switching. In the case of MTB, such mechanism would allow cells to "escape" from repellents, instead of becoming immobilized at a certain distance where $C(x) = C_0$. Furthermore, this mechanism allows cells to efficiently avoid repellants even in "noisy" concentration gradients, as expected in sediment, where has several local minima in which cells could be trapped.

This model needs to be tested against observations of oscillating cells in reversing fields. Figure 6.7c-f shows four cases where the field is reversed at different points of the cell trajectory, two when the cell is NS and two when the cell is SS. Depending on C_{int} at the moment when the field is switched and its subsequent evolution while the cell is swimming in the opposite direction, the cell might preserve its polarity or switch another time. The final result is a cell that is constantly NS in the reversed field – thus leaving the repellent zone, or constantly SS in the reversed field, in which case it irreversibly swims towards higher repellent concentrations. Because oscillatory cells spend most of their time in a region where the repellent concentration is zero, the probability for a cell to end in a SS state after field reversal is much lower than that of ending in a NS state, exactly as observed with *M. bavaricum* in zone B.

A final point to discuss is the reason for the lack of oscillating cells observations in gradients created with pH 1 or pH 12 solutions. In this case, cells enter zone C and abruptly stop to swim. A possible explanation of this phenomenon is related to the gradient steepness. As shown in Figure 6.7, a certain time is required for an external change in C

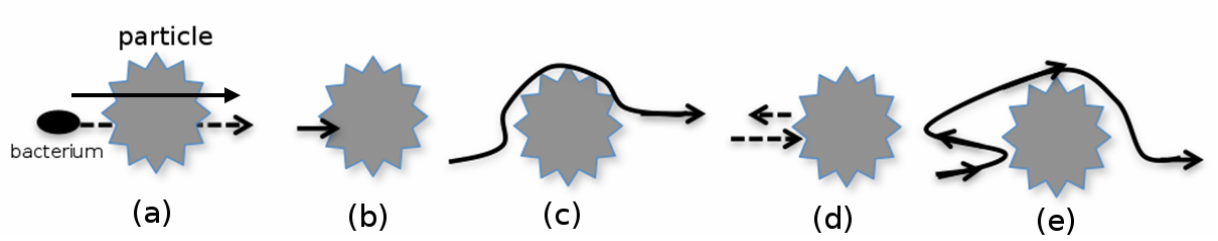

Figure 6.8: Observation of *M. bavaricum* trajectories intersecting sediment particles under the microscope. (a) The intersection is fictive, due to 2D projection, and cells swim undisturbed either above or below the particle. (b) The cell hits the particle and stop, permanently or for some time. If the field is reversed after a cell has stopped by a sediment particle, it might resume its motility. (c) The cell glides around sediment particles. (d) The cell become SS for a short time after hitting an obstacle and switches back to NS (e), hitting the obstacle a second time with a different angle that allows to glide around it.

to be perceived through C_{int} . If the pH gradient is excessively steep, the cell advances too much into the pH front and might be killed before it can switch its swimming direction.

6.4.3 Comparison with tactile responses

The swimming direction of *M. bavaricum* can be briefly switched after collision with sediment particles; however, this phenomenon is a tactile response that is different from the behaviour in a pH gradient as described in previous section. Figure 6.8 show different tactile responses observed under the optical microscope when the swimming trajectory of a cell intercepts a sediment particle. In most cases, the cell continues to swim and "glides" around the particle. In some cases, cells stop to swim as soon as they hit a particle, either permanently or for some seconds. Hitting a sediment particle can also switch the swimming direction for a brief time; however, the cell invariably returns NS and either hits the same particle again, or it "glides" around it. The same cell can perform several attempts to overcome an obstacle in what can be regarded as a strategy to move in a sedimentary environment with little available free space.

6.4.4 A testable model for polar magneto-chemotaxis

Model 2 appears capable of explaining the observations of *M. bavaricum* in zone B, i.e. the reaction of cells to a repellent. In reality, cells in zone B are exposed to two repellents,

namely oxygen and H^+ ions. In this case, the critical H^+-threshold C_0 might be interpreted as the point where the "adverse" effects of H^+ overcome those of oxygen, keeping the cell in a SS state. When C_{int} drops below C_0, the repellent effect of oxygen is dominant, and the cell reverts to its NS state. Under natural conditions (in the northern hemisphere), this state helps the cell "escaping" from excessive oxygen concentration. If MTB must react to more than one repellent, the signals $C_{int,i}$ arising from the detection of different substances needs to be combined into a single signal S that determines the swimming direction. In case of an additive combination,

$$S = \sum_i \chi_i C_{int,i} \tag{6.5}$$

where $C_{int,i}$ is the "perceived" concentration of the i-th repellent, and χ_i the sensitivity of the cell to this specific repellent. Chemoattractants (e.g. nutrients) can be included in eq. (6.5) by assigning them a negative value of χ_i : in this way, a chemoattractant decreases the total "repulsion".

In an ideal environment without repellents and with appropriated nutrients, cells have no need to be motile: flagella propulsion costs energy and, as demonstrated by Berg and Purcell (1977), it does not increase the intake rate of nutrients. Therefore, it is reasonably to assume that if $S<0$, as resulting from no repellents and some nutrients, MTB cells come to rest. Because of the difficulty of realize such conditions in the hanging drop assay, MTB always appear motile, except for some cases of interaction with sediment, where a cells stops swimming as it comes in contact with a sediment particle (section 6.4.3). In this case, the benefit of available nutrients might overcome the disadvantage of high oxygen concentrations. The main factor affecting S is probably the oxygen concentration, since the most obvious correlation between MTB distribution and chemical gradients in stratified environments is found with oxygen. For these reasons, if $S>0$ but below a positive threshold S_0, polar MTB cells display a "default" swimming direction that brings them deeper, where oxygen concentration is expected to decrease. In the northern hemisphere, this is the NS state. The absence of other important repellents in the oxic zone of the living environments of MTB might explain the benefit of this choice of cell polarity. In this way, MTB cells accidentally brought in the oxic zone, for example by bioturbation, will gain their typical living depth, where they might stop to swim. If other repellents capable of raising S above a threshold S_0 are mainly found in the anoxic zone, switching the swimming direction helps MTB moving towards the oxic zone, where such repellents

are not expected.

This model arises some fundamental questions. The first question concerns the comparison with axial magnetotaxis. Because polar magneto-chemotaxis is prone to errors in environments where the chemical gradient is reversed with respect to the magnetic field, it appears that gradient sensing, which leads to axial magnetotaxis, is a much more effective manner of finding most suited environmental conditions. Gradient sensing, on the other hand, is adversely affected by random environmental fluctuations, which might trap MTB cells inside microscopic local minima of repellent concentrations. A possible strategy for polar MTB to overcome "reversed" chemical gradients is the ability to "learn" from such situation and adapt to it by "reversing" the polar link between flagella rotation and sensing. In this case, cells that were normally NS under oxic conditions must become SS. This ability has indeed been observed for *M. bavaricum*. For example, a proportion of NS cells suddenly became SS when entering zone B, without engaging an oscillatory motion as most cells do. In this case, because of the impossibility to follow individual cells under the microscope for long time, it was not clear if this behaviour corresponds to an intrinsic change of polarity, or if the cell would eventually return NS after some time. More solid evidence for adaptation came from indirect observations of *M. bavaricum* in sediment (chapter 5): in this case, a minor fraction of cells were able to move in the right direction within few days despite wrong field polarity.

The abovementioned model for polar magneto-chemotaxis opens new testing possibilities. For example, experiments with pH gradients could be repeated under anoxic conditions to see whether cells engage the same oscillatory behaviour in front of an acidic solution, or if they just switch their swimming direction once, as observed in few cases under oxic conditions.

6.5 Conclusions

The experiments described in this chapter aimed at testing some important aspects of polar magnetotaxis on the example of *M. bavaricum*. Polar magnetotaxis, as hypothesized by Frankel et al. (1994) appears to be based on sensing concentrations, rather than gradients, with respect to one or more critical thresholds. In the magneto-aerotaxis model of Frankel et al. (1997), two oxygen thresholds have been used to explain the NS and SS polarities of cultured cocci. The lower threshold, supposed to induce a SS polarity, was never observed in wild-type cocci and *M. bavaricum* in the hanging drop assay under strictly anoxic con-

ditions. Because experiments with MTB migration in sediment indirectly confirmed the existence of SS cells, other factors must be responsible for the induction of a SS state. Hanging drop assays where a pH gradient was created by adding an acidic solution on one extremity of the drop led for the first time to the direct observation of SS cells of *M. bavaricum* as these cells were swimming from near-neutral water into a mixing front with pH 2-3. In this case, most cells engaged a stationary sequence of polarity changes that led them oscillate around a mean position for up to 30 min. This behaviour disappeared after a field reversal, with most cells ending in a NS state and swimming away from the pH front, and few cells ending in a SS state, in which case they swam further until a sudden stop, probably caused by excessive acidity. An axial magnetotactic model based on gradient sensing can explain the oscillatory behaviour, but not the small fraction of SS cells after field reversal. Furthermore, a gradient sensing model contradicts the observation of *M. bavaricum* cells with well-defined polarity in absence of chemical gradients. Polar magnetotaxis with a single pH threshold, on the other hand, can explain all experimental observations. Unlike in magneto-aerotaxis, SS cells are produced by the increasing concentration of other substances that might be commonly present in anoxic environments, rather than oxygen. For this reason polar magnetotaxis can be considered as a form of magneto-chemotaxis, where the polarity of MTB cells is determined by several substances.

As seen with hanging drop experiments in a pH gradient after field reversal, polar magnetotaxis does not always produce the correct polarity required for seeking ideal environmental conditions if the chemical gradient is reversed with respect to its usual orientation to the magnetic field in a horizontally stratified environment. This problem does not exist with axial magnetotaxis, where field polarity, and thus the direction of chemical gradients with respect to the field, appears irrelevant. Therefore, polar magnetotaxis might appear as a less efficient mean of performing chemotaxis. However, gradient sensing is expected to be more adversely affected by environments with microscopic concentration fluctuations: in this case, cells performing axial magnetotaxis might become entrapped by local minima of the concentration of some repellents, while polar magnetotaxis can better overcome local fluctuations. Furthermore, a minor fraction of *M. bavaricum* cells exposed to a mismatch between chemical gradients and magnetic field polarity appear to be capable to adapt to this situation by reversing the mechanism by which chemical sensing controls flagella rotation.

Similar observations could not be performed with wild-type cocci, which did not show any response to pH gradients, nor the capability to adapt to situations in which there

is a mismatch between oxygen gradient and field polarity. The reason for this difference is unclear. In any case, since the existence of wild-type SS cocci is supported by indirect observations in sediment, some not yet known substances might regulate their polar magnetotaxis in a similar manner as observed with *M. bavaricum*.

Appendix A

Supplementary materials in chapter 2: Magnetotaxis and acquisition of a detrital remanent magnetization by magnetotactic bacteria populations in sediment: first experimental results and theory

A.1 Observation of swimming trajectories in water

A.1.1 Sample preparation and MTB observation

The magnetodrome used for our experiments is shown in Figure A.1. MTB are observed with the hanging drop assay, in which a water drop on a cover slide is observed in presence of a magnetic field parallel to the slide (Figure A.2). Actively swimming bacteria will collect on the magnetic N or S side of the drop, depending on their polarity. Wild-type cocci, vibrios, and *M. bavaricum*, exhibit polar magnetotaxis (Frankel et al., 1997), i.e. they consistently swim to the magnetic N in the hanging drop assay (N-seeking, NS). Occasionally, few cells swim to the magnetic S (S-seeking, SS), as already observed by Blakemore (1982); however, the proportion of SS cells taken from microcosms that have been exposed only to geomagnetic fields typical of the N hemisphere, was always $<0.1\%$.

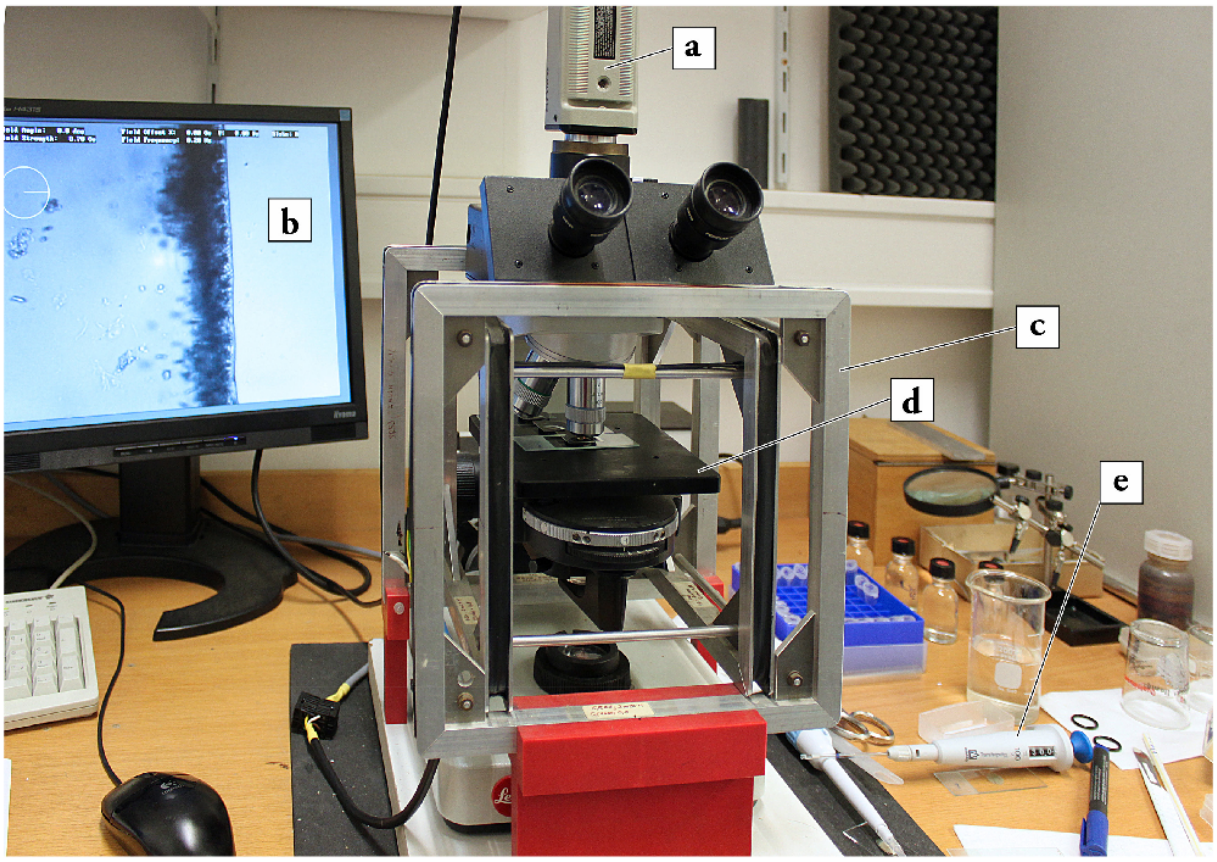

Figure A.1: Apparatus for the observation of magnetotactic bacteria (magnetodrome). (a) Camera attached to the optical microscope. (b) Live image from camera, showing *M. bavaricum* cells accumulating at the edge of the water drop in the hanging drop assay. (c) Helmholtz coils for providing controlled fields in horizontal direction. (d) Object stage. (e) Micropipette

Dissolved oxygen profiles in microcosms have been measured with a microprofiling system from Unisense (www.unisense.com), consisting of a computer-controlled vertical stage that moves an oxygen microsensor (OX50) with 50 μm outside tip diameter and 0.3 μM detection limit.

A.1.2 Swimming trajectories observation

Samples for swimming trajectory observations were prepared as follows. About 10 μl sediment were taken from microcosms with a micropipette and transferred on a glass slide. After adding a drop of pure water on one side of the sediment spot in order to provide a clear field of observation, the glass slide was further prepared for a hanging drop assay

Figure A.2: Preparation of the hanging drop assay. A vacuum-greased O-ring is placed on a microscope slide, providing the support for a cover slide carrying a drop of sediment-containing water. The cover slide (thin squared glass) is placed upside-down, so that the drop in enclosed in the space sealed by the O-ring. Contact sealing by the vacuum grease prevents evaporation, preserving the drop for long observation under the microscope. Bacteria migrating towards the drop edge become visible under the optical microscope.

(Figure A.2) and placed under the microscope. Application of a magnetic field pointing to the side where the water drop was added makes N-seeking bacteria exit the sediment and swim in water (see video Appendix C-1), until they collect on the drop edge. After a sufficient number of cells have been collected, the field is reversed in order to make the cell swim away from the drop edge. Finally, the field is reversed again, and the path of freely swimming cells is recorded.

The mean alignment of cells is defined by

$$\zeta = \frac{\|P_n - P_1\|}{\sum_{k=2}^{n} \|P_k - P_{k-1}\|} \tag{A.1}$$

where $\{P_1, P_2, \cdots\}$ is a sufficiently dense sequence of point coordinates along each trace. Over 1000 individual trajectories have been collected for each MTB type and each field intensity in order to ensure sufficient statistical significance. Eq. (A.1) was directly applied to manually digitized traces obtained in fields up to 10 μT for ovoid cocci and 2 μT for *M. bavaricum*. Alignments in larger fields have been estimated with a more efficient method based on the Fourier transform of trace images (e.g. Redon et al., 1998). In this case, the probability density function of trace directions with angle between trace vectors and

magnetic field is given by:

$$g(\theta) = \frac{\int_0^{\infty} |I^*(k, \theta + \pi/2)|\, k\mathrm{d}k}{\int_0^{2\pi} \mathrm{d}\psi \int_0^{\infty} |I^*(k, \psi)|\, k\mathrm{d}k} - C \tag{A.2}$$

where I^* is the Fourier transform of a trace image $I(x, y)$, expressed in polar coordinates, and C is a constant related to image noise. The distribution $f(\theta)$ of cell orientations is obtained from eq. (A.2) with $2g(\theta) = f(\theta) - f(\pi - \theta)$. The theoretical background of eq. (A.2) is explained in the following.

Swimming trajectory images $I(x, y)$ of black (I=0) and white (I=1) pixels (Figure 2.2a,b) provide a textured pattern whose Fourier spectrum convey information about the statistical distribution of cell orientations. For this purpose, we consider a function $T(u, v)$ that describes a certain anisotropic texture with respect to the principal axes u and v , and let $I(x, y)$ describe the same texture after it has been rotated counterclockwise by an angle φ . Relations between (x, y) and (u, v) coordinate systems are given by:

$$\begin{bmatrix} u \\ v \end{bmatrix} = \begin{bmatrix} \cos\varphi & \sin\varphi \\ -\sin\varphi & \cos\varphi \end{bmatrix} \cdot \begin{bmatrix} x \\ y \end{bmatrix} \tag{A.3}$$

and:

$$\begin{bmatrix} x \\ y \end{bmatrix} = \begin{bmatrix} \cos\varphi & -\sin\varphi \\ \sin\varphi & \cos\varphi \end{bmatrix} \cdot \begin{bmatrix} u \\ v \end{bmatrix} \tag{A.4}$$

The Fourier transform of the two-dimensional function $I(x, y)$ is defined as

$$I^*(k_x, k_y) = \int_{-\infty}^{+\infty} \int_{-\infty}^{+\infty} I(x, y) e^{-2\pi i(xk_x + yk_y)} \mathrm{d}x\mathrm{d}y \tag{A.5}$$

Applying the coordinate transformation of eq. (A.4), the same Fourier transform can be written as:

$$\begin{aligned} I^*(k_x, k_y) &= \int_{-\infty}^{+\infty} \int_{-\infty}^{+\infty} T(u, v) e^{-2\pi i k_x (u\cos\varphi - v\sin\varphi) - 2\pi i k_y (u\sin\varphi + v\cos\varphi)} \mathrm{d}x\mathrm{d}y \\ &= \int_{-\infty}^{+\infty} \int_{-\infty}^{+\infty} T(u, v) e^{-2\pi i u (k_x\cos\varphi + k_y\sin\varphi) - 2\pi i v (k_y\cos\varphi - k_x\sin\varphi)} \mathrm{d}x\mathrm{d}y \\ &= T^*(k_x\cos\varphi + k_y\sin\varphi, k_y\cos\varphi - k_x\sin\varphi) \end{aligned} \tag{A.6}$$

Defining

$$\begin{bmatrix} k_u \\ k_v \end{bmatrix} = \begin{bmatrix} \cos\varphi & \sin\varphi \\ -\sin\varphi & \cos\varphi \end{bmatrix} \cdot \begin{bmatrix} k_x \\ k_y \end{bmatrix} \tag{A.7}$$

we obtain the Fourier transform:

$$I^*(k_x, k_y) = T^*(k_u, k_v) \tag{A.8}$$

and because

$$\begin{bmatrix} k_x \\ k_y \end{bmatrix} = \begin{bmatrix} \cos\varphi & -\sin\varphi \\ \sin\varphi & \cos\varphi \end{bmatrix} \cdot \begin{bmatrix} k_u \\ k_v \end{bmatrix} \tag{A.9}$$

we see that I^* is identical to T^* after counterclockwise rotation by φ .

In the following, we consider the special case of a very anisotropic texture represented by:

$$T(u, v) = W(u)G(v), \tag{A.10}$$

where W is a wide function, and G represents the perpendicular profile across a series of narrow patterns (i.e. the cell trajectories). For example, if $T(u, v)$ represents a series of very long, parallel lines, then W is a box function and G is a Dirac comb. The Fourier transform of the rotated texture is given by:

$$I^*(k_x, k_y) = W^*(k_u)G^*(k_v). \tag{A.11}$$

Because W is a wide function, its Fourier transform is approximated by a Dirac impulse and we write:

$$I^*(k_x, k_y) = \delta(k_u)G^*(k_v) \tag{A.12}$$

As a result, the Fourier transform is everywhere zero, except when k_u=0 . This defines the condition $k_x \cos\varphi + k_y \sin\varphi$=0 , which can be rewritten as

$$\frac{k_y}{k_x} = -\cot\varphi \tag{A.13}$$

Introducing the polar coordinates (k, θ) with $k = \sqrt{k_x^2 + k_y^2}$ in Fourier space, eq. (A.13) becomes $\tan\theta = -\cot\varphi$ with solution $\theta = \varphi \pm \pi/2$. This means that the Fourier transform

of linear traces appears to be rotated by 90°. The argument of G^* in eq. (A.12) becomes:

$$\begin{aligned} k_v &= k\sin\theta\cos\varphi - k\cos\theta\sin\varphi \\ &= k\sin(\varphi \pm \pi/2)\cos\varphi - k\cos(\varphi \pm \pi/2)\sin\varphi \\ &= \pm k\cos^2\varphi \pm k\sin^2\varphi = \pm k \end{aligned} \tag{A.14}$$

and we obtain:

$$\begin{aligned} I^*(k,\theta) &= \delta[k(\theta-\varphi-\pi/2)]G^*(+k) + \delta[k(\theta-\varphi+\pi/2)]G^*(-k) \\ &= \frac{1}{k}\delta(\theta-\varphi-\pi/2)G^*(+k) + \frac{1}{k}\delta(\theta-\varphi+\pi/2)G^*(-k) \end{aligned} \tag{A.15}$$

Eq. (A.15) is the Fourier transform of straight trajectories (i.e. line segments) that from an angle φ with the x-axis. Curved traces can be considered as the overlap of straight segments, and because of the non-local property of Fourier transforms, the Fourier spectra of trajectories such as those of Figure 2.2a,b coincides with the sum of spectra obtained from straight segments with a certain distribution of orientations.

Therefore, we consider images obtained from overlapping the same texture after rotation by φ according to an axial (π-periodic) probability density function $g(\varphi)$. Such overlap represents traces with different orientations, as well as sections of curved traces approximated by straight segments. The expectation for the resulting Fourier spectrum is:

$$\langle I^*(k,\theta)\rangle = \frac{1}{k}\int_0^{2\pi} g(\varphi)[\delta(\theta-\varphi-\pi/2)G^*(+k) + \delta(\theta-\varphi+\pi/2)G^*(-k)]\mathrm{d}\varphi \tag{A.16}$$

Using the selection property of the Dirac impulse, the integral is eliminated and we obtain:

$$\langle I^*(k,\theta)\rangle = \frac{1}{k}g(\theta-\pi/2)G^*(+k) + \frac{1}{k}g(\theta+\pi/2)G^*(-k) \tag{A.17}$$

Because g is π-periodic and G^* is Hermitian (as for the Fourier transform of any real function), eq. (A.17) becomes:

$$\langle I^*(k,\theta)\rangle = \frac{2}{k}g(\theta-\pi/2)ReG^*(k) \tag{A.18}$$

with power spectrum

$$\langle P_I^*(k,\theta)\rangle = \frac{4}{k^2} g^2(\theta - \pi/2)[ReG^*(k)]^2 \tag{A.19}$$

Because G^* is independent of θ , eq. (A.19) implies that

$$g(\theta - \pi/2) \propto \sqrt{\langle P_I^*(k,\theta)\rangle} \tag{A.20}$$

for any $k \geq 1$, so that the power spectrum appears to be rotated by 90°with respect to the direction of the original texture. The proportionality in eq. (A.20) remains valid if the right-hand side is integrated over k . Therefore:

$$g(\theta) = \frac{\int_0^\infty |I^*(k,\theta+\pi/2)|\, k\mathrm{d}k}{\int_0^{2\pi} d\psi \int_0^\infty |I^*(k,\psi)|\, k\mathrm{d}k} \tag{A.21}$$

gives the π-periodic probability density function of trace directions over $0 \leq \theta \leq \pi$.

The Fourier transform $I^*(k,\theta)$ of single images containing few cell traces is subjected to statistical fluctuations. Because of the non-local nature of Fourier transforms, statistical noise is eliminated by averaging a large number of Fourier transforms obtained from individual trace images (Figure 2.2c). The π-periodic angular dependence of average spectra is overlaid with a constant background produced by image noise and by the finite thickness of traces, as well as a $\pi/2$-periodic contribution reflecting the effect of rectangular image frames. Therefore, $g(\theta)$ is parameterized, and distribution parameters are obtained by fitting eq. (A.2) with appropriated model functions (Figure 2.2d).

The distribution of trace directions is related to the distribution of bacteria orientations $f(\theta)$ by:

$$g(\theta) = \frac{f(\theta) + f(\pi - \theta)}{2} \tag{A.22}$$

If $f(\theta)$ is a Von-Mises Fisher distribution, then

$$g(\theta,\varkappa) = \frac{\varkappa}{4\pi \sinh \varkappa} \cosh(\varkappa \cos\theta) \tag{A.23}$$

is the parameterized function used to fit eq. (A.2).

In case of small alignment degrees (i.e.$\varkappa \to 0$), g converges to:

$$g(\theta,\varkappa) \approx \frac{1}{4\pi}[1 - \frac{5}{6}\varkappa^2 + \frac{1}{2}\varkappa^2 \cos^2\theta] \tag{A.24}$$

The sum of eq. (A.24) and a constant c is undistinguishable from $g[\theta, \varkappa/(1+c)]$ after renormalization. Therefore, the distribution g is uniquely determined only for sufficiently large values of $\varkappa$, and direct trace evaluation with eq. (A.1) has been used for cell alignment in small fields.

A.2 Cell dynamics during single magnetic pulses

A.2.1 Apparatus

A split pulse coil with ∼4 cm gap was mounted on the objective stage of the optical microscope in Figure A.3. The pulse coil is connected to a capacitor bank that is discharged through a thyristor, with peak currents attained in ∼50 μs. Pulse amplitudes up to ∼0.1 T can be regulated through charging voltage on the capacitor bank. Glass slides and plastic cubes filled with sediment (Figure A.4) can be placed in the pulse coil gap for pulse experiments on MTB in water and in sediment, respectively. The Helmholtz coil system around the microscope provides a homogeneous, constant field for aligning MTB. Sediment was allowed to rest for ∼20 min in order to obtain an equilibrium alignment with the field produced by the Helmholtz coils. Pulsed fields at different angles to the field provided by the Helmholtz coils can be applied by orienting the pulse coil.

A.2.2 Equations of motion

Consider a single bacterium with magnetic moment m immersed in a fluid medium permeated by a constant (weak) field H_0 along z. In absence of external disturbances, m is aligned with H_0 on average. A magnetic impulse field $H_p = H_p(t)$ starting at time t=0 is applied at an angle ψ to the z-axis (Figure A.5a). This impulse produces an almost instantaneous deviation of the magnetic moment from the chain axis by an angle , and, at the same time, a mechanical torque that rotates the chain axis by an angle towards the pulse field direction. The angle between magnetic moment and chain axis is obtained by minimization of the free energy:

$$E(\varepsilon, t) = E_a(\varepsilon) - \mu_0 m H_p(t) \cos[\psi - \beta(t) - \varepsilon(t)] \tag{A.25}$$

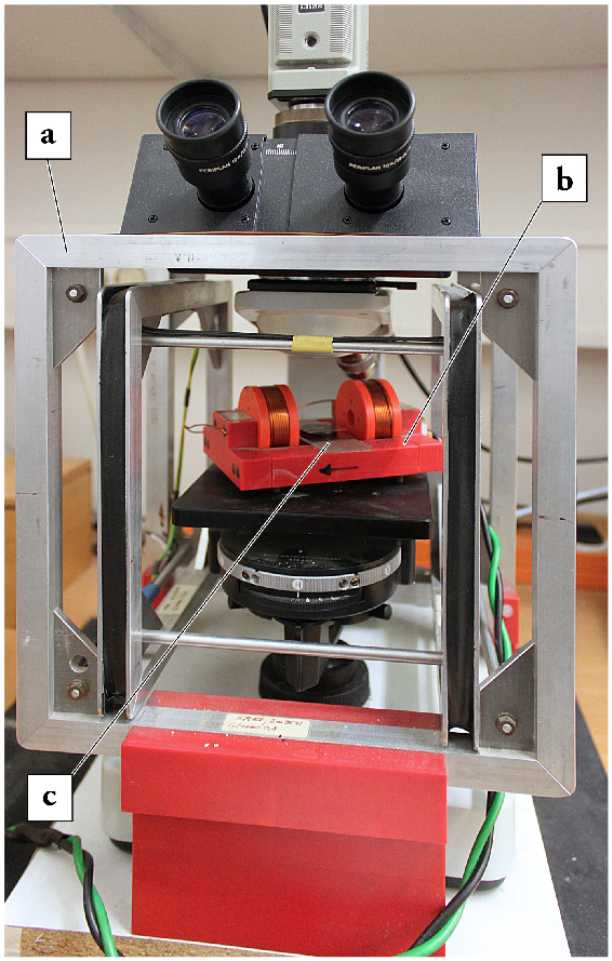

Figure A.3: Apparatus for pulsed field experiments, based on the magnetodrome shown in Figure A.1. (a) Helmholtz coils generating a continuous, horizontal field. (b) Coil for the generation of a pulse field, with visible copper windings. The pulse coil is placed on the object stage and can be oriented to give a horizontal pulse along any direction. (c) The pulse coil can accommodate a microscope slide for the observation of pulsed bacteria in the hanging drop assay, as shown in the photograph, as well as 2 cm cubes for pulse field experiments with sediment (see Figure A.4).

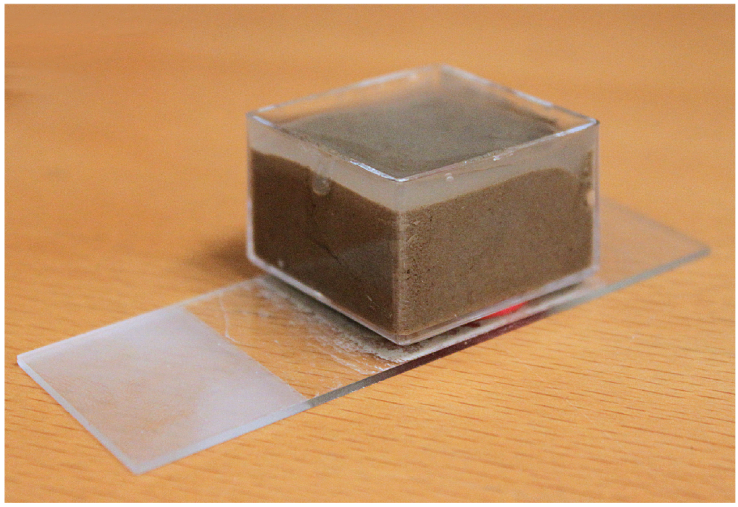

Figure A.4: 2 cm cube filled with sediment, fixed on a microscope slide that fits inside the pulse field coil.

where E_a is the energy contribution of uniaxial anisotropy. On the other hand, the mechanical torque exerted by H_p on the magnetic moment is given by

$$T(t) = \mu_0 m H_p(t) \sin[\psi - \beta(t) - \varepsilon(t)] \tag{A.26}$$

whereby H_0 has been neglected because $H_0 \ll H_p$. The equation of motion for the bacterium in a medium with dynamic viscosity η is given by

$$8\pi\eta f R^3 \dot{\beta}(t) = T(t) \tag{A.27}$$

where R is the radius of a sphere with same volume, and f a viscous resistance factor which depends on cell shape. For prolate rotation ellipsoids with ratio r between short and long axes, the resistance factor is

$$f = \frac{2}{3} \frac{1 - r^4}{\frac{2-r^2}{2\sqrt{1-r^2}} \ln \frac{1+\sqrt{1-r^2}}{1-\sqrt{1-r^2}} - 1} \tag{A.28}$$

with limit cases given by $f = 1$ for a sphere, and $f = 0$ for $r \to 0$ (Steinberger et al., 1994).

Combination of eq. (A.26) and (A.27) gives the differential equation

$$8\pi\eta f R^3 \dot{\beta}(t) = \mu_0 m H_p(t) \sin[\psi - \beta(t) - \varepsilon(t)] \tag{A.29}$$

for cell rotation. If the pulse is applied at an angle $0 \leq \varphi \leq \pi/2$ to H_0 , the angle between H_p and m is always $<\pi/2$, and, regardless of pulse intensity, the magnetic moment remains unswitched. Therefore, the chain axis realigns with H_0 after the pulse has been given. If the pulse is applied at an angle $\pi/2 \leq \varphi \leq \pi$ to H_0 , and H_p exceeds the switching field before the angle between H_p and m becomes $<\pi/2$, the magnetic moment is switched, converting a NS bacterium into a SS one. Two conditions are therefore required for H_p to switch the magnetic moment: (1) sufficient strength, and (2) sufficient pulse speed for switching before $\psi - \beta - \varepsilon$ becomes $<\pi/2$.

If whole chains are modeled as Stoner-Wohlfarth particles, the anisotropy energy is given by

$$E_a(\varepsilon) = \frac{1}{2} \mu_0 m H_K \sin^2 \varepsilon \tag{A.30}$$

Linear chains of SD particles, however, reverse by fanning (Jacobs and Bean, 1955). In

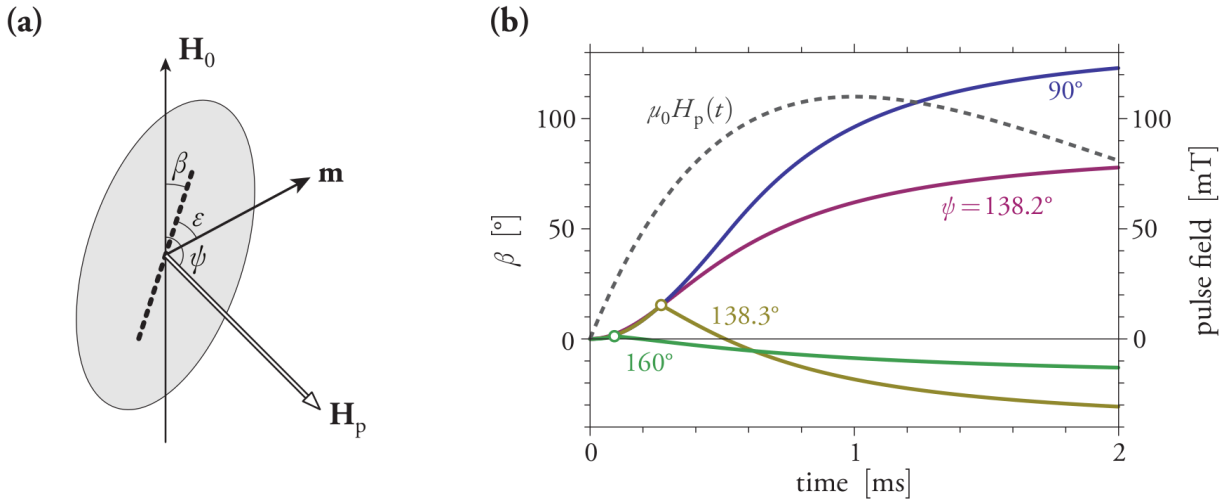

Figure A.5: (a) A magnetotactic bacterium (shaded ellipse), originally aligned with H_0 , is subjected to a pulse field H_p , which causes an instantaneous rotation of the magnetic moment **m** by ε , and a slower rotation of the whole cell by β . (b) Simulation of a pulse field experiment for *M. bavaricum* with 0.5 Hz critical escape frequency in a 0.1 mT rotating field. Magnetic pulse (dashed gray curve) and $\beta(t)$ for selected values of the pulse field angle ψ are shown as a function of time for the first 2 ms. The magnetic moment is switched for ψ>138.2°, as indicated by the sudden change in the first derivative of β (dots).

this case, an approximated solution is obtained with the modified anisotropy energy

$$E_a(\varepsilon, \varphi) = \frac{1}{2}\xi(\varphi)\mu_0 m H_K \sin^2 \varepsilon \tag{A.31}$$

where $\varphi = \psi - \beta$ is the angle between chain axis and pulsed field, and

$$\xi(\psi) \approx \frac{(1 - 0.375\cos\varphi)(1 + \tan^{2/3}\varphi)}{\sqrt{1 - \tan^{2/3}\varphi + \tan^{4/3}\varphi}} \tag{A.32}$$

is a correction factor for obtaining the same switching fields reported by Jacobs and Bean (1955).

The motion equation (eq. A.27) depends on the viscous drag of the cell, which is a complex function of its shape and of the flagellar structure. The same viscous drag also appears in the equation of motion of bacteria in weak rotating fields. In this case, $\varepsilon = 0$, because the applied rotating field $H_{rot}(\cos\psi, \sin\psi)$ is much smaller than the switching

field, and eq. (A.29) becomes

$$8\pi\eta f R^3 \dot{\beta}(t) = \mu_0 m H_{rot} \sin[\psi(t) - \beta(t)] \tag{A.33}$$

with $\psi(t) = 2\pi v t$ for a constant rotation frequency v . The angle $\psi - \beta$ between magnetic moment and field increases with v , until the cell escapes from circular orbit when $\psi - \beta$=90°. Therefore, the critical escape frequency $v = v_c$ above which the cell does no longer swim in circle satisfies the condition:

$$2\pi v_c = \frac{\mu_0 m H_{rot}}{8\pi\eta f R^3} \tag{A.34}$$

(Steinberger et al., 1994). Usually, eq. (A.34) is solved with respect to m in order to obtain the magnetic moment:

$$m = \frac{16\pi^2 v_c \eta f R^3}{\mu_0 H_{rot}} \tag{A.35}$$

In our case, eq. (eq. A.34) is used to calculated the viscous drag

$$8\pi\eta f R^3 = \frac{\mu_0 m H_{rot}}{2\pi v_c} \tag{A.36}$$

so that eq. (A.29) becomes:

$$\dot{\beta}(t) = 2\pi \frac{v_c}{H_{rot}} H_p(t) \sin[\varphi - \beta(t) - \varepsilon(t)] \tag{A.37}$$

where v_c/H_{rot} is determined experimentally. Examples of solutions of eq. (A.29) for realistic parameters are shown in Figure A.5b.

A.3 Magnetic measurements and analysis

A.3.1 Sample preparation

Plastic cups filled with pond sediment are shown in Figure A.6. These cups where chosen to fit the automatic sample handling system 'SushiBar' (Wack and Gilder, 2012) of our cryogenic magnetometer. Cups for samples A-C where kept open during the entire acquisition time, allowing for some water loss by evaporation. The maximum linear contraction caused by dewatering was ∼15% for 14 days acquisition time (Figure A.6b). Volume excess in the cups was carefully filled with plastic wrap, avoiding excessive pressure on the sediment

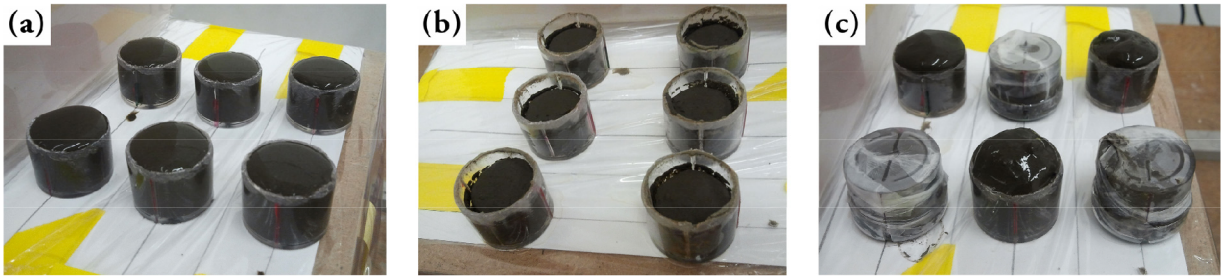

Figure A.6: (a) Plastic cups filled with sediment slurry at the beginning of the DRM experiments. Cups are placed in the center of a large Helmholtz coil system (not shown) on a board with marked positions. The magnetic field at the position occupied by each sample was measured at the beginning and at the end of the experiments. (b) Same cups after 14 days. Evaporation caused a ∼15% linear contraction of the sediment. (c) DRM experiments with three samples sealed and turned upside down for direction stability experiments.

surface. Finally, the caps were sealed with a lid and taped in order to avoid further drying during measurements. Samples D have been sealed after 52 hours and turned upside down for direction stability experiments (Figure A.6c).

A.3.2 CBD treatment

Modifications of the original CBD protocol of Mehra and Jackson (1958) have been successfully employed for the dissolution of ultrafine iron oxides – in particular magnetite – in soils and loess samples (Verosub et al., 1993; Vidic et al., 2000), due to its selectivity toward SD magnetite (Hunt et al., 1995). A CBD protocol optimized for selective magnetofossil dissolution in marine carbonates has been recently developed by Ludwig et al. (2013). We have used this protocol, which is summarized in the following.

About 30 g of sediment were added to 200 ml of water containing 5 g sodium dodecyl sulphate (a detergent for cell dissolution), 15 g sodium citrate, and 4 g sodium bicarbonate. After heating the sediment suspension to 50°C, 6 g sodium dithionite were added and the suspension was stirred at constant temperature for ∼1 h. Finally, vacuum filtration was used to rinse the sediment repeatedly with distilled water. This receipt has been adapted to the desired quantity of sediment, which was finally transferred in a container and mixed with distilled water to obtain a slurry with the same consistency as the original sediment.

A.3.3 Coercivity analysis of scalar measurements (ARM and IRM)

AF demagnetization curves of ARM and IRM were of sufficient quality and resolution for a direct calculation of corresponding coercivity distributions $f(H)$ as finite differences between magnetization intensities measured after consecutive AF steps:

$$f(\frac{H_i + H_{i+1}}{2}) = \frac{M(H_i) - M(H_{i+1})}{H_{i+1} - H_i} \tag{A.38}$$

where $M(H_i)$ is the magnetization measured after AF demagnetization with peak field H_i . The same coercivity distribution $f_{\log}$ on a logarithmic field scale is obtained by applying transformation rules for the new statistical variable $h = \log_{10} H$, i.e.:

$$f^*(h) = f(10^h)10^h \ln 10 \tag{A.39}$$

Coercivity distributions have been fitted with skewed generalized Gaussian functions

$$SGG(x, m, s, q, p) = \frac{1}{2^{1+1/p} s\Gamma(1 + 1/p)} \frac{\left|qe^{qx'} + q^{-1}e^{x'/q}\right|}{e^{qx'} + e^{x'/q}} \exp\left[-\frac{1}{2}\left|\ln\left(\frac{e^{qx'} + e^{x'/q}}{2}\right)\right|^p\right] \tag{A.40}$$

with $x' = (x - \mu)/s$ (Egli, 2003). The parameters m, s, q, and p control the distribution median, dispersion, skewness (i.e. asymmetry) and kurtosis (i.e. squareness), respectively. Because of the different relative weight of low- and high-coercivity ranges in f and f_{log} , fitting was performed by minimizing the mean square differences between model and measurements on both a linear and a logarithmic scale, which are defined as

$$\begin{aligned} e \;=\; & \sum_{i=1}^{N} \frac{1}{H_{1/2}} \left[\sum_{k=1}^{K} a_k SGG(\log H_i, \mu_k, s_k, q_k, p_k) - H_i f(H_i) \ln 10\right]^2 + \\ & \sum_{i=1}^{N} \left[\sum_{k=1}^{K} \frac{a_k}{H_i \ln 10} SGG(\log H_i, \mu_k, s_k, q_k, p_k) - f(H_i)\right]^2 \end{aligned} \tag{A.41}$$

where N is the number of points, K the number of components, and $H_{1/2}$ the median destructive field of the AF demagnetization curve. This expression reduces to the weighted sum

$$e = \sum_{i=1}^{N} \left[\frac{1}{H_{1/2}^2} + \frac{1}{(H_i \ln 10)^2}\right] \left[\sum_{k=1}^{K} a_k SGG(\log H_i, \mu_k, s_k, q_k, p_k) - H_i f(H_i) \ln 10\right]^2 \tag{A.42}$$

to be minimized with respect to the model parameters $a_k, \mu_k, s_k, q_k, p_k$.

All coercivity distributions have been modeled with three components ($K = 3$), which are sufficient for accurate fits of magnetofossil-bearing sediments up to ∼0.1 T. Furthermore, $p_k = 2$ has been chosen for all components, on the basis of systematic investigations by Egli (2004a,b). Best-fit parameters are summarized in Table A.1. Error estimates of fitted components have been obtained with a Monte Carlo method based on the empirical model residuals

$$\hat{r}_i = \sum_{i=1}^{K} \frac{a_k}{H_i \ln 10} SGG(\log H_i, \mu_k, s_k, q_k, p_k) - f(H_i)$$
$$\hat{r}_i^* = \sum_{i=1}^{K} \frac{a_k}{H_i \ln 10} SGG(\log H_i, \mu_k, s_k, q_k, p_k) - H_i f(H_i) \ln 10 \qquad \text{(A.43)}$$

on linear and logarithmic field scales, respectively. Each residual is the realization of a statistical variable representing the measurement error associated to the i-th point. Assuming that errors have a Gaussian probability distribution $\mathcal{N}(\mu, \sigma)$ with expectation $\mu = 0$, and standard deviation $\sigma = \hat{r}_i$ or $\sigma = \hat{r}_i^*$, synthetic measurements have been generated on the basis of synthetic errors $\hat{r}_i$ and $\hat{r}_i^*$ with distributions $\mathcal{N}(0, \hat{r}_i)$ and $\mathcal{N}(0, \hat{r}_i^*)$, respectively, obtained with a random number generator. This step was performed in Mathematica with the command

$$RandomVariate[NormalDistribution[0, r]] \qquad \text{(A.44)}$$

Finally, actual measurements in eq. (A.42) are replaced by synthetic measurements $f(H_i)+\hat{r}_i-r_i$ and $f^*(H_i)+\hat{r}_i^*-r_i^*$ in order to obtain a large number of simulated models. Confidence intervals of individual magnetic components are defined by Q and 1-Q quantiles of all solutions $a_k SGG(\log H_i, \mu_k, s_k, q_k, 2)$ obtained from synthetic measurements.

A.3.4 Comparison of single-axis and three-axis AF demagnetization curves

AF demagnetization along three orthogonal axes is more effective than the single-axis one, because the maximum angle between AF field and the direction of minimum switching field in individual magnetic particles is smaller. Let $h_s(\varphi)$ be the angular dependence of the switching field of uniaxial SD particles for an angle φ between field and easy axis. The mean switching field $\langle H_s \rangle$ of randomly oriented particles with anisotropy field H_K is given by weighted integration of $H_K h_s(\varphi)$ over all orientations. In case of single-axis AF

Table A.1: Coercivity analysis of ARM and IRM AF demagnetization curves of samples D (average of D1 and D2) with component 1 (LC: low-coercivity), component 2 (BS: biogenic soft) and component 3 (BH: biogenic hard). Cursive numbers in parentheses refer to the mean distribution parameters of components BS and BH in Egli (2004a). Median destructive fields (10^{μ}) from Egli (2004a) have been corrected for the expected difference between single-axis and three-axis AF demagnetization of SD particles.

component	a μAm^2	10^{μ} mT	s	q	p
D: ARM	0.544				
LC	0.062 ± 0.017	11.13	0.358	0.606	2
BS	0.323 ± 0.031	34.73 (*39.10*)	0.200 (*0.187*)	0.598 (*0.735*)	2
BH	0.161 ± 0.022	55.63 (*63.08*)	0.115 (*0.107*)	0.650 (*0.720*)	2
D: IRM	3.528				
LC	1.32 ± 0.33	13.5	0.371	0.641	2
BS	1.67 ± 0.11	31.49 (*36.36*)	0.233 (*0.209*)	0.620 (*0.726*)	2
BH	0.51 ± 0.26	57.79 (*58.52*)	0.124 (*0.132*)	0.828 (*0.773*)	2

demagnetization,

$$\langle H_{s1}\rangle = 2H_K \int_0^{\pi/2} h_s(\varphi)\cos\varphi\sin\varphi \mathrm{d}\varphi \tag{A.45}$$

In case of 3-axis demagnetization of a particle with easy axis defined by polar angle θ and azimuthal angle ψ , we have $\cos\varphi = \sin\theta\cos\psi$ for the x-axis, $\cos\varphi = \sin\theta\sin\psi$ for the y-axis, and $\varphi = \theta$ for the z-axis. The switching field is determined by the value of φ that yield the smallest $h_s(\varphi)$.

$$\langle H_{s3}\rangle = \frac{4}{\pi} H_K \int_{\psi}^{\pi/2} \mathrm{d}\psi \int_0^{\pi/2} min \begin{bmatrix} h_s\left[\arccos(\sin\theta\cos\psi)\right] \\ h_s\left[\arccos(\sin\theta\sin\psi)\right] \\ h_s(\theta) \end{bmatrix} \cos\theta\sin\theta \mathrm{d}\theta \tag{A.46}$$

Stoner-Wohlfarth particles are characterized by

$$h_s(\varphi) = \frac{\sqrt{1-\tan^{2/3}\varphi+\tan^{4/3}\varphi}}{1+\tan^{2/3}\varphi} \tag{A.47}$$

(Stoner and Wohlfarth, 1948), and the ratio between 3-axis and single-axis mean switching fields obtained from numerical evaluation of eq. (A.45,A.46) is $\gamma_{sw} = 0.972$. Magnetosome chains have a different switching mechanism based on a non-coherent, fanning-like rotation

of the magnetic moments of individual crystals. Calculations by Jacobs and Bean (1955) for infinite chains-of-spheres are well approximated by:

$$h_s(\varphi) = 1 - 0.375 \cos \varphi \tag{A.48}$$

in which case the ratio between 3-axis and single-axis mean switching fields obtained from numerical evaluation of eq. (A.45,A.46) is γ_f=0.922 .

A second effect responsible for differences between single-axis and 3-axis AF demagnetization of SD particles is the exposure time to the AF field. In case of single-axis demagnetization, this exposure time is inversely proportional to the field decay rate a . Egli and Lowrie (2002) found that the ARM intensity of SD particles is proportional to $\ln^{-1/3} a$, and that the dependence of the fluctuation field H_q , defined as the difference between switching field without and with thermal activations, on a is twice as large. Measurements on cultured magnetotactic bacteria give $H_q/H_s \approx 0.3$ and a 23% increase of ARM intensity for every factor 10 decrease of a . Therefore, a 10-fold increase of AF time produces a ∼7% reduction of the switching field. Because 3-axis AF demagnetization implies a 3-fold increase of the total AF time, the consequent switching field reduction must be multiplied by a factor $\log 3 / \log 10$, so that the expected effect of AF exposure time is ∼3.4%. If this effect is combined with the previous estimates of γ_{sw} and γ_f , we obtain $\gamma_{sw} \approx 0.94$ and $\gamma_f \approx 0.89$ for the expected ratios between mean destructive fields of 3-axis and single-axis AF demagnetization of Stoner-Wohlfarth particles, and magnetofossils, respectively.

A.3.5 Vectorial measurements (NRM)

Coercivity analysis of vectorial measurements is performed in analogy with the scalar measurements by considering the three orthogonal magnetization components along the sample axes, and assuming that each NRM-component has a coercivity-independent, fixed direction that is maintained until complete demagnetization. The directions of individual components, on the other hand, do not need to coincide. Because the quality of NRM AF demagnetization is less good than that of ARM and IRM, coercivity analysis was performed directly with the demagnetization curve, without calculating a coercivity distribution as intermediate step. In this case, each component is modeled by a cumulative, skewed

Gaussian function obtained by integrating the SGG function defined in eq. (A.40), i.e.:

$$SGGC(H, m, s, q, p) = \int_{\log H}^{\infty} SGG(x, m, s, q, p)\mathrm{d}x \tag{A.49}$$

In this case the AF demagnetization of NRM is the sum of SGGC-function multiplied by vector coefficients. Model parameters are obtained by minimization of:

$$e = \sum_{i=1}^{N} \left\| \sum_{k=1}^{K} \mathbf{a}_k SGGC(H_i, \mu_k, s_k, q_k, p_k) - M(H_i) \right\|^2 \tag{A.50}$$

where $\mathbf{M}(H_i)$ is the NRM remaining after the i-th AF demagnetization step. The direction of each NRM component is given by the unit vector $\mathbf{a}_k / \|\mathbf{a}_k\|$.

A.4 Determination of cell orientation with multiple pulses

A.4.1 Large number of bacteria after a single pulse

Consider a sediment sample containing NS bacteria whose chain axes, represented by unit vectors $\mathbf{u} = (\sin\theta\cos\lambda, \sin\theta\sin\lambda, \cos\theta)$, are distributed according to the probability density function $\mathcal{F}(\theta, \varkappa)$ of the angle θ with the constant field $\mathbf{H}_0$. A magnetic pulse is applied to the sediment at an angle ψ from $\mathbf{H}_0$, along the unit vector $\mathbf{p} = (\sin\psi, 0, \cos\psi$. A fraction $s(\cos\varphi)$ of all NS bacteria will become SS after the pulse, where φ is the angle between $\mathbf{p}$ and $\mathbf{u}$. This angle is given by:

$$\cos\varphi = \mathbf{u}\cdot\mathbf{p} = \sin\theta\sin\psi\cos\lambda + \cos\theta\cos\psi \tag{A.51}$$

The distribution of SS and NS bacteria orientations, created from an initial population of 100% NS bacteria after a single pulse, is then given by

$$\begin{aligned} s(\theta, \lambda; \psi) &= \mathcal{F}(\theta, \varkappa)\sigma(\sin\theta\sin\psi\cos\lambda + \cos\theta\cos\psi) \\ n(\theta, \lambda; \psi) &= \mathcal{F}(\theta, \varkappa)[1 - \sigma(\sin\theta\sin\psi\cos\lambda + \cos\theta\cos\psi)] \end{aligned} \tag{A.52}$$

with $n + s = \mathcal{F}$. The total fraction $S(\varphi)$ of SS bacteria is obtained by integration of s over the unit sphere:

$$S(\psi) = \int_{\lambda=0}^{2\pi} \int_{\theta=0}^{\pi} \mathcal{F}(\theta, \varkappa)\sigma(\sin\theta \sin\psi \cos\lambda + \cos\theta \cos\psi) \sin\theta \mathrm{d}\lambda \mathrm{d}\theta \tag{A.53}$$

Because λ appears only in $\cos\lambda$, eq. (A.53) can be rewritten as:

$$S(\psi) = 2 \int_{0}^{\pi} \int_{0}^{\pi} \mathcal{F}(\theta, \varkappa)\sigma(\sin\theta \sin\psi \cos\lambda + \cos\theta \cos\psi) \sin\theta \mathrm{d}\lambda \mathrm{d}\theta \tag{A.54}$$

In case of a completely random distribution of bacteria orientations, $\mathcal{F} = (4\pi)^{-1}$, and eq. (A.54) becomes:

$$S(\psi) = \frac{1}{2\pi} \int_{0}^{\pi} \int_{0}^{\pi} \sigma(\sin\theta \sin\psi \cos\lambda + \cos\theta \cos\psi) \sin\theta \mathrm{d}\lambda \mathrm{d}\theta \tag{A.55}$$

Because the same value of S is expected for any field orientation,

$$S(\psi) = S(0) = \frac{1}{2} \int_{0}^{\pi} \sigma(\cos\theta) \sin\theta \mathrm{d}\theta = S_0 \tag{A.56}$$

In case of immobilized bacteria, $\sigma(x) = \mathcal{H}(-x)$ and $S_0 = 1/2$, so that 50% of the bacteria are SS after pulse application. The empirical fit $\sigma(x) = \mathcal{H}(-x)\,|x|^q$, on the other hand, gives:

$$S_0 = \frac{1}{2} \int_{\pi/2}^{\pi} \sigma(\cos\theta) \sin\theta \mathrm{d}\theta = \frac{1}{2} \int_{-1}^{0} s(x) \mathrm{d}x = \frac{1}{2} \int_{0}^{1} x^q \mathrm{d}x = \frac{1}{2(q+1)} \tag{A.57}$$

with $S_0 \to 1/2$ for $q \to 0$.

A.4.2 Large number of bacteria after multiple pulses

The application of a single pulse does not allow the determination of two unknowns, namely the impulse response of individual bacteria, and their degree of alignment in an external field. Multiple pulses are necessary for this purpose. Therefore, we discuss the case of multiple pulses applied sequentially to the same sediment. Protocols for pulse applications are specified by the vector $\Phi = (\psi_0, \psi_1, \psi_2, \cdots)$, where the i-th pulse is applied at an angle ψ_i to $\mathbf{H}_0$. Accordingly, S_i is the relative amount of SS bacteria after application of the i-th pulse. The calculation of S_i depends on the degree of correlation existing between the cell

orientations after the $i-1$-th pulse and just before the i-th pulse. Let $s_i(\theta, \lambda, \varkappa, \psi_1, \cdots, \psi_i)$ and $n_i(\theta, \lambda, \varkappa, \psi_1, \cdots, \psi_i)$ be the statistical distributions of SS and NS bacteria orientations after the i-th pulse, respectively, and

$$\begin{aligned} S_i &= \int_{\lambda=0}^{2\pi}\int_{\theta=0}^{\pi} s_i(\theta, \lambda, \varkappa, \psi_i, \cdots, \psi_i) \sin\theta \mathrm{d}\lambda\mathrm{d}\theta \\ N_i &= \int_{\lambda=0}^{2\pi}\int_{\theta=0}^{\pi} n_i(\theta, \lambda, \varkappa, \psi_i, \cdots, \psi_i) \sin\theta \mathrm{d}\lambda\mathrm{d}\theta \end{aligned} \tag{A.58}$$

the corresponding relative amounts with $S_i + N_i = 1$. We distinguish the following cases:

A.4.3 No correlation between individual orientations during consecutive pulses

In this case, the orientation of NS and SS bacteria is independent of their past history. After a certain number of SS bacteria has been generated by a pulse, several interactions with the sediment make the probability density functions for the orientation of NS and SS bacteria converge to $\mathcal{F}(\theta, \varkappa)$ and $\mathcal{F}(\pi - \theta, \varkappa)$, respectively, *before* the next pulse is applied. Therefore,

$$\begin{aligned} s_i(\theta, \lambda, \varkappa, \psi_i, \cdots, \psi_i) &= S_i \mathcal{F}(\pi - \theta, \varkappa) \\ n_i(\theta, \lambda, \varkappa, \psi_i, \cdots, \psi_i) &= N_i \mathcal{F}(\theta, \varkappa) \end{aligned} \tag{A.59}$$

with

$$\begin{aligned} S_i &= S_{i-1}\int_{\lambda=0}^{2\pi}\int_{\theta=0}^{\pi} \mathcal{F}(\pi - \theta, \varkappa)\left[1 - \sigma(\theta, \lambda, \psi_i)\right] \sin\theta \mathrm{d}\lambda\mathrm{d}\theta \\ &\quad + N_{i-1}\int_{\lambda=0}^{2\pi}\int_{\theta=0}^{\pi} \mathcal{F}(\theta, \varkappa)\sigma(\theta, \lambda, \psi_i) \sin\theta \mathrm{d}\lambda\mathrm{d}\theta \end{aligned} \tag{A.60}$$

and $N_i = 1 - S_i$. Using eq. (A.58) we obtain the recursion formula:

$$\begin{aligned} S_i &= S_{i-1} - S_{i-1}\int_{\lambda=0}^{2\pi}\int_{\theta=0}^{\pi} \mathcal{F}(\pi - \theta, \varkappa)\sigma(\sin\theta \sin\psi_i \cos\lambda + \cos\theta \cos\psi_i) \sin\theta \mathrm{d}\lambda\mathrm{d}\theta \\ &\quad + (1 - S_{i-1})\int_{\lambda=0}^{2\pi}\int_{\theta=0}^{\pi} \mathcal{F}(\theta, \varkappa)\sigma(\sin\theta \sin\psi_i \cos\lambda + \cos\theta \cos\psi_i) \sin\theta \mathrm{d}\lambda\mathrm{d}\theta \end{aligned} \tag{A.61}$$

for the calculation of the SS fraction after each pulse.

A.4.4 Full correlation between individual orientations during consecutive pulses

In this case, the orientation of a given cell after the $(i-1)$-th pulse remains invariant until the i-th pulse is applied. Therefore, the orientation of individual cells can be considered as blocked during the whole experiment. The probability density functions for the orientations of NS and SS obey the equation:

$$n_i(\theta, \lambda, \varkappa, \psi_1, \cdots, \psi_i) + s_i(\theta, \lambda, \varkappa, \psi_1, \cdots, \psi_i) = \mathcal{F}(\theta, \varkappa) \tag{A.62}$$

with following recursive formula:

$$\begin{aligned} s_i(\theta, \lambda, \varkappa, \psi_1, \cdots, \psi_i) &= s_{i-1}(\theta, \lambda, \varkappa, \psi_1, \cdots, \psi_{i-1})\left[1 - \sigma(\pi - \theta, \pi + \lambda, \psi_i)\right] \\ &\quad + n_{i-1}(\theta, \lambda, \varkappa, \psi_1, \cdots, \psi_{i-1})\sigma(\theta, \lambda, \psi_i) \end{aligned} \tag{A.63}$$

Combining eq. (A.62) and (A.63) we obtain:

$$\begin{aligned} s_i(\theta, \lambda, \varkappa, \psi_1, \cdots, \psi_i) &= s_{i-1}(\theta, \lambda, \varkappa, \psi_1, \cdots, \psi_{i-1})\left[1 - \sigma(\pi - \theta, \pi + \lambda, \psi_i)\right] \\ &\quad + \left[\mathcal{F}(\theta, \varkappa) - s_{i-1}(\theta, \lambda, \varkappa, \psi_1, \cdots, \psi_{i-1}))\right]\sigma(\theta, \lambda, \psi_i) \\ &= \mathcal{F}(\theta, \varkappa)\sigma(\theta, \lambda, \psi_i) \\ &\quad + s_{i-1}(\theta, \lambda, \varkappa, \psi_1, \cdots, \psi_{i-1})[1 - \sigma(\theta, \lambda, \psi_i) - \sigma(\pi - \theta, \pi + \lambda, \psi_i)] \end{aligned} \tag{A.64}$$

and using eq. (A.51):

$$\begin{aligned} s_i(\theta, \lambda, \varkappa, \psi_1, \cdots, \psi_i) &= \mathcal{F}(\theta, \varkappa)\sigma(\sin\theta \sin\psi_i \cos\lambda + \cos\theta \cos\psi_i) \\ &\quad + s_{i-1}(\theta, \lambda, \varkappa, \psi_1, \cdots, \psi_{i-1}) \times \\ &\quad \begin{bmatrix} 1 - \sigma(\sin\theta \sin\psi_i \cos\lambda + \cos\theta \cos\psi_i) - \\ \sigma(-\sin\theta \sin\psi_i \cos\lambda - \cos\theta \cos\psi_i) \end{bmatrix} \end{aligned} \tag{A.65}$$

Because $\sigma = 0$ for positive arguments, eq. (A.65) simplifies to:

$$\begin{aligned} s_i(\theta, \lambda, \varkappa, \psi_1, \cdots, \psi_i) &= \mathcal{F}(\theta, \varkappa)\sigma(\sin\theta \sin\psi_i \cos\lambda + \cos\theta \cos\psi_i) \\ &\quad + s_{i-1}(\theta, \lambda, \varkappa, \psi_1, \cdots, \psi_{i-1})\left[1 - \sigma(-\left|\sin\theta \sin\psi_i \cos\lambda + \cos\theta \cos\psi_i\right|)\right] \end{aligned} \tag{A.66}$$

Integration over θ and λ gives the fraction:

$$S_i(\psi) = S_{i-1} + \int_{\lambda=0}^{2\pi}\int_{\theta=0}^{\pi} \mathcal{F}(\theta,\varkappa)\sigma(\sin\theta\sin\psi_i\cos\lambda+\cos\theta\cos\psi_i)\sin\theta\mathrm{d}\lambda\mathrm{d}\theta \quad (A.67)$$
$$-\int_{\lambda=0}^{2\pi}\int_{\theta=0}^{\pi} s_{i-1}(\theta,\lambda,\varkappa,\psi_1,\cdots,\psi_{i-1})\sigma(-|\sin\theta\sin\psi_i\cos\lambda+\cos\theta\cos\psi_i|)\sin\theta\mathrm{d}\lambda\mathrm{d}\theta$$

of SS bacteria after the i-th pulse.

A.4.5 Error calculation

After each magnetic pulse, NS and SS bacteria are counted according to the procedure described in section 2.2.3, and the relative amount of SS bacteria is defined as:

$$\hat{S}_i = \frac{\hat{c_S}}{\hat{c_N}+\hat{c_S}} \quad (A.68)$$

where $\hat{c_N}$ and $\hat{c_S}$ are NS and SS cell counts, respectively. These counts are modeled as statistical variables c_N, c_S resulting from a Poisson process with expected values $\hat{c_N}$ and $\hat{c_S}$, respectively. The probability density function of counts c is thus given by the Poisson distribution:

$$p(x) = \frac{\hat{c}^x}{x!}e^{-\hat{c}} \quad (A.69)$$

A generator of Poisson-distributed random numbers (i.e. built-in *Mathematica 9.0* function PoissonDistribution) is used to create large numbers of simulated cell counts (10,000 in our case) with expectations $\hat{c_N}$ and $\hat{c_S}$. These numbers define a list of simulated $\hat{S}_i$ - values, corresponding to an equal number of possible experimental outcomes. Next, a best-fit model is calculated for each simulated experiment by minimizing the sum of squared differences between $\hat{S}_i$ and the corresponding model values obtained with eq. (A.66) in case of fixed orientations, or eq. (A.67) in case of orientations that reach equilibrium with the applied field after each pulse.

The large number of best-fit models obtained with the Monte Carlo approach described above is summarized by pairs (ζ, q) of model parameters that can be interpreted as statistical realizations of a joint probability function $p = (\zeta, q)$ of ζ and q . The marginal cumulative distribution

$$P(\zeta) = \int_{u=\zeta}^{\infty}\mathrm{d}u\int_{q=0}^{\infty} p(u,q)\mathrm{d}q \quad (A.70)$$

defines the probability that the real MTB alignment is larger than a given value ζ . With

other words, the mean alignment of MTB in sediment, as deduced from the experiment, does not exceed a given value ζ at a confidence level 1-$P(\zeta)$.

A.5 NRM and IRM

A.5.1 Theory

The distribution of easy axes orientations in three dimensions is given by:

$$\begin{aligned} g(\theta,\varkappa) &= \mathcal{F}(\theta,\varkappa)+\mathcal{F}(\pi-\theta,\varkappa) \\ &= \frac{\varkappa}{4\pi\sinh\varkappa}\left[\exp(\varkappa\cos\theta)+\exp(-\varkappa\cos\theta)\right] = \frac{\varkappa}{2\pi\sinh\varkappa}\cosh(\varkappa\cos\theta) \end{aligned} \tag{A.71}$$

with $\theta\in[0,\pi/2]$. This distribution of easy axes defines the ratio

$$\frac{M_{rs}}{M_s} = 2\pi\int_0^{\pi/2} g(\theta,\varkappa)\cos\theta\sin\theta\mathrm{d}\theta = 1+\frac{1-\cosh\varkappa}{\varkappa\sinh\varkappa} \tag{A.72}$$

between saturation remanence M_{rs} and saturation magnetization M_s . On the other hand, the NRM is given by:

$$\frac{NRM}{M_s} = 2\pi\int_0^{\pi} f(\theta,\varkappa)\cos\theta\sin\theta\mathrm{d}\theta = \coth\varkappa-1/\varkappa \tag{A.73}$$

Therefore, the efficiency of NRM acquisition is quantified by:

$$\eta=\frac{NRM}{M_{rs}}=\frac{\coth\varkappa-1/\varkappa}{1+\frac{1-\cosh\varkappa}{\varkappa\sinh\varkappa}}=\frac{\varkappa\coth\varkappa-1}{\varkappa+\frac{1-\cosh\varkappa}{\sinh\varkappa}}=\frac{\varkappa\cosh\varkappa-\sinh\varkappa}{\varkappa\sinh\varkappa-\cos\varkappa+1} \tag{A.74}$$

A convenient approximation of eq. (A.74) with 0.2% maximum relative error and exact convergence to $\varkappa=0$ is:

$$\eta\approx\tanh(2\varkappa/3) \tag{A.75}$$

Using $\zeta=\mathcal{L}(\varkappa)$ with $\mathcal{L}(\varkappa)=\varkappa/3$ for $\varkappa\to 0$ we obtain $\eta=2\varkappa$ in case of weak alignments.

In case of weak alignments, the DRM acquisition efficiency of SD particles is expressed by the factor

$$Q=\frac{NRM}{M_{rs}H}\approx\frac{2\zeta(H)}{H} \tag{A.76}$$

which, in analogy with magnetic definitions of susceptibility, we call 'alignment susceptibility'. The unit of Q when H is expressed in A/m is m/A, like the unit of the ARM

susceptibility ratio χ_a/M_{rs} . The DRM acquired by independent SD particles in a field H is then given by $QM_{rs}H$. This expression can be generalized to the case of non-SD DRM carriers (i.e. true PSD particles or aggregates of SD particles). For this purpose we introduce the magnetization M'_{rs} , acquired in an ideal experiment by letting the magnetic moments of all DRM carriers align with a weak magnetic field that does not modify their magnetic moments m . Eq. (A.76) is then rewritten as

$$Q = 2\frac{NRM}{M'_{rs}H} \approx \frac{2\zeta(H)}{H} \tag{A.77}$$

This expression is valid for any type of DRM carriers, so that $NRM = QM'_{rs}H/2$. As next step, we calculate a general relationship between M'_{rs} and M_{rs} by considering that M_{rs} is acquired by applying a strong magnetic field that induces a 'saturation magnetic moment' $m_{rs} > m$ in each DRM carrier. If DRM carriers are isotropic and randomly oriented (up to a small alignment), $M'_{rs}/M_{rs} = 2m/m_{rs}$. Therefore, $M'_{rs} = 2M_{rs}r_d$, with $r_d = m/m_{rs}$ being the 'natural remanence' of the DRM carriers. Defining $r_s = M_{rs}/M_s$ as the saturation remanence of the bulk sample, we finally obtain $M'_{rs} = M_{rs}r_d/r_s$ and

$$NRM = QM_{rs}r_dH \tag{A.78}$$

A.5.2 Comparison with flocculation models

In the flocculation model of Tauxe et al. (2006), DRM carriers are aggregates of fundamental flocs with a magnetic moment of $\sim$2 aAm^2 (their Fig.6). According to their model, a composite floc of $\sim$3 μm radius is composed of $\sim$30 fundamental flocs and has a total magnetic moment of $\sim$6.6 aAm^2. In their DRM acquisition experiments, the fundamental flocs where previously magnetized with a saturation field, so that r_d is the ratio between the magnetic moment of a fundamental floc and that of the composite floc, i.e. $r_d \approx 0.11$. Using eq. (A.78) we obtain $NRM/Mrs \approx 0.18$ in a 10 μT field, compared to experimental values of 0.15-0.25 for $<$3 ppt salinity.

A.6 Complements to magnetotaxis models

A.6.1 Collision model of magnetotaxis

In the following, we consider a bacterium with magnetic moment **m** that is perfectly aligned with the magnetic field **B** when it swims in water without external perturbations. If a collision produces a deviation θ_0 of the original cell orientation, **m** will rotate back to **B** under the action of a magnetic torque $mB\sin\theta$, where θ is the angle between **m** and **B** . The motion equation for a spherical cell with radius R is

$$8\pi\eta R^3\dot{\theta}(t) = -mB\sin\theta(t) \tag{A.79}$$

where η is the dynamic viscosity of water. The solution of eq. (A.79) with initial condition $\theta(0) = \theta_0$ is

$$\theta(t) = 2\arctan\left[\tan\frac{\theta_0}{2}\exp\left(-\frac{mB}{8\pi\eta R^3}t\right)\right]. \tag{A.80}$$

The initial decay of θ can be approximated by the following linear expansion of eq. (A.80) at $t = 0$:

$$\theta(t) = \theta_0 - \sin\theta_0\frac{mB}{8\pi\eta R^3}t \tag{A.81}$$

Solution of eq. (A.81) with respect to t gives the typical time constant

$$\tau = \frac{\theta_0}{\sin\theta_0}\frac{8\pi\eta R^3}{mB} \tag{A.82}$$

for realignment with **B** . In this case, eq. (A.80) can be rewritten as

$$\theta(t) = 2\arctan\left[\tan\frac{\theta_0}{2}\exp\left(-\frac{\theta_0}{\sin\theta_0}\frac{t}{\tau}\right)\right] \tag{A.83}$$

If we assume $\theta_0 = \pi/2$ as the typical amplitude of disturbances caused by collisions, we finally obtain

$$\theta(t) = 2\arctan\left[\exp\left(-\frac{\pi t}{2\tau}\right)\right] \tag{A.84}$$

with

$$\tau = \frac{4\pi^2\eta R^3}{mB} = \frac{3\pi\eta V}{mB} \tag{A.85}$$

If collisions occur with a frequency v_c on average, the mean cell alignment is defined by integration of eq. (A.84) over a time interval $t_c = 1/v_c$:

$$\langle \cos\theta \rangle = \zeta = \int_0^{t_c} \cos\theta(t) \mathrm{d}t = 1 + \frac{\tau}{\pi t_c} \ln\left[\frac{(1+e^{-\pi t_c/\tau})^2}{4}\right] \tag{A.86}$$

An excellent approximation of eq. (A.86) with 2% maximum relative error is given by the Langevin function:

$$\zeta \approx \mathcal{L}\left(\frac{3\pi t_c}{4\tau}\right) \tag{A.87}$$

Using the definition of τ in eq. (A.85) we finally obtain

$$\zeta = \mathcal{L}\left(\frac{3\pi t_c}{4}\frac{mB}{3\pi\eta V}\right) = \mathcal{L}\left(\frac{mB}{4\eta V} t_c\right), \tag{A.88}$$

which is formally equivalent to the mean alignment for Brownian motion (eq. 2.2) if $k_B T$ is replaced by a 'perturbation energy' $E_c = 4\eta V v_c$.

The collision frequency of cells swimming with velocity v_0 in an environment containing randomly dispersed particles of identical size can be estimated by calculating the volume filled by the swimming path of a cell during the time interval $t_c = 1/v_c$ between consecutive collisions. For relatively infrequent collisions (i.e. the free swimming path is long in comparison with cell size), this volume is given by the product of the cell cross section and the path length $v_0 t_c$. If a single collision occurs in this volume, as expected from the definition of v_c , the particle density N corresponds to the inverse of this volume, i.e.:

$$N = \frac{v_c}{\pi R^2 v_0} \tag{A.89}$$

If colliding particles have the same volume V of MTB cells, the corresponding volume density is:

$$\phi_s = VN = \frac{V v_c}{\pi R^2 v_0} = \frac{4 R v_c}{3 v_0} \tag{A.90}$$

Solution of eq. (A.90) with respect to v_c gives

$$v_c = \frac{3 v_0 \phi_s}{4R} \tag{A.91}$$

In this case, k_BT in eq. (2.2) is replaced by:

$$E_c = (36\pi)^{1/3}\eta v_0 \phi_s V^{2/3} \tag{A.92}$$

In order for MTB to maintain the same mean alignment as in water without collisions, the condition $mB = 5E_0$ must be fulfilled. Solution with respect to m gives

$$m = \frac{20\eta v_c}{B} V \tag{A.93}$$

for given collision frequencies, and

$$m = \frac{5(36\pi)^{1/3}\eta v_0 \phi_s}{B} V^{2/3} \tag{A.94}$$

for given particle densities. These results can be compared with the dashed limits of Figure 2.7:

$$\begin{aligned} m\left[fAm^2\right] &\approx 5.89 \times V\left[\mu m^3\right] \\ m\left[fAm^2\right] &\approx 0.37 \times (V\left[\mu m^3\right])^{2/3} \end{aligned} \tag{A.95}$$

Using B=50 μT for mid latitudes, we obtain:

$$v_c = \frac{B}{20\eta}\left[\frac{m}{V}\right]_{empirical} \approx 15 collisions/s \tag{A.96}$$

and

$$\phi_s = \frac{B}{5(36\pi)^{1/3}\eta v_0}\left[\frac{m}{V^{2/3}}\right]_{empirical} \approx 0.008 \tag{A.97}$$

as the typical aqueous environment to which MTB appear have adapted. Using a mean density of 2.7 g/cm^3 for suspended particles ϕ_s corresponds to ∼21 g/l solid suspended matter.

A.6.2 Magnetotaxis in sediment

In three dimensions, the standard deviation of the displacement r produced by a random walk is given by $\langle r^2 \rangle = 6Dt$, where D is the equivalent diffusion coefficient (Berg, 1993). Therefore, the velocity of sediment particles subjected to solid biodiffusion between successive 'steps' of a random walk, is defined by $d_s^2 = 6D_{bt}t_s$, where d_s is the particle size,

t_s the time required to be displaced by d_s , and D_{bt} the biodiffusion coefficient. Particle velocity is thus given by $v_s = d_s/t_s = 6D_{bt}d_s$. This is the velocity with which any particle in sediment, including MTB, is forcedly moved by bioturbation. As next step we identify one such particle with a spherical cell with radius R , which, as any other particle, moves in a medium with low-shear viscosity η_{ls} , whereby η_{ls} includes the viscosity of water, as well as an additional term derived from the necessity to displace neighbour particles. The force required to move this particle is given by

$$F = 6\pi\eta_{ls}Rv_s \tag{A.98}$$

and the energy that accompanies this movement over the cell size $2R$ is $E_{bt} = 2FR$. Expressing R as function of the cell volume we obtain:

$$E_{bt} = 18\pi\frac{D_{bt}\eta_{ls}}{d_s}\left[\frac{6V}{\pi}\right]^{2/3} \tag{A.99}$$

as the typical energy of random disturbances produced by bioturbation.

A.6.3 Energy requirements for cell propulsion and magnetosome production

Cell propulsion with velocity v_0 through a medium with dynamic viscosity η requires a constant power $W = Fv_0$, to overcome the viscous drag force F , which, in case of a sphere with radius R , is given by $F = 6\pi\eta Rv_0$. In case of ellipsoidal cells with ratio r between short and long axis, moving parallel to the long axis, $F = 6\pi\eta fRv_0$, where R is the radius of a sphere with equivalent volume and

$$f = \frac{1}{\frac{1}{\sqrt{1-r^2}}\ln\frac{1+\sqrt{1-r^2}}{1-\sqrt{1-r^2}} - 1} \tag{A.100}$$

is a correction factor (Steinberger et al., 1994). The power required for cell propulsion is thus given by

$$W = 6\pi\eta fRv_0^2 \tag{A.101}$$

Flagellar propulsion implies additional viscous drags caused by cell and flagellum rotation, so that a higher power is required by the flagellar motor. The ratio between mechanical work of the flagellar motor and the power required for propulsion defines the propulsion

efficiency ε_p , which has been estimated to be comprised between 0.4% and 0.7% (Purcell, 1997). The flagellar motor is driven by proton flow and its energy is close to 100%, meaning that chemical energy is almost completely converted into chemical energy. The power of chemical reactions necessary to sustain propulsion (e.g. ATP consumption) is thus given by:

$$W_0 = \frac{6\pi\eta f R v_0^2}{\varepsilon_p} \tag{A.102}$$

Blakemore (1982) estimated a MTB cell yield of 10.5 μg dry cell weight per μmol ATP, which gives an ATP concentration of $\sim$0.1 mol(ATP)/(g dry cell). Assuming dry weight to be 20% of the total weight of a cell, and using $\varrho \approx$1 g/cm^3 for the cell density, we obtain a volume ATP concentration of 0.02 mol(ATP)/cm^3. Assuming that $\sim$40 kJ energy can be obtained from 1 mole ATP, the total energy stored in the cell is $\sim$3 pJ. If this energy is entirely available for cell propulsion, the bacterium can swim for $\sim$22 hours.

Appendix B

Data in chapter 4: Study of magnetotaxis advantage in stable sediment: magnetotactic bacteria in Earth's field, zero field and vertically alternating field

The population variation of *M. bavaricum* and coci in Earth's field, zero field and alternating field for Figure 4.7 are shown in Table B.1. The mean population of individual profiles of cocci and *M. bavaricum* are shown in Table B.2 and Table B.3 respectively.

Table B.1: Data of MTB population per μl for Figure 4.7

Field setting	Time/day	Date	*M. bavaricum*		Cocci		Each field setting
			Mean	Error	Mean	Error	Mean
Earth's field	28	10.29	19.01		12.79		
	36	11.6	8.58		20.27		
	49	11.19	18.34		15.75		
	56	11.26	5.25		10.86		*M. bavaricum*: 13.1±6.1
	70	12.10	13.59		7.76		
	74	12.14	14.56		16.27		Cocci: 11.7±4.5
	78	12.18	11.20		9.83		
	79	12.19	18.35		6.41		
	83	12.23	19.71		10.60		
	89	12.29	2.24		6.72		
Zero field	110	1.19	5.16	0.85	9.52	3.14	
	141	2.19	4.33	0.77	8.15	0.77	
	159	3.9	8.01	1.16	18.69	9.45	
	176	3.26	5.92	1.42	11.48	2.52	*M. bavaricum*: 5.8±1.2
	200	4.19	4.34	0.61	7.50	1.44	
	234	5.23	5.98	0.84	12.69	5.36	Cocci: 11.5±4.3
	250	6.8	7.06	0.94	10.25	2.71	
	270	6.28	6.30	0.82	17.98	5.94	
	283	7.11	5.17	1.27	6.87	2.70	
Earth's field	289	7.17	6.26	1.11	4.15	1.10	
	295	7.23	8.65	1.84	8.52	2.83	*M. bavaricum*: 12.2±5.3
	306	8.3	10.76		5.30		
	318	8.15	16.38	4.29	7.43	1.39	Cocci: 7.1±2.3
	333	8.30	18.78	4.58	9.87	1.18	
Zero field	347	9.13	9.93	3.81	5.75	1.54	
	362	9.28	8.79	1.08	7.72	1.81	*M. bavaricum*: 8.0±1.4
	377	10.13	8.13	1.49	7.19	1.53	
	383	10.19	6.52		8.91		Cocci: 9.5±4.7
	384	10.20	6.68		17.70		
Earth's field	403	11.8	8.81	2.23	17.85	4.21	
	420	11.25	10.37	2.00	15.76	4.59	*M. bavaricum*: 19.7±13.8
	445	12.20	11.26	2.97	10.02	4.39	
	476	1.20	13.66	2.88	10.29	2.67	Cocci: 13.9±3.1
	500	2.13	40.78	13.62	14.77	5.01	
	519	3.4	33.47	9.56	14.49	2.13	
Alternating field	530	3.15	10.02	2.83	1.39	0.38	
	537	3.22	8.32	1.54	0.30	0.10	
	549	4.3	7.24	1.34	0.22	0.13	*M. bavaricum*: 6.9±2.3
	566	4.20	6.70	1.62	0.33	0.17	
	582	5.6	8.23	1.64	0.70	0.56	Cocci: 0.5±0.5
	596	5.20	4.54	3.91	0.27	0.09	
	612	6.5	3.24	1.60	0.15	0.03	

Table B.2: Cocci population per μl of individual profiles. Cocci mean population in Earth's field in Table 4.2a is only based on profiles of day 28-89,318,333,445,476.

Field setting	Date	Time/day	**Cocci individual profiles**							
Earth's field	10.29	28	12.79							
	11.6	36	20.27							
	11.19	49	15.75							
	11.26	56	10.86							
	12.10	70	7.76							
	12.14	74	16.27							
	12.18	78	9.83							
	12.19	79	6.41							
	12.23	83	10.60							
	12.29	89	6.72							
Zero field	1.19	110	4.28	3.12	10.08	12.82	5.11	6.73	4.11	29.91
	2.19	141	4.97	7.82	5.95	9.29	10.51	6.85	8.56	11.25
	3.9	159	7.56	18.91	6.32	4.30	83.46	10.63	15.32	3.00
	3.26	176	9.30	9.92	18.88	9.10	8.08	25.54	7.27	3.74
	4.19	200	5.74	7.04	5.74	12.91	7.82	13.95	4.89	1.89
	5.23	234	16.10	48.12	0.78	12.97	6.13	7.11	7.69	2.61
	6.8	250	22.04	3.85	11.61	14.08	4.30	13.63	2.22	
	6.28	270	41.47	35.53	1.76	36.25	10.76	6.78	10.04	1.24
	7.11	283	10.43	1.63	6.26	15.19	0.85			
Earth's field	7.17	289	4.24	3.00	0.78	3.26	3.98	5.87	10.76	1.30
	7.23	295	1.17	27.19	4.37	7.30	6.26	10.69	5.35	5.80
	8.3	306	5.30							
	8.15	318	3.91	3.78	13.30	12.09	8.28	9.52	5.09	3.46
	8.30	333	5.28	8.61	7.24	15.45	11.67	9.00	13.24	8.48
Zero field	9.13	347	5.41	2.35	3.19	8.22	4.56	6.19	1.11	15.00
	9.28	362	7.17	2.28	10.24	11.61	15.52	0.78	3.72	10.43
	10.13	377	10.95	4.30	14.02	7.11	5.02	1.56	3.72	10.82
	10.19	383	8.91							
	10.20	384	17.70							
Earth's field	11.8	403	24.84	11.41	9.32	23.93	39.97	0.78	18.13	14.41
	11.25	420	43.10	8.02	20.41	16.10	17.34	1.17	15.84	4.11
	12.20	445	38.73	4.24	6.40	5.19	14.28	0.72	9.36	1.21
	1.20	476	25.88	6.94	9.00	7.75	6.18	5.91	10.39	
	2.20	507	41.65	15.45	19.97	11.46	3.54	4.75	6.58	
	3.4	519	22.35	16.12	14.15	17.46	13.21	14.37	3.76	
Alternating field	3.15	530	3.27	0.67	1.88	1.88	0.49	0.85	0.72	
	3.22	537	0.09	0.85	0.27	0.40	0.13	0.22	0.13	
	4.3	549	0.09	0.94	0.00	0.27	0.00	0.13	0.09	
	4.20	566	0.13	1.30	0.13	0.22	0.09	0.45	0.00	
	5.6	582	4.08	0.13	0.27	0.18	0.00	0.09	0.13	
	5.20	596	0.58	0.04	0.09	0.36	0.58	0.13	0.09	
	6.5	612	0.22	0.18	0.13	0.18	0.04			

Table B.3: *M.bavariucm* population of sing profiles. *M.bavariucm* mean population per μl in Earth's field in Table 4.2a is only based on profiles of day 28-89,318,333,445,476.

Field setting	Date	Time/day	***M. bavaricum* individual profiles**							
Earth's field	10.29	28	19.01							
	11.6	36	8.58							
	11.19	49	18.34							
	11.26	56	5.25							
	12.10	70	13.59							
	12.14	74	14.56							
	12.18	78	11.20							
	12.19	79	18.35							
	12.23	83	19.71							
	12.29	89	2.24							
Zero field	1.19	110	6.04	9.71	4.22	4.37	4.15	7.16	3.65	1.96
	2.19	141	7.91	5.46	3.42	4.97	2.28	0.98	3.75	5.87
	3.9	159	8.22	6.98	15.32	9.00	6.65	5.15	4.89	7.89
	3.26	176	5.84	2.51	4.41	8.49	4.01	4.69	2.72	14.67
	4.19	200	3.78	3.00	2.35	3.33	5.48	4.89	4.04	7.82
	5.23	234	4.24	3.85	2.80	4.89	6.32	8.74	8.08	8.93
	6.8	250	7.24	2.02	6.52	7.56	7.69	10.17	8.22	
	6.28	270	6.13	3.72	3.19	6.13	8.67	5.80	10.24	6.52
	7.11	283	4.11	1.83	3.65	7.76	8.48			
Earth's field	7.17	289	3.00	3.06	4.50	6.13	11.34	6.72	10.43	4.89
	7.23	295	2.15	3.00	4.43	15.97	10.11	10.76	14.80	7.95
	8.3	306	10.76							
	8.15	318	14.28	4.04	8.42	10.12	31.94	38.34	13.76	10.17
	8.30	333	15.26	12.52	10.30	17.21	48.51	24.38	13.50	8.54
Zero field	9.13	347	4.37	4.69	4.11	4.82	9.13	36.12	7.63	8.61
	9.28	362	8.08	5.09	6.91	15.65	8.80	8.15	8.41	9.26
	10.13	377	4.50	5.54	3.59	10.63	16.63	6.19	9.39	8.61
	10.19	383	6.52							
	10.20	384	6.68							
Earth's field	11.8	403	4.43	5.02	1.30	9.52	17.34	19.04	8.41	5.41
	11.25	420	7.69	3.59	5.22	8.80	21.32	14.87	11.67	9.78
	12.20	445	6.00	6.72	8.46	6.85	3.22	29.33	15.99	13.48
	1.20	476	10.30	4.21	9.22	8.51	16.43	22.75	24.23	
	2.20	507	7.79	4.12	20.38	68.02	40.08	39.54	105.55	
	3.4	519	49.44	4.52	7.57	25.52	34.66	34.30	78.28	
Alternating field	3.15	530	6.85	1.88	5.78	10.70	4.66	18.14	22.17	
	3.22	537	3.58	2.87	13.39	11.24	7.25	11.87	8.02	
	4.3	549	11.02	1.57	6.85	5.55	4.88	9.81	11.02	
	4.20	566	4.70	1.93	3.13	14.51	5.82	9.72	7.08	
	5.6	582	13.21	5.64	11.02	13.61	2.37	6.05	5.73	
	5.20	596	4.54							
	6.5	612	1.07	1.43	7.08	8.46	1.39			

Appendix C

List of online MTB videos

In order for better understanding of MTB behaviours discussed in this thesis, some MTB videos have been uploaded and are available online (www.youtube.com)

1. MTB in magnetic field

Description: *M. bavaricum* and cocci are fully aligned in a horizontal field and migrate along field lines. As the field direction is reversed, bacteria instantaneously reverse their swimming direction as well. Bacteria swim in circle when exposed in a rotating field. North seeking (NS) bacteria swim parallel to the field direction and south seeking (SS) which have been artificially converted from NS by a strong pulse field swim anti-parallel to the field direction.

Link: `http://www.youtube.com/watch?v=8Iyxqo_caSc&feature=youtu.be`

2. How to convert NS into SS by a strong pulse field

Description: When MTB are fully aligned along the applied field, a strong pulse field at 167°with applied field is applied. It leads to the occurrence of ∼64% switched SS bacteria which swim in opposite direction with respect to their NS counterparts.

Link: `http://www.youtube.com/watch?v=kLojgpz2sRE&feature=youtu.be`

3. *M. bavaricum* behaviour in pH 2 or pH 3 gradient

Description: *M. bavaricum* behaviours in pH 2 or pH 3 gradient are described in 3 zones. In zone A, cells keep swimming out of the sediment continuously. Cells in zone C are killed by excessively acidic condition. Cells in zone B (between zone A and zone C) display frequent back-and-forth oscillating phenomenon. Reversing field direction leads to the cease of this special behaviour and NS bacteria swim smoothly back towards sediment side. Meanwhile, a fraction of SS (∼5-10%) swim into zone C and are killed. Reducing pH solution diffusion rate allows to find out that the back-and-forth motion is evolved from an

evident SS behaviour (>50% SS) at the beginning of pH gradient formation. Oscillating swimming paths of 4 selected *M. bavaricum* have been digitized from the second video (the second link)

Link 1: `http://www.youtube.com/watch?v=KQnvclrQ2LE&feature=youtu.be`

Link 2: `https://www.youtube.com/watch?v=8nMPvD6ospg`

4. *M. bavaricum* behaviour in pH 4-11 gradients

Description: *M. bavaricum* swim smoothly in the pH gradient with relatively constant velocity except a slight back-and-forth motion in pH 4 gradient. As the bacteria emerge into pH solution, they stop forward swimming meanwhile keep shaking cell body. These cells will not swim back when applied field is reversed. In a rotating field, they rotate around one end of cell body

Link: `http://www.youtube.com/watch?v=ddUL_VeU2HE&feature=youtu.be`

5. MTB in CO_2 atmosphere

Description: In CO_2 atmosphere, *M. bavaricum* becomes less motile and inefficient for forward swimming. Cocci, on the other hand, are rarely detected in same condition.

Link: `http://www.youtube.com/watch?v=FQlWpzkzptU&feature=youtu.be`

6. Slightly magnetic cells in anaerobic environment

Description: when the sediment in the glove box is in anaerobic atmosphere (filled with N_2 gas), many undefined cells appear. They are slightly magnetic when tested by rotating field. These cell disappear when exposed in air.

Link: `http://www.youtube.com/watch?v=1tsSqin0XHk&feature=youtu.be`

7. Bacteria "hunters" in anaerobic environment

Description: As the sediment in the glove box is in anaerobic atmosphere (filled with N_2 gas), some giant hunter-like organisms seemingly swallow magnetotactic bacteria.

Link: `http://www.youtube.com/watch?v=DEjAo16PS1Y&feature=youtu.be`

Bibliography

Adler, J. (1975). Chemotaxis in bacteria. *Annu. Rev. Biochem.*, 44:341–56. Cited in section(s) 5.1.

Barnes, A. H. (1997). Thixotropy– a review. *J.Non-Newtonian Fluid Mech.*, 70(1):1–33. Cited in section(s) 2.6.2.

Bazylinski, D. A. (2003). Biologically controlled mineralization in Prokaryotes. *Rev. Mineral. Geochem.*, 54(1):217–247. Cited in section(s) 3.1.

Bazylinski, D. A. & Frankel, R. B. (2004). Magnetosome formation in prokaryotes. *Nat. Rev. Microbiol.*, 2(3):217–230. Cited in section(s) 1, 2.1 and 3.1.

Bazylinski, D. A., Frankel, R. B., Heywood, B. R., Mann, S., King, J. W., Donghay, P. L., & Hanson, A. K. (1995). Controlled biomineralization of magnetite (Fe_3O_4) and greigite (Fe_3S_4) in a magnetotactic bacterium. *Appl. Environ. Microbiol.*, 61:3232–3239. Cited in section(s) 5.1.

Bazylinski, D. A., Schlezinger, D. R., Howes, B. H., Frankel, R. B., & Epstein, S. S. (2000). Occurrence and distribution of diverse populations of magnetic protists in a chemically stratified coastal salt pond. *Chem. Geol.*, 169(3):319–328. Cited in section(s) 3.3.1.

Bellini, S. (2009a). Further studies on "magnetosensitive bacteria". *Chin. J. Oceanol. Limnol.*, 1:6–12. Cited in section(s) 1.

Bellini, S. (2009b). On a unique behavior of freshwater bacteria. *Chin. J. Oceanol. Limnol.*, 27:3–5. Cited in section(s) 1.

Berg, H. C. (1993). *Random walks in biology.* Princeton University Press. Cited in section(s) 2.6.1 and A.6.2.

Berg, H. C. & Brown, D. (1972). Chemotaxis in Escherichia coli analysed by three-dimensional tracking. *Nature*, 239(5374):500–504. Cited in section(s) 5.1.

Berg, H. C. & Purcell, E. M. (1977). Physics of chemoreception. *Biophys. J.*, 20(2):193–219. Cited in section(s) 6.1, 6.4.2 and 6.4.4.

Berner, R. A. (1980). *Early diagenesis: a theoretical approach (No.1)*. Princeton University Press. Cited in section(s) 2.6.1 and 2.6.1.

Bishop, S. & Egli, R. (2011). Discovery prospects for a supernova signature of biogenic origin. *Icarus*, 212(2):960–962. Cited in section(s) 1.

Blakemore, R. (1975). Magnetotactic bacteria. *Science*, 190:377–379. Cited in section(s) 1, 3.1, 5.2.2 and 6.1.

Blakemore, R. (1982). Magnetotactic bacteria. *Annu. Rev. Microbiol.*, 36:217–238. Cited in section(s) 1, 2.6.1, 3.1, 5.1, 5.2.2, 6.1, A.1.1 and A.6.3.

Blakemore, R., Maratea, D., & Wolfe, R. (1979). Isolationand pure culture of a freshwater magnetic spirillum in chemically defined medium. *J. Bacteriol.*, 140:720–729. Cited in section(s) 3.1 and 6.1.

Blakemore, R. P., Short, K. A., Bazylinski, D. A., Rosenblatt, C., & Frankel, R. B. (1985). Microaerobic conditions are required for magnetite formation within aquaspirillum magnetotacticum. *Geomicrobiol. J.*, 4(1):53–71. Cited in section(s) 3.1.

Canfield, D. E. & Berner, R. A. (1987). Dissolution and pyritization of magnetite in anoxic marine sediments. *Geochim. Cosmochim. Acta*, 51:645–659. Cited in section(s) 1.

Carter-Stiglitz, B., Valet, J., & Legoff, M. (2006). Constraints on the acquisition of remanent magnetization in fine-grained sediments imposed by redeposition experiments. *Earth Planet. Sci. Lett.*, 245(1-2):427–437. Cited in section(s) 2.5, 2.6.2 and 2.8.

Chang, S. B. R. & Kirschvink, J. L. (1989). Magnetofossils, the magnetization of sediments, and the evolution of magnetite biomineralization. *Annu. Rev. Earth Planet. Sci.*, 17:169–195. Cited in section(s) 1 and 3.1.

Chen, C., Ma, Q., Jiang, W., & Song, T. (2011). Phototaxis in the magnetotactic bacterium Magnetospirillum magneticum strain AMB-1 is independent of magnetic fields. *Appl. Microbiol. Biotechnol.*, 90(1):269–275. Cited in section(s) 5.1 and 6.1.

Cheng, Z., Zhu, J., Chaikin, P., Phan, S.-E., & Russel, W. (2002). Nature of the divergence in low shear viscosity of colloidal hard-sphere dispersions. *Phys. Rev. E*, 65(4):041405. Cited in section(s) 2.6.1 and 2.7.

Cox, B. L., Popa, R., Bazylinski, D. a., Lanoil, B., Douglas, S., Belz, A., Engler, D. L., & Nealson, K. H. (2002). Organization and elemental analysis of P-, S-, and Fe-rich inclusions in a population of freshwater magnetococci. *Geomicrobiol. J.*, 19(4):387–406. Cited in section(s) 5.3.

Davila, A. F. (2005). *Detection and funtion of biogenic magnetite*. PhD thesis, LMU. Cited in section(s) 4.2.3.

Dunin-Borkowski, R. E. (1998). Magnetic microstructure of magnetotactic bacteria by electron holography. *Science*, 282(5395):1868–1870. Cited in section(s) 2.3 and 2.7.

Egli, R. (2003). Analysis of the field dependence of remanent magnetization curves. *J. Geophys. Res.*, 108(B2):1–25. Cited in section(s) 2.5 and A.3.3.

Egli, R. (2004a). Characterization of individual rock magnetic components by analysis of remanence curves, 1. unmixing natural sediments. *Stud. Geophys. Geod.*, 48(2):391–446. Cited in section(s) 1, 2.5, A.3.3 and A.1.

Egli, R. (2004b). Characterization of individual rock magnetic components by analysis of remanence curves.2. fundamental properties of coercivity distributions. *Phys. Chem. Earth, Parts A/B/C*, 29(13-14):851–867. Cited in section(s) A.3.3.

Egli, R., Chen, A. P., Winklhofer, M., Kodama, K. P., & Horng, C. S. (2010). Detection of noninteracting single domain particles using first-order reversal curve diagrams. *Geochem. Geophys. Geosyst.*, 11:Q01Z11. Cited in section(s) 1 and 2.1.

Egli, R. & Lowrie, W. (2002). Anhysteretic remanent magnetization of fine magnetic particles. *J. Geophys. Res.*, 107(B10):EPM 2 1–21. Cited in section(s) A.3.4.

Eisenbach, M. (2004). *Chemotaxis*. Imperial College Press. Cited in section(s) 6.1.

Erglis, K., Wen, Q., Ose, V., Zeltins, A., & Al, E. (2007). Dynamics of magnetotactic bacteria in a rotating magnetic field. *Biophys. J.* Cited in section(s) 2.7.

Esquivel, D. M. S. & De Barros, H. G. P. (1986). Motion of magnetotactic microorganisms. *J. Exp. Biol.*, 121(1):153–163. Cited in section(s) 2.3, 2.1, 2.6.1 and 2.7.

Faivre, D. & Schüler, D. (2008). Magnetotactic bacteria and magnetosomes. *Chem. Rev.*, 108(11):4875–4898. Cited in section(s) 1 and 2.1.

Faucheux, L. & Libchaber, A. (1994). Confined Brownian motion. *Phys. Rev. E*, 49(6):5158–5163. Cited in section(s) 2.6.1.

Flies, C. B., Jonkers, H. M., de Beer, D., Bosselmann, K., Böttcher, M. E., & Schüler, D. (2005a). Diversity and vertical distribution of magnetotactic bacteria along chemical gradients in freshwater microcosms. *FEMS Microbiol. Ecol.*, 52:185–195. Cited in section(s) 2.6.1, 3.1, 4.3.3 and 5.1.

Flies, C. B., Peplies, J., & Schüler, D. (2005b). Combined approach for characterization of uncultivated magnetotactic bacteria from various aquatic environments. *Appl. Environ. Microbiol.*, 71(5):2723–2731. Cited in section(s) 3.4.1.

Frankel, R. B. (1984). Magnetic guidance of organisms. *Annu. Rev. Biophys. Bioeng.*, 13(1):85–103. Cited in section(s) 1, 2.6.1, 3.1 and 6.1.

Frankel, R. B. (2009). The discovery of magnetotactic/magnetosensitive bacteria. *Chin. J. Oceanol. Limnol.*, 27(1):1–2. Cited in section(s) 1.

Frankel, R. B. & Bazylinski, D. A. (2009). Magnetosomes and magneto-aerotaxis. *Bacterial Sensing and Signaling*, pages 182–193. Cited in section(s) 3.1 and 3.4.1.

Frankel, R. B., Bazylinski, D. A., Johnson, M. S., & Taylor, B. L. (1997). Magneto-aerotaxis in marine coccoid bacteria. *Biophys. J.*, 73(2):994–1000. Cited in section(s) 1, 1, 2.2.1, 3.1, 3.1, 3.4.1, 4, 4.1, 4.4.1, 4.4.2, 5.1, 5.2.1, 5.3.3, 5.5.3, 6, 6.1, 6.5 and A.1.1.

Frankel, R. B. & Blakemore, R. (1980). Navigational compass in magnetic bacteria. *J. Magn. Magn. Mater.*, 15-18:1562–1564. Cited in section(s) 2.3, 2.3 and 2.1.

Frankel, R. B., Blakemore, R., Torres De.Araujo, F., Esquivel, D., & Danon, J. (1981). Magnetotactic bacteria at the geomagnetic Equator. *Science*, 212(4):1269–1270. Cited in section(s) 5.5.7.

Frankel, R. B., Blakemore, R. P., & Wolfe, R. S. (1979). Magnetite in freshwater magnetotactic bacteria. *Science*, 203(4387):1355–1356. Cited in section(s) 1.

Froelich, P. N., Klinkhammer, G. P., Bender, M. L., Luedtke, N. A., Heath, G. R., Cullen, D., Dauphin, P., Hammond, D., & Hartman, B. (1979). Early oxidation of organic matter

in pelagic sediments of the eastern equatorial Atlantic : suhoxic diagenesis. *Geochimica et cosmochimica acta*, 43:1075–1090. Cited in section(s) 6.1.

Galindo-Gonzalez, C., Feinberg, J. M., Kasama, T., Gontard, L. C., Posfai, M., Kosa, I., Duran, J. D., Gil, J. E., Harrison, R. J., & Dunin-Borkowski, R. E. (2009). Magnetic and microscopic characterization of magnetite nanoparticles adhered to clay surfaces. *Am. Mineral.*, 94(8-9):1120–1129. Cited in section(s) 2.6.2.

Hanzlik, M. (1999). *Elektronenmikroskoishe und magnetomineralogische Untersuchungen an magnetotaktischen Bakterien des Chiemsees und an bakteriellem Magnetit eisenreduzierender Bakterien.* PhD thesis, Ludwig-Maximilians University, Germany. Cited in section(s) 2.7 and 2.6.1.

Hanzlik, M., Winklhofer, M., & Petersen, N. (1996). Spatial arrangement of chains of magnetosomes in magnetotactic bacteria. *Earth Planet. Sci. Lett.*, 145:125–134. Cited in section(s) 3.2.

Hanzlik, M., Winklhofer, M., & Petersen, N. (2002). Pulsed-field-remanence measurements on individual magnetotactic bacteria. *J. Magn. Magn. Mater.*, 248:258–267. Cited in section(s) 2.2.3 and 4.2.3.

Hesse, P. P. (1994). Evidence for bacterial palaeoecological origin of mineral magnetic cycles in oxic and sub-oxic Tasman Sea sediments. *Mar. Geol.*, 117:1–17. Cited in section(s) 1 and 2.1.

Hunt, C. P., Singer, M. J., Kletetschka, G., TenPas, J., & Verosub, K. L. (1995). Effect of citrate-bicarbonate-dithionite treatment on fine-grained magnetite and maghemite. *Earth Planet. Sci. Lett.*, 130(1-4):87–94. Cited in section(s) A.3.2.

Jacobs, I. & Bean, C. (1955). An approach to elongated fine-particle magnets. *Phys. Rev*, 100:1060–1067. Cited in section(s) A.2.2, A.2.2 and A.3.4.

Jogler, C., Niebler, M., Lin, W., Kube, M., Wanner, G., Kolinko, S., Stief, P., Beck, a. J., De Beer, D., Petersen, N., Pan, Y., Amann, R., Reinhardt, R., & Schüler, D. (2010). Cultivation-independent characterization of 'Candidatus Magnetobacterium bavaricum' via ultrastructural, geochemical, ecological and metagenomic methods. *Environ. Microbiol.*, 12(9):2466–2478. Cited in section(s) 2.2.1, 3.2, 3.4.1, 4.2.3, 4.3.3, 4.4.1, 5.1, 6.1 and 6.4.1.

Kalmijn, A. (1981). Biophysics of geomagnetic field detection. *IEEE Trans. Magn.*, 17(1):1113–1124. Cited in section(s) 2.3 and 2.3.

Karlin, R. (1990). Magnetite diagenesis in marine sediments from the Oregon continental margin. *J. Geophys. Res.*, 95(B4):4405. Cited in section(s) 1.

Katari, K. & Tauxe, L. (2000). Effects of pH and salinity on the intensity of magnetization in redeposited sediments. *Earth Planet. Sci. Lett.*, 181(4):489–496. Cited in section(s) 2.6.2 and 2.6.2.

Kim, B. Y., Kodama, K. P., & Moeller, R. E. (2005). Bacterial magnetite produced in water column dominates lake sediment mineral magnetism: Lake Ely, USA. *Geophys. J. Int.*, 163(1):26–37. Cited in section(s) 2.6.1, 2.6.2, 4.3.3 and 5.1.

Kim, I. C. & Torquato, S. (1992). Diffusion of finite-sized Brownian particles in porous media. *J. Chem. Phys.*, 96(2):1498–1503. Cited in section(s) 2.6.1.

Kirschvink, J. L. (1980). South seeking magnetotactic bacteria. *J. Exp. Biol.*, 86:345–347. Cited in section(s) 4.1.

Kirschvink, J. L. (1982). Paleomagnetic evidence for fossil biogenic magnetite in western Crete. *Earth Planet. Sci. Lett.*, 59(2):388–392. Cited in section(s) 1.

Kirschvink, J. L. & Chang, S. B. R. (1984). Ultrafine-grained magnetite in deep-sea sediments: Possible bacterial magnetofossils. *Geology*, 12(9):559–562. Cited in section(s) 1.

Kluijtmans, S. G. J. M. & Philipse, A. P. (1999). First in situ determination of confined Brownian tracer motion in dense random sphere packings. *Langmuir*, 15(6):1896–1898. Cited in section(s) 2.6.1.

Kobayashi, A., Kirschvink, J. L., Nash, C. Z., Kopp, R. E., Sauer, D. a., Bertani, L. E., Voorhout, W. F., & Taguchi, T. (2006). Experimental observation of magnetosome chain collapse in magnetotactic bacteria: Sedimentological, paleomagnetic, and evolutionary implications. *Earth Planet. Sci. Lett.*, 245(3-4):538–550. Cited in section(s) 1 and 2.6.2.

Kolinko, S., Wanner, G., Katzmann, E., Kiemer, F., M Fuchs, B., & Schüler, D. (2012). Clone libraries and single cell genome amplification reveal extended diversity of uncultivated magnetotactic bacteria from marine and freshwater environments. *Environ. Microbiol.* Cited in section(s) 2.2.1.

Kopp, R. E. & Kirschvink, J. L. (2008). The identification and biogeochemical interpretation of fossil magnetotactic bacteria. *Earth-Sci. Rev.*, 86:42–61. Cited in section(s) 1 and 2.1.

Lefèvre, C. T., Frankel, R. B., Pósfai, M., Prozorov, T., & Bazylinski, D. A. (2011). Isolation of obligately alkaliphilic magnetotactic bacteria from extremely alkaline environments. *Environ. Microbiol.*, 13(8):2342–50. Cited in section(s) 6.1.

Li, J. & Pan, Y. (2012). Environmental factors affect magnetite magnetosome synthesis in Magnetospirillum magneticum AMB-1: implications for biologically controlled mineralization. *Geomicrobiol. J.*, 29(4):362–373. Cited in section(s) 3.1.

Li, J., Pan, Y., Liu, Q., Kui, Y., Menguy, N., Che, R. C., Qin, H. F., Lin, W., Wu, W., Petersen, N., & Yang, X. (2010). Biomineralization, crystallography and magnetic properties of bullet-shaped magnetite magnetosomes in giant rod magnetotactic bacteria. *Earth Planet. Sci. Lett.*, 293:368–376. Cited in section(s) 3.2.

Lins, U., McCartney, M. R., Farina, M., Frankel, R. B., & Buseck, P. R. (2005). Habits of magnetosome crystals in coccoid magnetotactic bacteria. *Appl. Environ. Microbiol.*, 71(8):4902–4905. Cited in section(s) 2.7.

Lippert, P. C. & Zachos, J. C. (2007). A biogenic origin for anomalous fine-grained magnetic material at the Paleocene-Eocene boundary at Wilson Lake, New Jersey. *Paleoceanography*, 22(4):n/a–n/a. Cited in section(s) 1.

Ludwig, P., Egli, R., Bishop, S., & Chernenko, V. (2013). Quantification of primary and secondary magnetite in marine sediment by combining chemical and magnetic unmixing techniques. *Global Planetary Change*, page In press. Cited in section(s) 2.5 and A.3.2.

Lyle, M., Dadey, K. A., & Farrell, J. W. (1995). The Late Miocene (11-8 Ma) Eastern Pacific carbonate crash: Evidence for reorganization of deep-water circulation by the closure of the Panama gateway. In: *Proceedings of the Ocean Drilling Program, Scientific Results*, volume 138, pages 821–838. Cited in section(s) 2.8.

Macnab, R. M. & Koshland, D. E. (1972). The gradient-sensing mechanism in bacterial chemotaxis. *Proc. Natl. Acad. Sci. U. S. A.*, 69(9):2509–2512. Cited in section(s) 5.5.1.

Mann, S., Sparks, N. H., & G, B. R. (1990). Magnetotactic bacteria: micorbiology, biomineralization, palaeomagnetism and biotechnology. *Adv. Microb. Physiol.*, 31:125–181. Cited in section(s) 6.1.

Martatea, D. & Blakemore, R. P. (1981). Aquaspirillum magnetotacticum sp. nov., a magnetic spirillum. *Int. J. Syst. Bacteriol.*, 31(4):452–455. Cited in section(s) 6.1.

Mcneill, D. F. & Kirschvink, J. L. (1993). Early dolomitization of platform carbonates and the prservation of magnetic polarity. *J. Geophys. Res.*, 98:7977–7986. Cited in section(s) 1.

Mehra, O. P. & Jackson, M. L. (1958). Iron oxide removal from soils and clays by a dithionite-citrate system buffered with sodium bicarbonate. *Clays Clay Min.*, 7:317–327. Cited in section(s) 2.2.4 and A.3.2.

Meldrum, F. C., Mann, S., Heywood, B. R., Frankel, R. B., & Bazylinski, D. A. (1993). Electron microscopy study of magnetosomes in a cultured coccoid magnetotactic bacterium. *Pro.R.Soc.Lond*, 251:231–236. Cited in section(s) 2.7.

Meynadier, L., Valet, J.-P., & Shackleton, N. J. (1995). Relative geomagnetic intensity during the last 4 m.y. from the Equatorial Pacific. In: *Proceedings of the Ocean Drilling Program, Scientific Results*, volume 138, pages 779–795. Cited in section(s) 2.8.

Meysman, F. J., Boudreau, B. P., & Middelburg, J. J. (2005). Modeling reactive transport in sediments subject to bioturbation and compaction. *Geochim. Cosmochim. Acta*, 69(14):3601–3617. Cited in section(s) 2.6.1.

Moskowitz, B. M., Bazylinski, D. A., Egli, R., Frankel, R. B., & Edwards, K. J. (2008). Magnetic properties of marine magnetotactic bacteria in a seasonally stratified coastal pond (Salt Pond, MA, USA). *Geophys. J. Int.*, 174(1):75–92. Cited in section(s) 4.3.3 and 5.1.

Mulsow, S., Boudreau, B. P., & Smith, J. A. (1998). Bioturbation and porosity gradients. *Limn. Oceanogr.*, 43:1–9. Cited in section(s) 2.6.1 and 2.6.2.

Nogueiral, F. S. & Barros, H. (1995). Study of the motion of magnetotactic bacteria. *Eur. Biophys. J.*, 24(1):13–21. Cited in section(s) 2.2 and 2.7.

Paasche Øand Larsen, J. (2010). Changes in lake stratification and oxygen distribution inferred from two contrasting records of magnetotactic bacteria and diatoms. *J. Geophys. Res.*, 115(G2):G02012. Cited in section(s) 3.1 and 5.1.

Pan, Y., Lin, W., Li, J., Wu, W., Tian, L., Deng, C., Liu, Q., Zhu, R., Winklhofer, M., & Petersen, N. (2009). Reduced efficiency of magnetotaxis in magnetotactic coccoid bacteria in higher than geomagnetic fields. *Biophys. J.*, 97:986–991. Cited in section(s) 3.2.

Pan, Y., Petersen, N., Davila, A. F., Zhang, L., Winklhofer, M., Liu, Q., Hanzlik, M., & Zhu, R. (2005a). The detection of bacterial magnetite in recent sediments of Lake Chiemsee (southern Germany). *Earth Planet. Sci. Lett.*, 232:109–123. Cited in section(s) 3.1, 3.2, 4.2.1 and 6.1.

Pan, Y., Petersen, N., Winklhofer, M., Davila, A. F., Liu, Q., Frederichs, T., Hanzlik, M., & Zhu, R. (2005b). Rock magnetic properties of uncultured magnetotactic bacteria. *Earth Planet. Sci. Lett.*, 237:311–325. Cited in section(s) 1 and 2.2.1.

Petermann, H. (1994). *Magnetotaktische Bakterien und ihre Magnetosome in Oberflächensedimenten des Südatlantiks*. PhD thesis, Bremen University, Germany. Cited in section(s) 2.6.2 and 2.7.

Petermann, H. & Bleil, U. (1993). Detection of live magnetotactic bacteria in South Atlantic deep-sea sediments. *Earth Planet. Sci. Lett.*, 117(1-2):223–228. Cited in section(s) 2.6.1, 2.6.2, 3.1, 4.3.3 and 5.1.

Petermann, H., Weiss, D. G., Bachmann, L., & Petersen, N. (1989). Motile behaviour and measurement of the magnetic moment of magnetotactic bacteria in rotating magnetic fields. *Lecture Notes in Biomathematics*, 89:387–395. Cited in section(s) 2.3 and 4.2.3.

Petersen, N., von Dobeneck, T., & Vali, H. (1986). Fossil bacterial magnetite in deep-sea sediments from the South Atlantic Ocean. *Nature*, 320:611–615. Cited in section(s) 1.

Petersen, N., Weiss, D. G., & Hojatollah, V. (1989). Magnetic bacteria in lake sediments. *Geomagnetism and paleomagnetism*, 261:231–241. Cited in section(s) 2.3, 3.1 and 3.2.

Powell, M. (1979). Site percolation in randomly packed spheres. *phy. Rev. B*, 20(10):4194–4198. Cited in section(s) 2.6.2 and 2.8.

Proksch, R. B., Scha, T. E., Moskowitz, B. M., Dahlberg, E. D., Bazylinski, D. A., & Frankel, R. B. (1995). Magnetic force microscopy of the submicron magnetic assembly in a magnetotactic bacterium. *Appl. Phys. Lett.*, 66(19):2582–2584. Cited in section(s) 2.3 and 2.7.

Purcell, E. M. (1997). The efficiency of propulsion by a rotating flagellum. *Proc. Natl. Acad. Sci. U. S. A.*, 94(21):11307–11. Cited in section(s) 2.6.1 and A.6.3.

Rabouille, C. & Gaillard, J.-F. (1991). A coupled model representing the deep-sea organic carbon mineralization and oxygen consumption in surficial sediments. *J. Geophys. Res.*, 96(C2):2761. Cited in section(s) 2.6.2.

Redon, C., Chermant, L., Chermant, J., & Coster, M. (1998). Assessment of fibre orientation in reinforced concrete. *J.Micros*, 191:258–265. Cited in section(s) 2.2 and A.1.2.

Roberts, A. P., Chang, L., Heslop, D., Florindo, F., & Larrasoaña, J. C. (2012). Searching for single domain magnetite in the "pseudo-single-domain" sedimentary haystack: Implications of biogenic magnetite preservation for sediment magnetism and relative paleointensity determinations. *J. Geophys. Res.*, 117(B8):B08104. Cited in section(s) 1 and 2.1.

Roberts, A. P., Florindo, F., Villa, G., Chang, L., Jovane, L., Bohaty, S. M., Larrasoaña, J. C., Heslop, D., & Fitz Gerald, J. D. (2011). Magnetotactic bacterial abundance in pelagic marine environments is limited by organic carbon flux and availability of dissolved iron. *Earth Planet. Sci. Lett.*, 310(3-4):441–452. Cited in section(s) 1 and 2.1.

Schumann, D., Raub, T. D., Kopp, R. E., Guerquin-Kern, J.-L., Wu, T.-D., Rouiller, I., Smirnov, A. V., Sears, S. K., Lücken, U., Tikoo, S. M., Hesse, R., Kirschvink, J. L., & Vali, H. (2008). Gigantism in unique biogenic magnetite at the Paleocene-Eocene Thermal Maximum. *Proc. Natl. Acad. Sci. U. S. A.*, 105(46):17648–17653. Cited in section(s) 1.

Shapiro, O. H., Hatzenpichler, R., Buckley, D. H., Zinder, S. H., & Orphan, V. J. (2011). Multicellular photo-magnetotactic bacteria. *Environ. Microbiol. Rep.*, 3(2):233–238. Cited in section(s) 5.1 and 6.1.

Shcherbakov, V. & Shcherbakova, V. (1987). On the physics of acquisition of post-depositional remanent magnetization. *Phys. Earth Planet. Inter.*, 46(1-3):64–70. Cited in section(s) 2.6.2.

Simmons, S. L., Bazylinski, D. A., & Edwards, K. J. (2006). South-seeking magnetotactic bacteria in the Northern Hemisphere. *Science*, 311(5759):371–374. Cited in section(s) 5.1.

Simmons, S. L., Sievert, S. M., Frankel, R. B., Bazylinski, D. A., & Edwards, K. J. (2004). Spatiotemporal distribution of marine magnetotactic bacteria in a seasonally stratified coastal salt pond. *Appl. Environ. Microbiol.*, 70:6230–6239. Cited in section(s) 2.6.1, 2.6.2 and 5.1.

Smith, M. J., Sheehan, P. E., Perry, L. L., Connor, K. O., Csonka, L. N., Applegate, B. M., & Whitman, L. J. (2006). Quantifying the magnetic advantage in magnetotaxis. *Biophys. J.*, 91:1098–1107. Cited in section(s) 4.1 and 5.1.

Snowball, I., Zillén, L., & Sandgren, P. (2002). Bacterial magnetite in Swedish varved lake-sediments: a potential bio-marker of environmental change. *Quaternary International*, 88(1):13–19. Cited in section(s) 3.1.

Solan, M., Cardinale, B. J., Downing, A. L., Engelhardt, K. a. M., Ruesink, J. L., & Srivastava, D. S. (2004). Extinction and ecosystem function in the marine benthos. *Science*, 306(5699):1177–80. Cited in section(s) 2.6.1.

Spormann, A. M. & Wolfe, R. S. (1984). Chemotactic, magnetotactic and tactile behaviour in a magnetic spirillum. *FEMS Microbiol. Lett.*, 22(3):171–177. Cited in section(s) 6.1.

Spring, S., Amann, R., Ludwig, W., Schleifer, K. H., van Gemerden, H., & Petersen, N. (1993). Dominating role of an unusual magnetotactic bacterium in the microaerobic zone of a freshwater sediment. *Appl. Environ. Microbiol.*, 59(8):2397–2403. Cited in section(s) 1, 3.1, 3.2, 5.3 and 6.4.1.

Steinberger, B., Petersen, N., Petermann, H., & Weiss, D. G. (1994). Movement of magnetic bacteria in time-varying magnetic fields. *J. Fluid Mech.*, 273:189–211. Cited in section(s) 6.4, A.2.2, A.2.2 and A.6.3.

Stoner, E. & Wohlfarth, E. (1948). A mechanism of magnetic hysteresis in heterogeneous alloys. *Phil. Trans. Royal Sco. London*, A240:599–642. Cited in section(s) A.3.4.

Tarduno, J. a. (1994). Temporal trends of magnetic dissolution in the pelagic realm: Gauging paleoproductivity? *Earth Planet. Sci. Lett.*, 123(1-3):39–48. Cited in section(s) 1.

Tauxe, L., Steindorf, J. L., & Harris, A. (2006). Depositional remanent magnetization: Toward an improved theoretical and experimental foundation. *Earth Planet. Sci. Lett.*, 244(3-4):515–529. Cited in section(s) 2.6.2, 2.7 and A.5.2.

Taylor, B. L., Zhulin, I. B., & Johnson, M. S. (1999). Aerotaxis and other energy-sensing behavior in bacteria. *Annu. Rev. Microbiol*, 53(1):103–128. Cited in section(s) 3.4.2.

Thomas-Keprta, K. L., Bazylinski, D. a., Kirschvink, J. L., Clemett, S. J., McKay, D. S., Wentworth, S. J., Vali, H., Gibson, E. K., & Romanek, C. S. (2000). Elongated prismatic magnetite crystals in ALH84001 carbonate globules: Potential Martian magnetofossils. *Geochimica et cosmochimica acta*, 64(23):4049–4081. Cited in section(s) 1.

Trauth, M. H., Sarnthein, M., & Arnold, M. (1997). Bioturbational mixing depth and carbon flux at the seafloor. *Paleoceanography*, 12(3):517–526. Cited in section(s) 2.6.2.

Vali, H., Förster, O., Amarantidis, G., & Petersen, N. (1987). Magnetotactic bacteria and their magnetofossils in sediments. *Earth Planet. Sci. Lett.*, 86:389–400. Cited in section(s) 1.

Vali, H. & Kirschvink, J. L. (1991). Observations of magnetosome organization, surface structure, and iron biomineralization of undescribed magnetic bacteria: Evolutionary speculations. In: *Iron biominerals*, R. B. Frankel & R. P. Blakemore, ed., pages 97–116. Plenum Press. Cited in section(s) 1.

Verosub, K. L., Fine, P., Singer, M. J., & TenPas, J. (1993). Pedogenesis and paleoclimate: Interpretation of the magnetic susceptibility record of Chinese loess-paleosol sequences. *Geology*, 21(11):1011–1014. Cited in section(s) A.3.2.

Vidic, J., Tenpas, J. D., Verosub, K. L., & Singer, M. J. (2000). Separation of pedogenic and lithogenic components of magnetic susceptibility in the Chinese loess / palaeosol sequence as determined by the CBD procedure and a mixing analysis Natas. *Geophys. J. Int.*, 142:551–562. Cited in section(s) A.3.2.

Wack, M. R. & Gilder, S. A. (2012). The SushiBar: An automated system for paleomagnetic investigations. *Geochem. Geophys. Geosyst.*, 13:Q12Z38. Cited in section(s) 2.2.4 and A.3.1.

Wheatcroft, R. A., Jumars, P. A., Smith, C. R., & Nowell, A. R. M. (1990). A mechanistic view of the particulate biodiffusion coefficient: Step lengths, rest periods and transport directions. *J. Mar. Res*, 48(1):177–207. Cited in section(s) 2.6.1.

Winklhofer, M., Abraçado, L. G., Davila, A. F., Keim, C. N., & Lins de Barros, H. G. P. (2007). Magnetic optimization in a multicellular magnetotactic organism. *Biophys. J.*, 92(2):661–670. Cited in section(s) 2.7.

Yamazaki, T. & Ikehara, M. (2012). Origin of magnetic mineral concentration variation in the Southern Ocean. *Paleoceanography*, 27(2):PA2206. Cited in section(s) 1 and 2.1.

Yamazaki, T. & Kawahata, H. (1998). Organic carbon flux controls the morphology of magnetofossils in marine sediments. *Geology*, 26(12):1064–1066. Cited in section(s) 1.

Yamazaki, T. & Solheid, P. (2011). Maghemite-to-magnetite reduction across the Fe-redox boundary in a sediment core from the Ontong-Java Plateau: influence on relative palaeointensity estimation and environmental magnetic application. *Geophys. J. Int.*, 185(3):1243–1254. Cited in section(s) 1.

Zhang, W. J., Chen, C., Li, Y., Song, T., & Wu, L. F. (2010). Configuration of redox gradient determines magnetotactic polarity of the marine bacteria MO-1. *Environ. Microbiol. Rep.*, 2(5):646–650. Cited in section(s) 3.4.1 and 5.1.

Acknowledgement

I would like to express my deepest gratitude to the following people and organizations who make this thesis possible

- My supervisor Ramon Egli. His broad and profound knowledge often guides me to find solutions and explanations for complex problems. He teaches me how to carefully design experiments and inspires me with brilliant idea.
- Nikolai Petersen. As expert of magnetotactic bacteria, he encourages me to try and find something interesting in this field. Thanks for his patience to discuss results with me.
- Stuart Gild, Michael Winklhofer, Julia Linder, Michael Wack, Qingguo Wei and Annica Ferk for the discussion in rock magnetism.
- Kerstin Reimer and Xiangyu Zhao for their assistance in experiments and discussion about the data. Marianne Hanzlik for her wonderful work in Transmission electron micrograph (TEM) . Most TEM pictures in this thesis come from her.
- Very grateful to my former supervisor Xiuming Liu who kindly supports me to start my PhD study in Munich.
- Tobias Megies, Simon Marek and other colleagues in the institute for fun in coffee break.
- China Scholarship Council (CSC) for three-year funding.
- Joanna Markut for management of the Hiwi contract with the university, Jens Oeser for computer help and other nice staffs in the institute
- My wife, my parents, my family and many nice friends for their understanding and supports during my PhD period.